# HAND POSTURE RECOGNITION USING DISCRETE ORTHOGONAL MOMENTS

***S. Padam Priyal***

# HAND POSTURE RECOGNITION USING DISCRETE ORTHOGONAL MOMENTS

*A*

*Thesis submitted*

*for the award of the degree of*

**DOCTOR OF PHILOSOPHY**

By

**S. PADAM PRIYAL**

DEPARTMENT OF ELECTRONICS AND ELECTRICAL ENGINEERING

INDIAN INSTITUTE OF TECHNOLOGY GUWAHATI

GUWAHATI - 781 039, ASSAM, INDIA

APRIL 2014

கேடுஇல் விழுச்செல்வம் கல்வி ஒருவற்கு
மாடுஅல்ல மற்றை யவை.

- திருக்குறள் (400)

***Learning is excellence of wealth that none destroy;***
***To man nought else affords reality of joy.***

***- Thirukkural*** (400)

*This thesis is dedicated to*

*My Teacher, Prof. Bora;*

*My Husband, Shyam;*

*and*

*My Friends and Family.*

# Certificate

This is to certify that the thesis entitled "**HAND POSTURE RECOGNITION USING DISCRETE ORTHOGONAL MOMENTS**", submitted by **S. Padam Priyal** (06610210), a research scholar in the *Department of Electronics and Electrical Engineering, Indian Institute of Technology Guwahati*, for the award of the degree of **Doctor of Philosophy**, is a record of an original research work carried out by her under my supervision and guidance. The thesis has fulfilled all requirements as per the regulations of the institute and in my opinion has reached the standard needed for submission. The results embodied in this thesis have not been submitted to any other University or Institute for the award of any degree or diploma.

Dated:

Guwahati.

Dr. Prabin Kumar Bora

Professor

Dept. of Electronics and Electrical Engineering

Indian Institute of Technology Guwahati

Guwahati - 781 039, Assam, India.

# Acknowledgements

The successful completion of this thesis is benefited from the contributions and the support of many individuals, to whom I feel indebted. At the outset, I would like to express my heartfelt gratitude to my thesis supervisor, *Prof. Prabin Kumar Bora* for his support and encouragement. He has trained me in research and imparted discipline for being a good academician and person. I would particularly like to thank him for the patience he has shown in carefully correcting my manuscripts.

I am very thankful to my doctoral committee members, *Prof. S. Dandapat*, *Prof. Chitralekha Mahanta* and *Prof. S.R.M. Prasanna* for their moral support, thorough evaluations and suggestions that improved my research work. I am very much indebted to *Prof. S.R.M. Prasanna* for providing me the additional computing resources to complete my research work.

I owe my deepest gratitude to *Dr. J.S. Sahambi*, who had been on my doctoral committee for a brief period and has given valuable advices for improving my skills as a researcher. I would like to extend my gratitude to *Prof. Anil Mahanta* for his kindness and motivation to stay focussed in work.

I am also thankful to the Head of the Department and the other faculty members for their kind help in carrying out this work. I express my gratitude to all the members of the research and technical staff of the Department for their timely help. My special thanks go to *Mr. Sanjib Das* for providing excellent computing facilities and helping me with various resources that were useful for the research work.

I have been very fortunate to have a great group of friends in IITG. They have immensely contributed to my research work, by spending their time with me and helping me in database collection. Without their support, this research would have been incomplete. I would like to convey my special thanks to my friends *Mr. T. Kannan* and *Ms. Babita Jajodia* for being there for me at all the times. I could not have completed this manuscript without their supports. My heartfelt thanks to my friends *Mrs. Sumitra Shukla*, *Dr. S. R. Nirmala* and *Dr. Amrita Ganguly* for the love and the care they have been showing to me, ever since I joined IITG. I would like to express my sincere thanks to *Mr. Ramesh Kumar Mishra* for his kindness.

I would like to express my heartfelt gratitude to *Ms. V. Kohila* for being a great friend. I gratefully acknowledge my friends like brothers, *Mr. V. Satheesh Kumar*, *Mr. S. Arun* and *Mr. R. Vinoth Kumar* for their constant support and unconditional help. My heartfelt thanks to *Ms. D. J. Sheeba* and *Ms. N. Sharmila* for the great companionship that they both have shared with me. All my other friends have also helped me in several ways and so, I would like to say a big thank you to all of them for their friendship and support.

My sincere thanks goes to the following friends, who during their stay in IITG have been a great support to me and took part in my database collection.

*Dr. Amrita Ganguly, Assam engineering college, Guwahati.*
*Dr. S.R. Nirmala, Guwahati university, Guwahati.*
*Dr. Rupaban Subadar, North-eastern hill university, Shillong.*
*Dr. C. Shyam Anand, Samsung research and development institute, Delhi.*
*Dr. D. Senthil Kumar, GE global research, Bengaluru.*
*Dr. S. S. Karthikeyan, Indian institute of information technology, Kancheepuram.*
*Dr. Sarada Prasad Dakua, Quatar foundation, Doha.*
*Dr. Himanshu Katiyar, BBD university, Lucknow.*
*Dr. K.C.Narasimhamurthy, Siddaganga institute of technology, Tumkur.*
*Dr. D. Govind, Amrita vishwa vidyapeetham, Coimbatore.*
*Mrs. Sowmya Athreya, Central research lab-BEL, Bengaluru.*
*Ms. Anushree Neogi, Cambridge institute of technology, Ranchi.*
*Mr. S. Hemanth Kumar, IISC, Bengaluru.*
*Ms. V. Kohila, National institute of technology, Warangal.*
*Ms. Sumithra Das, National institute of technology, Warangal.*
*Ms. R. Vinnarasi, Sharda university, Noida.*
*Ms. Ellanti Saranya, NetApp, Inc. , Bengaluru.*
*Ms. Anusha, IIT Hyderabad.*
*Mrs. Sumitra Shukla, IIT Guwahati.*
*Mrs. G. Aruna, IIT Guwahati.*
*Mr. CH. Nagesh, IIT Guwahati.*
*Mr. Kuntal Deka, IIT Guwahati.*
*Mr. T. Kannan, IIT Guwahati.*
*Ms. Nabanita Adhikary, IIT Guwahati.*
*Ms. Bhavana.*
*Ms. Anupa Majumdar.*
*Ms. Poornima.*
*Ms. Durga.*

My deepest gratitude goes to my husband *Dr. C. Shyam Anand* and my parents *Dr. S. Soundararajan* and *Mrs. S. Brinda Devi* for their continuous love and support throughout my studies. I would like to convey my sincere thanks to my father-in-law *Mr. A. Chandran* and my mother-in-law *Mrs. C. Suseela* for the opportunity they have given me to pursue my interest in research. The unlimited sacrifices of my family are the reasons where I am and what I have accomplished so far.

My deepest and heartfelt thanks to my Godfather in my uncle *Mr. S. Chandrasekaran*, who molded me into the person I am today. I take this opportunity to thank him for all the love, care and the support he is giving to me ever since my childhood. Without him, I could have never pursued this career.

Finally, I thank the great God for guiding my life through these wonderful people. I pray to Him to watch over them every day and night and give them all, a blissful life.

*S. Padam Priyal*

# Abstract

Hand posture recognition involves interpretation of hand shapes by a computer. To find an appropriate shape descriptor for uniquely characterising this, has been a major issue in hand posture recognition. This thesis develops a novel hand posture recognition technique based on discrete orthogonal moments (DOMs). These moments are derived from the approximation of the image by the two-dimensional discrete orthogonal polynomials (DOPs).

The theory of the DOPs is studied and the Krawtchouk and the discrete Tchebichef moments are considered for shape representation. The experiments conducted on the MPEG-7 (CE Shape-1, Part-B) shape database confirm that these moments are robust to shape deformations and hence they form potential descriptors for recognising the hand postures.

The proposed DOM based hand posture recognition technique takes the hand image as the input. A rule based technique depending on the anthropometric dimensions of the hand is developed to segment the hand from the forearm. An adaptive rotation normalisation procedure based on the abducted fingers and the major axes of the hand is proposed. The normalised hand shapes are represented using the Krawtchouk and the discrete Tchebichef moments. The technique is analysed for robustness against scale, user and view-angle variations on a hand posture database containing $4,230$ samples of 10 gesture signs. The experiments on the classification of hand postures suggest that the DOMs are robust to user and view-angle variations. The performance of the DOMs is analysed in comparison with the other shape descriptors like the geometric moments, the Zernike moments, the Fourier descriptors, the Gabor wavelets and the principal component analysis (PCA). Comparative studies show that the DOMs are superior to the Gabor wavelets, the Fourier descriptors, the geometric moments and the Zernike moments. The DOM based classification offer high accuracies and is comparable to the PCA based classification. Particularly, the discrete Tchebichef moments show marginally better performance than the Krawtchouk moments.

The proposed DOM based recognition technique is applied for the recognition of 32 single-hand postures of Bharatanatyam known as the Asamyuta hastas. The performances of the Krawtchouk

and the discrete Tchebichef moments are compared with that of the PCA technique. The experiments are performed on a hand posture database containing $8,064$ samples of 32 Asamyuta hastas. The results show that the discrete Tchebichef moments offer better classification performance than the Krawtchouk moments and the PCA. The proposed system aims towards promoting hand postures as data cues to automatically annotate and retrieve Bharatanatyam dance videos.

# Contents

# List of Figures

# List of Tables

# List of Acronyms

| | |
|---|---|
| 1D | One Dimensional |
| 2D | Two Dimensional |
| 3D | Three Dimensional |
| 1/4L | One-quarter Left |
| 1/4R | One-quarter Right |
| 3/4L | Three-quarter Left |
| 3/4R | Three-quarter Right |
| CBA | Computer Based Automation |
| CSS | Curvature Scale Space |
| DCT | Discrete Cosine Transform |
| DFT | Discrete Fourier Transform |
| DIP | Distal interphalangeal |
| DOG | Difference-of-Gaussian |
| DOP | Discrete Orthogonal Polynomials |
| DOM | Discrete Orthogonal Moments |
| DTP | Discrete Tchebichef Polynomials |
| ESD | Energy Spectral Density |
| FB | Full Back |
| FD | Fourier Descriptor |
| FF | Full Front |
| FOM | Figure-of-Merit |
| FOV | Field-of-View |

| | |
|---|---|
| HCI | Human-Computer Interaction |
| HMM | Hidden Markov Models |
| IP | Interphalangeal |
| LBP | Local Binary Patterns |
| LDA | Linear Discriminant Analysis |
| LLE | Local Linear Embedding |
| MCT | Modified Census Transform |
| MHD | Modified Hausdorff Distance |
| MP | Metacarpophalangeal |
| PCA | Principal Component Analysis |
| PIP | Proximal Interphalangeal |
| PL | Profile Left |
| PR | Profile Right |
| PZM | Pseudo-Zernike Moment |
| QMF | Quadrature Mirror Filters |
| SIFT | Scale Invariant Feature Transform |
| SSIM | Structural Similarity |
| STFT | Short-time Fourier Transform |
| TMC | Trapeziometacarpal |
| WKP | Weighted Krawtchouk Polynomial |
| ZM | Zernike Moment |

# List of Symbols

| | |
|---|---|
| $(a)_k$ | Pochhammer symbol |
| $\mathbb{B}$ | Shape boundary |
| $C_\theta$ | Angle of view |
| $e_k$ | $k$th eigenvector |
| ${}_rF_s\,(a_1 \cdots a_r; b_1 \cdots b_s; z)$ | Hypergeometric function |
| $f(x, y)$ | Binary shape image |
| $F(\omega)$ | Fourier transform of f(t) |
| $G_{nm}$ | Geometric moments of order $(n + m)$ |
| $G_{\vartheta,\theta}$ | Gabor wavelets of scale $\vartheta$ and orientation $\theta$ |
| $G\,(x, t)$ | Generating function |
| $K_n\,(x; p)$ | $1D$ Krawtchouk polynomial basis of order $n$ |
| $\overline{K}_n\,(x; p)$ | $1D$ Weighted Krawtchouk polynomial basis of order $n$ |
| $\overline{\mathcal{K}}_n\,(\omega)$ | Discrete Fourier transform of $\overline{K}_n\,(x; p)$ |
| $\lambda_k$ | $k$th eigenvalue |
| $M_n$ | $1D$ Discrete orthogonal moments of order $n$ |
| $M_{nm}$ | $2D$ Discrete orthogonal moments of order $(n + m)$ |
| $\omega_p$ | Peak frequency |
| $\omega_{BW}$ | Bandwidth |
| $\psi_n\,(x)$ | Discrete orthogonal polynomials of order $n$ |
| $\Psi_n\,(\omega)$ | Discrete Fourier transform of $\psi_n\,(x)$ |
| $\Psi_n\,(r, \omega)$ | Short-time Fourier transform of $\psi_n\,(x)$ |

| | |
|---|---|
| $p$ | Shifting parameter |
| $\mathrm{p}_n$ | Noise level |
| $Q_{nm}$ | $2D$ Krawtchouk moments of order $(n+m)$ |
| $\sigma$ | scale parameter |
| $T_n(x)$ | $1D$ discrete Tchebichef polynomial basis of order $n$ |
| $\overline{\mathcal{T}}_n(\omega)$ | Discrete Fourier transform of $T_n(x)$ |
| $V_{nm}$ | $2D$ discrete Tchebichef moments of order $(n+m)$ |
| $W_{pca}$ | PCA projection matrix |
| $W_{lda}$ | LDA projection matrix |
| $w(x)$ | Weight function |
| $\xi(l)$ | Hanning window function |
| $Z_{nm}$ | Zernike moment of order $n$ and repetition $m$ |

# 1

# Introduction

**Contents**

Computer based automation (CBA) systems can be defined as the computing systems for automatic data analysis and process control via computers. The CBA system is basically an information processing system in which the characteristics of the input data and the man-machine interface for providing the input data are important factors along with the techniques for data processing. Thus, a CBA system can be considered to comprise of two functional units. They are: (a) the *user interface* and (b) the *information processing unit*.

The user interface acts as the channel for interaction between the humans and the computer. Thus, as a functional unit, the user interface provides the means for

**Input,** allowing the users to pass the data and the instructions to the computer in order to execute the desired process.

**Output,** allowing the computer to present to the user the outcome of the executed process.

This activity of communication between the human and the computer is generally stated as the human-computer interaction (HCI). The main objective in the design of a user interface is to provide an efficient interaction unit that correlates with the user's knowledge, skills and the capabilities. The widely employed input interfaces for HCI in CBA systems are the keyboard and the mouse. The other input interfaces for voice and video inputs are the microphone and the camera respectively. The processed output data can be of any form such as the textual data, image, video and audio. Accordingly, the commonly used output interfaces are a monitor, a printer and the speakers.

The information processing unit is the software unit that comprises of programs, algorithms and instructions related to automatic data processing.

The advancements in data representation techniques allow complex data such as the text, image, video and sound to be digitally represented. This enables the information processing unit of a computer to handle and process the complex data types. From the past few decades, more research is oriented towards developing computational algorithms for processing the image and the sound data. In this context, several image, video and sound processing algorithms are successfully developed for exploiting the information underlying the raw data. The success of these information processing algorithms encourages advanced user interfaces that are capable of providing image, video or sound inputs to CBA systems. Hence, the goal of HCI is intended towards developing interactive user interfaces that emulate the 'natural' way of interaction among humans.

The futuristic technologies in CBA systems attempt to incorporate communication modalities like speech, hand writing and hand gestures with HCI. Among these, the gesture based user interfaces offer several advantages in CBA systems for supervision and control. Further, the inclusion of computer technology in the fields like cognitive linguistics and sign language communication has increased the role of hand gestures as an element for user interface.

## 1.1 Hand gestures in CBA systems

Gestures are a means of non-verbal interaction among people through modes like facial expressions, hand poses and bodily movements specific to the hand, the head, the shoulder and the leg. Among these, the most participating and meaningful elements while gesturing are the hands and the facial expressions.The hand gestures comprise of specific postures and movements that are relative or non-relative to the semantic of the spoken language. For this reason, it is possible to have a structured gesture language based on hand gestures that can act as a substitute for the spoken language. On the other hand, the facial expression can only emphasise the underlying emotions in a sentence and it cannot be a stand-alone structured language. Therefore, it is understood that in a structured gesture language the level of semantic content conveyed through the hand gestures is more significant than the other gesturing entities. Hence, hand gesture based user interfaces are considered as an interesting alternative to achieve natural interaction between the humans and the computer. This section explains the types of gestures and their applicability in CBA system.

### 1.1.1 Hand gesture taxonomy

From the study of literature on the role of gestures in communication [8–12], the hand gestures can be broadly classified into three categories based on the context of their occurrence:

(i) The **gestures that accompany speech** are spontaneous and unintentional gestures that may or may not relate to the semantic content of the speech. The gestures that accompany speech are usually hand movements. The taxonomy of the gestures belonging to this class includes [8]

- *Iconic gestures* that are used as referential symbols to illustrate the concrete features relative to the semantics of speech.
- *Metaphoric gestures* are those used to illustrate abstract contents in effect towards imagining the nonexisting aspects of the speech.
- *Deictic gestures* are known as the pointing gestures. They involve pointing through fingers to illustrate the *where* and the *who* aspects that occur within the context of the speech.
- *Beat gestures* are unintentional hand movements that occur along with the rhythmical pulsation of speech. The beat gestures are not correlated to the semantic of the speech and are used to draw the

attention of the listeners.

(ii) The **gestures that substitute speech** are communicative gestures and they are independent of the spoken language. These gestures combine to frame an autonomous gesture system that assumes a language like form structured at the syntactic, morphological and the phonological levels. The system of gestures with this kind of linguistic structure is known as the *sign language* [8]. The sign language comprises of several units of meaningful hand poses and hand movements. The other class under the communicative gestures is the class of *emblems*.Unlike the sign language, the emblems do not have a linguistic structure and are mere hand poses with specific meanings [8]. They can occur independent of the speech and the gestures under this class have standard meanings that clearly substitute for a spoken word. The emblems are otherwise known as the *hand postures* or *static hand gestures* [11, 12].

(iii) **Pantomime** is a combination of meaningful hand poses and hand movements that may or may not accompany speech [12]. The gestures in pantomime are consciously communicative and stand-alone as a substitute for the spoken word even if accompanied with speech. However, the pantomime does not have a formal linguistic structure as the sign language [10].

### 1.1.2 Applicability in CBA

The choice on the type of gestures to be employed for the HCI in a CBA system depends on the application domain. Based on these applications they may serve as user interface data for HCI or as data cue for analyzing image or video sequences containing gestures. These applications are outlined below.

#### 1.1.2.1 Application as user interface data

In the context of user interface, the gestures are employed to replace the mouse and the keyboard. The gestures made by a person are captured using sensing devices that are interfaced to the computer. The input gesture acquired using the sensors/camera is then interpreted by the information processing unit in order to execute a specific task associated with the input. According to Nielsen et al. [11], the functions of the hand gestures as a user interface language are summarised as follows.

(i) The gestures are used to issue ***commands*** for executing system functions that occur within the context of the application. For example, the system commands such as the cut, copy, paste, delete and refresh can be executed with the use of gestures. Typically, hand postures can be used for the command function, so that the appearance of each hand pose can be specified to relate to a particular system command [13].

(ii) The deictic gestures are commonly used as an alternative to the mouse. In the HCI, these gestures are used as ***pointers*** to select an object or to specify the spatial location of an object in application domains including the desktop computer [13] and virtual reality systems [14, 15].

(iii) The other important function of gestures as a user interface is ***manipulation***. The gestures for manipulation are related to functions such as editing an object and moving an object to a specific location. The useful gesture types for manipulation are the iconic and the deictic gestures [11].

(iv) The gesture as the interactive element for the ***control*** function enables supervising and manipulating a process from distance. The gestures used for the control process can use any of the gesture types [11]. The application domains of such gestures are the robotic systems, avatar animation, interactive gaming and assistive systems.

(v) The gestures act as the ***communication language*** in automatic sign translation systems. The automatic sign translation systems are higher end applications in which the sign language performed by a person is interpreted by the computer and converted to other communication modes like speech and text [16, 17].

Except for the communicate function, the choice of the gesture type for the command, point, manipulate and control operations is subjective. For example, a sequence of hand postures can be used to execute the point and the manipulate operations instead of the hand movements.

#### 1.1.2.2 Application as a data cue

Because of the advancements in computer and internet technology, a large number of data are stored, shared and accessed by the users world wide. Likewise, there are several samples of images and videos related to gestures such as the sign-language and the pantomime sequences that are digitally stored and shared across the web.

With the enormous volume of data available for access, the major concern that needs to be addressed is the effective retrieval of the desired data. The current techniques for data retrieval rely on keyword indexing and textual annotations. The procedure is performed manually and hence, it is subjective and prone to errors. Therefore, automation systems for annotation and retrieval of data based on the information processing techniques have evolved.

The CBA systems for annotation and retrieval of images and/or videos containing a particular gesture require *cues* that are relative to the content to be processed. The data cues here will be the samples of the hand gesture that are acquired *a priori* through the input interface.

### 1.1.3 Significance of hand postures in CBA

From the details on the gestures, it can be inferred that the gesture types beneficial for HCI are the iconic gestures, deictic gestures and the hand postures. The characteristics of hand gestures that are of principal importance in CBA are the hand movements and the hand postures. The choice of the gesture type depends on the demand of the application. Thus, the HCI in a CBA system can involve hand movements or hand postures or a combination of both.

The hand postures are relatively more meaningful and their usefulness can be conveniently extended to all the functional requirements in CBA. The applicability of hand movements is convenient only as the user interface component and it is very difficult to analyse meaningful gesture events such as those in the sign-language by using the hand movements as a data cue. On the other hand, a sequence of relative hand postures can be used effectively as data cues for analyzing the gesture events and may be useful in annotation and retrieval systems for large digital gesture libraries.

The steps involved in processing the hand movements are complex due to the spatio-temporal variations such as the speed and the duration of the gesture event. Also, in real time applications, tracking the hand movements are relatively difficult when compared to detecting the hand postures. Despite these difficulties, the role of hand movements in HCI cannot be ignored in sophisticated applications such as avatar animation, automatic sign translation systems and interactive gaming. For applications like assistive systems, robotics, annotation and retrieval systems, the hand postures can effectively satisfy the requirement as a user interface component and a data cue.

## 1.2 Structure and the movements of the hand

The user interface unit in a gesture based CBA system refers to the data acquisition device through which the hand posture input is provided to the computer. Therefore, the gesture interface device should be designed in such a way that the variations in the hand structure are properly defined to the information processing unit.

The structure of the human hand is primarily attributed to the bones comprising the hand and the element responsible for the varied hand postures is the anatomical position of the bone segments of the fingers. The anatomy of the hand shown in Figure 1.1 illustrates the hand joints and the bone segments that constitute the hand structure [18]. From the figure, it can be observed that each of the five fingers has three joints. The joints corresponding to the thumb are the *interphalangeal joint* (IP), the *metacarpophalangeal* (MP) and the *trapeziometacarpal* (TMC) joints. The joints of the other four fingers are the *distal interphalangeal* (DIP),

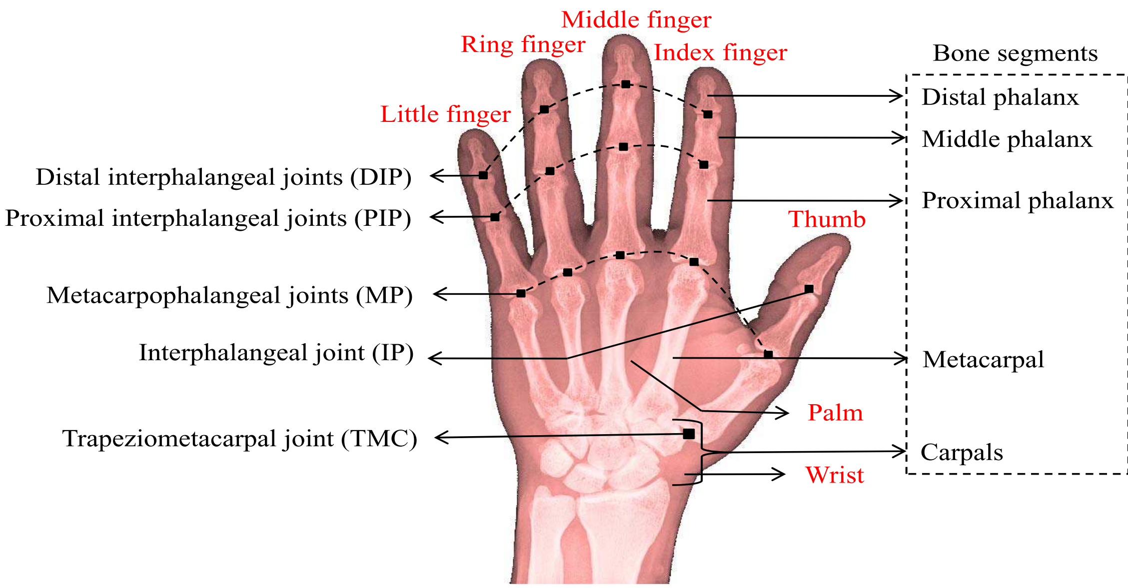


**Figure 1.1:** Illustration of anatomy of the human hand explaining the bone segments and the joints of the hand. Image courtesy www.ossurwebshop.co.uk

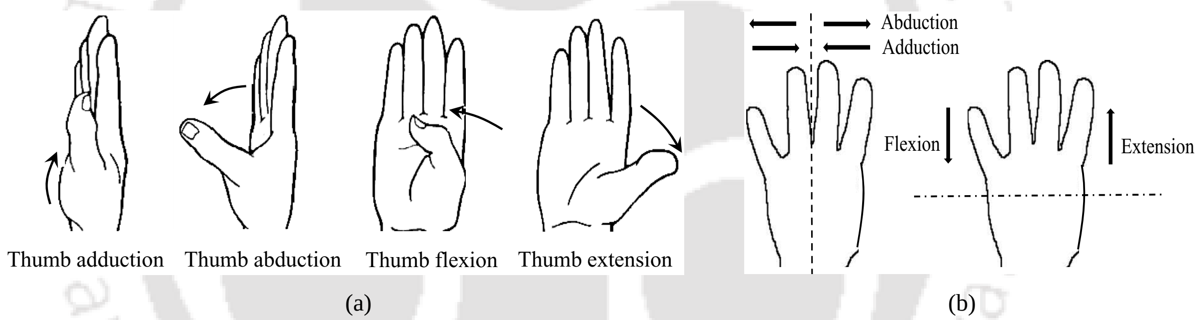


**Figure 1.2:** Illustration of anatomical movements with respect to (a) thumb and (b) four fingers of the hand.

the *proximal interphalangeal* (PIP) and the *metacarpophalangeal* (MP) joints. The various hand movements because of which the position of the bone segments vary are known as the *flexion, extension, adduction* and *abduction*. These hand movements are defined as follows [7, 18, 19].

(i) Flexion is a bending movement in which the relative angle of a joint between two adjacent bone segments decreases. This involves moving the bone segments towards the palm.

(ii) Extension is a straightening movement in which the relative angle between the two adjacent bone segments increases as a joint returns to the zero or reference position. The extension motion permits the fingers to move away from the palm.

(iii) Adduction is the movement of a finger towards the median plane of the hand.

(iv) Abduction is the movement of a finger away from the median plane of the hand.

**Table 1.1:** Details of anatomical movements associated with the joints between the bone segments of the hand.

| | DIP | PIP | IP | MP | TMC |
|---|---|---|---|---|---|
| Thumb | - | - | Flex, Extend | Flex, Extend Adduct, Abduct | Flex, Extend Adduct, Abduct |
| Index finger | Flex, Extend | Flex, Extend | - | Flex, Extend Adduct, Abduct | - |
| Middle finger | Flex, Extend | Flex, Extend | - | Flex, Extend Adduct, Abduct | - |
| Ring finger | Flex, Extend | Flex, Extend | - | Flex, Extend Adduct, Abduct | - |
| Little finger | Flex, Extend | Flex, Extend | - | Flex, Extend Adduct, Abduct | - |

Figure 1.2(a) and 1.2(b) illustrate the anatomical movements with respect to the thumb and the other four fingers respectively. It can be noticed that the adduction and the abduction movements of the thumb occur at 90° with respect to the palm [19]. The degree of movement varies from joint to joint and the movement of the bone segments are relatively dependent. The details of the movements associated with the joints between the adjacent bone segments are given in Table 1.1. A few examples of hand postures obtained through varied motion of the hand joints are shown in Figure 1.3.

## 1.3 Hand posture based user interfaces

From the discussion on the anatomical movements of the hand joints, it is evident that the appearance of a hand shape is based on the angles made by the finger joints. Thus, the cues acquired by the gesture interface device for HCI can be direct measurement of the parameters defining the anatomical motion or they can be visual cues such as the colour, texture, disparity and geometry [20]. The gesture based user interface for HCI is broadly classified as

1. Sensor based interface

2. Vision based interface

A brief outline of these gesture interfaces, their advantages and limitations are discussed as follows.

### 1.3.1 Sensor based interfaces

The sensor based interfaces are electronic devices that employ sensors to provide information about the motion, the orientation and the position of the fingers to the computer. The key element in a sensor based interface is the hand glove to which the flex sensors, the abduction sensors and the palm-arch sensors are

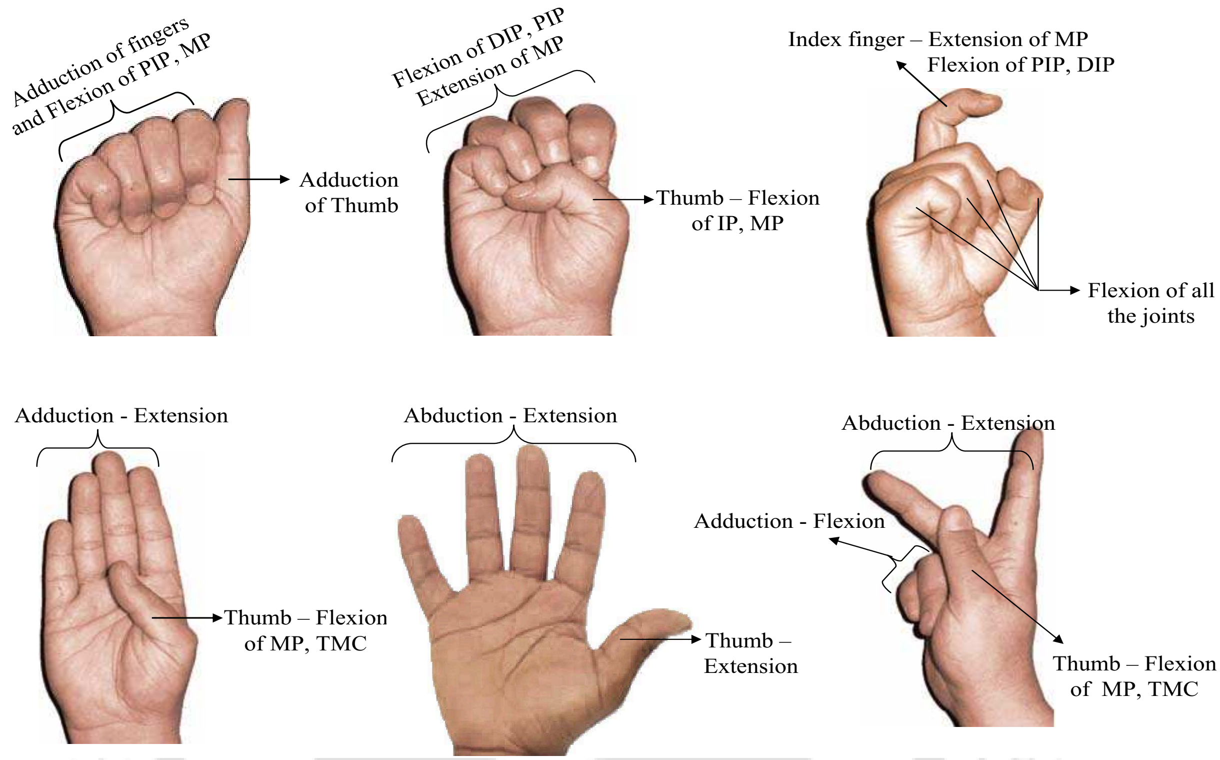


**Figure 1.3:** Examples of hand postures to illustrate the variations in the hand shape relative to the anatomical movements of the hand joints. Image courtesy wikimedia.org/wiki/File:ABC_pict.png

attached [21]. The flex sensors are placed at the finger joints to measure the angular information at the finger joints. The abduction sensors are placed between the adjacent fingers for measuring the abduction angle. The palm-arch sensors measure the bending of the palm. Along with these, additional sensors such as the magnetic or acoustic sensors are used to measure the relative orientation and the position of the hand in the three dimensional (3D) space [22, 23]. The angular and the positional information measured by the sensors is then passed to the computer through a wired or wireless connection. Such sensor based hand gloves are generally known as the instrumented gloves or the data gloves.

The sensor measurements relative to a hand posture are the cues provided to the information analysis unit. Depending on the application, the information analysis unit either directly interprets the hand posture or it maps to an animated hand such that it mirrors the shape of the user's hand posture. There are different types of data gloves that are designed specific to an application. Detailed surveys on the types of data gloves developed so far and their relative applications are given in [22], [24] and [25]. The design of a data glove varies based on the sensor technology, the number of sensors and the sensor precision [22]. The types of sensors used in the instrumented gloves include the accelerometer, conductive pads, Hall effect sensors, capacitive bend sensors, piezo-sensitive sensors, resistive ink sensors and the fiber optic sensors.

The Sayre glove is the first instrumented glove developed by Thomas DeFanti and Daniel Sandin in 1977.

(a) (b) (c)

(d) (e) (f)

**Figure 1.4:** Sensor based glove interfaces. (a) Dataglove. Image courtesy www.dipity.com; (b) CyberGlove II; (c) Example of hand gesture animation using CyberGlove II. Copyright ©2011 CyberGlove Systems LLC All rights reserved; (d) 5DT data glove. Image courtesy www.5dt.com; (e) Humanglove. Image courtesy Humanware (www.hmw.it) and (f) Pinch glove. Image courtesy Fakespace Labs (www.fakespacelabs.com).

The glove consists of light based sensors to measure the finger flexion and it was designed for multidimensional control of sliders and other two dimensional (2D) widgets [24]. The digital data entry glove developed in 1983 by the Bell telephone laboratories is the first to be designed for manual data entry using single-hand postures in sign language [26]. The glove consists of optical sensors for measuring the finger flexion, conductive pads for sensing proximity, tilt and inertial sensors for measuring the orientation and the position of the hand respectively. In 1987, Zimmerman et al. [27] developed the DataGlove for manipulating 3D virtual objects with hand gestures. The device consists of fibre optic sensors to measure the finger flexion and the magnetic sensors to measure the orientation of the hand. The DataGlove is the first commercially successful device that has been widely used.

James Kramer developed the cyberglove in 1991 to translate the American sign language to spoken English [28]. The cyberglove was commercialised by the virtual technologies and it is one of the leading instrumented gloves in terms of accuracy [22]. The cyberglove consists of piezo-sensitive sensors to measure the flexion, abduction and adduction at the finger joints and the wrist [29].

5DT data glove is another successful glove system developed by the fifth dimension technologies [30]. The

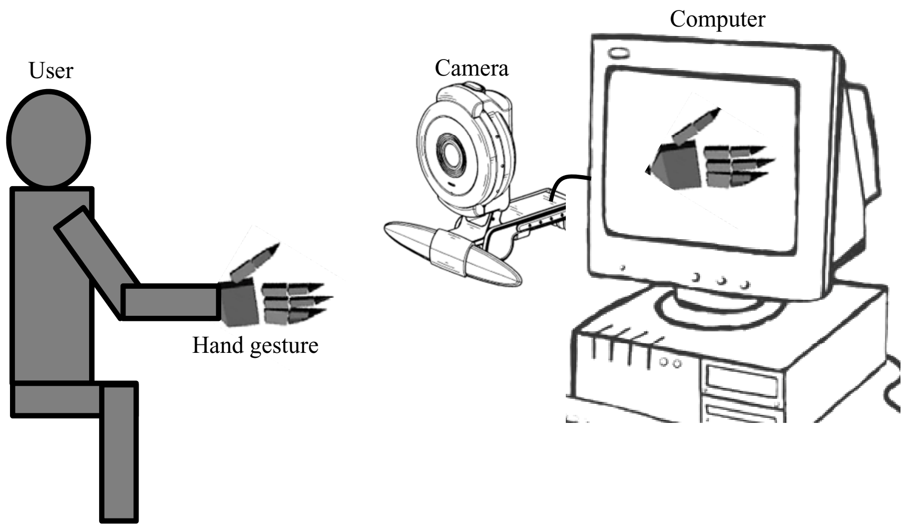


**Figure 1.5:** Illustration of the monocular vision based interface unit for CBA systems.

5DT data gloves consist of fiber optic sensors for measuring the joint movements of the hand [31]. Similarly, the other commercially available glove systems are the Humanglove [32] and the pinch glove [33]. The Humanglove consists of Hall effect sensors to measure the joint movements [34] and the pinch glove consists of two or more electrical contacts placed at specific parts of the hands. When a hand posture is made, the electrical contacts meet to complete a conductive path [34].

These sensor based glove interfaces facilitate accurate interpretation or mapping of the hand postures and hence, they find wide applications in sign-to-speech/text translation systems [35, 36], animation [37–39] and virtual reality [40–42].

### 1.3.2 Vision based interfaces

The vision based interfaces for CBA involve acquisition of hand postures using one or more cameras that are connected to the computer [43]. The vision based system using single camera is referred as the monocular vision system and that with multiple camera is referred as the multi-vision system. The schematic diagram of a monocular vision based interface setup for CBA systems is shown in Figure 1.5.

Unlike the sensor based interface, a computer vision method does not permit direct measurement of the hand posture parameters and hence, the images of the hand postures are the only cues provided to the information analysis unit. The information analysis unit employs image processing techniques for modelling and estimating the hand postures from the acquired hand posture image. The key factor in vision based interface is to ensure sufficient visibility such that the hand posture and the parameters pertaining to it are properly defined to the computer [44]. Accordingly, the camera's angle of view with respect to the user's hand should be chosen in such a way that there is no self-occlusion between the fingers and the shape of the hand is accurately captured [44]. In real time, the choice of the angle of view varies with respect to every hand posture. Thus, in order to accurately recover the hand posture, the vision based interface should either employ one moving camera or multiple still cameras for capturing the posture images at different angles of view. However, the choice of one moving camera is not a feasible solution in most of the practical applications of CBA. Hence, multiple cameras are placed at different angles of view to accurately capture the hand posture [45]. Bebis et al. [46], have employed one moving camera and multiple still cameras for HCI in virtual environments.

The multi-vision system offers the advantages of the accurate reconstruction of hand posture and the elimination of occlusion [44]. As a result the multi-vision systems are successful in higher-end applications like robotics, virtual reality, 3D object manipulation and animation. Despite these advantages, the multi-vision based interface is resource-intensive and requires computationally complex algorithms for hand pose estimation [44, 47]. Due to the difficulties associated with the multi-vision systems, the monocular vision based interfaces are widely employed.

In a monocular vision based system, the hand postures are acquired using one camera and the visual features extracted through image processing techniques are used for the interpretation of hand postures. Several researchers have already shown that the hand posture image acquired at one angle of view is accurate and effective for HCI. Further, the development of estimation methods [48] for 3D reconstruction from a 2D image encourages the use of monocular vision based interface in high-end applications. Accordingly, several estimation methods are being proposed for reconstructing $3D$ hand postures from the corresponding $2D$ images [49–54]. The reduced computational complexity and the availability of image processing algorithms for accurate modelling and interpretation of $2D$ images make the monocular vision based interface more suitable for real time CBA systems.

### 1.3.3 Merits of vision based interfaces over sensor based interfaces

The choice of the type of interface depends on the requirements of the CBA system such as accuracy, the size of the gesture vocabulary, ease while interaction and adaptability. In this context, the sensor based interfaces facilitate precise estimation of posture parameters and modelling/interpretation of hand postures [47]. As a result, the sensor based interfaces are capable of accurately interpreting a large class of gesture vocabulary that includes hand postures with minor differences.

Despite the advantages, the sensor based glove interfaces are obtrusive and they hinder the naturalness of the user interacting with the computer. They are not user adaptive and it requires to calibrate the device with respect to each user [22, 47]. Other drawbacks associated with them are the expensiveness and the limited portability [44]. Further, they cannot be used for generating data cues required in other CBA applications such as the content-based annotation and retrieval of images/videos containing the hand postures.

The vision based interfaces are non-intrusive and they facilitate natural HCI. They are robust to user variations and do not involve calibration in order to adapt to the varying users [44, 47]. The other advantages of vision based interfaces include cost effectiveness and the scope beyond HCI that includes generating data cues for content-based annotation and retrieval of images/videos containing the hand postures. The major limitation of the vision based interfaces is that the accuracy of the system is compromised due to the occlusion errors and the structural variations with the angle of view of the camera. As a result, the vision based interfaces facilitate only partial estimation of the hand posture and so the size of the gesture vocabulary that can be accurately interpreted is also restricted [47]. However, the advancements in pattern recognition algorithms favor effective and accurate interpretation of hand postures from the partial estimation [47]. Therefore, the vision based interface is considered as one of the potential elements for HCI in CBA systems.

## 1.4 Vision based hand posture recognition: the information processing step

The procedures involved in interpreting the acquired hand posture constitute the information processing unit of the CBA system. The key idea in automatically recognizing the hand posture is to search for similar hand postures that are already stored as templates. Accordingly, the development of the hand posture recognition unit is divided into two major phases. They are the training and the testing phases.

**Training** is the process of deriving decision functions based on the samples of the hand posture that are acquired *a priori* to constitute the training data. The decision rule required for the classification of hand postures is formulated through the extraction of significant properties of each hand posture image contained in the training set. Based on the properties, the postures are associated with different classes through a decision function. The mode of training can be *supervised* or *unsupervised*.

In supervised training, for a given a set of $P$ number of training samples $X = \{x_1, x_2, \ldots, x_P\}$, the corresponding class labels $Y = \{y_1, y_2, \ldots, y_P\}$ will be priorly available. Hence, the supervised training involves deriving or learning a decision function that relates $X$ to $Y$. In the case of unsupervised learning, the class labels are not known and only the training samples $X = \{x_1, x_2, \ldots, x_P\}$ are used for learning. Unsupervised learning involves analyzing the underlying structure of $X$ and grouping the data into clusters based on the analysis. Supervised training is employed in pattern recognition application.

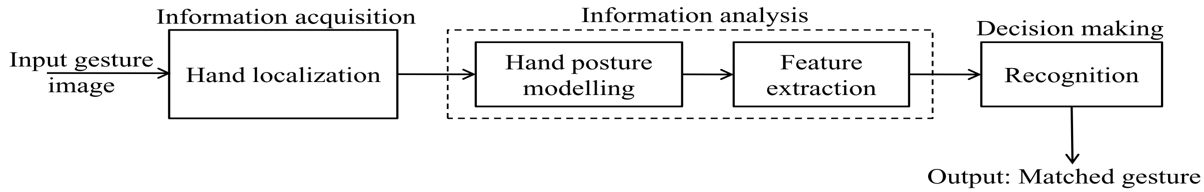


**Figure 1.6:** General block diagram representation of a hand posture recognition unit for CBA systems.

**Testing** refers to verifying the performance of the recognition unit in accurately classifying the test patterns based on the decision function derived while training. The correct classification ($CC$) accuracy of the hand posture recognition unit is defined as

$$CC = \frac{\text{Total number of correctly classified test patterns}}{\text{Total number of test patterns}} \tag{1.1}$$

The information processing unit for recognizing the hand postures employs image processing algorithms to analyse the hand postures and derive the decision functions. The procedure for analysis includes hand localization and hand modelling. The decision function is derived through feature extraction and the decision label associated with a sample is obtained through classification. The general block diagram representation of the procedures involved in hand posture recognition is shown in Figure 1.6. The procedures are explained briefly as follows.

### 1.4.1 Hand localization

The primary aspect in developing a vision based CBA system is to ensure that the hand posture and its relative parameters are properly emphasised to aid information analysis. The common method employed to highlight the posture parameters in vision based interface is through the use of optical markers and the coloured gloves. Traditional methods use retro-reflective markers or light emitting diodes (LEDs) placed at various finger joints in order to track the posture parameters [24,55]. However, the use of such optical markers is obtrusive [55] and finding the correspondence between the markers and the relative joints is a major problem [56]. Hence, colour-coded gloves are used as an effective alternative [44, 55, 56]. The colour-coded glove is made of fabric and designed to consist of different colours for every joint and the bone segment of the hand. These colours are used as cues to detect the segments of the hand and the hand posture parameters.

Even though the colour-coded gloves are simple and effective as a vision based interface, ideally it is not desirable for the gesturer to rely on the colour-coded gloves in practical applications. Hence, glove-free and markerless vision based interfaces in which the hand region is extracted from the image are employed. The commonly employed technique reported in the literature for hand extraction in a vision based interface

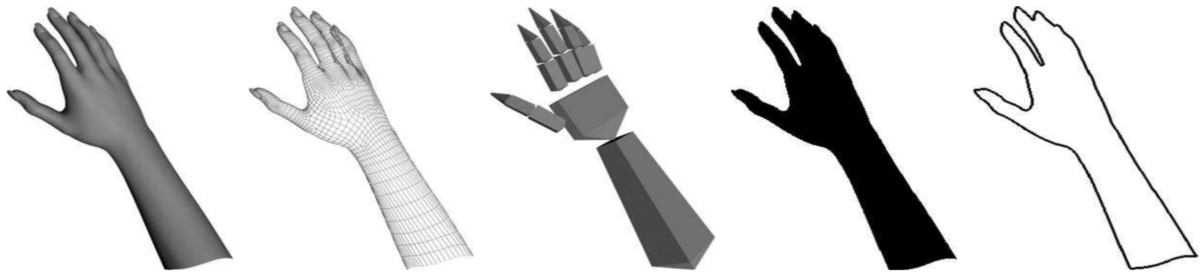

(a) (b) (c) (d) (e)

**Figure 1.7:** Illustration of different hand posture models. (a) 3D textured volumetric model; (b) 3D wireframe volumetric model; (c) 3D skeletal model; (d) Binary silhouette and (e) Contour. Image courtesy Wikipedia [1].

is through skin colour detection [47]. Some of the methods for hand detection use background subtraction techniques [57, 58], object contours [59] or a combination of the colour and the edge characteristics for hand localization [60].

### 1.4.2 Hand posture modelling

The detected hand posture can be considered as the configuration of the hand in the 3D space. Hence, the description of the hand posture through information analysis involves the characterization of their spatial properties. The approaches to spatial modelling of the hand postures are the *model based approach* and the *appearance based approach* [47, 61].

The model based approach to spatial modelling of the hand involves synthesizing 3D hand models to analyse the hand posture. The important parameters of the model based approach are the angles made by the hand joints and the palm position [61]. The 3D hand models are mainly classified into the *volumetric* and the *skeletal* models. The volumetric models describe either the 3D visual appearance or the 3D geometric appearance of the human hand. The geometric appearance in volumetric modelling is achieved through the use of generalised cylinders and superquadrics which encompass cylinders, spheres, ellipsoids and hyper-rectangles. The skeletal models are constructed using simple geometric structures such as the rectangular segments and lines. The illustrations of these different hand posture models are in Figure 1.7.

Unlike the model-based approach, the appearance based approaches are based on the projection of the 3D object into a 2*D* plane. Therefore, the appearance based models are the 2D images of the hand postures. This implies that the 2D appearance based modelling does not recover the entire hand posture and it results in loss of information in comparison to 3D modelling methods. However, the computational cost in fully recovering the 3D hand posture state is very high for real-time recognition and slight variations in the model parameters greatly affect the system performance. By contrast, processing the 2D appearance based models offers low computational cost and high accuracy for a modest gesture vocabulary [62]. Thus, the 2D models are well pertinent for real time processing in CBA systems.

### 1.4.3 Feature extraction

The general approach to deriving the decision function is through analyzing the unique set of visual features that accurately represent the hand postures. The procedure of deriving the features that describe the given object is known as feature extraction and it is one of the most crucial steps that directly influence the performance efficiency of the hand posture based CBA systems. The features employed for describing the hand posture vary depending on the type of hand posture models. In the case of 3D hand models, the direct parameters defining the hand postures such as the joint angles, the palm position, the height and the width of the fingers can be accurately estimated and they form the feature set representing the hand postures [61].

In the appearance based models, the 2D images of the hand postures are used as the templates. The feature describing the hand posture images can be derived either from the spatial domain or the transform domain representation of the binary hand shapes or the gray-level hand images. In the spatial domain representation, the features are directly derived by analyzing the pixel values constituting the hand posture image. The transform domain representation is the projection of the image from spatial domain on another domain in such a way that the distinct characteristics of the image are emphasised. Some of the image properties that are characterised by the extracted features are the spatial distribution of the intensity values, the magnitude and the orientation properties of the image gradients or the edges and the shape. These feature descriptors are derived either from the gray-level images or the binary silhouette images of the hand posture. Some of the other visual features derived from the appearance based models include the geometric features such as the number of extended fingers, their spatial positions and the inclination angles. Among these features, the shape is an important visual feature and it has been successfully used for representing the hand postures. The computational requirements in shape based object analysis is less when compared to processing the gray-level and the colour images.

A large number of features based on the above image properties are reported in the area of hand posture recognition. The efficiency of the extracted features for object recognition is generally evaluated based on the compactness in representation, robustness to spatial transformations, sensitivity to noise, accuracy in classification and the complexity of computation [63]. In this context, the moments are transform domain representations that are known to be efficient for shape representation [64]. Accordingly, some of the robust moments based features reported for hand posture recognition are the geometric moments [65] and the continuous orthogonal Zernike moments [66, 67]. The moment based features are simple, robust and offer compact representations. A detailed review on the feature descriptors used for hand posture recognition is presented in Chapter 2.

### 1.4.4 Classification

Classification is the process of assigning the class label to a given hand posture input. The class label is chosen through classifying the test hand posture as one of the classes of hand postures that constitute the training set. The classification is performed by analyzing the similarity between the features of the test hand posture and each of the hand posture in the training set. Some of the classification methods employed in pattern recognition are the minimum distance classifiers, probability based classifiers, discriminant functions and neural networks [60].

## 1.5 Issues in vision based hand posture recognition

The efficiency of the hand posture recognition unit depends on the accurate representation of hand postures. The features used for representation must be capable of uniquely describing the hand postures such that the recognition system is robust to variations that affect its performance efficiency. The important factors that affect the performance efficiency of the vision based hand posture recognition system are (a) the segmentation errors and (b) the geometrical distortions.

### 1.5.1 Segmentation errors

The accurate representation of a hand posture based on its features relies on the proper segmentation of the hand posture from the acquired image. Image segmentation is an ill-posed problem that relies on the depth cues, the colour cues and the geometric properties of the object to be segmented. The depth cues can be obtained only in multi-vision systems and the monocular vision systems have to rely only on the colour and the geometrical properties of the hand region. As mentioned in Section 1.4.1, the commonly employed method for hand localization is the skin colour detection.

The proper segmentation of hand postures based on the skin colour is affected by the illumination changes because of the non-uniform illumination of the hand region. Improper illumination also affects the dynamic range of the image intensity values contained within the hand region. As a result, it is difficult to choose an adaptive threshold for proper segmentation of hand postures under illumination changes. This leads to segmentation errors. Figure 1.8 presents hand posture captured under three different illumination conditions. The corresponding plots of the image histograms shown in Figure 1.9 illustrate the distribution of the intensity values with respect to the hand posture region. Figure 1.8(a) is an example of the hand posture image captured

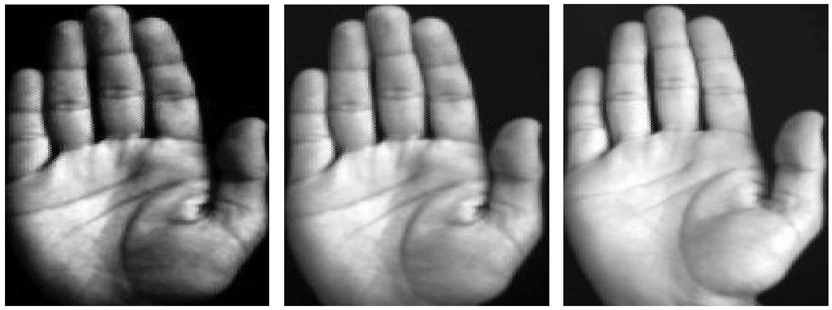

(a) (b) (c)

**Figure 1.8:** Illustration of variations in the details of the hand posture image with respect to illumination changes. (a) Poor illumination - dark image; (b) Normal (average) illumination - average contrast and (c) High illumination - high contrast.

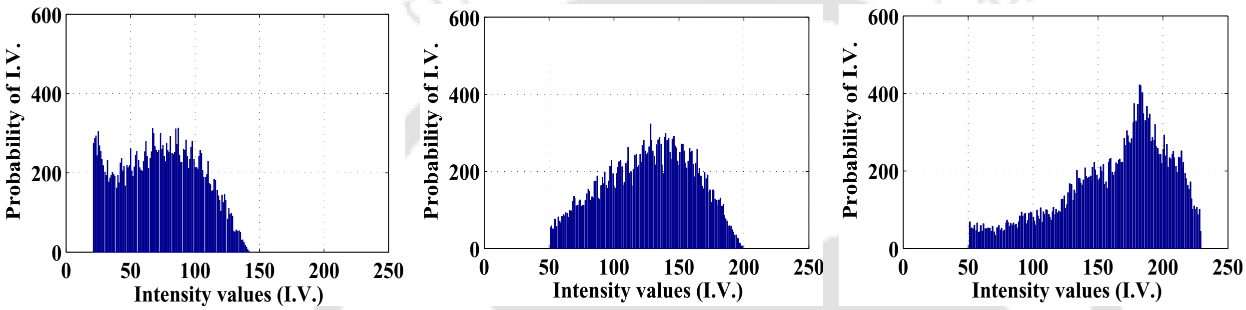


(a) (b) (c)

**Figure 1.9:** Histograms of (a) the dark image; (b) the average contrast image and (c) the high contrast image shown in Figure 1.8.

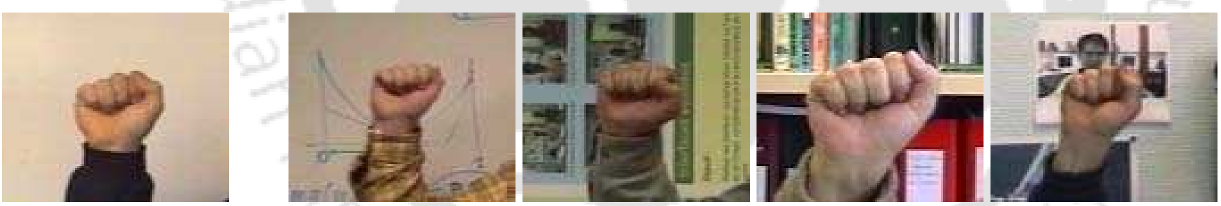

(a) (b)

**Figure 1.10:** Examples of hand posture images taken in varying background: (a) hand posture acquired in a uniform background and (b) hand posture images acquired in complex backgrounds. The hand posture images are taken from the Jochen Triesch static hand posture database [2].

under poor illumination with the corresponding histogram shown in Figure 1.9(a). The hand posture captured under normal illumination and the corresponding plot of image histogram are shown in Figure 1.8(b) and Figure 1.9(b) respectively. Similarly, Figure 1.8(c) is an example of the hand posture image captured under relatively high illumination and the corresponding plot of histogram is shown in Figure 1.9(c). Under poor illumination, the dynamic range of the intensity values is low and hence, the resultant image is dark and has a poor contrast. In the case of normal illumination, the dynamic range of the intensity values has increased and distribution of the intensity values within the range is almost uniform. Hence, the resultant image is relatively bright and has good contrast. Similarly, under high illumination the dynamic range of the intensity values is relatively more and the resultant image has higher contrast than the poor and the normal illumination images.

Additionally, segmentation errors also occur while segmenting the hand postures from a complex or cluttered background that contains several other objects with almost similar colour or geometrical characteristics as the hand region. The proper segmentation of hand postures is also affected if the colour of the user's clothing coincides the skin colour. Some examples of the hand posture captured under different backgrounds are shown in Figure 1.10.

### 1.5.2 Geometrical distortions

The other major issue involved in accurate recognition of the hand postures is the geometrical distortions that occur due to geometrical transformations, variations in the hand posture parameters and variations due to changes in the angle of view.

#### 1.5.2.1 Geometrical transformations

The geometrical transformations affecting the performance of the recognition unit includes the *scale*, the *rotational* and the *translational* changes induced during gesture acquisition as described below.

- The scale represents the spatial resolution of the acquired hand posture. The resolution will differ with respect to the variations in the hand geometry of the users and the distance between the gesturer and the camera.
- Rotation changes refer to the variation in the orientation of the hand posture that occurs either when the user rotates the hand while gesturing or when the camera is rotated along its plane within the field-of-view (FOV).
- Translational changes represent the variation in the spatial location of the hand posture that occurs due to the user's movement of the hand.

#### 1.5.2.2 Variations in the hand posture parameter

As explained in Section 1.2, the parameters that characterise the hand shape are the angles caused by the flexion/extension and the abduction/adduction movements of the finger joints. Among these, the flexion and the adduction movements are positive joint excursions and the extension and the abduction movements are negative joint excursions. The joint angle between two adjacent bone segments is measured by considering one

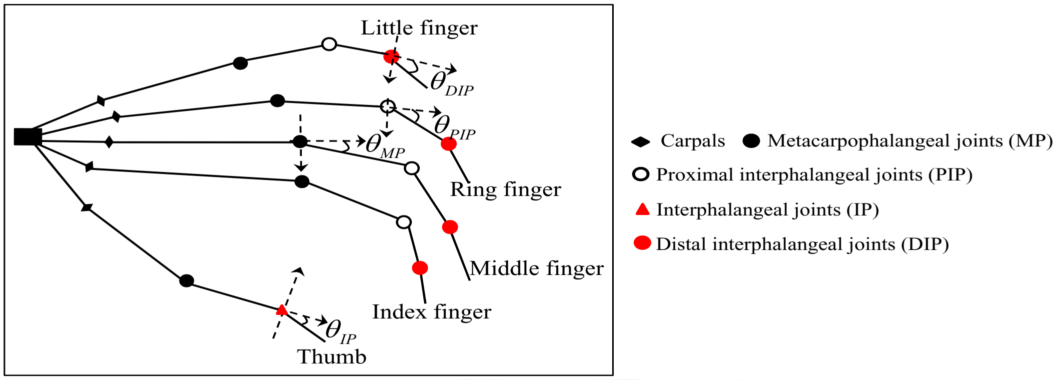


(a)

**Figure 1.11:** Illustration of hand posture parameters using the hand skeleton. The joint angles represent the hand posture parameters.

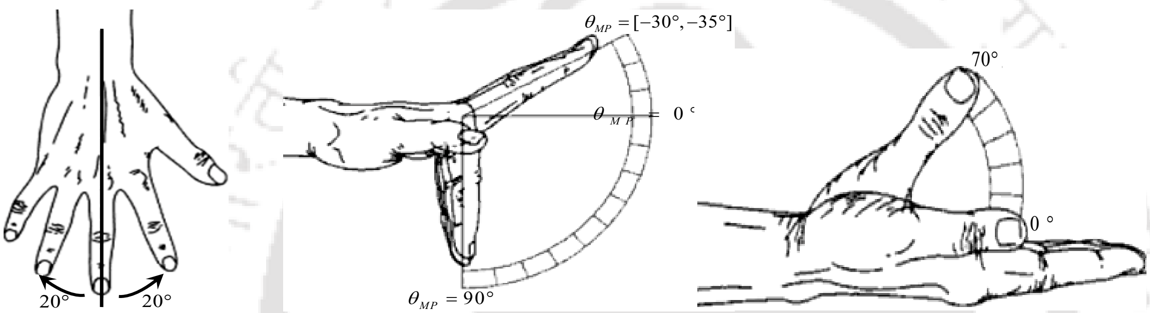


(a) (b) (c)

**Figure 1.12:** Illustration of (a) finger abduction; (b) MP joint range of motion, flexion-extension and (c) Palmar abduction and adduction of the thumb at the MP joint. The negative angle in (b) refers to the extension movement.

of the bone segments at close distance to the carpals as the reference axis. The procedure for measuring the hand posture parameters at the finger joints is illustrated using a hand skeleton in Figure 1.11(a). Similarly, a few examples illustrating the angular positions of the bone segments with respect to the abduction and the flexion movements of the metacarpal joints (MP) are shown in Figure 1.12. The maximum value of the motion parameters with respect to each finger joints are given in Table 1.2.

Based on these movement parameters, the hand postures can be considered as *simple postures* and *complex postures*. With simple postures, every individual finger is either extended or flexed to the maximum range. Complex postures are those in which the fingers can be bent at any angle within the maximum range of motion in order to constitute a hand posture. In the case of complex postures, the joint angles defining a hand posture are only approximations that lie within a defined range of angular values. The structural variations with respect to a hand posture occur due to the changes in the flexibility of the user's hand joints within the defined range.

Similarly, the hand posture parameters vary due to the variations in the hand geometry. An experimental study on the effects of the hand length and the flexibility of the joint angles in [68] states that the joint flexibility

(a)

(b)

**Figure 1.13:** Examples of a hand posture taken at various angles of view. The figure illustrates the structural deviations or deviations in the appearance of the hand posture. Similarly, occlusion of certain parts of the hand can be observed at each angle of view. The hand posture images are taken from the Massey hand posture database for the American sign language [3].

**Table 1.2:** Maximum range of motion parameters defining the movements with respect to the thumb and the finger joints [7].

| | Extension | | | Flexion | | | Abduction | Adduction |
|---|---|---|---|---|---|---|---|---|
| Fingers | $\theta_{MP}$ | $\theta_{PIP}$ | $\theta_{DIP}$ | $\theta_{MP}$ | $\theta_{PIP}$ | $\theta_{DIP}$ | 20° | 0° |
| | [−30°, −35°] | 0° | −20° | 90° | [100°, 120°] | [80°, 90°] | | |
| Thumb | $\theta_{MP}$ | $\theta_{IP}$ | | $\theta_{MP}$ | $\theta_{IP}$ | | 70° | 0° |
| | 0° | −20° | | 50° | 90° | | | |

of the fingers increase with the increase in the hand length. Therefore, the variations in the flexibility of the user's hand and the hand geometry result in the deviation of hand posture parameters due to which there is diversity in the appearance of a hand posture.

#### 1.5.2.3 Variations due to the angle of view

In the field of imaging, the angle of view is known as the view-angle. The viewpoint refers to the position of the camera with respect to the object of focus [69]. The optimal choice of the viewing angle or the viewpoint is determined by the amount of perspective distortion. Perspective distortion is a phenomenon in which, the part of the object present at a larger distance from the camera appears to be smaller than the closer part of the same object and vice versa [69, 70]. As a result, the perceived shape of the object is distorted / altered. The distortion is caused if the focal plane is not parallel to the objects surface and/or not in level with the centre of the object.It means that the camera is not at equidistance from all the parts of the object [70]. The variations in the viewpoint result in structural deviations and self-occlusion of the fingers. A few examples illustrating the structural variations and the occlusion errors in a hand posture due to variations in the view-angle are shown in Figure 1.13.

## 1.6 Motivation for the present work

Vision based hand posture recognition is one of the important research areas spawning advanced HCI techniques for intelligent interaction in CBA systems. The efficiency of these systems depends on the accuracy of the features used for describing the input hand postures. For improved performance, the features defining the hand postures should be robust to geometrical distortions caused by the similarity transformations, user and the view-angle variations. Among these, the geometrical transformations can be easily addressed through proper normalization techniques. Unlike geometrical transformations, it is very difficult to model and develop techniques for normalizing user and view-angle variations.

Only very few works in hand posture recognition have concentrated in developing user and view invariant recognition techniques. The comparative evaluation of the existing feature descriptors and their robustness to user and view-angle variations are not yet explored. Hence, this research is motivated towards identifying features that are robust to user and view-angle changes. Accordingly, the goal is to develop a robust monocular vision based hand posture recognition system that is capable of handling simple and complex hand postures.

Recently, the discrete orthogonal moments are introduced as efficient approximations for image analysis. These discrete orthogonal moments were shown to be efficient in terms of compact representation, robustness to noise and accurate reconstruction [71–73]. However, they are yet to be explored for shape description and classification. In this research work, two discrete orthogonal moments , namely the *Krawtchouk* and the *discrete Tchebichef* moments are proposed as features for shape representation. Based on the validation in representing the general shapes, a vision based hand posture recognition system using the discrete orthogonal moments as feature descriptors is proposed.

The thesis also aims at assessing the user and the view invariant characteristics of the proposed and other existing descriptors. Accordingly, the geometric moments, the Zernike moments, the Fourier descriptors, the Gabor wavelets and the principal component analysis (PCA) based descriptors will be evaluated.

The proposed discrete orthogonal moment based hand posture recognition system and the various feature descriptors are to be tested on two different classes of hand postures that are intended to find the applicability in different CBA systems. The first class of postures consists of 10 simple single-hand postures formed by extension/flexion and abduction/adduction of fingers to the maximum range. These simple hand postures can be used to command, control and manipulate operations in HCI. The second class of gestures consists of 32 complex single-hand postures taken from Bharatanatyam, a pantomimic dance form in India [74, 75]. The recognition technique for recognizing the hand postures in Bharatanatyam is aimed at developing content-based dance annotation and retrieval systems for Bharatanatyam.

## 1.7 Contributions of the thesis

The contributions of this research work are as follows.

(i) Discrete orthogonal moments, namely the Krawtchouk moments and the discrete Tchebichef moments are introduced as features for shape representation. The accuracy of the discrete orthogonal moments in representing the shapes from the MPEG 7 shape database is experimentally studied. The study is considered as validation towards using the discrete orthogonal moments as features for hand posture recognition.

(ii) A monocular vision based hand posture recognition system that is robust to geometrical transformations, user and view-angle variations is developed based on the discrete orthogonal moments.

(iii) For comparative evaluation, the user and the view-angle invariance characteristics of the proposed method and the state-of-the art methods like the Fourier descriptors, the geometric moments, the Zernike moments, the Gabor wavelets and the PCA descriptors are studied in detail.

(iv) In this research work, two different hand posture databases are developed. The first database consists of $4,230$ samples of 10 simple hand postures acquired at varied scales, orientations and view-angles. The database is collected from 23 users. The gesture recognition technique developed on this database may find applicability in hand posture based HCI to perform command, control and manipulation functions in CBA systems.

The second database consists of $8,064$ samples of 32 complex single-hand postures in Bharatanatyam, known as the *Asamyuta hastas*. The images are acquired by varying the scale and view-angle. The database is collected from 6 female subjects. The hand posture recognition technique developed on this database aims towards promoting hand postures as data cues to automatically annotate and retrieve Bharatanatyam dance videos.

## 1.8 Organization of the thesis

The rest of this thesis is organised as follows.

Chapter 2 presents a review on the feature descriptors used for hand posture recognition. The chapter concludes with an insight into the applicability of discrete orthogonal moment based descriptors for hand posture analysis.

Chapter 3 presents the theory of discrete orthogonal moments and the formulation of Krawtchouk and Tchebichef moments. The chapter includes experimental studies on the spatial- and the spectral-domain properties of the Krawtchouk and the discrete Tchebichef polynomials. The efficiency of the discrete orthogonal moments in shape representation and shape classification is studied using the MPEG 7 shape database. The experimental study presented in this chapter validates the discrete orthogonal moments as efficient shape descriptors.

Chapter 4 elaborates the proposed discrete orthogonal moment based hand posture recognition technique that is robust to similarity transformations and user and view-angle variations. The system deals with the silhouette model of the simple hand postures that are intended for application in HCI. In this chapter, anthropometry based normalization techniques for the removal of the forearm and orientation correction are proposed. The chapter includes details about the database development and the analysis on structural variations in a hand posture with respect to user variations and view-angle changes. The experiments on hand posture classification validate the efficiency of the discrete orthogonal moments in comparison to the other considered methods.

Chapter 5 explains the hand posture recognition technique developed for recognizing the single-hand postures in Bharatanatyam known as the *Asamyuta hastas*. The chapter explains the development of the Asamyuta hastas database and the system implementation procedure. The representation methods for analyzing the complex hand postures in Bharatanatyam are chosen based on the experimental results in Chapter 4. Accordingly, the Krawtchouk moments and the discrete Tchebichef moments and the PCA descriptors are considered. The experiments validate that the Tchebichef and the Krawtchouk moments are efficient features for representing these complex hand postures.

Chapter 6 concludes this thesis with suggestions for the application of the proposed discrete orthogonal moment based hand posture recognition technique for the automatic annotation of the Bharatanatyam video and content-based retrieval Bharatanatyam video from a database.

# 2

# A Review on Feature Extraction in Hand Posture Recognition

## Contents

In this chapter we present the existing state-of-art methods in hand posture recognition. The methods are categorised based on the features derived from the hand posture images for description. The advantages and the limitations of the existing methods in terms of the computational complexity, robustness to similarity transformations, user and view-angle invariance, classification rate and the supported size of the posture vocabulary are reviewed.

## 2.1 Introduction

The recognition of an object in an image requires the extraction of some features that uniquely characterise the object. These features are called the descriptors for the object and represented in a form suitable for the classifier used for mapping the object into a known class. The descriptor may be derived from the geometric shape in the form of the binary silhouette image that is obtained by the segmentation of the original image. Alternatively, the descriptor may be derived from the variation of intensity in the gray-level image containing the object.

There are large number of descriptors derived from the silhouette image and the gray level image to represent the hand posture. We classify these methods into two category they are: (a) the silhouette image based methods and (b) the gray-level image based methods. The important descriptors belonging to both the categories are described below.

## 2.2 Silhouette image based methods

The silhouette image based methods derive features that represent the hand posture by its shape. The procedure for recognizing the shape of a given object requires to derive parameters that uniquely characterise the shape [76]. The efficiency of a method used for representing the shapes is evaluated in terms of retrieval accuracy, compactness of representation, hierarchy of coarse to fine representations, computational complexity, robustness to geometrical transformations and robustness to shape defections [77]. The geometrical transformations include rotation, scaling, translation and affine variations of a given shape. The shape defections are structural distortions caused by noise, boundary distortions and the segmentation errors that occur while binarisation [63]. The retrieval efficiency represents the ability of the shape descriptor to effectively recognise similar shapes inspite of the above mentioned geometrical transformations and the shape defections. The silhouette image based methods generally derive the important features by using either the shape boundary or the interior points of the shape along with the boundary [63]. Hence, the silhouette based shape features can be classified into *contour features* and *region features*. The contour features exploit only the pixels that form the shape boundary and the region features take in to consideration all the pixels constituting the shape region or the entire silhouette image. The details of several contour-based features and region-based features used for hand posture analysis are discussed below.

### 2.2.1 Geometric features

The geometric features of the hand posture are the simple shape descriptors that can be derived both from the shape boundary and the shape region. The geometric features for defining the entire shape are derived by extracting the morphological characteristics of the finger and the palm regions of the hand. Accordingly, the location, the position and the inclination angles of the fingers are among the geometric features employed for representing the hand posture.

In [78], a hand posture recognition technique using the boundary profile of the hand postures as features was proposed. Let $\mathbb{B}$ define the boundary of the hand posture and $(x_c, y_c)$ be its centroid of the hand posture region. Then, for $(x, y) \in \mathbb{B}$, the boundary profile ($BP$) describing the hand posture is computed as

$$BP\,(x,y) = \sqrt{(x - x_c)^2 + (y - y_c)^2} \tag{2.1}$$

The number of peaks in the boundary profile represents the number of extended fingers with the peaks corresponding to the finger tips. The positions of the peaks of the BP denotes the positions of the fingers with respect to the centroid of the hand posture. The BP was used to classify a database consisting of 6 distinct static hand gestures. The classification was performed with the minimum distance classifier and the average recognition rate obtained was 95%.

Jag et al. [79] proposed a view-point invariant hand posture recognition technique combining the silhouette model and 3D-hand posture model for recognition. The method derived the centroidal profile from the boundary of the hand posture. Given the shape boundary, the centroidal profile is obtained by mapping the boundary points into a polar $(r, \theta)$ representation. The radius $r$ describes the distance between the shape centroid and the boundary points. The $\theta$ value describes the inclination angle of the extended fingers. The system was tested on a dataset containing 5 distinct hand postures that were captured at 15 different viewing directions. Their technique achieved a classification rate of 90.8%.

The above methods based on the shape boundary are sensitive to noise, rotation variations and there may be two different hand postures with almost similar boundaries. Also, the locations of the peaks vary according to the user's hand geometry and hence, it is not possible to handle gestures with various finger flexions. In order to overcome this, different region based techniques for detecting the number of extended fingers, their positions and the relative length of the fingers are employed in [80–84]. In [80], a circle that intersects all the abducted fingers was drawn with respect to the centroid of the hand posture. The diameter of the circle was fixed as 0.7 of the farthest distance from the centroid. The number of extended fingers was estimated by counting the number of background-to-foreground transitions and used as the feature. The technique was tested on a small gesture library consisting of 5 distinct hand postures and was shown to be invariant to the similarity transformations. Yin and Xie [82] employed a similar technique for finding the number of extended fingers. However, the circle that intersects the abducted fingers was obtained iteratively. The other features used in this technique include the positions of the fingers with respect to the circle. The method was tested on a database consisting of 8 gesture signs.

The skeleton of the hand posture image was used in [81] for extracting the geometric features such as the position, the orientation and the number of extended fingers. These features were employed for classifying the basic hand shapes in the Japanese sign language. Stergiopoulou and Papamarkos [83] proposed a graph based searching method for deriving the morphological features of the palm and the finger regions of the hand posture. The shape of a given hand posture was approximated using the Self-Growing and Self-Organised Neural Gas (SGONG) network. The morphological features of the hand such as the number of the extended fingers, palm centre, slope of the hand, inclination angles of the extended fingers relative to the hand slope were derived from the SGONG approximation of the hand posture. A probabilistic classifier that is based on the choice of the most probable finger combination of a set of feasible gestures was used for recognition. The system was tested on a dataset of 180 images of 31 hand postures. The system achieved a maximum classification rate of 90% and is invariant to similarity transformations. However, the system is computationally complex and very sensitive to the errors in extracting the geometric features. In [84], the concave and the convex points in the boundary profile of the hand posture were used for partitioning the finger and the palm regions. Based on these points, the extended fingers were identified and the length and the width of the detected fingers were employed as features for classifying the hand postures. The geometric measures of each finger were determined based on the anthropometric measurements. The system achieved a classification rate of 91.4% in classifying 12 hand postures from the Arabic sign language.

Flasiński and Myśliński [85] have used boundary-based graph models and a parsing method for the recognition of hand postures in the Polish sign language. In general, the model graph of a given hand posture is obtained by deriving the polygonal approximation of its contour. the nodes of the graph are the vertices of the polygon and are labeled with the vertex angles. The nodes are connected by directed lines known as the edges. The orientations of the edges with respect to a reference node are used for labeling the edges. The obtained graph is called the *indexed edge-unambiguous graph* (IE-graph) and the vertex angles and the edge orientations are the feature descriptors. In [85], a set of IE-graphs representing the hand postures was treated as a formal language generated with the ETPL($k$) (Embedding transformation preserved production ordered $k$-left nodes unambiguous) graph grammar. The graph grammar was used for classifying 48 hand posture signs in the Polish sign language. It was shown that the system is robust to moderate changes in the view-angle and variations in the user hand anatomy. However, the system is sensitive even to small variations in the geometry of the hand posture induced due to user variations. Further experiments are required to verify the robustness of the system to perspective distortions induced by the view-angle changes.

Dias et al [86] developed a system known as the *Open Gestures Recognition Engine* (O.G.R.E) for recognizing the hand postures in the Portuguese Sign Language. The histogram of the distances and the angle between the contour edges were used to derive a contour signature known as the pair-wise geometrical histogram. The classification was performed by comparing the pair-wise geometrical histograms representing the gestures.

The above discussed geometric features are simple shape descriptors and usually can discriminate only hand postures with large differences. Further, these simple shape descriptors cannot handle hand postures that are deformed due to segmentation errors and self-occlusion.

### 2.2.2 Curvature scale space

The curvature scale space (CSS) representation of the hand posture is a boundary based shape description method. In this technique, the evolution of the zero-crossing points with respect to the multi-scale representations of the shape boundary is used as the features for hand posture recognition [87]. Consider the shape boundary $\mathbb{B}$, which is assumed to be a planar curve. Then, the curvature function $\kappa(u)$ is computed as

$$\kappa(u) = \frac{\dot{x}(u)\,\ddot{y}(u) - \ddot{x}(u)\,\dot{y}(u)}{\left(\dot{x}(u)^2 + \dot{y}(u)^2\right)^{3/2}} \tag{2.2}$$

where $u$ is the length parameter. Convolving $\mathbb{B}$ with a $1D$ Gaussian kernel $g(u,\sigma)$ of standard deviation $\sigma$ results in the smoothed curve $\mathbb{B}_\sigma$. The smoothed boundary points are given by

$$\begin{aligned} X(u,\sigma) &= x(u) * g(u,\sigma) \\ Y(u,\sigma) &= y(u) * g(u,\sigma) \end{aligned} \tag{2.3}$$

where $*$ denotes the convolution operation.

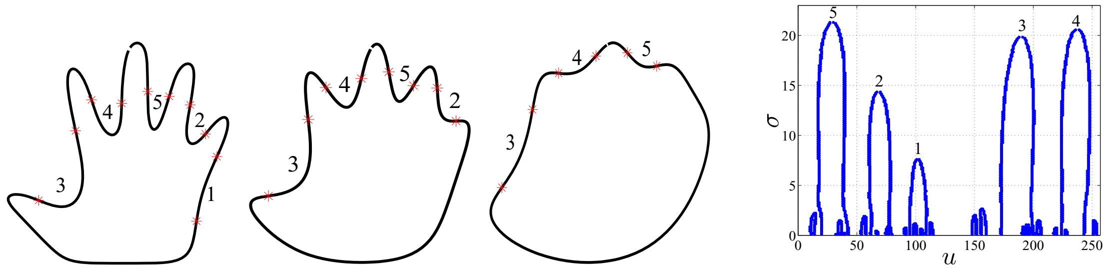


(a) (b) (c) (d)

**Figure 2.1:** Illustration of smoothing of the shape boundary and the evolution of the inflection points at different scales ($\sigma$). (a) $\sigma = 3.5$; (b) $\sigma = 8.2$ and (c) $\sigma = 14.6$. The concave segments at each scale are enumerated. The number of concavities decreases with the increase in the scale. (d) The CSS image constructed from the locations of the inflection points at various scales.

Accordingly, the curvature $\kappa(u,\sigma)$ at a scale $\sigma$ is computed as

$$\kappa(u,\sigma) = \frac{\dot{X}(u,\sigma)\,\ddot{Y}(u,\sigma) - \ddot{X}(u,\sigma)\,\dot{Y}(u,\sigma)}{\left(\dot{X}(u,\sigma)^2 + \dot{Y}(u,\sigma)^2\right)^{3/2}} \tag{2.4}$$

The CSS descriptors represent the location of the inflection points on the curve at different scales and are extracted as the CSS image. The CSS image $I_{CSS}(u,\sigma)$ is defined as

$$I_{CSS}(u,\sigma) = \{(u,\sigma)\,|\,\kappa(u,\sigma) = 0\} \tag{2.5}$$

An example illustrating the evolution of the concave segments in the hand posture boundary for different values of $\sigma$ and the corresponding CSS image are shown in Figure 2.1. The shape boundary is convolved with the smoothing kernel iteratively until there are no inflection points on the smoothened boundary. The scale of the smoothing kernel increases with the number of iterations. The peaks in the CSS image correspond to the concavities in the hand posture contour and the height of the peaks depends on the depth and the size of the concave segments. In general, the CSS image is used as the feature descriptor and the classification is performed using nearest neighbor classifier.

Kopf et al [88] employed CSS descriptors for classifying a class of 3 simple hand postures. They proposed a modified CSS approach in which the convex segments of the shapes were also represented in the CSS image. Chang et al [89, 90] proposed a feature alignment approach for making the CSS image invariant to translation, scale and rotation changes. The feature alignment involved circularly shifting the coordinate peaks of the CSS image with respect to the coordinate containing the largest peak. The proposed approach was tested on a hand posture database consisting of 600 images of 6 hand postures. It was shown that the performance of the aligned CSS descriptors is better than that of the Zernike and the pseudo-Zernike moment invariants representing the hand posture. The major drawback of the CSS image based approach is that the locations of the peaks are highly unstable making it difficult to adapt to user variances and perspective distortions induced by view-angle changes. The number of peaks representing the number of concave or convex segments are stable features and hence, CSS image might be useful only for classifying distinct hand signs. Also, two different shapes with the same sets of concavities will have the same CSS representations resulting in misclassification.

### 2.2.3 Modified Hausdorff distance based matching

The modified Hausdorff distance (MHD) based matching is a contour-based shape matching technique introduced by Dubuisson and Jain in [91]. The method employs the nearest point search strategy for computing the similarity between two shapes. The MHD is used for hand posture recognition in [92] and [93]. Let $A = \{\alpha_1, \alpha_2, \cdots, \alpha_{N_A}\}$ and $B = \{\beta_1, \beta_2, \cdots, \beta_{N_B}\}$ be the two point sets to be compared, where $N_A$ and $N_B$ represent the cardinality of the set $A$ and $B$ respectively.

Sánchez-Nielsen et al [92] used the $L_1$ norm and computed the bidirectional partial Hausdorff distance as

$$H = \max\{h(A,B), h(B,A)\} \tag{2.6}$$

where $h(A,B)$ is the directed distance between the point sets $A$ and $B$ and it is defined as

$$h(A,B) = {}^{i}K^{th}_{\alpha\in A} \|\alpha - \beta\|_1, \tag{2.7}$$

${}^{i}K^{th}_{\alpha\in A}$ represents the $K^{th}$ ranked distance such that $K/N_A = i\,\%$. The distance measure $H$ was used to classify a set of 26 static hand postures and the experiments show that the system achieved an average classification accuracy of 90%. The MHD based shape matching is a widely employed technique robust to outlier points and similarity transformations. However, the MHD technique is a point-wise correspondence based method and hence, it exhibits high computational complexity.

### 2.2.4 Fourier descriptors

Fourier descriptors are boundary based representations that are robust to noise and invariant to translation, scale and rotation changes. Given a shape boundary $\mathbb{B}$ of size $L$ and the points $(x,y) \in \mathbb{B}$, the Fourier descriptors are obtained through the Fourier transform on a complex vector derived from the coordinates $(x,y)$. For $u = \{0, 1, \cdots, L-1\}$, the complex co-ordinates characterizing the shape boundary are obtained as

$$f(u) = (x(u) - x_c) + i\,(y(u) - y_c) \tag{2.8}$$

where $(x_c, y_c)$ is the centroid of the shape. For $\omega = \frac{2\pi k}{L}$, $k = 0, 1, \cdots, L-1$, the Fourier transform of (2.8) is given by

$$F(\omega) = \sum_{u=0}^{L-1} f(u) \exp(-j\omega u) \tag{2.9}$$

The magnitude of $|F(\omega)|$ is known as the Fourier descriptor and it is invariant to rotation and translation changes. In order to achieve scale-invariance, the spectrum is normalised as

$$\left|\bar{F}(\omega)\right| = \frac{|F(\omega)|}{|F(0)|} \tag{2.10}$$

Chen et al [57] developed a system based on the Fourier descriptors and the hidden-Markov model (HMM) for classifying gestures in the Taiwanese sign language. The Fourier descriptors were used as features for representing the hand postures contained in the gesture sign. The Fourier descriptors along with the other temporal features were used to build the HMM model for gesture classification. In [94], the Fourier descriptors were used as features for user-adaptive hand posture classification. The Fourier descriptors were used to classify a database of 1600 samples of 9 hand postures. Similarly, Yang et al [95] developed a command system using hand posture as the user-interface element. The system employed the Fourier descriptors as features for classifying 4 hand posture signs that are used for specifying the commands in human-computer interaction. Bourennane and Fossati [96] have shown that the Fourier descriptors are efficient over region-based features like moments. They performed experiments on two different hand posture databases and the results confirm Fourier descriptors as efficient features for scale and rotation invariant hand posture classification.

The works on Fourier descriptor based hand posture recognition have considered only a few distinct hand postures and the performance of the Fourier descriptors in the case of more gesture classes, view-angle variations and user-independence needs to be evaluated.

### 2.2.5 Moments and moment invariants

Moments are region based descriptors in which all the pixels within a shape region are taken into account to obtain the shape representation [63, 97]. The moments extract statistical description of the pixels in the shape region [63]. The moment functions allow to derive moment invariants that are robust to geometrical transformations and less sensitive to shape defections [98].

Moments can be defined as the projection of a given function onto the polynomials that form the basis set [99]. The polynomials can be orthogonal or non-orthogonal. Accordingly, the moments are categorised as non-orthogonal moments and orthogonal moments [99]. The simple and the widely used non-orthogonal moments in hand posture description are the geometric moment invariants.

Consider $f(x, y)$ to represent a binary image of size $(N+1) \times (M+1)$ such that $x \in \{0, 1, \cdots, N\}$ and $y \in \{0, 1, \cdots, M\}$. The function $f(x, y)$ takes the unity value inside the shape region and otherwise it takes the zero value. The geometric moments of order $(n+m)$ representing the image is defined as

$$G_{nm} = \sum_{x=0}^{N} \sum_{y=0}^{M} x^n y^m f(x, y), \quad n, m = 0, 1, 2, \cdots \tag{2.11}$$

Using non-linear combinations of the lower order geometric moments, Hu [100] derived a set of moment invariants called as *geometric moment invariants* that are invariant under image scaling, translation and rotation. Previous works on shape classification [63] have shown that the geometric moment invariants are not sufficient for describing arbitrarily distorted contour-based shapes and perspectively transformed shapes. Hence, the geometric moment invariants are used along with other geometric properties for representing hand postures.

Chalechale et al [65] used geometric moment invariants and geometric properties (area, perimeter, major axis length, minor axis length and eccentricity) as features for representing 25 hand posture signs. The classification was based on Bayesian rule assuming Gaussian distribution for the extracted features. The descriptors were used to classify a database consisting of 2080 hand posture samples and achieved a classification accuracy of 98%. Similarly, in [101], the geometric moment invariants were combined with features like normalised length of the contour and directional gradients for representing hand postures. The classification was performed using weighted nearest neighbor-based classification scheme. The technique was tested on a database consisting of 700 samples of 3 hand postures acquired under various lighting conditions. Out of 700 samples 200 samples were used for testing and the technique achieved an average performance of 95%. Tofighi et al [102] derived geometric moment invariants from the shape boundary of the hand postures as feature descriptors. Along with the geometric moments, the convex points on the hand posture were also employed to form the feature vector. The classification was performed using the minimum distance classifier. The efficiency of the geometric moment was tested on a database of 500 samples of 10 gesture classes and their results reported an average classification rate of 90%.

The studies suggest that the geometric moment invariants are suitable for describing simple shapes and not sufficient to accurately describe large number of shapes. The basis functions of the geometric moments are correlated implying that these moment features are redundant [98]. Teague [103] suggested image representation through orthogonal moments that are derived from the orthogonal polynomials. The Zernike moments (ZMs) and the pseudo-Zernike moments (PZMs) are among the efficient orthogonal moments used for hand posture

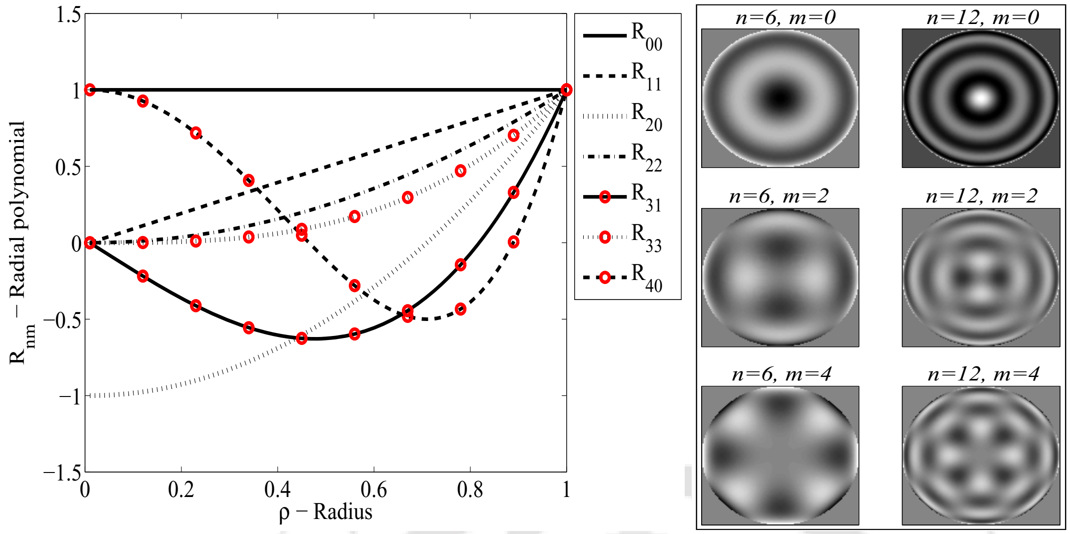


(a) (b)

**Figure 2.2:** (a) $1D$ Zernike radial polynomials $R_{nm}(\rho)$ and (b) $2D$ complex Zernike polynomials $V_{nm}(\rho, \theta)$ (real part).

representation. The ZMs and the PZMs are rotation invariant descriptors that are derived using the complex Zernike polynomials and pseudo-Zernike polynomials respectively as basis functions.

The ZMs and PZMs are defined on the polar coordinates $(\rho, \theta)$, such that $0 \leq \rho \leq 1$ and $0 \leq \theta \leq 2\pi$. The complex Zernike polynomial $V_{nm}(\rho, \theta)$ of order $n \geq 0$ and *repetition* $m$ is defined as [99]

$$V_{nm}(\rho, \theta) = R_{nm}(\rho)\exp(-jm\theta) \tag{2.12}$$

For even values of $n - |m|$ and $|m| \leq n$, $R_{nm}(\rho)$ is the real-valued radial polynomial given by

$$R_{nm}(\rho) = \sum_{s=0}^{(n-|m|)/2} \frac{(-1)^s (n-s)!\rho^{n-2s}}{s!((n+|m|)/2-s)!((n-|m|)/2-s)!}$$

The plots of the radial polynomials $R_{nm}(\rho)$ for different orders $n$ and repetition $m$ are given in Figure 2.2(a). The $2D$ complex Zernike polynomials $V_{nm}(\rho, \theta)$ obtained for different values of $n$ and $m$ are shown in Figure 2.2(b). From the plots, we can infer that the Zernike polynomials have wider supports. Therefore, the Zernike moments characterise the global shape features.

The complex Zernike polynomials satisfy the orthogonality property,

$$\int_0^{2\pi}\int_0^1 V^*_{nm}(\rho, \theta)\, V_{lk}(\rho, \theta)\, \rho\, d\rho\, d\theta \;=\; \frac{\pi}{n+1}\,\delta[n-l]\;\delta[m-k]$$

where $\delta[.]$ is the Kronecker delta function. The Zernike moment $Z_{nm}$ of order $n$ and repetition $m$ is given by

$$Z_{nm} = \frac{n+1}{\pi} \int_0^{2\pi} \int_0^{1} V_{nm}^{*}(\rho,\theta)\; f(\rho,\theta)\; \rho\; d\rho\, d\theta \tag{2.13}$$

where $|m| \leq n$ and $n - |m|$ is even.

The integration in (2.13) needs to be computed numerically. The magnitude $|Z_{nm}|$ is invariant to rotation and hence, used for rotation invariant gesture representation [66, 67].

The pseudo-Zernike basis polynomials exhibit properties similar to those of Zernike basis polynomials. The pseudo-Zernike basis polynomials differ only in terms of the radial polynomials. The radial basis of the pseudo-Zernike polynomials are real-valued functions and defined as

$$R_{nm}(\rho) = \sum_{s=0}^{(n-|m|)} \frac{(-1)^s (2n+1-s)! \rho^{n-2s}}{s!(n-|m|-s)!(n+|m|+1-s)!}$$

Chang et al [66] used the ZMs and the PZMs as combined features for hand posture classification. The experiments were performed on a database consisting of 600 hand postures of 6 gesture signs collected from 10 subjects. The ZMs and PZMs features representing the hand postures were classified using the nearest neighborhood classification technique and achieved a classification rate of 97.3%.

Gu and Su [67] have shown that the ZMs as efficient descriptors for view and user invariant representation of the hand postures. A hierarchial classifier based on the multivariate decision tree was employed for classifying the hand posture features. The database used for the experiment consisted of 3850 samples of 11 gesture signs. The images were acquired from 5 subjects and at 7 different viewing directions with the frontal view-angle varying between $-60^{\circ}$ to $60^{\circ}$. The results have shown that the ZMs are robust to large variations in the viewing angle and the user's hand shape.

### 2.2.6 Multi-fusion features

A few works in hand posture recognition have combined various contour and region based descriptors to derive multiple features for representing hand postures. In [104], the geometrical features like the location of the fingertips, convex and concave points of the fingers, area and the principal axes were combined with the geometric moments to form a feature vector for classification. Kelly et al [105] have derived features from the binary silhouette and the one dimensional boundary profile to represent the hand postures. The binary silhouette was represented using the geometric moments. The size functions were derived from the boundary profile to describe the hand shape. The dimensionality of the size functions was reduced using the principal component analysis. The reduced size functions are known as the *eigen space size functions*. The geometric moments and the eigen space size functions were combined to achieve user independent gesture recognition. In [106], the eigen features are extracted from the contour of the hand posture and is combined with the mean shape of the hand posture samples for finding the exact match.

Feng et al [107] have proposed a two-step feature extraction procedure in which the first and the second steps are known as the coarse location phase (CLP) and the refined location phase (RLP) respectively. In the CLP phase, the hand posture features like the convex and the concave points of the hand and the intersection of knuckle on different fingers were used for coarse representation. In the RLP phase, the features were derived from the multi-scale space representation of the hand postures. The multi-scale space representation characterises the blob, ridge, corner and edge features of the hand posture at different scales. The integration of these features were used for classifying 26 hand posture signs.

Yun et al [108] combined the geometric moment invariants and the colour cues derived from the hand posture regions to form a feature vector for the description of hand postures. These features were classified using the Euclidean distance based matching technique. The method was tested on a database consisting of 1000 samples of 10 hand posture signs acquired at different backgrounds. Using these multiple features, a classification accuracy of 91% was achieved.

## 2.3 Gray-level image based methods

The gray-level image based approaches use image features derived using the gray-level or the intensity values of the acquired hand posture image. The gray-level image based methods are also known as the appearance based approaches [109]. The hand postures are modeled based on these appearance features and used as predefined templates for classifying the test hand postures. These features characterise the image parameters such as the intensity distribution around a neighborhood and the edge characteristics of the hand postures. Similar to the silhouette image based methods, the efficiency of the gray-level image based methods is also evaluated in terms of retrieval efficiency, computational complexity and robustness to geometric and perspective distortions. In addition to these, the gray-level image based methods must also be robust to illumination variations that occur while acquisition. The various gray-level image based approaches used for hand posture analysis are discussed as follows.

### 2.3.1 Edge-based Features

The shape and the appearance of an object in an image can be represented by the local distribution of magnitudes and the orientations of the gradient image. A few descriptors for the hand posture are based on the edge maps. They are discussed as follows.

#### 2.3.1.1 Orientation histograms

Orientation histograms are edge based features that are derived from the edge map or the gradient map of the hand posture image. The orientation histogram represents summarised information on the orientations of the edges or the gradients constituting the hand posture image. The orientation histogram can be computed as a global feature or as a local feature.

Freeman [110] derived the orientation histogram from the intensity values of the hand posture image. The gradients were computed using two-tap derivative filters along the $x$ and the $y$ directions. If $I_x$ and $I_y$ are the outputs of the $x$ and the $y$ derivative operators, then the gradient direction is derived as $\tan^{-1}\left(\frac{I_y}{I_x}\right)$. The probability distribution of the gradient orientation gives the orientation histogram of the hand posture. The feature vectors were formed by the orientation histograms and classified using the nearest neighborhood classification. The experiments performed on a dataset of 10 different hand postures show that the orientation histograms are robust to illumination variations.

The orientation histograms computed from the local gradients were used as features and classified through Euclidean distance matching in [111]. Zhou et al [112] and Sha et al [113] derived the orientation histograms from the local gradient directions computed by dividing the image into over-lapping blocks of uniform size. The accumulated orientation histogram is known as the *histogram of oriented gradients*. Zhou et al [112] classified the histogram features using the $k-means$ clustering algorithm. In [113], the classification was performed by calculating the similarity between the histograms in terms of the Bhattacharyya coefficient.

Above studies on the orientation histogram features for hand posture description have shown that they are invariant to translation, scale and illumination changes. However, they are sensitive to rotation variations and a hand posture acquired at two different orientations yields different orientation histograms. Further, it is possible that two different hand postures exhibit similar orientation histograms and hence, it requires that the gesture vocabulary should have only gestures with distinct orientation characteristics. The studies in [110] show that the orientation histogram is sensitive to the perspective distortions.

#### 2.3.1.2 Hough transform

One of the simplest method for pattern analysis is the Hough transform that extracts and describes parametrically the important structural features such as the lines, circles and ellipses. Munib et al [114] developed a system based on the Hough transform and the neural networks for the recognition of hand postures in American sign language. The desired hand region was segmented from the background and the edge maps of the hand postures were derived using the Canny edge operator. The Hough features derived from the edge maps form the feature vector representing the hand posture. The feature vectors corresponding to each hand posture was classified using the feed-forward back propagation neural network. The dataset used for the experiment consisted of 330 samples of 20 hand posture signs. The hand postures were collected from 15 users at various scales and orientations. The scale invariance was achieved by fixing the scale of the hand posture to a predefined value through image interpolation. In order to achieve rotation invariance, the system was trained with samples taken at several orientations. The developed system achieved an average classification rate of 92%. Altun and Albayrak [115] employed the generalised Hough transform for classifying 29 classes of hand postures in the Turkish sign language. Instead of the edge maps, the interest regions were derived using the scale invariant feature transform (SIFT). Using the Hough transform, the system attained a classification rate of 93%. The main drawbacks of the Hough transform are its substantial computational and storage requirements that become acute when the object orientation and the scale have to be considered.

### 2.3.2 Image transform features

The image transforms map the image to the frequency domain or spatio-frequency domain. Common linear transformations used for image representation include the discrete Fourier transform (DFT), discrete Cosine transform (DCT), principal component analysis (PCA), linear discriminant analysis (LDA) and the wavelet transforms. Among these, the wavelet transforms are multi-resolution, spatio-frequency representations that extract the localised spatio-frequency features for image description.

#### 2.3.2.1 DCT features

AL-Rousan et al [116] developed a system for user-independent representation of 30 gesture signs in the Arabic sign language. The gesture signs in their experiments are composed of hand shapes and hand movements. The hand shapes were represented using the DCT features. The DCT features were combined with the hidden Markov modelling (HMMs) for classifying the gesture signs. The database consisted of 7860 samples collected from 18 users. The system achieved an overall high classification rate of 94.2%. The DCT features are only frequency localised and hence, the loss of spatial localization may limit the applicability of these features to large gesture classes.

#### 2.3.2.2 PCA and LDA based features

The PCA and the LDA are important multivariate data analysis methods used in pattern recognition. The LDA is also known as the Fisher's discriminant analysis method. The PCA finds a set of the most representative projection vectors such that the projected samples retain most information about original samples. The dimensionality of the projected samples is less than the dimensionality of the original samples yielding compact representations.

Consider a set of $I$ images $\{f_1, f_2, \cdots, f_I\}$ each of dimension $(N+1)\times(M+1)$. Assume that there are $P$ classes with $Q$ number of samples belonging to each class, such that $I = PQ$. The $2D$ images are represented as 1-dimensional vectors by concatenating the rows. Therefore, we get $I$ vectors of size $l = (N+1)(M+1)$ represented as $\{\boldsymbol{f}_1, \boldsymbol{f}_2, \cdots, \boldsymbol{f}_I\}$. The steps in PCA are as follows.

Step 1: Compute the mean centered image vectors $\overline{\boldsymbol{f}}_i$ by

$$\overline{\boldsymbol{f}}_i = \boldsymbol{f}_i - \frac{1}{I}\sum_{i=1}^{I}\boldsymbol{f}_i \tag{2.14}$$

Step 2: Find the eigen vectors and the eigen values of the covariance matrix

$$R = \frac{1}{I}\sum_{i=1}^{I}\overline{\boldsymbol{f}}_i\overline{\boldsymbol{f}}_i^T \tag{2.15}$$

The eigenvectors $\{e_1, e_2, \cdots, e_k\}$ corresponding to the $k$ largest eigenvalues $\{\lambda_1, \lambda_2, \cdots, \lambda_k\}$ of $R$ form a transformation matrix

$$W_{pca} = [e_1 \;\; e_2 \;\; e_3 \;\; \ldots \;\; e_k], \tag{2.16}$$

for $k << l$. The matrix $W_{pca}$ forms the orthonormal basis that projects each $l-$ dimensional vector $\boldsymbol{f_i}$ in the original space to an $k-$ dimensional vector $\boldsymbol{g_i}$ defined as

$$\boldsymbol{g}_i = W_{pca}^T\boldsymbol{f}_i \tag{2.17}$$

The $k$ largest eigenvalues $\{\lambda_1, \lambda_2, \cdots, \lambda_k\}$ are known as the principal components and the corresponding eigenvectors $\{e_1, e_2, \cdots, e_k\}$ are known as the eigenimages. The subspace spanned by the eigenvectors is known as the eigenspace. Each eigenimage forms the feature descriptor for image classification. The classification is performed by finding a match that minimises the Euclidean distance between the input image projected in to the eigenspace and an image class represented in the eigenspace.

Unlike the PCA, the LDA uses the class information and finds a set of vectors that maximise the between-class scatter while minimizing the within-class scatter of the original samples. In the LDA technique, the projection vector is selected in such a way that the ratio of the between-class scatter and the within-class scatter is maximised.

Consider a set of $I$ image vectors $\{\boldsymbol{f}_1, \boldsymbol{f}_2, \cdots, \boldsymbol{f}_I\}$ with $I = PQ$. For notational convenience, let us label the image vectors in terms of the image class and rewrite $\{\boldsymbol{f}_1, \cdots, \boldsymbol{f}_I\}$ as $\{\boldsymbol{f}_{11}, \cdots, \boldsymbol{f}_{1Q}, \cdots, \boldsymbol{f}_{P1}, \cdots, \boldsymbol{f}_{PQ}\}$. The steps involved in the LDA are summarised as follows.

Step 1: For $p \in \{1, 2, \cdots, P\}$ and $q \in \{1, 2, \cdots, Q\}$ , compute the mean image vectors for each image class by

$$\boldsymbol{f}_{mean}^{p} = \frac{1}{Q}\sum_{q=1}^{Q} \boldsymbol{f}_{pq} \tag{2.18}$$

Compute the global mean image vector $\boldsymbol{f}_{mean}$ through

$$\boldsymbol{f}_{mean} = \frac{1}{P}\sum_{p=1}^{P} \boldsymbol{f}_{mean}^{p} \tag{2.19}$$

Step 2: Compute the between-class scatter matrix ($\boldsymbol{S}_b$) and the within-class scatter matrix ($\boldsymbol{S}_w$) as

$$\boldsymbol{S}_b = \sum_{p=1}^{P} pr(p)\left(\boldsymbol{f}_{mean}^{p} - \boldsymbol{f}_{mean}\right)\left(\boldsymbol{f}_{mean}^{p} - \boldsymbol{f}_{mean}\right)^T \tag{2.20}$$

$$\boldsymbol{S}_w = \sum_{p=1}^{P} pr(p)\sum_{q=1}^{Q}\left(\boldsymbol{f}_{pq} - \boldsymbol{f}_{mean}^{p}\right)\left(\boldsymbol{f}_{pq} - \boldsymbol{f}_{mean}^{p}\right)^T \tag{2.21}$$

respectively. $pr(p)$ denotes the probability of the image class $p$.

Step 3: Compute the transformation matrix $\boldsymbol{W}_{lda}$ such that it maximises the class separability with regard to a chosen separability criterion. One of the most widely used discriminant criteria is given by

$$W_{lda} = \underset{W}{argmax}\frac{\left|W^T\boldsymbol{S}_bW\right|}{\left|W^T\boldsymbol{S}_wW\right|} \tag{2.22}$$

If $\boldsymbol{S}_w$ is non-singular, $\boldsymbol{W}_{lda}$ is formed by the $k$ eigenvectors $\{\overline{e}_1, \overline{e}_2, \cdots, \overline{e}_k\}$ of the matrix $(\boldsymbol{S}_w)^{-1}\boldsymbol{S}_b$ corresponding to the $k$ largest eigenvalues $\left\{\overline{\lambda}_1, \overline{\lambda}_2, \cdots, \overline{\lambda}_k\right\}$. However, if $\boldsymbol{S}_w$ is singular, $\boldsymbol{W}_{lda}$ is computed by first projecting the images in to a lower dimensional space through PCA so that $\boldsymbol{S}_w$ is non-singular. Then, the standard definition in (2.21) is applied to the reduced data set. Accordingly, the transformation matrix is defined as [117]

$$W_{lda}^T = W_{fld}^T W_{pca}^T \tag{2.23}$$

where

$$W_{fld} = \underset{W}{argmax} \frac{\left| W^T W_{pca}^T \boldsymbol{S}_b W_{pca} W \right|}{\left| W^T W_{pca}^T \boldsymbol{S}_w W_{pca} W \right|} \tag{2.24}$$

The projected image vectors $g_{pq}$ are obtained using the following linear transformation.

$$\boldsymbol{g}_{pq} = W_{lda}^T \boldsymbol{f}_{pq} \tag{2.25}$$

In the case of LDA, the upper bound on $k$ is $P - 1$, where $P$ is the number of classes. The classification is performed by computing the minimum distance between the projected image vectors.

The efficiency PCA and the LDA methods is widely studied in the field of face recognition. The comparative studies show that the PCA and the LDA features are robust under varying view-angle, illumination changes and other variations [118, 119].

A few works on hand posture recognition based on the PCA have been reported in [120–123]. The gray-values of the segmented hand posture regions constitute the desired input for PCA based classification. Birk et al [121] combined PCA based description with the Bayes classifier for classifying 25 hand signs in the American sign language. The segmented gray-level images were normalised for geometric transformations during the preprocessing stage. The database used for the experiment consisted of 2500 samples of 25 hand postures. The results demonstrated an over-all recognition rate of 99% on a test database containing 1500 images. Dardas and Petriu [123] developed a robust hand posture classification system using the PCA features derived from hand posture images with different scales, orientations and illumination variations. The features were used to classify 4000 samples of 4 gesture signs acquired at various scales, orientations and illumination conditions. The system achieved an average recognition rate of 93%.

The LDA based features were employed for hand posture analysis in [124–127]. The performance of the PCA and the LDA features in hand posture classification is studied in detail in [124, 125]. The hand postures were segmented from the background and the intensity maps in the posture segment are used as the input. The gesture signs used in their experiment were dynamic gestures in which the hand posture changes with time. The system was trained with 504 samples of 28 gesture signs acquired at varying illumination. Similarly, the test dataset consisted of 540 samples of 28 gesture signs. The performance of the LDA features were shown to be superior to the PCA based classification method. Deng and Tsui [127] investigated the performance of the LDA features in classifying 100 hand gesture signs taken from the American sign language. The dimensionality of the dataset was initially reduced through the PCA and the discriminant features were derived from the reduced dataset as defined in (2.25). They combined the LDA features with the HMM classifier and achieved a classification accuracy of 93.5%. In [126], LDA was employed to classify the hand posture signs in the Japanese sign language. The LDA features representing the hand postures were classified through the $K$-means clustering method. The system achieved an average recognition accuracy of 98% on the samples of 41 hand posture signs taken from 4 subjects.

From the above studies we can infer that the PCA and the LDA techniques provide potential features for classifying large classes of hand postures and results in dimensionality reduction offering efficient compact representations and better discriminations. However, more research is required to examine the performance of these multivariate data analysis methods in the presence of view-angle distortions and user-variations.

#### 2.3.2.3 Wavelet transform based descriptors

The wavelet transforms using the Gabor basis functions offer spatio-frequency representations that overcome the limitations of the frequency localised features. The Gabor wavelets are multi-scale and multi-orientation representations that allow to derive the image features at different scales and orientations. Gabor wavelets are derived by sinusoidally modulating Gaussian functions of different scales and orientations. Let $P$ be the maximum number of scales and $Q$ be the maximum number of orientations such that $p \in \{0, 1, \cdots, P-1\}$ and $q \in \{0, 1, \cdots, Q-1\}$. The Gabor wavelets $G_{\vartheta,\theta}$ are defined as [4]

$$G_{\vartheta,\theta}(x, y) = \frac{U_{\vartheta}^2}{\sigma^2} \exp\left(\frac{-U_{\vartheta}^2}{2\sigma^2}\left(x^2 + y^2\right)\right)\left[\exp\left(iU_{\vartheta}\left(x\cos\theta + y\sin\theta\right)\right) - \exp\left(-\frac{\sigma^2}{2}\right)\right] \tag{2.26}$$

where the radial $U_{\vartheta}$ and the orientation $\theta$ are given by

$$U_{\vartheta} = \frac{\omega_{\max}}{(\Delta f)^{\vartheta}} \quad \text{and} \quad \theta = \frac{\pi q}{Q}$$

respectively. In the above, $\omega_{max}$ is the centre frequency of the highest band and $\Delta f$ is the spacing factor between the kernels in the frequency domain. Figure 2.3 shows the plot of real part of the Gabor kernels for $P = 4$ and $Q = 8$.

Amin and Yan [128] used Gabor wavelet transforms as feature descriptors for the classification of hand posture signs in the American sign language. The desired hand region was segmented from the background and normalised for scale, translation and orientation changes. The intensity values of the segmented hand posture region was normalised for illumination variations. The normalised hand posture image was convolved with Gabor kernels of 5 different scales and 8 different orientations. Thus, the obtained 40 filter responses form the feature vector for each hand posture image. The dimensionality of the feature vector was reduced using the

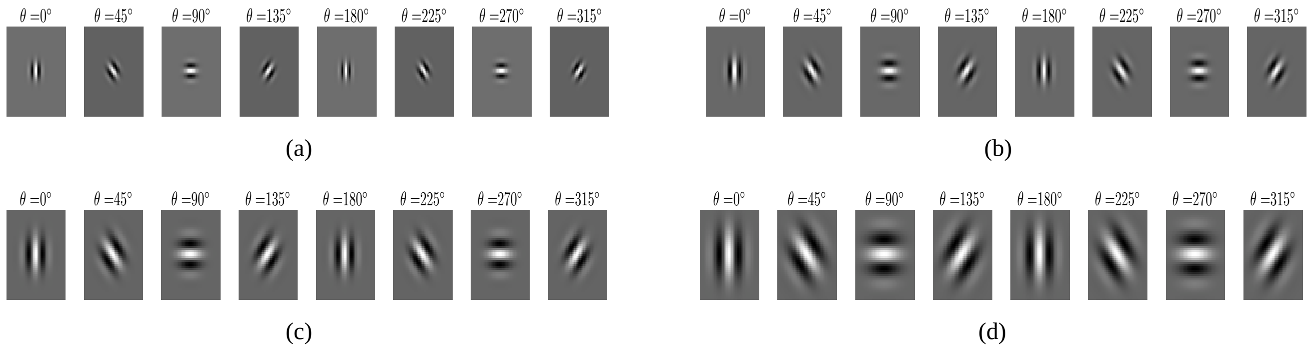


**Figure 2.3:** Plots of the real part of the Gabor wavelet kernels $G_{\vartheta,\theta}$ obtained at 4 scales ($P = 4$) and 8 orientations ($Q = 8$). The parameters are chosen as $\sigma = \pi$, $\omega_{\max} = \frac{\pi}{2}$ and $\Delta f = \sqrt{2}$ [4].

PCA method. The reduced feature set was classified using the fuzzy C-means classifier. The experiment was performed on a database consists of 3432 images of 26 hand posture signs performed by 11 persons. Among these 572 images were used for testing and the method achieved an average classification rate of 93.23%. In [129], a similar technique combining the Gabor-PCA features with neural network based classifier was employed for the recognition of hand posture signs in the Ethiopian sign language.

Huang et al [130] derived the Gabor-PCA features from the binary silhouette of the hand postures and used support vector machines for the classification stage. The rotation variations of the hand postures were normalised based on the Gabor wavelet responses. The orientation at which the Gabor wavelet response exhibits maximum energy was shown to be the orientation of the hand posture. Using the estimated angle values, the orientation of the hand postures were aligned to a fixed degree. The Gabor feature vectors were then derived from the rotation normalised images and the dimensionality of the feature vector was reduced using PCA. The gesture dataset used in the experiment consisted of 1320 samples of 11 gestures performed by 10 people. Among these, 660 samples were used for testing and the recognition rate achieved was 96.1%.

The wavelet features derived using the Haar bases were used for recognizing the hand postures in the Persian sign language [131]. The Haar wavelet transform was applied on the segmented gray-level images containing the hand posture and the higher-scale transform coefficients were used as the feature descriptors. The extracted features were used to train a multi-layered perceptron neural network. The technique was implemented and tested on a data set of 640 samples of 32 hand postures among which 224 samples were used for testing. The experimental results show that the technique offers an average classification accuracy of 94.06%.

From the above studies, we infer that the wavelet transforms are successfully employed for classifying large number of posture classes. However, the performance of the wavelet features in representing the hand shapes that are distorted due to view-angle variations and user dependencies is yet to be explored.

### 2.3.3 Elastic Graph matching

Elastic graph matching is an image matching problem in which the images are represented by the graph structures. Given a model image, a regular or an irregular grid is superimposed and the image features computed at the intersections of the grid lines used as the feature descriptors [132]. During the classification phase, an isomorphic grid is superimposed on the test image, and then deformed in order to have the best matching between the features computed at the sample grid points of the model image.

Triesch et al [2, 133] employed elastic graph matching to develop a system for user-independent classification of hand postures against a complex background. The system does not require a separate segmentation stage and is robust to various background conditions. The structural information of the hand postures was represented by a graph composed of irregular grid. The grid intersections are the graph nodes and the lines connecting the grids constitute the edges. The edges were labeled with a distance vector and the nodes were labeled with local image descriptions derived from the Gabor wavelet responses of the hand posture. The Gabor wavelet responses were obtained at three different scales and eight orientations. Thus, there were 24 feature descriptors representing each node and they were used for classifying the hand postures.

The developed system was tested on a dataset consisting of 10 hand postures performed by 24 persons against different types of backgrounds. The system reached 86.2% correct classification for 239 test samples of 10 postures. The experimental results showed that the elastic graph matching technique is robust to background changes and is user-independent. The major drawbacks of the system are the high computational complexity and the sensitivity to geometric distortions induced due to view-angle variation. Further, the nodes in the model graph are required to be constructed manually.

### 2.3.4 Local spatial pattern analysis

Local spatial pattern analysis involves analyzing the local structural properties at each pixel of the image. The local spatial patterns derived encode the structural information like the oriented edges and the curvature points within a local region of the image. The local structural information are accumulated as feature descriptors for classification. Some of the local spatial pattern analysis methods employed in hand posture classification include local binary patterns, modified Census transform and Haar-like feature descriptors and scale invariant feature transforms (SIFTs).

#### 2.3.4.1 Local binary patterns

Local binary patterns (LBP) are illumination invariant descriptors that characterise the local spatial patterns at each pixel of the image. The descriptors are derived from the gray-values of the pixels and they involve labelling each pixel value in terms of the radiometric distance between the pixels in the neighbourhood. Given a pixel $f(x, y)$, let $g(k), k = 1, 2, \cdots, m^2 - 1$ denote the intensity values of the pixels in a $m \times m$ neighborhood of $f(x, y)$, excluding $(x, y)$. Then, the LBP descriptor is derived as follows

$$LBP(x, y) = \sum_{k=1}^{m^2-1} T(g(k) - f(x, y))2^{k-1} \tag{2.27}$$

where $T(.)$ is the thresholding operator given by

$$T(c) = \begin{cases} 1 & c > threshold \\ 0 & other\ wise \end{cases} \tag{2.28}$$

Ding et al [134] employed the LBP descriptors for representing a class of 12 hand postures. The threshold was chosen based on the minimum and the maximum difference values of $g(k)$. The experiment was performed on a database consisting of 600 samples and the Adaboost classifier [135] was employed for classifying the LBP descriptors. It was shown that the LBP descriptors are robust to scale changes and non-linear illumination conditions.

#### 2.3.4.2 Modified census transform

Similar to the local binary pattern, the modified census transform (MCT) is also local spatial pattern descriptor proposed in [136] for face recognition. The MCT is similar to the LBP descriptor except that in MCT the pixel differences are computed with respect to the mean intensity value within the considered neighborhood. Accordingly, the MCT is defined as

$$MCT(x, y) = \underset{k=1}{\overset{m^2-1}{\otimes}} T\left(g(k) - \overline{f}(x, y)\right) \tag{2.29}$$

where $\overline{f}(x, y)$ is the mean intensity of the pixel at $(x, y)$ computed with respect to its neighborhood and $\otimes$ denotes the concatenation operation. The thresholding operator $T(.)$ is given by

$$T(c) = \begin{cases} 1 & c > \overline{f}(x, y) \\ 0 & other\ wise \end{cases} \tag{2.30}$$

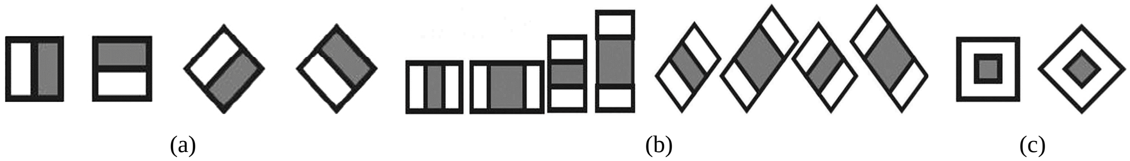


**Figure 2.4:** Haar-like rectangular kernels used for feature extraction. The rectangular kernels are capable of extracting (a) Edge features; (b) Line features and (c) Center-surround features.

The MCT value corresponding to each pixel is a binary string of $\left(m^2 - 1\right)$ bits. The MCT values are used as the local feature descriptors and classified through the Adaboost classification scheme. Just et al [137] computed the MCT features for classifying hand postures against a complex background. The efficiency of the technique was verified on the Jochen Triesch database reported in [133]. Similar to the elastic graph matching method, the MCT technique does not require segmentation and is capable of recognizing the hand postures under illumination variations and different background conditions. The major drawback of the method is its sensitivity to the scale, translation and the rotation variations. The technique depends on the choice of the neighborhood window size and hence, more experiments are required in order to evaluate the influence of the neighborhood size.

#### 2.3.4.3 Haar-like features

The Haar-like feature descriptors combined with the Adaboost classification scheme were proposed by Viola and Jones for real-time face detection [138]. The Haar-like features are robust to noise and illumination variations. The kernels used for computing the Haar-like features are shown in Figure 2.4. The features can be derived by convolving the image with these kernels. Since the convolution with several kernels is computationally demanding, the concept of *integral image* was introduced in [138] for computing the kernel responses. Using the technique in [138], several works have been done for illumination invariant hand posture classification [139–141].

Wachs et al [139] used the Haar-like features for fuzzy c-means clustering based classification of three distinct hand posture signs. Chen et al [140] and Tran et al [141] employed Haar-like features and the Adaboost classifier for recognizing a class of 4 hand posture signs. In [140], the experiments were performed on a database of 450 samples for each posture that were acquired at different scales. Among these, 100 samples were used for testing and an average classification accuracy of 97% was achieved. In [141], the hand region was obtained through skin colour detection and the Haar-like features were derived with respect to the detected hand region. The database used in their experiments was composed of an average of 1000 samples per hand posture acquired at varying illumination. The experiments in [140, 141] involved studying the efficiency of the Haar-like features in classifying hand postures against varying background and illumination changes. The Haar-like features are found to be sensitive to rotation variations.

The above techniques based on the local spatial pattern analysis are shown to be efficient for illumination changes and robust to complex backgrounds. Particularly, the LBP and the MCT methods do not require a separate segmentation stage and hence are effective for real-time hand posture recognition based systems. Despite its robustness, the training phase is very demanding and it requires large number of training samples including the samples of the background images in order to reduce the false classification rate. The performance of these techniques also depends on the efficiency of the classifier and hence it requires to combine more complex classifiers in a cascaded structure for achieving high recognition rate.

#### 2.3.4.4 Scale invariant feature transform

The scale invariant feature transform (SIFT) is an efficient image descriptor developed by Lowe [142]. The SIFT is robust under translation, scaling, rotation and intensity variations. The basic idea in SIFT is to describe the local image features in terms of key points that are invariant to geometrical transformations. The scale-invariant key features are identified using the multi-scale representation of the image derived by convolving the image with Gaussian functions of different variances.

Given an image $f(x,y)$ and the Gaussian function $g(x,y,\sigma)$ of standard deviation $\sigma$, the corresponding scale space images $F_{\sigma}(x,y)$ for multi-scale representation are derived as

$$F_{\sigma}(x,y) = g(x,y,\sigma) * f(x,y) \tag{2.31}$$

where

$$g(x,y,\sigma) = \frac{1}{2\pi\sigma^2} \exp\left(\frac{-\left(x^2+y^2\right)}{2\sigma^2}\right) \tag{2.32}$$

and $*$ is the convolution operation. At each up scale, the standard deviation $\sigma$ is varied by a constant multiplicative factor $k$. The key points for feature description are detected from the extrema points in the multi-scale representation. The extrema points are obtained by computing the difference-of-Gaussian (DOG) images $D_{\sigma}(x,y)$ given by [143]

$$D_{\sigma}(x,y) = F_{k\sigma}(x,y) - F_{\sigma}(x,y) \tag{2.33}$$

Using (2.31), $D_\sigma(x, y)$ can be rewritten as

$$D_\sigma(x, y) = (g(x, y, k\sigma) - g(x, y, \sigma)) * f(x, y) \tag{2.34}$$

Accordingly, the difference between the scale-space images at a scale $i$ can be written as

$$D_\sigma^i(x, y) = \left(g\left(x, y, k^{i+1}\sigma\right) - g\left(x, y, k^i\sigma\right)\right) * f(x, y) \tag{2.35}$$

The local maxima and the minima points in the difference image $D_\sigma^i(x, y)$ are determined by comparing the magnitude of the pixels in $D_\sigma^i(x, y)$ with respect to its 8-neighbors in the current scale $i$ and 9-neighbors in the adjacent scales $\{i-1, i+1\}$. The unstable extrema points are identified and eliminated using the ratio of principal of curvature s along the scales. The resultants are the keypoints used for image description. The SIFT descriptors are obtained from the local gradient magnitude and orientation characteristics of the image pixels that lie around the neighborhood of the detected keypoints.

The SIFT features were classified using the Adaboost classifier for view-angle independent hand posture recognition in [144]. The experiments demonstrated the performance of the SIFT feature in recognizing three hand posture classes and the average classification rate obtained was 95.6%. The results have shown that the SIFT features are robust to background noise issues, rotation changes and achieve satisfactory multi-view hand detection.

Though the SIFT features are very robust, the main drawbacks are that the computational complexity of the algorithm increases rapidly with the number of keypoints and the dimensionality of the SIFT descriptors is high.

### 2.3.5 Local linear embedding

Local linear embedding (LLE) is a non-linear multivariate data analysis method. LLE maps the high dimensional data to a low dimensional space that preserves the relationship between the local neighborhood pixels. The LLE algorithm consists of three different steps. The first step selects a number of nearest neighbors of each data pixel based on the Euclidean distance. The second step computes the the optimal reconstruction weights for each pixel within the neighborhood. The optimal weights are obtained from the covariance matrix computed within the considered neighborhood. The third step performs the embedding by preserving the local geometry represented by the reconstruction weights. The embedded matrix is constructed from the largest eigenvectors of the reconstruction weights.

Teng et al [62] and Ge et al [145] developed hand posture recognition systems based on LLE. The hand posture regions were segmented from the background and normalised for scale changes. The LLE features were derived from the normalised gray-level images of the hand posture. In [62], the experiments were performed on a dataset consisting of 4125 images of 30 hand postures in the Chinese sign language. Among these, 2475 samples were used for training and 1650 samples for testing. The results obtained show an average classification accuracy of 92.2%. Ge et al [145] combined LLE features with probabilistic neural networks for classifying 280 samples of 14 hand postures. The system was trained with 1120 samples and high recognition rate of 93.2% was achieved. Despite the recognition rate, the LLE technique is scale and rotation variant. It is also sensitive to structural variations in the hand posture images that occur due to boundary distortions. The efficiency of LLE is controlled by the number of neighbors of each data point and involves several computations.

## 2.4 Summary and conclusion

In this chapter, existing hand posture representation techniques have been reviewed. The feature extraction methods are broadly classified in to two classes: silhouette image based methods and gray-level image based methods. The silhouette image based methods can be further divided as boundary based and region based techniques. The gray-level image based methods use the edge maps or the intensity values for feature extraction.

The silhouette image based methods are simple, robust and fast to compute. Hence, they are preferred in real-time systems for hand posture classification. The contour based features of the hand posture silhouettes are compact representations and they can be easily made robust to scale, translation and orientation changes. Among the contour based techniques, the Fourier descriptors are robust to similarity transformations and shape distortions. Basically, the important primitives characterised by the contour based features are the number of extended fingers. In practical applications, this primitives may not sufficiently represent a large posture class. Hence, the contour based features have shown high classification accuracy only in handling hand postures with distinct shape boundaries. The CSS images are efficient boundary representations in which the multi-scale evolution of the contour can be used for classifying large posture classes. But, the limitation is due to the sensitivity of the CSS technique even to small variations in the shape boundary. The number of concave points detected at each scale is not stable and hence, it is difficult to achieve view and user independent representations of large posture classes. The above limitations can be overcome by using region based features. Region based features are more robust than contour features as they use the entire shape information for representation. However, the region based features are not necessarily more complex than contour based methods. The Zernike moments are the promising region based features that are successfully employed for view and user invariant hand posture classification. The implementation of the Zernike moments are simple and they provide compact representation of the images. The moments are in general robust to noise and can cope well with shape defections.

Compared with the silhouette image based approaches, the gray-level image based methods are too complex to implement and some methods like Haar-like features, Gabor wavelet transform and SIFT are over-complete representations. Hence, these methods require feature selection techniques and more efficient matching algorithms for accurate retrieval. Also, since the methods are based on the intensity values, it is required that they are invariant to illumination changes. The gray-level image based methods mostly characterise the shape information in terms of primitives such as the orientation of the edge structures and the radiometric similarity between the pixels within a neighborhood. Therefore, these methods are extremely useful in dealing with large posture classes. Another important advantage is that the gray-level image based methods are comparatively more robust in partial matching. From the review, it can be inferred that the some of the gray-level image based methods are robust to the background conditions and hence, the system based on those methods does not require a segmentation stage. Though this can be seen an important advantage over the silhouette image based systems, the overload appears in the training stage. In order to achieve robustness against background changes, the system also requires to be trained with several samples of background images. Such methods require complex algorithms to achieve invariance to geometrical transformations. The multivariate data analysis methods that include the PCA and the LDA are efficient techniques and can handle large variations between the hand postures. Compared with other gray-level image based approaches, the PCA and the LDA features are compact representations and also offer accurate retrieval efficiency.

In summary, gray-level image based methods are useful in classifying large posture classes and they are useful in locating the hand postures in an image or sub-image matching. The silhouette image based methods ignore the internal contours and hence, their applicability is limited to a moderate posture library. However, applications that use hand postures as user-interface entities and data cues can be efficiently realised with silhouette image based approaches. Hence, the choice between the silhouette and the gray-level image based methods is clearly limited to the demand of the application. Therefore, deriving features from the silhouettes are advantageous in terms of the computational requirements, compact representation and robust retrieval efficiency. It should also be noted that some of the techniques like the Gabor wavelet transform and the PCA that are discussed under gray-level image based approaches can also be used for deriving features from the silhouette image. In terms of the compact representation and robustness to shape distortions, the review shows that the Fourier descriptors, the Zernike moments and the PCA and the LDA are the best choices. The Fourier descriptors have offered good retrieval efficiency in classifying samples belonging to a small posture class. Some of the works in shape retrieval show the Fourier descriptors to be efficient for classifying large shape classes. Hence, it is required to study the efficiency of the Fourier descriptors in representing large hand posture classes. The performance of the Zernike moments has been tested and they are shown to be robust for view-angle and user invariant hand posture representations. Though, the efficiency of the PCA in view and user invariant classification is yet to be studied, the success of these techniques in the field of face recognition promises them to be robust to view-and user variations. Similarly, the Gabor wavelets also offer high classification accuracy. But the Gabor wavelets are over-complete representations and hence, the dimensionality of the feature vectors is more than the dimensionality of the original image.

We infer that the Zernike moments, the Gabor wavelets and the PCA based techniques as efficient methods in terms of retrieval efficiency. Despite these advantages, these techniques also have certain limitations. The Zernike moments are derived from the continuous orthogonal polynomials. For computation, the Zernike moments have to be approximated in the discrete domain and the discretization error increases for higher orders. As a result, the choice of the order of the Zernike moments for accurate representation is limited due to the numerical errors at higher orders. Though the PCA method offer best compact representations, the complexity involved in computing the covariance values and the computation of eigen vectors is high and increases with the increase in the size of the database.

Recently the discrete orthogonal moments like the discrete Tchebichef moments and the Krawtchouk moments were introduced for image analysis [71, 72]. It is shown that these moments are compact representations and provide higher approximation accuracy than the existing moment based representations. The discrete orthogonal moments are derived from the discrete orthogonal polynomials defined in the image coordinate space. Hence, the computation of the discrete orthogonal moments does not involve any numerical approximation and they offer higher representation accuracy with the increase in the order. A few works in image retrieval show that they are potential features for pattern classification [71, 72, 146]. Our subsequent research works concentrate on applying the discrete orthogonal moments for hand posture classification.

# 3

# A Study on the Characteristics of Discrete Orthogonal Moments for Shape Representation

**Contents**

Discrete orthogonal moments derived from discrete orthogonal polynomials are efficient tools for image analysis. This chapter empirically studies the characteristics of two discrete orthogonal moments, namely the Krawtchouk and the discrete Tchebichef moments for representing shapes. The analysis is performed in terms of the shape reconstruction and shape classification accuracies. The study includes exploring the band-pass filter like characteristics of the discrete orthogonal moments. Particularly, the Krawtchouk polynomials are shown as quadrature mirror functions exhibiting a wavelet like property. Based on these studies, the applicability of the discrete orthogonal moments to hand posture recognition is validated.

## 3.1 Introduction

Image understanding through digital image processing is an elementary step in developing computer vision based techniques for applications like content-based image retrieval, character recognition and gesture recognition. Image understanding involves recognizing objects that constitute the image content [76]. It can be considered as an object recognition problem that relies on the visual features such as the colour, the texture and the shape of the objects. Among these features, the shape is an important visual feature and it has been successfully used as a cue in various applications that involve object recognition [63].

The shape of an object is a binary image representing the extent of the object and it can be thought as the silhouette of the object [76]. The procedure for recognizing the shape of a given object requires to derive parameters that uniquely characterise the object's shape. This step is known as the feature extraction or shape description and the features are known as the shape descriptors [76].

The methods for representing and describing the shapes are broadly classified into the *contour based* and the *region based* methods [63]. Moment-based shape description is one of the popular region based methods and widely used for object recognition [63, 97]. The major advantage of the moment based representation is the compactness due to which the amount of data needed for storage and/or analysis is reduced. The moments explored widely in object recognition are the geometric moments. However, the geometric moments are nonorthogonal and so image reconstruction from the geometric moments is an intricate task. Teague [103] suggested image representation through orthogonal moments that are derived from the orthogonal polynomials.

Teague [103] introduced two classes of orthogonal moments, namely, the Legendre moments derived from the Legendre polynomials and the Zernike moments derived from the Zernike polynomials as features for image analysis. These polynomials are continuous functions that form a complete orthogonal basis set on the unit circle. The feature representation capability of the Zernike moments is shown to be superior to those of the geometric and the Legendre moments [147]. Also, the Zernike moments are less sensitive to noise and rotation invariant [99, 147]. Therefore, the Zernike moments are extensively used in object classification [77], optical character recognition [148], face recognition [149] and hand gesture recognition [66].

Despite their advantages, the reconstruction error of the Zernike moments increases due to the numerical instability that arises with the approximation of the continuous Zernike polynomials in the discrete domain [99]. This led to the evolution of discrete orthogonal moments (DOMs) for image analysis. The discrete orthogonal moments derived from the discrete orthogonal polynomials (DOPs) are advantageous in the absence of discretization errors and for the high reconstruction accuracy. The DOPs are defined in the image domain itself and hence, do not require coordinate transformation as in the case of Legendre and Zernike polynomials. Some of the DOPs explored for image analysis are the discrete Tchebichef polynomials [71], Krawtchouk polynomials [72], Hahn polynomials [150, 151] and the Racah polynomials [152]. The moments derived using the Krawtchouk polynomials act as local descriptors such that the moments of a particular order emphasise only the features within a certain region of the image [72, 153]. Conversely, the discrete Tchebichef moments are global descriptors in which the features are extracted from the image as a whole. Yap et al [151] have shown that the discrete Hahn polynomials are the generalization of the discrete Tchebichef and the Krawtchouk polynomials. Zhu et al [152], in their study on image analysis using the Racah moments have shown that the reconstruction accuracy of the Racah moments depends on the proper choice of parameters and exhibits almost similar characteristics as the Krawtchouk moments. It is also shown that the Krawtchouk moments are more robust to noise than the discrete Tchebichef and the Racah moments.

From the previous works, we can infer that the Krawtchouk and the discrete Tchebichef moments are unique with diverse properties in terms of global and local feature descriptions. The invariants of the discrete Tchebichef and the Krawtchouk moments that are robust to rotation, scale and translation changes have been derived in [71] and [72]. However, the efficiency of those Krawtchouk and the discrete Tchebichef moment invariants is yet to be well explored. Similarly, a few studies have concentrated on analyzing the energy compaction ability of the DOPs [153]. The characteristics of these DOPs in representing the binary shapes and their responses to the structural variations need to be explored.

This chapter empirically analyses the accuracy of the Krawtchouk moments and the discrete Tchebichef moments in representing binary shapes with different structural variations. It presents the formulations, the spatial and the frequency domain properties of the Krawtchouk and the discrete Tchebichef polynomials. The behaviour of these DOPs in shape approximation is explained in terms of their frequency domain characteristics. It is experimentally shown that the Krawtchouk polynomials and the discrete Tchebichef polynomials of different orders act as band-pass functions. Experiments are performed to analyse the relation between the structural characteristics of the shape and the accuracy of the DOP based approximations. The experiments also include a study on the reconstruction accuracy of the orthogonal moments in the presence of noise.

## 3.2 Theory of discrete orthogonal polynomials

This section outlines the theory of discrete orthogonal polynomials. The details are available in [154–158]. The analysis here is based on the excellent text in [158].

Consider a set of non-negative numbers $\{w(x) \,|\, x \in \mathrm{Z}\}$, where Z is the set of integers. Let $\psi$ and $\phi$ be real functions defined on Z with the corresponding inner product

$$\langle \psi, \phi \rangle = \sum_{x=-\infty}^{\infty} \psi(x)\, \phi(x)\, w(x) \tag{3.1}$$

The functions $\psi(x)$ and $\phi(x)$ are called orthogonal with respect to the weight $w(x)$ if

$$\langle \psi, \phi \rangle = \begin{cases} 0 \;;\; \psi \neq \phi \\ \|\psi\|_w^2 \;;\; \psi = \phi \end{cases} \tag{3.2}$$

where, $\|\psi\|_w = \left( \sum\limits_{x=-\infty}^{\infty} \psi^2(x)\, w(x) \right)^{1/2}$ is the norm induced by the inner product. The weight $w(x)$ is normalised such that $\sum\limits_{x=-\infty}^{\infty} w(x) = 1$. The set of all such functions on Z with the inner product defined as in (3.1) constitutes the $\mathbf{L}_w^2$ *subspace*. In particular cases, $w(x)$ may be nonzero only for $x \in \mathbb{Z}_{\geq 0} = \{0, 1, \cdots\}$ or for $x \in \mathbb{Z}_{N+1} = \{0, 1, \cdots N\}$. In the later case, $\mathbf{L}_w^2$ is of dimension $N + 1$.

Under the condition

$$\sum_{x=0}^{\infty} x^{2n} w(x) < \infty, \tag{3.3}$$

we can get a set of degree $n$ polynomials $\left\{\psi_n(x) \in \mathbf{L}_w^2\right\}$ such that for $n, m \in \mathbb{Z}_{\geq 0}$, $\psi_n(x)$ and $\psi_m(x)$ satisfy the orthogonality relation in (3.2). These polynomials $\psi_n(x)$, $n \in \mathbb{Z}_{\geq 0}$ are called discrete orthogonal polynomials (DOPs). The DOP $\psi_n(x)$ of degree $n$ is given by

$$\psi_n(x) = \kappa_{n,0} x^n + \kappa_{n,1} x^{n-1} + \cdots + \kappa_{n,n-1} x + \kappa_{n,n} \tag{3.4}$$

where $\kappa_{n,i}$ s are appropriate real constants.

The DOPs constitute an orthogonal basis set of $\mathbf{L}_w^2$ and under the condition,

$$\sum_{x=0}^{\infty} e^{2c|x|} w(x) < \infty, \tag{3.5}$$

for $c > 0$, this basis set is complete [158]. Thus, any function $f(x) \in \mathbf{L}_w^2$ can be expressed as

$$f(x) = \sum_{n \leq \infty} \langle f(x), \psi_n(x) \rangle \psi_n(x) \tag{3.6}$$

Just like the continuous orthogonal polynomials, the DOPs are widely studied and applied. Some important properties of the DOPs are listed below.

***Property 1:*** DOPs satisfy a second-order linear difference equation.

Consider the second-order difference equation

$$P_1(x)[\Delta\nabla u(x)] + Q(x)\nabla u(x) + R\,u(x) = 0, \tag{3.7}$$

where $\nabla u(x) = u(x) - u(x-1)$ is the backward difference and $\Delta u(x) = u(x+1) - u(x)$ is the forward difference operations, $P_1(x)$, $Q(x)$ and $u(x)$ are real functions defined for $x \in \mathbb{Z}_{\geq 0}$ and $R$ is a constant. Using the finite difference expansions, the difference equation (3.7) can be rewritten as

$$P_1(x)\Delta u(x) - P_2(x)\nabla u(x) + R\,u(x) = 0, \tag{3.8}$$

where $P_2(x) = Q(x) - P_1(x)$.

The DOPs satisfy the second-order difference equations in (3.7) and (3.8). In the operator notation (3.8) can be written as

$$\Upsilon u(x) = 0 \tag{3.9}$$

where $\Upsilon = P_1\Delta - P_2\nabla + R$ is a linear operator. The DOPs form the eigen functions of the operator $\Upsilon$ if

(i) $\Upsilon$ is symmetric with respect to the weight $w(x)$.

(ii) $P_1(x)$ and $P_2(x)$ are polynomials of at most degree 2.

(iii) $R$ is a constant which is assumed to be zero.

Given the real functions $\psi(x)$ and $\phi(x)$, the symmetry of $\Upsilon$ implies that

$$\langle \Upsilon\psi, \phi \rangle - \langle \psi, \Upsilon\phi \rangle = 0 \tag{3.10}$$

From (3.10), we can derive

$$P_2(x)\,w(x) = P_1(x-1)\,w(x-1) \tag{3.11}$$

(3.11) implies that for $\Upsilon$ to be symmetric, the weight $w(x)$ should be a recursive function of the form

$$w(x) = \frac{P_1(x-1)}{P_2(x)} w(x-1) \tag{3.12}$$

Because of the above conditions, the eigenfunctions of (3.8) are the polynomials $\psi_n(x)$ which are orthogonal with respect to $w(x)$. The eigen value equation corresponding to (3.9) can be written as

$$P_1(x)\{\Delta\psi_n(x)\} - P_2(x)\{\nabla\psi_n(x)\} + \lambda_n\psi_n(x) = 0 \tag{3.13}$$

where

$$\lambda_n = n\Delta(P_2(x) - P_1(x)) + \sum_{j=1}^{n-1} \Delta P_1(x) - \Delta P_1(x+j) \tag{3.14}$$

By solving (3.13), the general form for the $n^{th}$ degree DOP is obtained as

$$\psi_n(x) = \sum_{k=0}^{n} (-1)^{n-k} \begin{pmatrix} n \\ k \end{pmatrix} \prod_{j=0}^{n-k-1} P_1(x+j) \prod_{j=0}^{k-1} P_2(x-j) \tag{3.15}$$

***Property 2:*** DOPs can be expressed using the generalised Rodrigues formula.

The discrete Rodrigues formula associated with the DOP solution in (3.15) can be derived as

$$\psi_n(x) = B_n w(x)^{-1} \nabla^n \left[ w(x) \prod_{k=0}^{n-1} P_1(x+k) \right] \tag{3.16}$$

where $B_n$ is a normalizing constant.

***Property 3:*** DOPs satisfy a three term recurrence relation.

The three-term recurrence associated with the DOPS can be derived as

$$x\psi_n(x) = \alpha_n\psi_{n+1}(x) + \beta_n\psi_n(x) + \gamma_n\psi_{n-1}(x) \tag{3.17}$$

where $\alpha_n, \beta_n$ and $\gamma_n$ are the constants. Using (3.4), the constants in the recurrence relation are computed as

$$\alpha_n = \frac{\kappa_{n,0}}{\kappa_{n+1,0}} \;\; ; \;\; \beta_n = \frac{\kappa_{n,1}}{\kappa_{n,0}} - \frac{\kappa_{n+1,1}}{\kappa_{n+1,0}} \;\; ; \;\; \gamma_n = \frac{\kappa_{n-1,0}}{\kappa_{n,0}} \frac{\langle\psi_n, \psi_n\rangle}{\langle\psi_{n-1}, \psi_{n-1}\rangle}$$

***Property 4:*** The DOP can be represented in terms of the hypergeometric series.

Any series $\sum_k C_k$ is known as the *hypergeometric series* [156] if $C_0 = 1$ and

$$\frac{C_{k+1}}{C_k} = \frac{(k+a_1)(k+a_2)\cdots(k+a_r)}{(k+1)(k+b_1)(k+b_2)\cdots(k+b_s)}\, z \tag{3.18}$$

where, the function defined by

$${}_rF_s\left(a_1\cdots a_r; b_1\cdots b_s; z\right) = \sum_{k=0}^{n} \frac{(a_1)_k\cdots(a_r)_k}{(b_1)_k\cdots(b_s)_k}\frac{z^k}{k!} \tag{3.19}$$

is called the hypergeometric function [156, 157].

In (3.19), $(a)_k$ denotes the *Pochhammer symbol* given as

$$(a)_k = a\,(a+1)\cdots(a+k-1) = \frac{\Gamma\,(a+k)}{\Gamma\,(a)}, \tag{3.20}$$

$r$ and $s$ are the constants denoting the number of terms in the numerator and the denominator respectively and $z$ may be a constant or variable.

The classical DOPs, namely, the Charlier, the Meixner, the Krawtchouk and the Tchebichef-Hahn polynomials are the only DOPs that occur as eigenfunctions of $\Upsilon u\,(x)$ with respect to the choices of $P_1(x)$ and $P_2(x)$. The discrete Tchebichef polynomials are the special case of Tchebichef-Hahn polynomials. The formulation of the Krawtchouk and the discrete Tchebichef polynomials of a fixed degree are presented below. Through out this thesis, the degree of the polynomial is synonymously mentioned as the order of the polynomial.

## 3.3 Formulation of the Krawtchouk polynomials

The Krawtchouk polynomials are defined over a finite set $\mathbb{Z}_N = \{0, 1, \cdots, N\}$. Suppose in (3.8),

$$P_1\,(x) = p\,(N-x) \quad \text{and} \quad P_2\,(x) = qx$$

with $p, q > 0$ and $p + q = 1$. Then, from (3.12)

$$w(x) = \frac{p^x N\,(N-1)\,(N-2)\ldots(N-x+1)}{q^x x!} w\,(0)\,. \tag{3.21}$$

We can write, $(N-x+1)_x = \dfrac{N!}{(N-x)!}$

Therefore,

$$w\,(x) = \frac{p^x N!}{q^x x!\,(N-x)!} w\,(0) \tag{3.22}$$

By assuming $w(0) = q^N$, $w(x)$ is given by

$$w(x) = \binom{N}{x} p^x q^{N-x} \tag{3.23}$$

Note that $w(x)$ is the binomial probability mass function and the polynomials associated with it are the Krawtchouk polynomials. Substituting $P_1(x)$ and $P_2(x)$ in (3.14) and (3.15), we get $\lambda_n = n$ and

$$\begin{aligned}\psi_n(x) &= \sum_{k=0}^{n} (-1)^{n-k} \binom{n}{k} \prod_{j=0}^{n-k-1} p(N-x-j) \prod_{j=0}^{k-1} q(x-j) \\ &= \sum_{k=0}^{n} (-1)^{n-k} \binom{n}{k} p^{n-k} q^k \left\{ \begin{array}{l} (N-x)(N-x-1)\cdots(N-x-n+k+1) \\ x(x-1)\cdots(x-k+1) \end{array} \right\}\end{aligned} \tag{3.24}$$

$\psi_n(x)$ can be simplified as

$$\psi_n(x) = n! \sum_{k=0}^{n} (-1)^{n-k} p^{n-k} q^k \binom{N-x}{n-k} \binom{x}{k} \tag{3.25}$$

The standard form of the Krawtchouk polynomials defined after normalization is given by [158]

$$\overline{\psi}_n(x) = \frac{(-1)^n}{n! p^n} \psi_n(x) = \sum_{k=0}^{n} \binom{N-x}{n-k} \binom{x}{k} \left(-\frac{q}{p}\right)^k \tag{3.26}$$

### 3.3.1 Rodrigues formula

Using (3.16), the discrete Rodrigues formula associated with the Krawtchouk polynomials $\overline{\psi}_n(x)$ can be derived as

$$\overline{\psi}_n(x) = q^N \binom{N}{n} w(x)^{-1} \nabla^n \left[ \binom{N-n}{x} \left(\frac{p}{q}\right)^x \right] \tag{3.27}$$

Clearly, $\overline{\psi}_0(x) = 1$, $\overline{\psi}_1(x) = N - xp^{-1}$ and so on.

### 3.3.2 Recurrence relation

From the series expansion, the three-term recurrence relation for computing the Krawtchouk polynomials of order $n > 1$ is obtained as [72, 157, 158]

$$p(n+1)\overline{\psi}_{n+1}(x) = (pN + n - 2pn - x)\overline{\psi}_n(x) + (1-p)(N-n+1)\overline{\psi}_{n-1}(x). \tag{3.28}$$

It is easy to verify that the Krawtchouk polynomials exhibit symmetry with respect to the parameters $n$ and $x$ [72, 157]. The symmetry properties of the Krawtchouk polynomials are stated below.

(i) For $p = 0.5$, the symmetry along $x$-axis is given by

$$\overline{\psi}_n(x) = (-1)^n \overline{\psi}_n(N-x) \tag{3.29}$$

(ii) For $p = 0.5$, the symmetry along $n$-axis is expressed as

$$\overline{\psi}_n(x) = (-1)^x \overline{\psi}_{N-n}(x) \tag{3.30}$$

(iii) For any $p$, the diagonal symmetry with respect to $n = x$ is defined as

$$\overline{\psi}_n(x) = \overline{\psi}_x(n) \tag{3.31}$$

By using the symmetry property, the Krawtchouk polynomials can be efficiently computed for large $N$.

### 3.3.3 Hypergeometric representation

The Krawtchouk polynomial in (3.26) can be written as

$$\overline{\psi}_n(x) = \begin{pmatrix} N-x \\ n \end{pmatrix} \sum_{k=0}^{n} \begin{pmatrix} x \\ k \end{pmatrix} \frac{n!}{(n-k)!\,(N-x-n+1)\cdots(N-x-n+k)} \left(-\frac{q}{p}\right)^k \tag{3.32}$$

By defining,

$$C_k = \begin{pmatrix} x \\ k \end{pmatrix} \frac{n!}{(n-k)!\,(N-x-n+1)\cdots(N-x-n+k)} \left(-\frac{q}{p}\right)^k \tag{3.33}$$

the ratio in (3.18) is obtained as

$$\frac{C_{k+1}}{C_k} = \frac{(k-n)(k-x)}{(k+N-x-n+1)(k+1)} \left(-\frac{q}{p}\right) \tag{3.34}$$

Thus, the hypergeometric representation of the Krawtchouk polynomials is given by

$$\overline{\psi}_n(x) = \begin{pmatrix} N-x \\ n \end{pmatrix} {}_2F_1\left(-n, -x; N-x-n+1; \frac{p-1}{p}\right) \tag{3.35}$$

Using the hypergeometric identity [159],

$${}_2F_1(-n, b; c; z) = \frac{(c-b)_n}{(c)_n} {}_2F_1(-n, b; b+1-n-c; 1-z),$$

(3.35) can be further simplified as

$$\overline{\psi}_n(x) = \begin{pmatrix} N \\ n \end{pmatrix} {}_2F_1\left(-n, -x; -N; \frac{1}{p}\right) \tag{3.36}$$

An alternative form of the normalised Krawtchouk polynomials as defined in [72, 157] is

$$K_n(x;p) = \begin{pmatrix} N \\ n \end{pmatrix}^{-1} \overline{\psi}_n(x) \tag{3.37}$$

$$= {}_2F_1\left(-n, -x; -N; \frac{1}{p}\right) \tag{3.38}$$

### 3.3.4 Derivation of $\left\|\overline{\psi}_n\right\|_w^2$

The squared norm $\left\|\overline{\psi}_n\right\|_w^2$ of the Krawtchouk polynomials is derived using the method of generating function $G(x,t)$ that is defined as

$$G(x,t) = \sum_{n=0}^{\infty} \overline{\psi}_n(x)\, t^n \tag{3.39}$$

The definition in (3.39) implies that $\overline{\psi}_n(x)$ appears as the coefficient of $t^n$. By substituting $\overline{\psi}_n(x)$ in (3.39), we have

$$G(x,t) = \sum_{k=0}^{\infty} \begin{pmatrix} x \\ k \end{pmatrix} \left(-\frac{q}{p}\right)^k t^k \sum_{n-k=0}^{\infty} \begin{pmatrix} N-x \\ n-k \end{pmatrix} t^{n-k} \tag{3.40}$$

Using the binomial theorem, the generating function for the Krawtchouk polynomials in (3.40) can be simplified as [155, 160]

$$G(x,t) = \left(1 - \frac{q}{p}t\right)^x (1+t)^{N-x} \tag{3.41}$$

Based on (3.41), we determine the inner product

$$\langle G_t, G_r \rangle_w = \sum_{x=0}^{N} \begin{pmatrix} N \\ x \end{pmatrix} p^x q^{N-x} \overline{\psi}_n(x) t^n \, \overline{\psi}_n(x)\, r^n \tag{3.42}$$

$$= \sum_{x=0}^{N} \begin{pmatrix} N \\ x \end{pmatrix} p^x q^{N-x} \left\{\left(1 - \frac{q}{p}t\right)^x (1+t)^{N-x}\right\} \left\{\left(1 - \frac{q}{p}r\right)^x (1+r)^{N-x}\right\}$$

$$= \left(1 + \frac{q}{p}rt\right)^N \tag{3.43}$$

Thus

$$\langle G_t, G_r \rangle_w = \sum_{k=0}^{N} \begin{pmatrix} N \\ k \end{pmatrix} \left( \frac{q}{p} tr \right)^k \tag{3.44}$$

In (3.44), it is clear that $\left\| \overline{\psi}_n \right\|_w^2$ appears as the coefficient of $t^n r^n$. Therefore,

$$\left\| \overline{\psi}_n \right\|_w^2 = \begin{pmatrix} N \\ n \end{pmatrix} \left( \frac{q}{p} \right)^n \tag{3.45}$$

From (3.37), the squared norm of the normalised Krawtchouk polynomials can be easily derived as

$$\|K_n\|_w^2 = \begin{pmatrix} N \\ n \end{pmatrix}^{-1} \left( \frac{q}{p} \right)^n \tag{3.46}$$

Substituting $q = 1 - p$ and $\frac{N!}{(N-n)!} = (-N)_n (-1)^n$, the squared norm can be rewritten as

$$\|K_n\|_w^2 = \frac{(-1)^n n!}{(-N)_n} \left( \frac{1-p}{p} \right)^n \tag{3.47}$$

The Krawtchouk polynomial basis can be made orthonormal by dividing the polynomial by its norm $\|K_n\|_w$ [72]. Thus, the orthonormal Krawtchouk polynomial can be defined as

$$\tilde{K}_n (x; p) = \frac{K_n (x; p)}{\|K_n\|_w} \tag{3.48}$$

### 3.3.5 Weighted Krawtchouk polynomials (WKPs)

From the definition of the orthonormal Krawtchouk polynomials in (3.48), it can be seen that the range of the polynomial values increases by a factor of $N^{n/2} (n!)^{-1/2}$ with respect to the order $n$. For large values of $N$, the order of magnitude of the polynomial values exceeds 5 [72]. Hence, in order to ensure numerical stability, Yap et al [72] introduced a set of WKPs that are obtained through multiplying $\tilde{K}_n (x; p)$ with a scaling factor. The scaling factor is simply the square root of the binomial weight function. Therefore, the set of WKPs $\left\{ \overline{K}_n (x; p; N) \right\}$ is defined by [72]

$$\overline{K}_n (x; p) = K_n (x; p) \frac{\sqrt{w (x; p)}}{\|K_n\|_w} \tag{3.49}$$

Replacing $K_n(x;p)$ in (3.28) with $\overline{K}_n(x;p)$, the recurrence relation for the WKPs can be derived as

$$\begin{aligned} p(N-n)\overline{K}_{n+1}(x) &= \sqrt{\frac{(1-p)(n+1)}{p(N-n)}}(pN+n-2pn-x)\overline{K}_n(x) \\ &\quad + \sqrt{\frac{(1-p)^2 n(n+1)}{p^2(N-n)(N-n+1)}}n(1-p)\overline{K}_{n-1}(x) \end{aligned} \tag{3.50}$$

## 3.4 Formulation of discrete Tchebichef polynomials (DTPs)

For $x \in \mathbb{Z}_N$, let the real valued functions in (3.8) be assumed as [158]

$$P_1(x) = (N-x)(x+1) \quad ; \quad P_2(x) = x(N-x+1)$$

Using (3.12), the weight function for the DTPs can be derived as

$$\begin{aligned} w(x) &= 1.w(x-1) \\ &= (1)^x w(0) \end{aligned} \tag{3.51}$$

By assuming $w(0) = 1$, the weight function associated with the DTPs is given by $w(x) = \frac{1}{N+1}$.

Substituting $P_1(x)$ and $P_2(x)$ in (3.14) gives $\lambda_n = n(n+1)$. Similarly, by substituting $P_1(x)$ and $P_2(x)$ in (3.15), the DTP of order $n$ can be derived as

$$\begin{aligned} \psi_n(x) &= \sum_{k=0}^{n}(-1)^{n-k}\begin{pmatrix} n \\ k \end{pmatrix}\prod_{j=0}^{n-k-1}(x+1+j)(N-x-j)\prod_{j=0}^{k-1}(x-j)(N-x+1+j) \\ &= \sum_{k=0}^{n}(-1)^{n-k}\begin{pmatrix} n \\ k \end{pmatrix}\left\{ \begin{array}{l} (x+1)\cdots(x+n-k)(N-x)\cdots(N-x-n+k+1) \\ x(x-1)\cdots(x-k+1)(N-x+1)\cdots(N-x+k) \end{array} \right\} \end{aligned} \tag{3.52}$$

The above equation can be simplified as

$$\psi_n(x) = \sum_{k=0}^{n}(-1)^{n-k}\begin{pmatrix} n \\ k \end{pmatrix}\frac{(x+n-k)!\,(N-x+k)!}{(x-k)!\,(N-x-n+k)!} \tag{3.53}$$

The simple form of DTPs is obtained by normalizing by the factor $n!$ and is given as [158]

$$T_n(x) = \frac{1}{n!}\sum_{k=0}^{n}(-1)^{n-k}\begin{pmatrix} n \\ k \end{pmatrix}\frac{(x+n-k)!\,(N-x+k)!}{(x-k)!\,(N-x-n+k)!} \tag{3.54}$$

### 3.4.1 Rodrigues formula

Using (3.16), the discrete Rodrigues formula for the DTPs is derived as

$$T_n(x) = \nabla^n \left[ \binom{x}{n} \binom{N-x+n}{n} \right] \tag{3.55}$$

Clearly, $T_0(x) = 1$, $T_1(x) = 2x - N$ and so on.

### 3.4.2 Recurrence relation

For $n > 1$, the three term recurrence relation for the discrete Tchebichef polynomial can be derived as [71, 154]

$$(n+1)\,T_{n+1}(x) = (2n+1)(2x-N)\,T_n(x) - n\left((N+1)^2 - n^2\right) T_{n-1}(x), \tag{3.56}$$

From (3.54), it is easy to show that the DTPs are symmetric with respect to $x$ as given by

$$(-1)^n\, T_n(x) = T_n(N-x) \tag{3.57}$$

### 3.4.3 Hypergeometric representation

Expanding the terms in the series in (3.54) gives

$$\tilde{\psi}_n(x) = \frac{(-1)^n (N-x)!\,(x+n)!}{n!\,x!\,(N-x-n)!} \sum_{k=0}^{n} (-1)^k \binom{n}{k} \frac{\begin{array}{c} x(x-1)\cdots(x-k+1)(x+n-1)\cdots(x+n-k) \\ (N-x+1)\cdots(N-x+k) \end{array}}{(N-x-n+1)\cdots(N-x-n+k)} \tag{3.58}$$

Assuming,

$$C_k = (-1)^k \binom{n}{k} \frac{x(x-1)\cdots(x-k+1)(x+n-1)\cdots(x+n-k)(N-x+1)\cdots(N-x+k)}{(N-x-n+1)\cdots(N-x-n+k)}$$

in (3.18), we get

$$\frac{C_{k+1}}{C_k} = \frac{(k-n)(k-x)(N-x+k+1)}{(k+1)(k-x-n)(N-x-n+k+1)}$$

Therefore,

$$T_n(x) = \frac{(-1)^n (N-x-n+1)_n (x+1)_n}{n!}\, {}_3F_2(-n, -x, N-x+1; -x-n, N-x-n+1; 1) \tag{3.59}$$

Using the hypergeometric identity [159],

$$ {}_3F_2\left(-n,a,b;d,e;1\right)=\frac{(d-a)_n\,(e-a)_n}{(d)_n\,(e)_n}{}_3F_2\left(-n,a,a+b-n-d-e+1;a-n-d+1,a-n-e+1;1\right) $$

$T_n(x)$ in (3.59) can be simplified as

$$ T_n(x)=(-N)_n\,{}_3F_2\left(-n,-x,1+n;1,-N;1\right) \tag{3.60} $$

$T_n(x)$ in (3.60) defines the standard form of the DTPs [71, 154].

### 3.4.4 Derivation of $\|T_n\|_w^2$

The squared norm $\|T_n\|_w^2$ can be derived using the Rodrigues type formula given in (3.55). Suppose

$$ V(x)=\binom{x}{n}\binom{x-N-1}{n}=\frac{1}{(n!)^2}x(x-1)\cdots(x-n+1)(x-N-1)\cdots(x-N-n). \tag{3.61} $$

Accordingly, (3.56) can be written as $T_n(x)=\nabla^n V(x)$. The squared norm $\|T_n\|_w^2$ is computed as

$$ \|T_n\|_w^2=\frac{1}{N+1}\sum_x T_n(x)\,T_n(x)=\frac{1}{N+1}\sum_x T_n(x)\,\Delta^n V(x) \tag{3.62} $$

Using the analog of integration by parts, the solution for (3.62) as derived in [161] is given by

$$ \|T_n\|_w^2=\frac{(N+1)\left((N+1)^2-1\right)\left((N+1)^2-2^2\right)\cdots\left((N+1)^2-n^2\right)}{2n+1} \tag{3.63} $$

The orthonormal discrete Tchebichef polynomial basis $\overline{T}_n(x)$ is obtained by normalization as

$$ \overline{T}_n(x)=\frac{T_n(x)}{\|T_n\|_w} \tag{3.64} $$

## 3.5 Least squares approximation of functions by DOPs

A function $f(x)$ defined for $x\in\{0,1,\cdots,N\}$ can be approximated in terms of the orthogonal polynomials defined through (3.15) and the approximation is given by

$$ \overline{f}(x)\cong\sum_{u=0}^{n}M_u\psi_u(x)\,w(x) \tag{3.65} $$

where $M_u$ is the coefficient of the polynomial $\psi_u(x)$ and $n\leq N$ is the highest order of the polynomials.

The optimal $M_u$ parameters are obtained by solving the least-squares problem:

$$\text{Minimise } \left\|\overline{f} - f\right\|^2 = \sum_{x=0}^{N} \left|\overline{f}(x) - f(x)\right|^2 \tag{3.66}$$

with respect to $M_u$, $u = 0, 1, \cdots, n$. Since $\{\psi_0(x), \psi_1(x), \cdots, \psi_N(x)\}$ form an orthogonal system, the coefficient $M_u$ is computed by

$$M_u = \frac{1}{\|\psi_u(x)\|_w^2} \sum_{x=0}^{N} f(x)\, \psi_u(x)\, w(x) \tag{3.67}$$

The coefficients $M_0, M_1, \cdots, M_n$ are known as the *discrete orthogonal moments* (DOMs). The Krawtchouk moments and the discrete Tchebichef moments are obtained by assuming $\psi_u(x) = \overline{K}_u(x)$ and $\psi_u(x) = \overline{T}_u(x)$ respectively in (3.67).

### 3.5.1 Image representation using two-dimensional DOPs

Using the separability property, the one-dimensional ($1D$) polynomial bases can be extended to two or more dimensions. Therefore, the two-dimensional ($2D$) DOP $\psi_{uv}(x, y)$ of order $(u + v)$ is given by

$$\psi_{uv}(x, y) = \psi_u(x)\, \psi_v(y) \tag{3.68}$$

Given a $2D$ image function $f(x, y)$ defined over a rectangular grid $\mathbb{G} = \{0, 1, \cdots, N\} \times \{0, 1, \cdots, M\}$, the approximation is defined as

$$\overline{f}(x, y) = \sum_{u=0}^{n} \sum_{v=0}^{m} M_{uv} \psi_{uv}(x, y)\, w(x)\, w(y) \tag{3.69}$$

where, $M_{uv}$ denotes the discrete orthogonal moment of order $(u + v)$ given by

$$M_{uv} = \frac{1}{\|\psi_{uv}(x, y)\|_w^2} \sum_{x=0}^{N} \sum_{y=0}^{M} f(x, y)\, \psi_{uv}(x, y)\, w(x)\, w(y) \tag{3.70}$$

Using (3.70), the Krawtchouk moments $Q_{uv}$ of order $(u + v)$ is obtained by

$$Q_{uv} = \sum_{x=0}^{N} \sum_{y=0}^{M} \overline{K}_u(x; p_1) \overline{K}_v(y; p_2) f(x, y) \tag{3.71}$$

Similarly, the discrete Tchebichef moments $V_{uv}$ of order $(u + v)$ is computed as

$$V_{uv} = \sum_{x=0}^{N} \sum_{y=0}^{M} \overline{T}_u(x) \overline{T}_v(y) f(x, y) \tag{3.72}$$

## 3.6 Spatial domain behaviour of the DOPs

In this section, the spatial characteristics of the WKPs and the normalised DTPs of various orders are analysed. The spatial characteristics of the DOPs is studied in terms of the spatial support and the oscillatory nature of the basis. This study on the spatial properties of the DOPs provides insight into their behaviour in approximating different functions.

The plots and basis images of the WKPs and the DTPs of various orders are shown in Figure 3.3 and Figure 3.4 respectively. From the plots, we infer that the DOPs show oscillating behaviour and the number of zero-crossings increases with the order of the polynomial. This variation implies that the DOPs exhibit different frequency characteristics with respect to the order.

The plots of $1D$ WKPs for $N = 60$, $n = 0, 1,$ and 2 for different values of $p$ are shown in Figure 3.1. It can be observed that, for $p = 0.5$ each polynomial is symmetric with respect to $x = N/2$. As $p$ deviates from the value of 0.5 by $\Delta p$, the support of WKP are approximately shifted by $N\Delta p$ [72]. The direction of shifting is dependent on the sign of $\Delta p$. Thus, the parameter $p$ of the WKPs can be considered as the translation parameter controlling the polynomial shift along the $x$-axis. As a result, the WKPs are localised functions and allow local approximation of functions by varying the value of $p$ [72, 153].

The basis images of $2D$ WKPs of various orders for different values of $p_1$ and $p_2$ are shown in Figure 3.2. The parameters $p_1$ and $p_2$ can be tuned to shift the polynomials in the horizontal and the vertical direction respectively. As a result, the appropriate selection of $p_1$ and $p_2$ enables local features of an image at the region-of-interest (ROI) to be extracted by the Krawtchouk moments. The $1D$ and the $2D$ WKPs of higher orders are shown in Figure 3.3(a) and Figure 3.3(b) respectively. From the illustrations in Figure 3.1-3.3, it is evident that the support of the WKP increases with the increase in the order. This implies that the lower order moments characterise the local features and as the higher order moments characterise the global features. Therefore, the WKPs are spatially localised and hence, exhibit a wavelet-like property.

The plots and the basis images of the normalised DTPs in Figure 3.4 show that the support of the polynomials extends over the entire range of the $x-$axis. This implies that the discrete Tchebichef moments of any order provide global description of the function. As the number of zero crossing increases with the order, the discrete Tchebichef moments represent the structural characteristics of the given image at different scales.

Except for the spatial localization property, the oscillatory behaviour of the DTPs is almost similar to that of the WKPs. However, the difference in the polynomial characteristics are seen to be more prominent at lower orders. From the plots of the lower order polynomials in Figure 3.1 and Figure 3.4, it is observed that the number

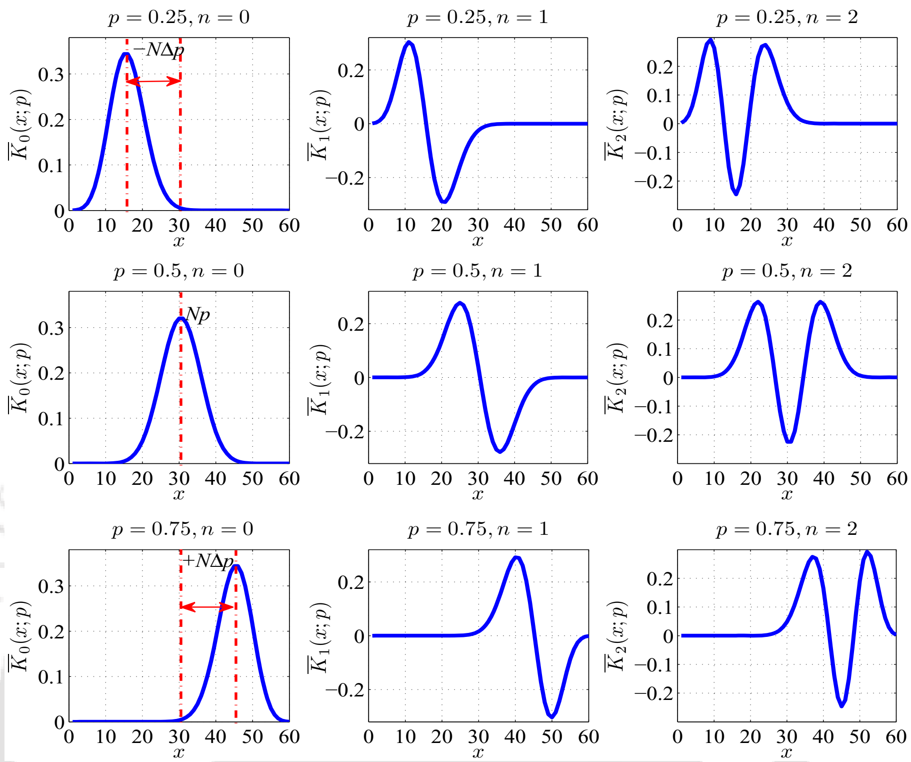


**Figure 3.1:** Plots of the WKPs for different values of $p$ and order $n$. The plots illustrate the translation of $\overline{K}_n(x)$ with respect to the value of $p$. For $p = 0.5 \pm \Delta p$, the polynomial is shifted by a factor of $\pm N\Delta p$. The value of $N = 60$.

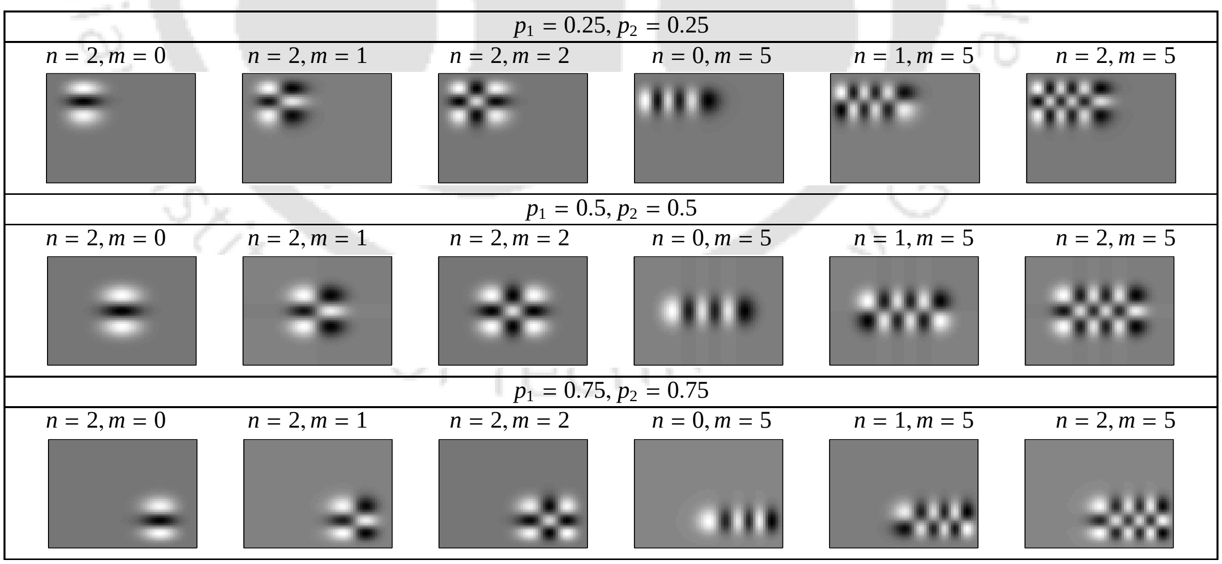


**Figure 3.2:** Basis images of $2D$ WKPs for different values of $p_1$ and $p_2$. The parameters $p_1$ and $p_2$ control the polynomial position in the vertical ($x-$ axis) and the horizontal direction ($y-$ axis) respectively. From the illustration, it can also be observed that the spatial support of the polynomial increase in the $x-$ direction as the value of $n$ increases. Similarly, the support increases in the $y-$ direction as the value of $m$ increases.

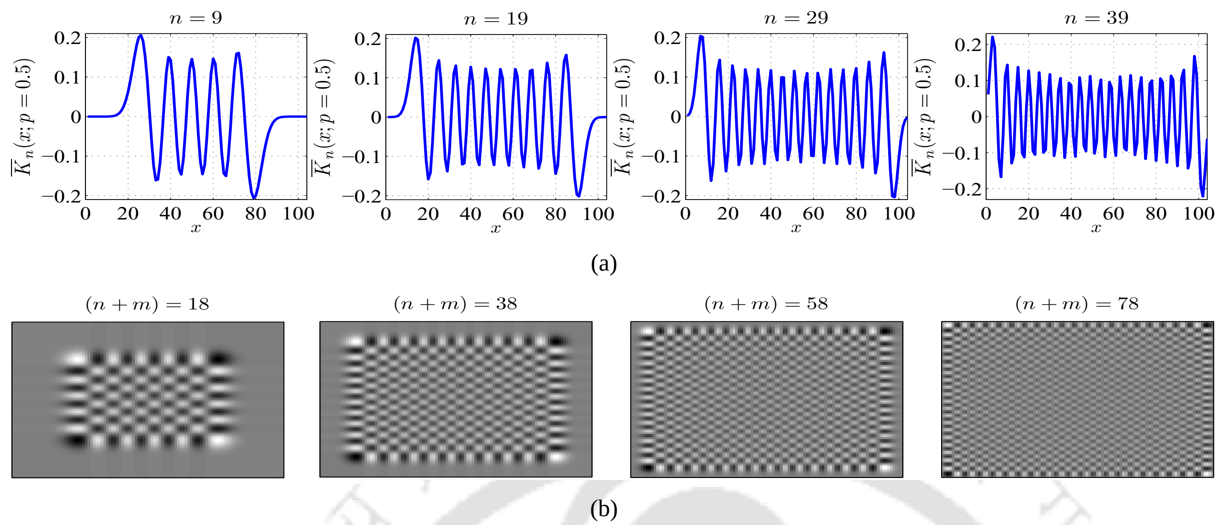


**Figure 3.3:** (a) Plots of the 1D WKPs of higher order $n$ and (b) Basis images of the 2D WKPs for higher values of $(n + m)$. The parameters $n = m$ and $N = 100$.

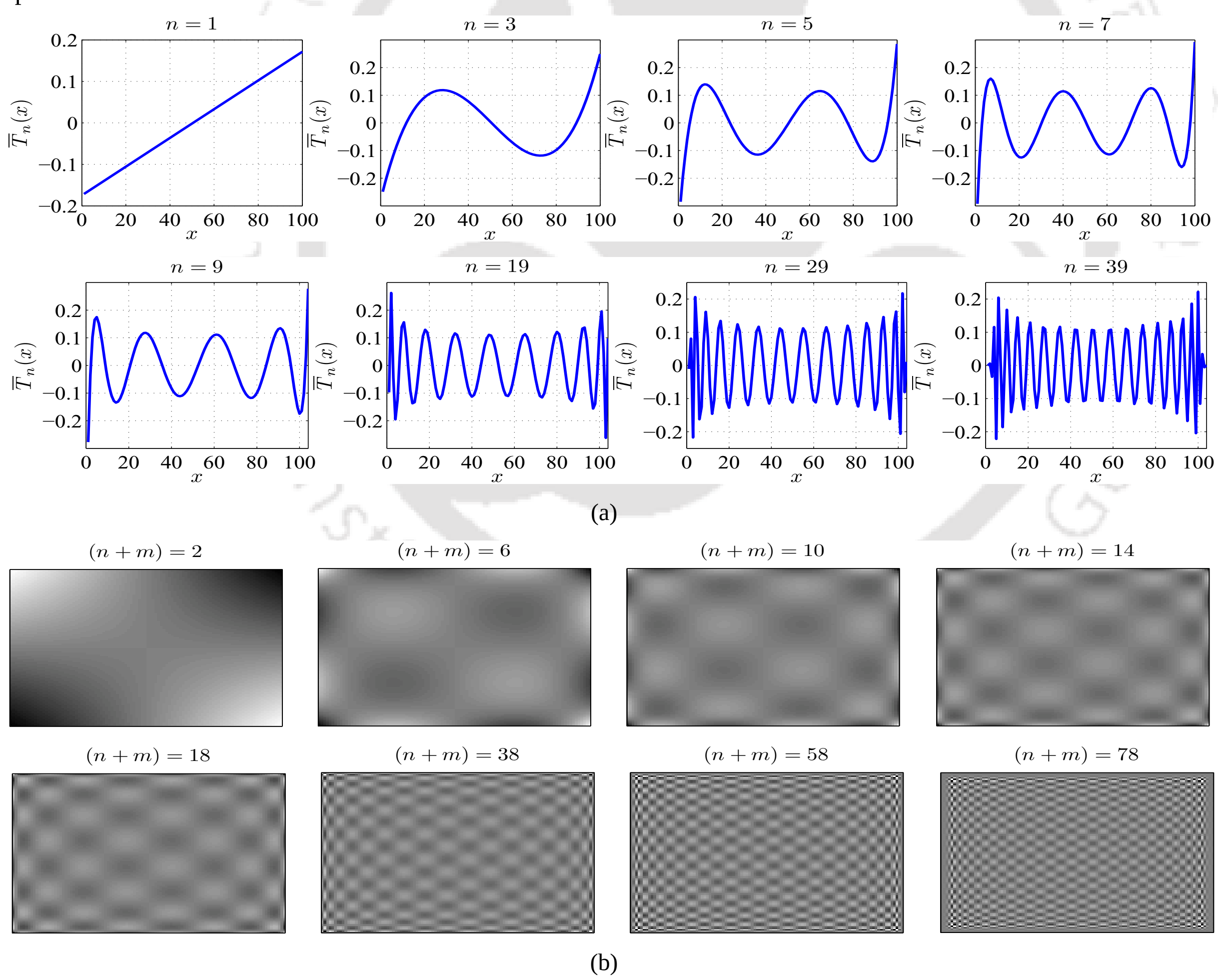


**Figure 3.4:** (a) Plots of the 1D normalised DTPs and (b) Basis images of the 2D normalised DTPs of different orders. The order $(n + m)$ of the 2D normalised DTPs is chosen such that $n = m$. The value of $N = 100$.

of zero crossing at a given order is comparatively higher in WKPs. It is further observed that the densities of zero crossings slightly vary along its support. This variation in the oscillatory nature is comparatively more noticeable in the normalised DTPs.

This study on the spatial behaviour of the DOPs suggests that the WKPs and the normalised DTPs are band-pass functions and the moments of different orders approximate different frequency bands of the function being approximated. The variation in the frequency characteristics of the DOPs can be studied in detail through their frequency domain representations.

## 3.7 Frequency domain behaviour of the DOPs

In this section, we empirically analyse the frequency domain characteristics of the WKPs and the normalised DTPs. The frequency domain representation of an *nth* order DOP is obtained by computing the discrete Fourier transform (DFT) of the polynomial function $\psi_n(x)$. The DFT of the polynomial function $\psi_n(x)$ is given by [162]

$$\Psi_n(\omega) = \sum_{x=0}^{N} \psi_n(x) \exp(-j\omega x) \tag{3.73}$$

where, $\omega = \frac{2\pi k}{N+1}$, $k = 0, 1, \cdots, N$. The *energy spectral density* (ESD) of the function $\psi_n(x)$ is given by $|\Psi_n(\omega)|^2$. It gives the contribution of the frequency component at $\omega$ to the total energy.

The Fourier transforms $\overline{\mathcal{K}}_n(\omega)$ and $\overline{\mathcal{T}}_n(\omega)$ are obtained by substituting $\psi_n(x) = \overline{K}_n(x)$ and $\psi_n(x) = \overline{T}_n(x)$ respectively in (3.73).

The plot of the ESD $\left|\overline{\mathcal{K}}_n(\omega)\right|^2$ of the WKPs obtained for $p = 0.5$ is shown in Figure 3.5. From the plots we can infer that the Krawtchouk polynomials act as band-pass functions and exhibit quadrature mirror symmetry with respect to the order $n$. The quadrature mirror property of the WKPs can also be verified by solving the frequency domain representation obtained through (3.73). Accordingly, by substituting (3.73) it is straightforward to show

$$\left|\overline{\mathcal{K}}_n\left(\left(\omega - \frac{\pi}{2}\right)\right)\right| = \left|\overline{\mathcal{K}}_{N-n}\left(\left(\omega + \frac{\pi}{2}\right)\right)\right| \tag{3.74}$$

The condition in (3.74) ensures that the WKPs of orders $n$ and $N - n$ exhibit quadrature mirror symmetry with respect to the quadrature frequency $\omega = \frac{\pi}{2}$. The proof for (3.74) is given in the Appendix 3.10. Using the quadrature mirror property of the WKPs, Akansu et al [163] derived a class of orthonormal binomial quadrature mirror filters (QMF) for multiresolution signal decomposition. The binomial QMFs are shown to be identical to

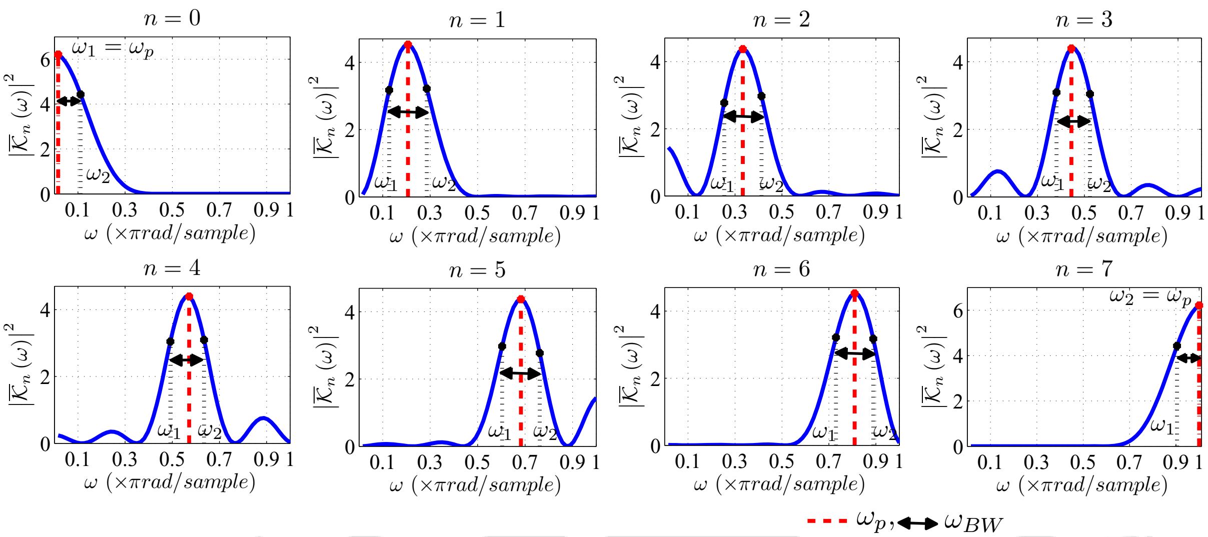


**Figure 3.5:** Plots of the ESD of the 1D WKPs for $(N + 1) = 8$, $p = 0.5$ and $n = \{0, 1, \cdots, 7\}$. $\omega_{BW} = |\omega_2 - \omega_1|$. The figure illustrates the QMF property of the WKPs with respect to the frequency $\omega = \frac{\pi}{2}$. The frequency characteristics implies that the polynomials act as band-pass functions. The WKPs exhibit sidelobes at the lower as well as the higher frequencies. For $n < \frac{N+1}{2}$ the sidelobes at lower frequencies have higher energy. On the contrary, for $n > \frac{N+1}{2}$ the sidelobes present at the higher frequencies exhibit higher energy.

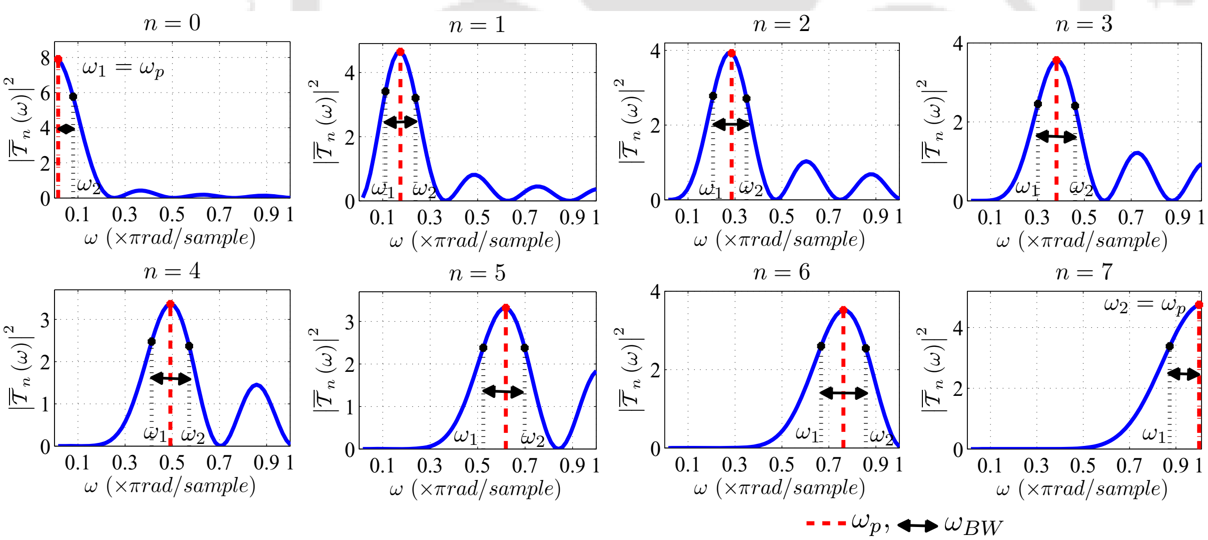


**Figure 3.6:** Plots of the ESD of the 1D normalised DTPs for $(N + 1) = 8$, $p = 0.5$ and $n = \{0, 1, \cdots, 7\}$. $\omega_{BW} = |\omega_2 - \omega_1|$. The frequency characteristics implies that these polynomials act as band-pass functions. It is also observed that the DTPs contain sidelobes at higher frequencies. The energy of the sidelobes is more in the middle-order polynomials. It can be observed that the sidelobe energy of the DTPs is higher than that of the WKPs. The DTPs do not exhibit quadrature symmetry.

**Table 3.1:** Frequency domain characteristics of WKPs and the normalised DTPs for various order $n$. The length of the sequence $N+1=8$.

| Order $n$ | WKPs | | normalised DTPs | |
|---|---|---|---|---|
| | Peak frequency $\omega_p$ ($\times\pi rad/\sec$) | Bandwidth $\omega_{BW}$ ($\times\pi rad/\sec$) | Peak frequency $\omega_p$ ($\times\pi rad/\sec$) | Bandwidth $\omega_{BW}$ ($\times\pi rad/\sec$) |
| 0 | 0.016 | 0.0952 | 0.016 | 0.0635 |
| 1 | 0.206 | 0.159 | 0.175 | 0.127 |
| 2 | 0.333 | 0.159 | 0.286 | 0.143 |
| 3 | 0.444 | 0.143 | 0.381 | 0.159 |
| 4 | 0.571 | 0.143 | 0.492 | 0.159 |
| 5 | 0.683 | 0.159 | 0.619 | 0.175 |
| 6 | 0.810 | 0.159 | 0.762 | 0.191 |
| 7 | 1 | 0.0952 | 1 | 0.127 |

the Daubechies wavelet filters and binomial QMF based signal decomposition exhibit higher energy compaction than the discrete cosine transform.

The plots of $\left|\overline{\mathcal{T}}_n(\omega)\right|^2$ for different values of $n$ are shown in Figure 3.6. From these plots, it is evident that normalised DTPs show the behaviour of the band-pass functions. However, $\left|\overline{\mathcal{T}}_n(\omega)\right|^2$ does not exhibit the property of quadrature mirror symmetry.

### 3.7.1 Quantitative analysis

Similar to the spectral analysis of moments in [164], the frequency domain characteristics of the DOPs are analysed in terms of the peak frequencies and the bandwidths.

The *peak frequency* $\omega_p$ is the frequency at which energy of the function is the highest. The *bandwidth* $\omega_{BW}$ is computed as the difference between the frequencies for which the energy value is 0.707 times of the highest energy.

The values of $\omega_p$ and the corresponding $\omega_{BW}$ for different orders of 8-point WKP and DCP sequences are given in Table. 3.1. From the table, it is inferred that the peak frequencies of the normalised DTPs are comparatively smaller than that of the WKPs of the same order. Further, it is also observed that the bandwidth of the normalised DTPs increases with the order. At higher orders, the normalised DTPs behave as wide-band band-pass functions and the WKPs are relatively narrow-band functions.

### 3.7.2 Short-time Fourier transform (STFT) analysis

The plots of the WKPs and the DTPs in the spatial domain, as in Figure 3.3 and Figure 3.4 respectively, show slightly varying densities of zero-crossings along the support. This suggests the variation of oscillatory nature of the polynomials along $x$. The frequency variation of the polynomial functions with respect to $x$ is

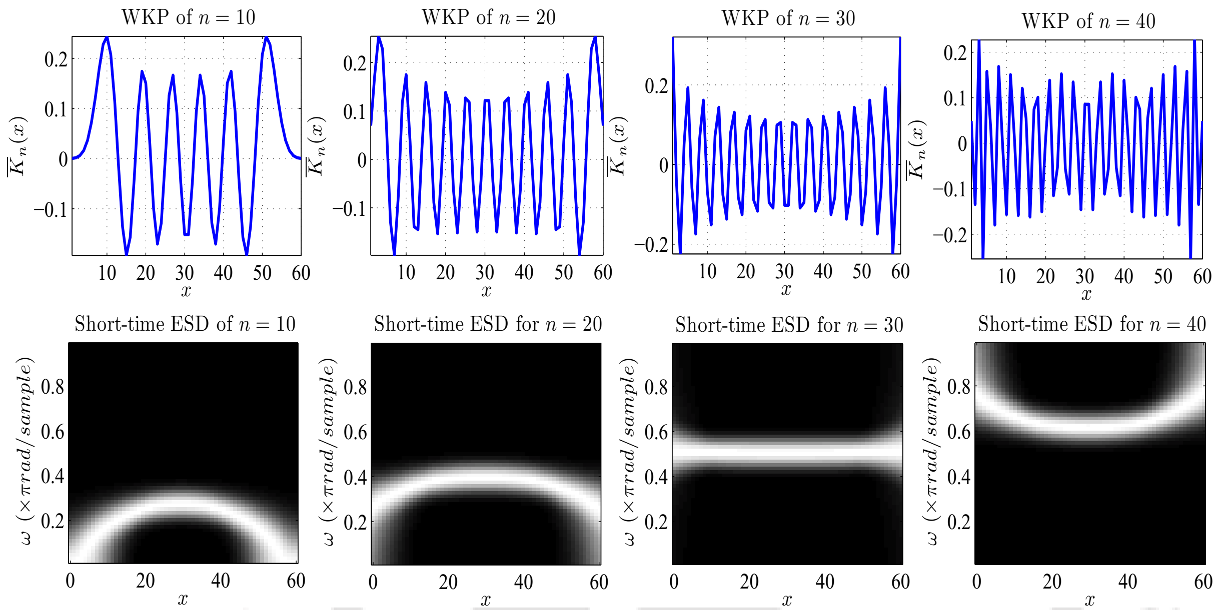


**Figure 3.7:** Plots of the 1D WKPs and corresponding ESD obtained using STFT as functions of $x$. The plots are obtained for $(N + 1) = 60$ and $p = 0.5$. The illustration shows that for order $n < \frac{N+1}{2}$, the low-frequency ESD of the polynomial increases for the values of $x$ close to $x = 0$ and $x = N$. For $n > \frac{N+1}{2}$, the high-frequency ESD with respect to these values gradually increases. The length of the sliding window $\xi(.)$ is chosen as 30 and the number of frequency points is 128.

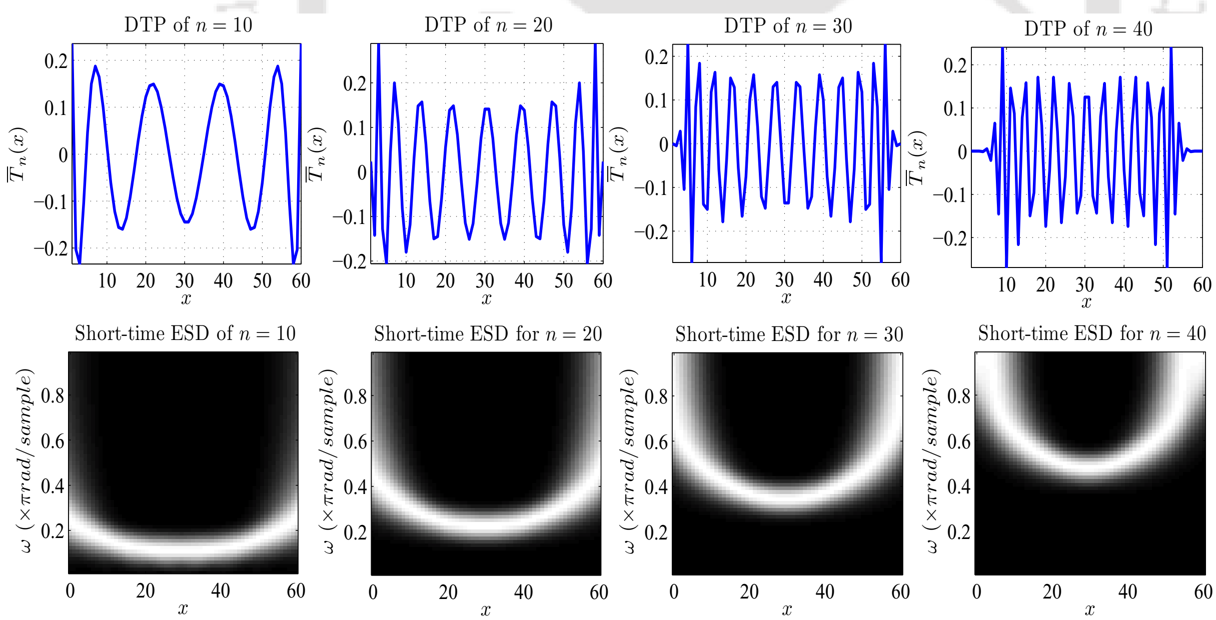


**Figure 3.8:** Plots of the 1D normalised DTPs and corresponding ESD obtained using STFT as a function of $x$. The plots are obtained for $(N + 1) = 60$. The illustration shows that for any given order $n$, the high-frequency ESD increases for the values of $x$ close to $x = 0$ and $x = N$. The length of the sliding window $\xi(.)$ is chosen as 30 and the number of frequency points is 128.

studied from the time-frequency representation of the DOPs. The time-frequency representation is obtained by computing the *short-time fourier transform* (STFT) of the DOPs. The procedure for deriving the STFT involves multiplying the polynomial with a window function of compact support and then compute the DFT for each windowed portion of the polynomial [165]. Accordingly, the expression for STFT can be written as

$$\Psi_n(r,\omega) = \sum_{x=0}^{N} \psi_n(x)\,\xi(x-r)\exp(-j\omega x) \tag{3.75}$$

where, $\xi(.)$ denotes the window function. The Hanning window is used for experimentation and the coefficients of an $L-$ point symmetric Hanning window are computed from the following equation.

$$\xi(l) = 0.5\left(1-\cos\left(\frac{2\pi l}{L-1}\right)\right),\ \ 0 \le l \le L-1 \tag{3.76}$$

The ESD of the STFT response corresponding to the WKP and the normalised DTP bases of different orders are shown in Figure 3.7 and Figure 3.8 respectively.

The time-frequency images in Figure 3.7 show that the low-frequency ESD of the WKPs up to order $n < 0.5(N+1)$ increases as the value of $x$ deviates from $x = N/2$ and approaches the values 0 and $N$. As the order becomes $n > 0.5(N+1)$, the high-frequency ESD increases for the values close to $x = 0$ and $x = N$. Contrary to the WKPs, the STFT response of the DTPs in Figure 3.8 exhibits stronger high frequency response as the value of $x$ deviates from $N/2$ approaching towards $x = 0$ and $x = N$.

From this frequency characteristics of the DOPs, it clear that the WKPs exhibit better band-pass behaviour than the DTPs and the energy of the frequency components varies with the derivation from the middle of the support of the polynomials.

## 3.8 Shape approximation using DOPs

The studies on the spatial and the frequency domain behaviour of the WKPs and DTPs have shown that these DOPs are band-pass functions and they exhibit varied characteristics in terms of the spatial localization and band-pass characteristics. Therefore, these DOPs can be considered as efficient tools for approximating different shapes. The shape features that are acquired by the Krawtchouk and the discrete Tchebichef moments will significantly vary due to the varying spatial and the frequency domain characteristics. This section presents the empirical studies performed to comparatively analyse the performance of the Krawtchouk and the discrete Tchebichef moments based approximations for shape representation and shape classification. The objective of this experimentation is to study the efficiency of these DOPs in accurately representing shapes with different structural characteristics and defections induced by noise.

The shapes required for the experiments are taken from the MPEG-7 (CE Shape-1, Part-B) database. The dataset used in the experimentation consists of 20 different shape classes containing 20 samples in each class. Two sets of experiments were performed. The first set studies the efficiency of the WKPs and DTPs in shape representation. The results include accuracy in approximating different shapes and sensitivity to noise. The second set of the experiments validates the discrete orthogonal moments as features for shape classification.

### 3.8.1 Metrics for reconstruction accuracy

The reconstruction accuracy of the DOMs is evaluated using the structural similarity index and the modified Hausdorff distance as defined below:

The **Structural similarity (SSIM) index** [166] is a region based similarity measure. The SSIM index between the shapes $f$ and $\hat{f}$ is computed locally by dividing the image into $L$ blocks of uniform size $11 \times 11$. For $l \in \{1, 2, \cdots, L\}$, the SSIM between the $l^{th}$ blocks of $f$ and $\hat{f}$ is evaluated as

$$SSIM\left(f, \hat{f}\right)_l = \frac{\left(2\mu_f \mu_{\hat{f}} + c_1\right)\left(2\sigma_{f\hat{f}} + c_2\right)}{\left(\mu_f^2 + \mu_{\hat{f}}^2 + c_1\right)\left(\sigma_f^2 + \sigma_{\hat{f}}^2 + c_2\right)} \tag{3.77}$$

where $\mu_f$ and $\mu_{\hat{f}}$ denote the mean intensities, $\sigma_f^2$ and $\sigma_{\hat{f}}^2$ denote the variances and $\sigma_{f\hat{f}}$ denotes the covariance. The constants $c_1$ and $c_2$ are included to avoid unstable results when $(\mu_f^2 + \mu_{\hat{f}}^2)$ and $(\sigma_f^2 + \sigma_{\hat{f}}^2)$ are very close to zero. We chose $c_1 = 0.01$ and $c_2 = 0.03$ [166]. The SSIM index between $f$ and $\hat{f}$ $SSIM\left(f, \hat{f}\right)$ is given by

$$SSIM\left(f, \hat{f}\right) = \frac{1}{L} \sum_{l=1}^{L} SSIM\left(f, \hat{f}\right)_l \tag{3.78}$$

The value of SSIM index lies in $[-1, 1]$ and a larger value means high similarity between the compared shapes.

The **modified Hausdorff distance (MHD)** [91] is employed to measure the similarity based on the shape boundary. Let $A = \{\alpha_1, \alpha_2, \cdots, \alpha_{N_A}\}$ and $B = \{\beta_1, \beta_2, \cdots, \beta_{N_B}\}$ be the two point sets representing the boundaries in the shapes $f$ and $\hat{f}$ respectively and $N_A$ and $N_B$ represent the corresponding cardinalities. The directed distance between the point sets $A$ and $B$ is defined as

$$D(A, B) = \frac{1}{N_A} \sum_{\alpha \in A} \min_{\beta \in B} (\|\alpha - \beta\|) \tag{3.79}$$

where, $\|.\|$ denotes the Euclidean norm. Based on the directed distances $D(A, B)$ and $D(B, A)$, the MHD is computed as [91]

$$MHD = \max\left(D(A, B), D(B, A)\right) \tag{3.80}$$

The similarity between the compared shapes $f$ and $\hat{f}$ is high, if the corresponding MHD is small.

Given the binary shape $f(x,y)$, its approximation $\hat{f}(x,y)$ is obtained using the Krawtchouk and the discrete Tchebichef moments defined through (3.71) and (3.72) respectively. The approximated shape is binarised through thresholding. In these experiments, the threshold for binarisation is chosen as 0.5. The reconstruction accuracy of the DOMs is quantitatively compared by using the values of the SSIM index and the MHD. The performance of the orthogonal moments is analysed by varying the order of the moments used for approximation.

### 3.8.2 Experiments on shape representation

In this experiment, we analyse the efficiency of the DOP approximations of different orders in representing the structural variations in shapes under different spatial scales. The structural variation in the shapes are studied using the curvature variations in the boundary contour. Accordingly, the shapes used for the experiments are chosen based on their curvature properties. The difference in the structural characteristics of the shapes are compared based on the number of concave segments and their geometrical properties. The properties of the concavities on the shape boundary are represented through the curvature scale space (CSS) representation. This section explains the distinct variation in the structural characteristics of shapes using the CSS and details the experimental analysis performed to study the accuracy of DOMs in representing different shapes.

#### 3.8.2.1 Characterizing shapes using curvature properties

The curvature properties of the shape boundary are among the important perceptual features describing the shape. The curvature can be defined as the rate of change of slope along the shape boundary and it can be expressed in terms of the first and the second order derivatives.

Let $f$ denote a binary shape and $\mathbb{B}$ be the corresponding shape boundary. Assume, $\mathbb{B}(u)$=$(x(u), y(u))$ as a continuous vector valued function defined by the position vectors $(x(u), y(u))$. Given the boundary points $(x,y) \in \mathbb{B}$ of length $L$, the curvature function is computed as [87]

$$\kappa(u) = \frac{\dot{x}(u)\,\ddot{y}(u) - \ddot{x}(u)\,\dot{y}(u)}{\left(\dot{x}(u)^2 + \dot{y}(u)^2\right)^{3/2}} \tag{3.81}$$

where $u$ is a real value such that $0 \leq u \leq (L-1)$. For the discrete case, the derivatives of $x$ and $y$ are approximated by the corresponding finite differences.

The zero-crossings of the curvature function are the *inflection points* on the shape boundary. The local absolute maximum in the curvature corresponds to a generic corner in the shape [167]. If the maximum value

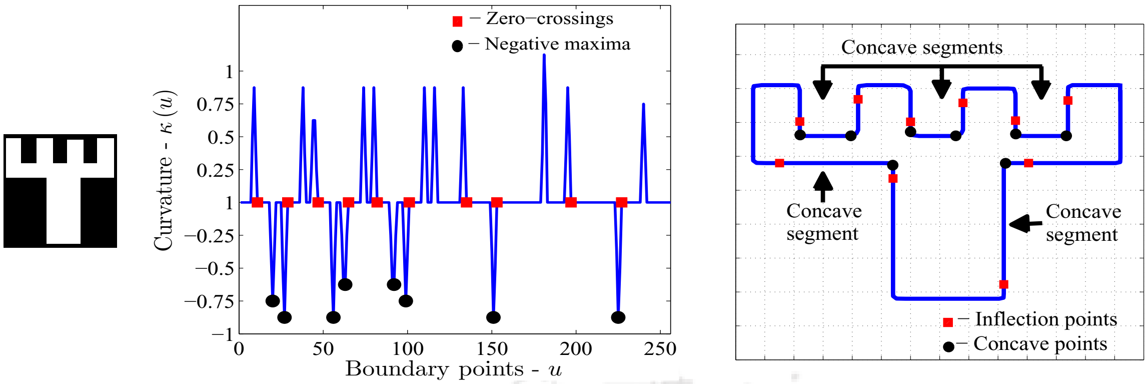


**Figure 3.9:** Illustration of finding the concave segments of a shape from the curvature function derived from the corresponding shape boundary. (a) Geometric shape used for illustration; (b) The curvature function derived from the boundary of the geometric shape and (c) Representing the inflection points and the concave segments on the shape boundary. The zero-crossings correspond to the inflection points. Similarly, the negative maxima correspond to the concave points.

**Table 3.2:** Types of concavities based on the width and the depth of the concave segments.

| Width | Depth | Type of concavity |
|---|---|---|
| Small | Small | Narrow - Shallow concavity |
| Small | High | Narrow - Deep concavity |
| High | Small | Wide - Shallow concavity |
| High | High | Wide - Deep concavity |

is positive, the corner is considered as the convex point and if the maximum is negative, the corner is considered as the concave point. The boundary section between the inflection points that contain the convex point is the *convex segment* and the section constituting the concave point comprises the *concave segment*.

Since, the shape boundary is a closed curve, the concave segments provide comparatively more detailed information and they constitute the transition between different parts of the shape. An example illustrating the inflection points and the concave segments of a geometric shape along with the corresponding curvature function is shown in Figure 3.9.

The structural variations in shape can be characterised by the variations in the width and the depth of the concave segments. The width of a concave segment can be computed as the length of the line connecting the corresponding two inflection points. The depth of the concave segment is the distance between the concave point and the line connecting the corresponding inflection points. Based on the width and the depth values, the concavities can be divided in to four types as listed in Table 3.2.

The characteristics of the concavities present in the shape can be represented using the curvature scale space (CSS) representation. The CSS representation is a map of the location of the zero-crossings in the curvature function $\kappa(u)$ obtained over successive smoothing of the shape boundary [87]. Convolving $\mathbb{B}$ with a $1D$ Gaussian kernel $g(u,\sigma)$ of standard deviation $\sigma$ results in the smoothed curve $\mathbb{B}_\sigma = \{(X,Y)\}$. The smoothed boundary points are given by

$$\begin{aligned} X(u,\sigma) &= x(u) * g(u,\sigma) \\ Y(u,\sigma) &= y(u) * g(u,\sigma) \end{aligned} \tag{3.82}$$

Accordingly, the curvature on $\mathbb{B}_\sigma$ is computed as

$$\kappa(u,\sigma) = \frac{\dot{X}(u,\sigma)\,\ddot{Y}(u,\sigma) - \ddot{X}(u,\sigma)\,\dot{Y}(u,\sigma)}{\left(\dot{X}(u,\sigma)^2 + \dot{Y}(u,\sigma)^2\right)^{3/2}} \tag{3.83}$$

The CSS descriptors that represent the location of the inflection points on the curve are extracted for varying values of $\sigma$ and are used to obtain the CSS image that is defined as

$$I_{CSS}(u,\sigma) = \{(u,\sigma)\,|\,\kappa(u,\sigma) = 0\} \tag{3.84}$$

The CSS map consists of several arch-shaped contours, each related to the concave segments of the shape boundary. The height and the base width of the arch-shaped contours reflect the depth and the width of the concavities respectively [168, 169]. The height of the CSS contours is larger for wide-shallow, wide-deep and narrow-deep concavities.

A few examples of the shapes used in this experiment and the corresponding CSS representations are shown in Figure 3.10 and Figure 3.11. The CSS representations of three star-shaped polygons consisting of 16 concave segments of almost same width and varying depth are illustrated in Figure 3.10. It can be observed that the number of arch-shaped contours in the CSS map is equal to the number of concave segments in the shape boundary. The shape in Figure 3.10(a) consists of shallow concave segments in comparison to the shapes illustrated in Figure 3.10(b) and 3.10(c). The star-shaped polygon in Figure 3.10(c) exhibits deeper concave segments and hence, the height of the arch-shaped contours in the corresponding CSS map is comparatively higher. By comparing the CSS maps in Figure 3.10, it can easily inferred that the height of the contours in the CSS map increases with the depth of the concave segments.

Figure 3.11 illustrates the CSS representation of three different shapes composed of different number of concave segments of different width. The shape of the character ‘T’ in Figure 3.11(a) consists of two wide-deep concave segments and hence, the corresponding CSS map exhibits two arch-shaped contours representing the concavities. Similarly, the CSS representations of a cross-shaped and the fork-shaped polygons in Figure 3.11(b) and Figure 3.11(c) respectively reflect the number of concavities in the shape boundary. The cross-shaped polygon is composed of concave segments of almost same width and depth. Hence, the arch-shaped contours in the corresponding CSS map are of approximately same height and base width. The fork-shaped

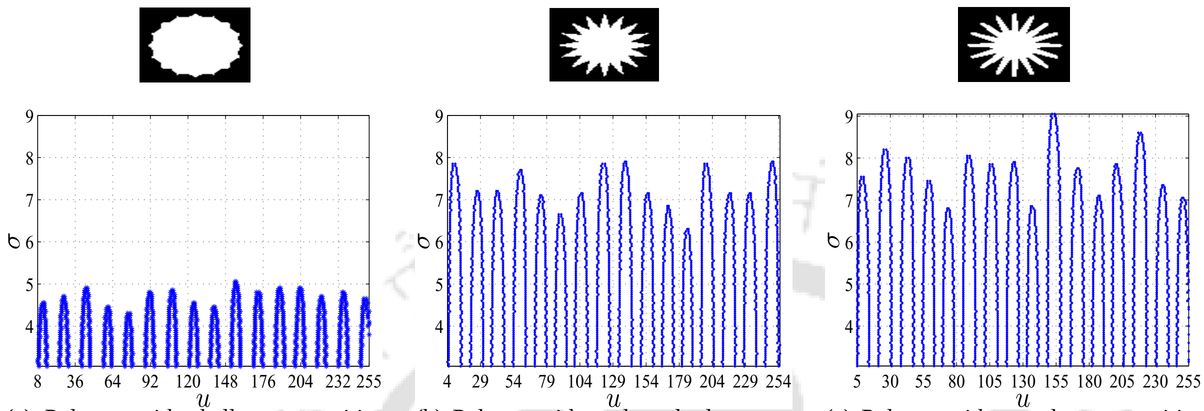


(a) Polygon with shallow concavities and its CSS map

(b) Polygon with moderately deep concavities and its CSS map

(c) Polygon with very deep concavities and its CSS map

**Figure 3.10:** CSS representation of star-shaped polygons composed of 16 concave segments of varying depth. The polygon shape in (a) consists of shallow concave segments and (c) consists of deeper concave segments. The figure illustrates the variation in the height of the arch-shaped contours in the CSS map with respect to the variation in the depth of the concavities.

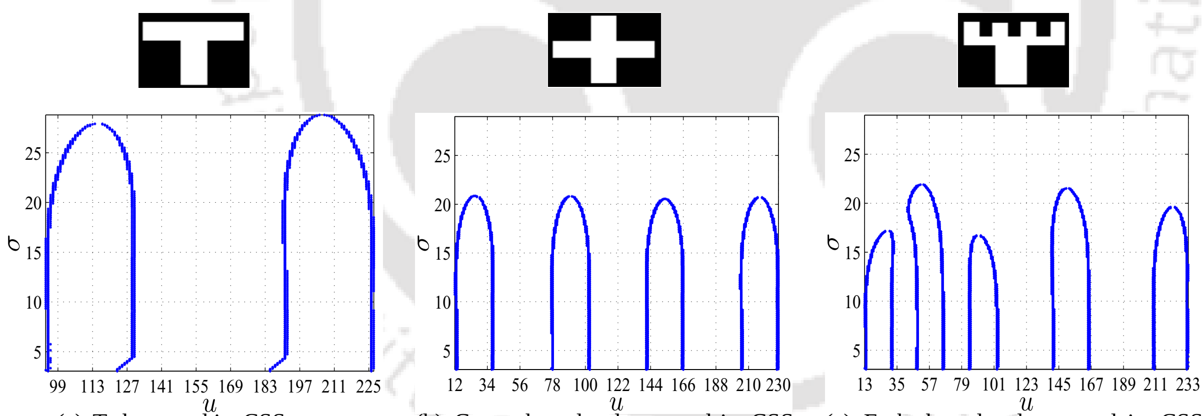


(a) T-shape and its CSS map

(b) Cross-shaped polygon and its CSS map

(c) Fork-shaped polygon and its CSS map

**Figure 3.11:** CSS representation of four different geometric shapes with varying number of concave segments and width. The figure illustrates the variation in the base width of the arch-shaped contours relative to the variation in the width of the concavities. Also, the number of arch-shape contours is proportional to the number of concavities. The shape of character 'T' has comparatively less number of concave segments and the concavities are more wide. The cross-shaped polygon has concave segments of similar width and depth. Conversely, the fork-shaped polygon is composed of concave segments of different widths and depth.

polygon consists of five deep concave segments. Based on the base width of the arch-shaped contours in the CSS map, it can be easily verified that the fork-shaped polygon is composed of two wide concavities and three comparatively narrow concavities. The base width of the CSS contours in Figure 3.11(b) and Figure 3.11(c) is less than that of the CSS contours illustrated in Figure 3.11(a). This implies that the T-shape is composed of comparatively wide concavities. By comparing the base widths of the arch-shaped contours in the CSS maps shown in Figure 3.10 and Figure 3.11, it can be inferred that the shapes presented in Figure 3.10 are composed of comparatively narrow concave segments.

Using the above curvature properties of the shape boundaries, it is also possible to infer the various spatial frequency structures of the shapes. It can be easily verified that the shapes composed of many number of deep concave segments consists of large number of transitions between the background and the object regions. Such shapes can be considered as complex shapes with higher spatial frequency regions and hence, exhibit large structural details. The shapes composed of shallow segments such as the star-shaped polygon in Figure 3.10(a) consist of less number of transitions between the background and the object regions. Hence, such shapes are composed of low spatial frequency regions with less structural details. On the other hand, the shapes presented in Figure 3.11 consist of less number of concave segments than the star-shaped polygon in Figure 3.10(a). However, the concave segments of the shapes presented in Figure 3.11 are comparatively deeper exhibiting high spatial frequency regions. From this discussion on the curvature properties, it is understood that the complexity of the shapes in terms of the structural details increases with the number of concavities and the depth of the concavities.

#### 3.8.2.2 Spatial scale of the shapes

Another important factor considered in this experiment is the spatial scale of the foreground region containing the shape with respect to the enclosed background region. Generally, in shape based object representation methods, the objects to be recognised are segmented from a scene and hence, the size of the object may vary depending upon the spatial resolution of the scene. Since the scenes are unconstrained, the size of the segmented object that constitutes the foreground region is unpredictable. As the DOPs are computed over the entire shape grid, the representation accuracy of the DOPs may vary with the spatial scale of the foreground object.

The images containing the shapes are binarised such that the pixels belonging to the object region are assigned the intensity value '1' and the pixels constituting the background are assigned the intensity value '0'.The size of the image grid is fixed at $90 \times 90$. The scale of the object's shape is varied as $40 \times 40$, $60 \times 60$ and $80 \times 80$. The parameters $p_1$ and $p_2$ of the WKPs are chosen as 0.5 so that the emphasis of the polynomial is with respect to the centroid of the shape.

#### 3.8.2.3 Variation in shapes versus reconstruction accuracy

The experiments are performed on the shapes presented in Figure 3.10 and Figure 3.11 and the results obtained are presented in the illustrations given through Figure 3.12 - Figure 3.17. The efficiency of the DOMs in accurately approximating different shapes is tested and discussed in terms of variation in the spatial scale of the shape and different structural characteristics.

From the results shown in Figure 3.12 - Figure 3.17, we can observe that the performance of the Krawtchouk moments in terms of the SSIM index and the MHD is consistently higher at all the orders while approximating shapes of lower scale $40 \times 40$. As the scale increases to $60 \times 60$ and $80 \times 80$, it is noticed that the reconstruction accuracy of the WKPs decreases for lower order approximations. This occurs due to the variation in the spatial support of the WKPs with respect to its order. As mentioned earlier, the lower order WKPs have smaller spatial supports and the support increases only with the order. In the case of shapes with lower scale values, most of the shape region lies within the spatial support of the WKPs yielding higher reconstruction accuracy at the lower order itself. As the scale of the shape increases, the entire shape region is not sufficiently spanned by the lower order WKPs. Hence, under this condition, the order of the WKPs has to be high for better reconstruction accuracy.

Converse to the performance of WKPs, it can be observed that the lower order DTPs offer poor reconstruction accuracy while approximating shapes of lower scale. It is known that the spatial support of the DTP extends over the entire range of the image grid offering a global support. The lower order DTPs exhibit less peak frequencies and hence, while approximating shapes they more or less behave like averaging functions resulting in excessive smoothing. As the order increases, the high frequency response of the DTP increases providing effective reconstruction of the high spatial frequency structures of the shape. While approximating shapes of lower scales, the background region is more dominating than the shape region and hence the averaging effect on the shapes is more than in the case of shapes with higher scales.

The results of DOM based approximation of the star-shaped polygons with varying depth of concavities are shown in Figure 3.12, Figure 3.13 and Figure 3.14. These results illustrate the efficiency of the DOMs in approximating the concave segments that constitute the structure of the shape. From the corresponding plots of the SSIM index and the MHD values obtained for various orders of the DOM based approximation, it is observed that the performance of the DOMs significantly varies at the lower orders.

The star-shaped polygon in Figure 3.12 consists of shallow concave segments and the shape is composed

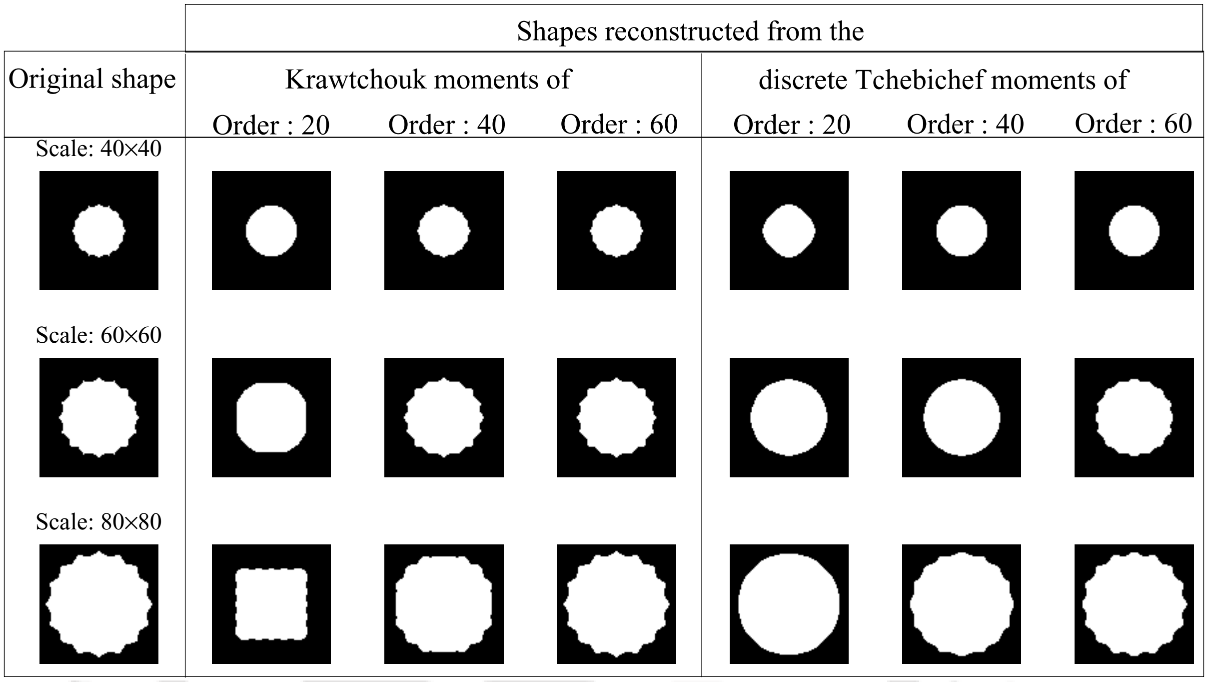


(a) Results of shape reconstruction obtained from DOM based approximations at various orders $(n+m)$, such that $n = m$.

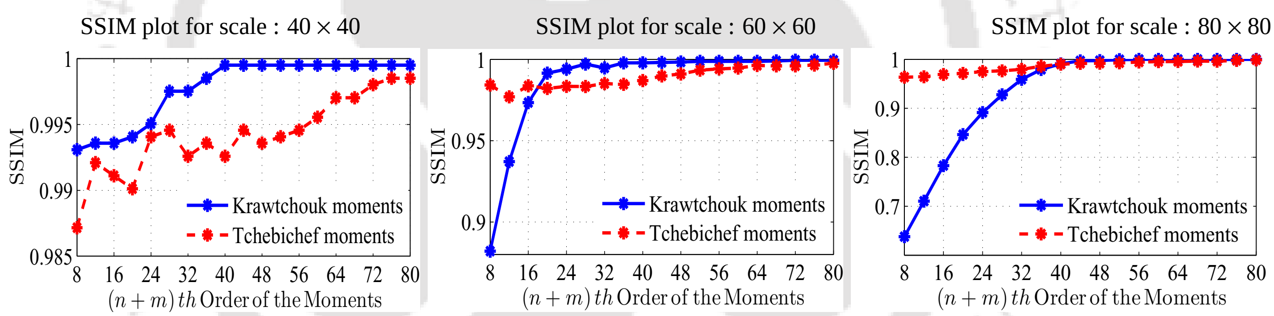


(b) Comparative plot of the SSIM index values obtained for different values of order $(n+m)$.

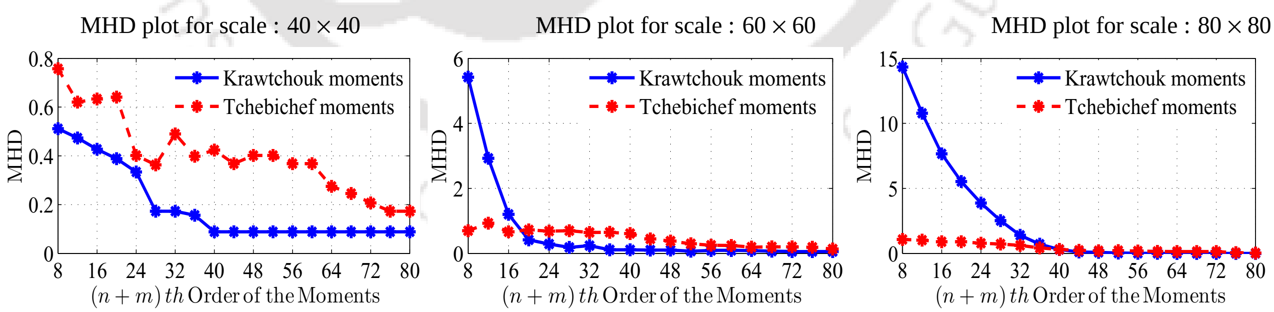


(c) Comparative plot of the MHD values obtained for different values of order $(n+m)$.

**Figure 3.12:** Illustration of reconstruction accuracy with respect to the star-shaped polygon consisting of shallow concavities. The illustration shows that the WKP based approximation is better for lower scales of the shape. For approximating shapes at lower scales, the DTPs require higher orders. At large scales the DTPs offer better reconstruction accuracy. However, as the order increases both the moments exhibits similar performance. In the case of lower order Krawtchouk moments, only a local region of the original shape that lie within the spatial support of the corresponding polynomials is efficiently reconstructed. Hence, the reconstruction accuracy evaluated in terms of the SSIM and MHD of the lower order Krawtchouk moments is comparatively less for scales $60 \times 60$ and $80 \times 80$.

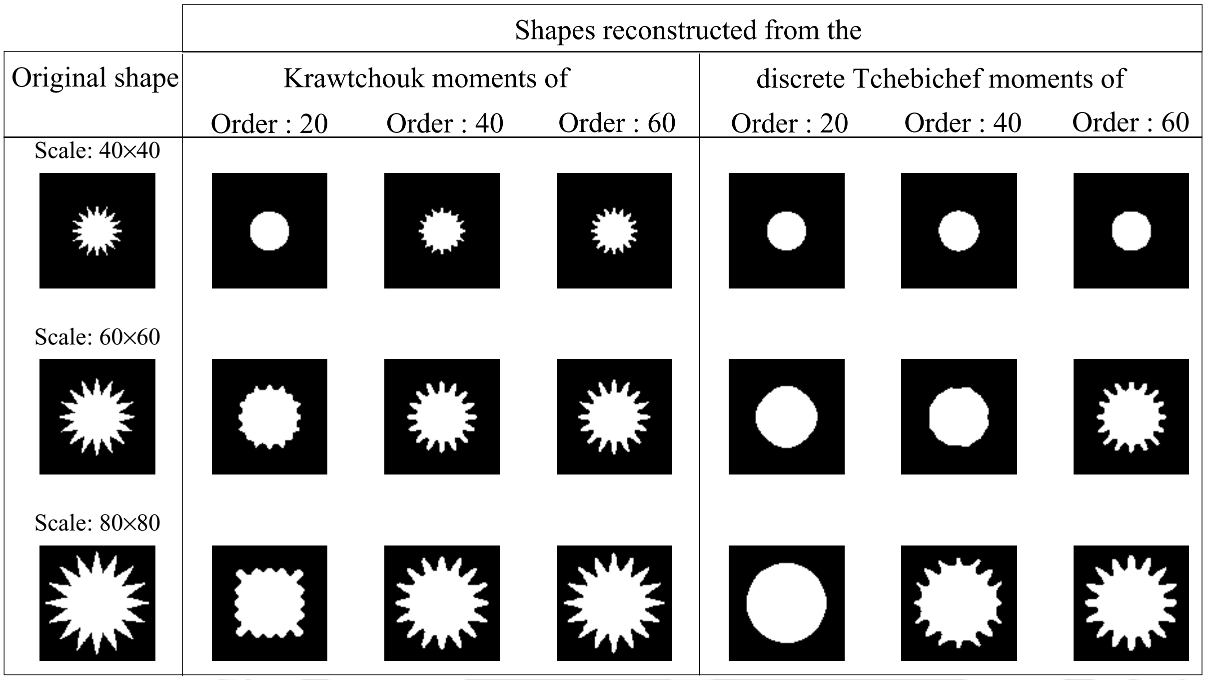


(a) Results of shape reconstruction obtained from DOM based approximations at various orders ($n + m$), such that $n = m$.

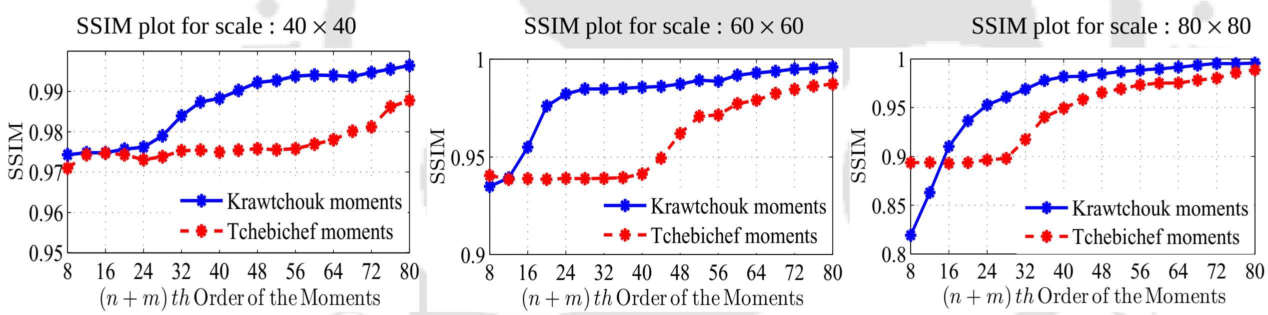


(b) Comparative plot of the SSIM index values obtained for different values of order ($n + m$).

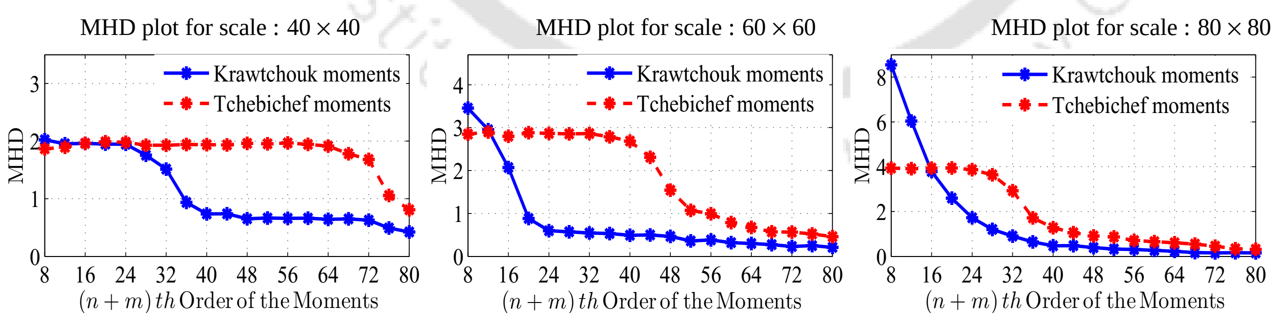


(c) Comparative plot of the MHD values obtained for different values of order ($n + m$).

**Figure 3.13:** Illustration of reconstruction accuracy with respect to the star-shaped polygon with moderately deep concavities. The results in terms of the SSIM and MHD indicates that the accuracy of the WKPs is comparatively higher than the DTPs in approximating shapes at different scales. The concavities are more accurately reconstructed by the Krawtchouk moments and the Tchebichef moments result in smoothened reconstruction of the sharp concave segments.

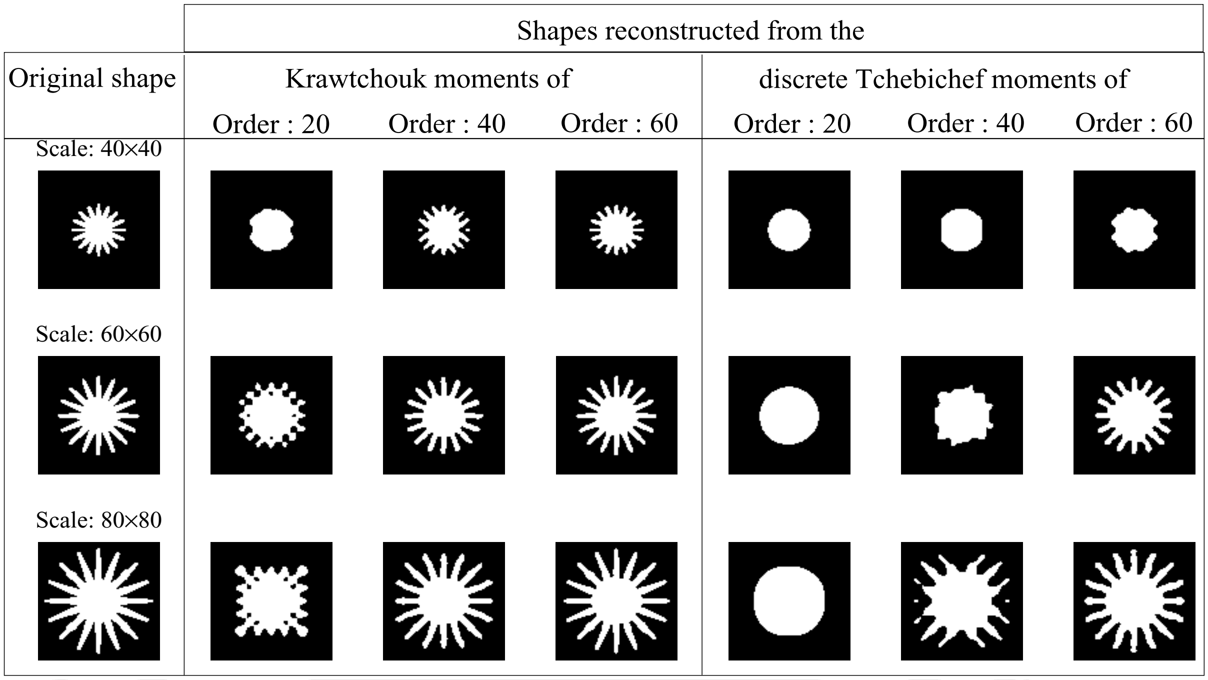


(a) Results of shape reconstruction obtained from DOM based approximations at various orders $(n + m)$, such that $n = m$.

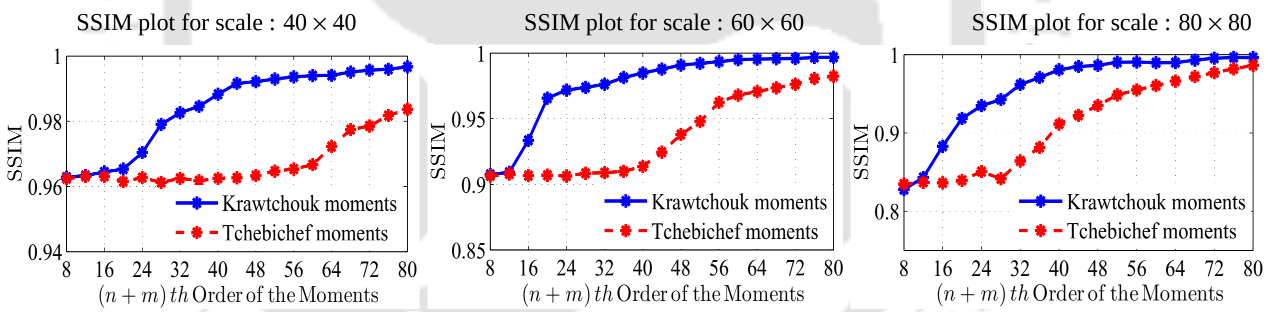


(b) Comparative plot of the SSIM index values obtained for different values of order $(n + m)$.

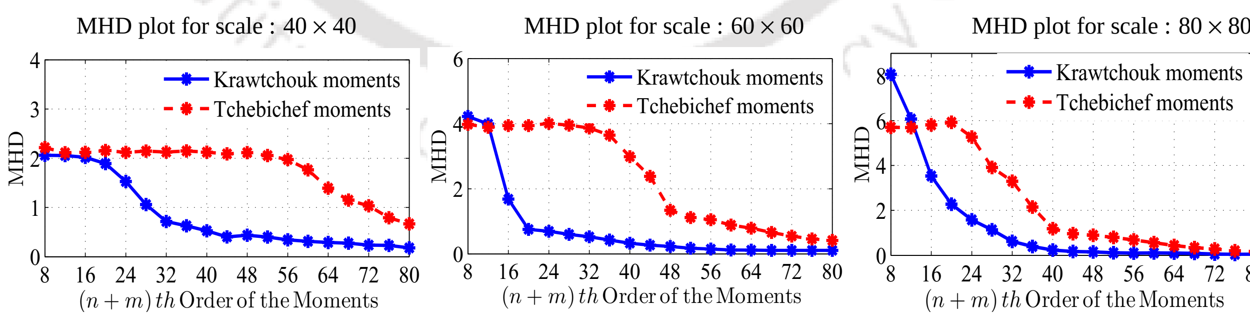


(c) Comparative plot of the MHD values obtained for different values of order $(n + m)$.

**Figure 3.14:** Illustration of DOM based approximation of a star-shaped polygon consisting of deep concave segments. The illustration shows that the performance of the Krawtchouk moments at all the orders is consistently superior to the discrete Tchebichef moments in approximating the shapes at all three different scales.

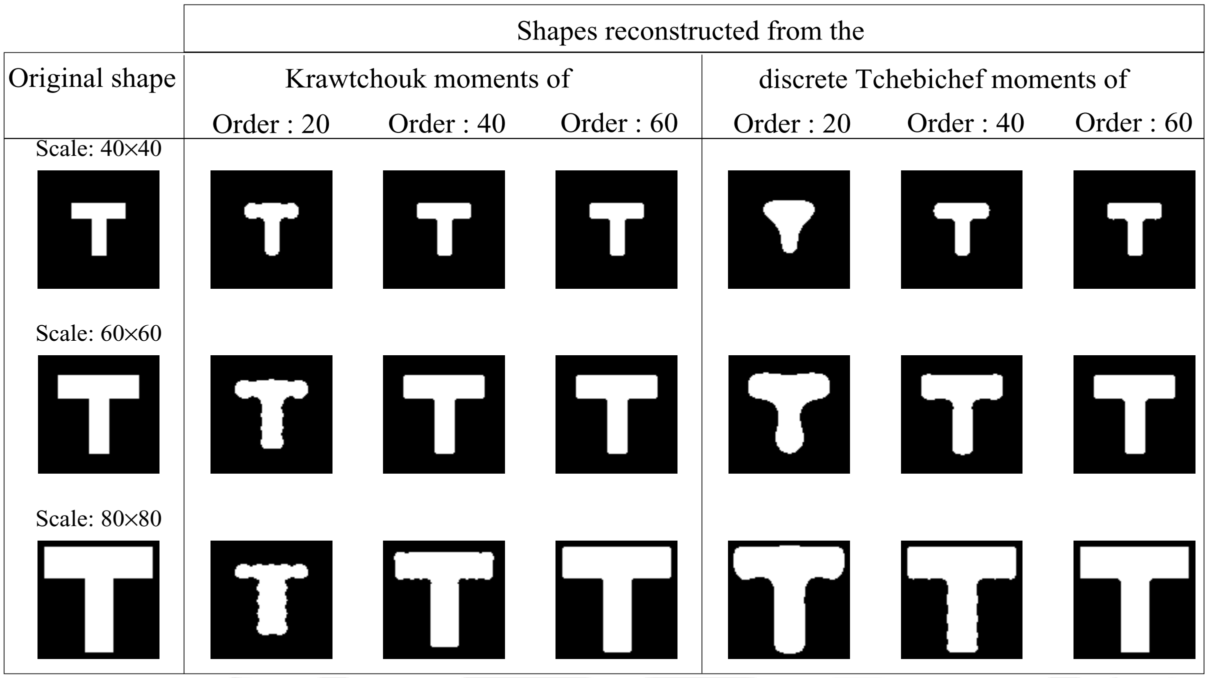


(a) Results of shape reconstruction obtained from DOM based approximations at various orders $(n+m)$, such that $n = m$.

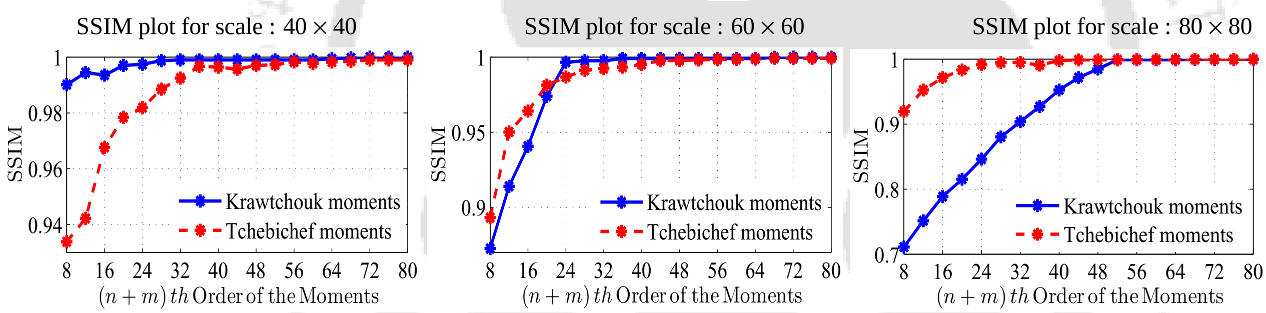


(b) Comparative plot of the SSIM index values obtained for different values of order $(n+m)$.

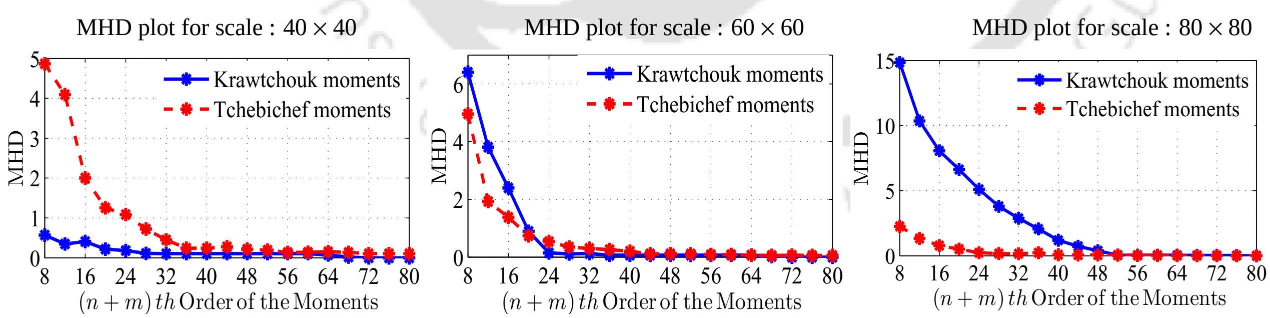


(c) Comparative plot of the MHD values obtained for different values of order $(n+m)$.

**Figure 3.15:** Illustration of reconstruction accuracy for varying orders of DOP based approximations of the shape of character 'T'. The shape is composed of two wide-deep concave segments. The values of the SSIM index and the MHD show that the WKP based approximations give high reconstruction accuracy at scale $40 \times 40$. At scale $60 \times 60$, the performance of both the moments are very close in terms of SSIM index and MHD. The DTP based approximation results in excessive smoothing. For scale $80 \times 80$, the DTP based approximation shows better performance. For scale $40 \times 40$, the accuracy of DTPs at lower orders is reduced due to excessive smoothing and for scale $80 \times 80$, the performance of WKPs at lower orders is affected due to the compact spatial support of the polynomials.

of a low spatial frequency region. The plots of the SSIM index and the MHD obtained between DOM based approximation and the original shape are shown in Figure 3.12(b) and Figure 3.12(c) respectively. From the values obtained, we infer that the WKP based reconstruction yields higher representation accuracy for the scales of $40 \times 40$ and $60 \times 60$. From the corresponding reconstructed shapes shown in Figure 3.12(a), it is evident that the shallow concavities are accurately reconstructed in the Krawtchouk moments based approximation. We observe that the DTPs require higher orders to accurately approximate the shallow concave segments. Since the shape is composed of a low spatial frequency region, the lower order DTP based approximations at higher scale $80 \times 80$ is comparatively superior. Though, the performance of lower order WKPs is limited due to compact support, it should be noted that the concavities are better represented in the WKP based approximation of the shapes at various scales.

The star-shaped polygons presented in Figure 3.13 and Figure 3.14 are composed of deep concave segments exhibiting high spatial frequency regions. Particularly, the polygon in Figure 3.14 exhibits comparatively more structural variations. The reconstructed shapes shown in Figure 3.13(a) and Figure 3.14(a) show that the WKP based approximation results in perceptually more similar reconstruction than the DTPs based approximation. The plots of the SSIM index and the MHD values also confirm the efficiency of the WKPs. By comparing the results obtained for the three different star-shaped polygons, we can infer that the DTPs are not efficient in accurately representing the sharp transitions such as the concave segments of the shapes. The efficiency of the DTPs decreases if the shape consists of more high spatial frequency regions. On the other hand, even the lower order Krawtchouk moments are more efficient in representing the high spatial frequency regions in the star-shaped polygons discussed above.

Similar evaluations are performed on the geometric shapes shown in Figure 3.11. Accordingly, the evaluations reflect the behaviour of the DOMs in representing shapes composed of deep concave segments of various widths. Figure 3.15 illustrates the efficiency of the DOMs in representing the shape of character T. The T-shape consists of only two deep concave segments with less number of transitions between the background and the foreground. However, the T-shape is composed of two regions of different spatial supports and in comparison to the cross-shaped and fork-shaped polygons, the T-shape exhibits less structural variations. From the reconstructed shapes shown in Figure 3.15(a), it is evident that at lower order approximations the WKPs result in better approximation of the sharp structural details. The plots of the SSIM index and the MHD show that at lower scales, the performance of the Krawtchouk moments is significantly better than the DTP based approximations. As the scale increases to $60 \times 60$, the efficiency of the DOPs in terms of the SSIM index and the MHD

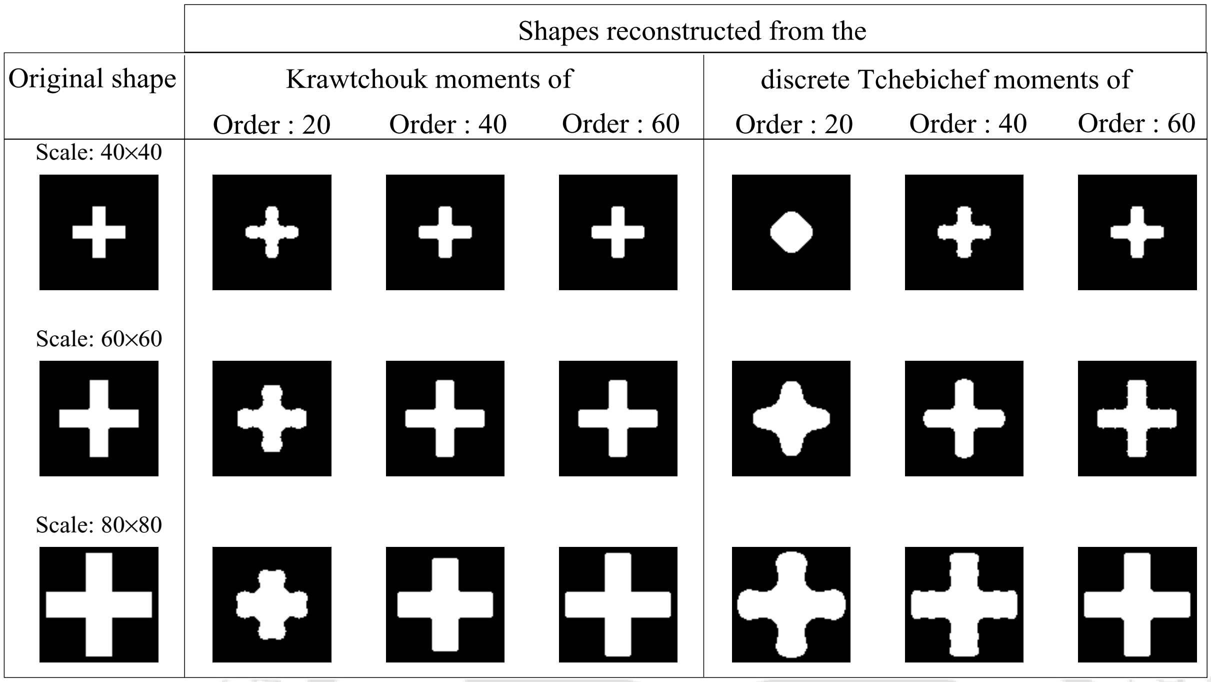


(a) Results of shape reconstruction obtained from DOM based approximations at various orders $(n + m)$, such that $n = m$.

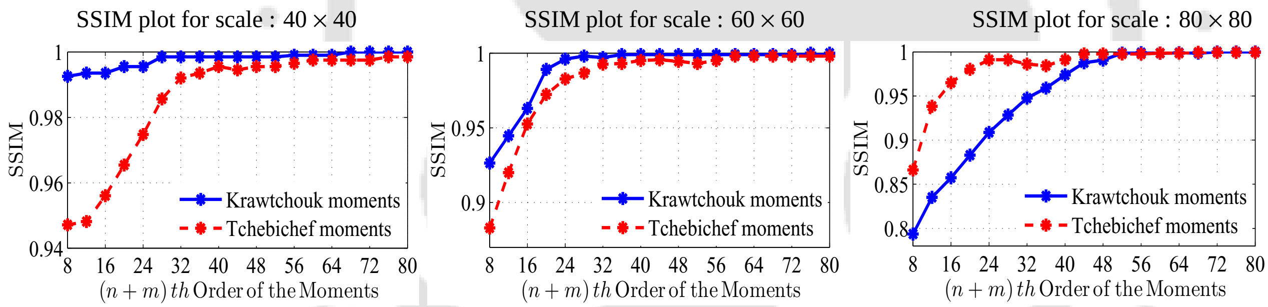


(b) Comparative plot of the SSIM index values obtained for different values of order $(n + m)$.

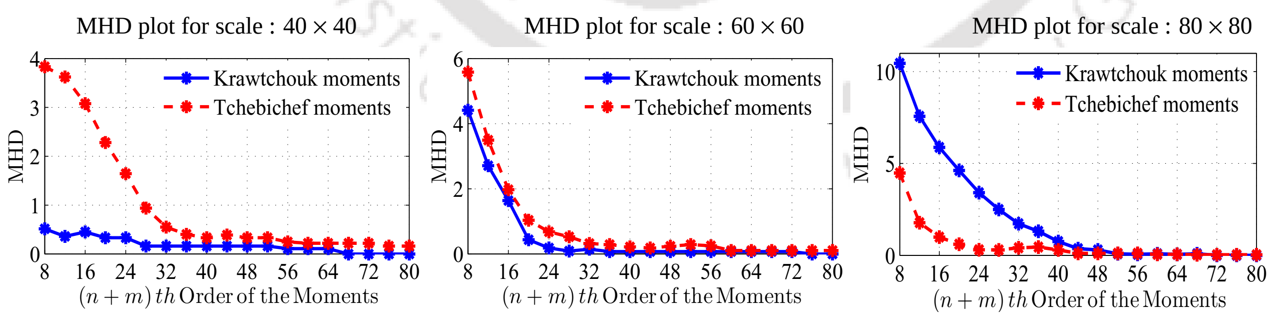


(c) Comparative plot of the MHD values obtained for different values of order $(n + m)$.

**Figure 3.16:** Illustration of reconstruction accuracy with respect to the cross-shaped polygon. The shape is composed of four concave segments of same width and depth. The SSIM index and the MHD show that the WKP based approximations give high reconstruction accuracy for scales $40 \times 40$ and $60 \times 60$. The shapes reconstructed from DTP based approximation are over-smoothened. At higher scale $80 \times 80$, the spatial support of the lower order WKPs is not sufficiently large and hence, the reconstruction error is more at these orders.

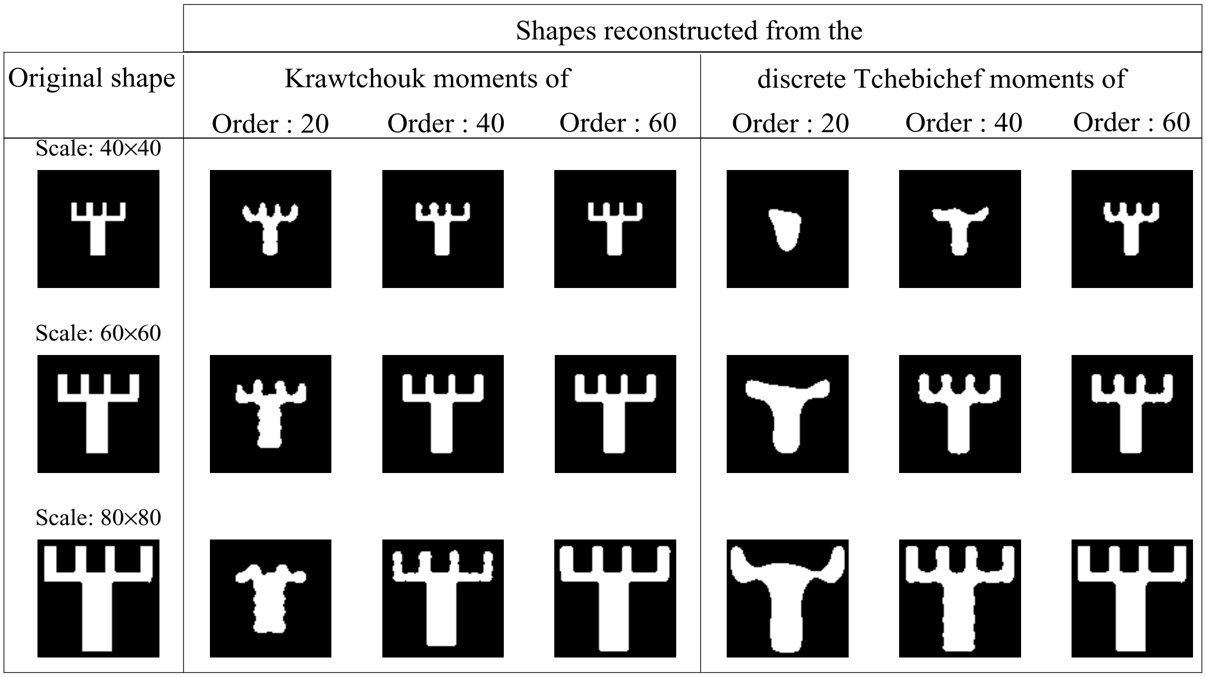


(a) Results of shape reconstruction obtained from DOM based approximations at various orders $(n + m)$, such that $n = m$.

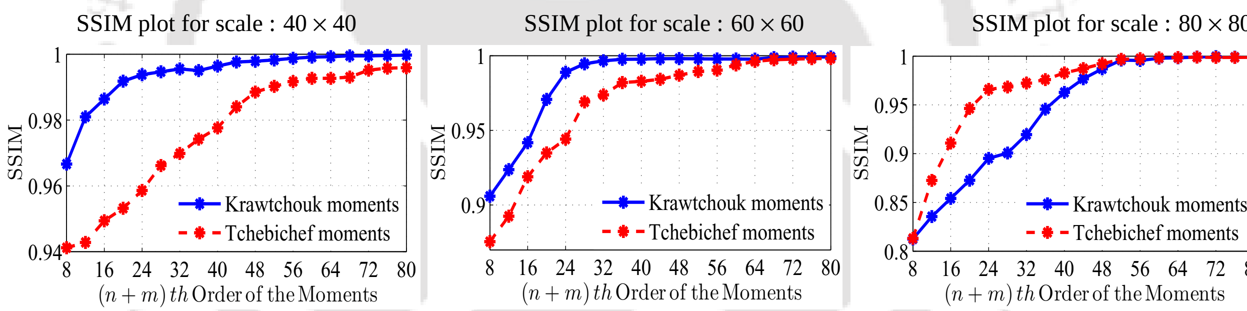


(b) Comparative plot of the SSIM index values obtained for different values of order $(n + m)$.

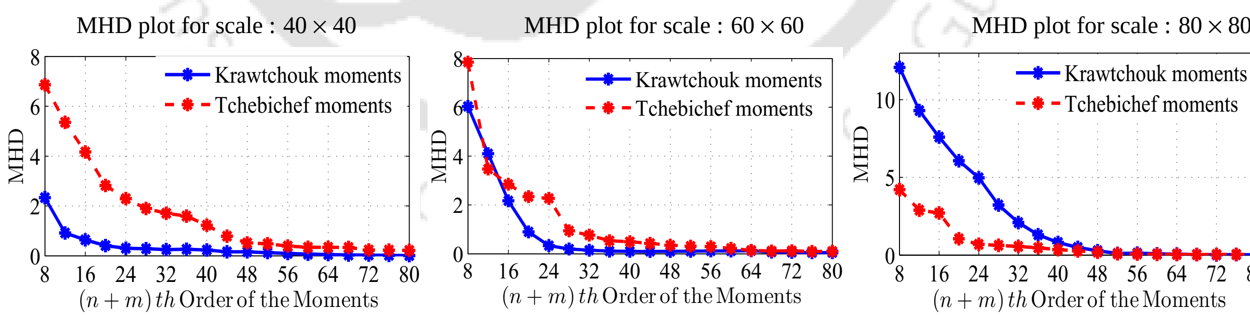


(c) Comparative plot of the MHD values obtained for different values of order $(n + m)$.

**Figure 3.17:** Illustration of reconstruction accuracy with respect to a fork-shaped polygon. The shape is a high spatial frequency structure consisting of five concave segments of different width and depth. The accuracy in reconstruction evaluated in terms of the SSIM index and the MHD show that the Krawtchouk moments based approximation is comparatively high for scales $40 \times 40$ and $60 \times 60$. It is observed that the shapes reconstructed from Tchebichef moments are more smoothened and the high spatial frequency regions are not properly reconstructed at lower orders. At a higher scale of $80 \times 80$, the accuracy of the WKP based approximation is poor due to the limited spatial support of the polynomial basis.

are very close even at lower orders.

The cross-shaped polygon illustrated in Figure 3.16 consists of more concave segments and exhibits more structural details than the T-shape. In comparison to the behaviour of DTPs in approximating the T-shape, we can observe that its performance is decreased in approximating the cross-shaped polygon. This can be clearly inferred by comparing the plots in Figure 3.15(b) and Figure 3.16(b). The DTPs require comparatively higher orders for approximating the cross-shaped polygon. Similarly, by comparing the plots in Figure 3.15(c) and Figure 3.16(c), we can infer that the order of the DTPs required for approximating shapes of scale $80 \times 80$ depends on the complexity of the shape i.e., the structural details. It can observed that the order of the DTPs required for accurately representing the cross-shaped polygon at scale $80 \times 80$ is more than that required for the T-shape.

Similar variations in the performance of the DOPs can be observed from the results obtained for the approximation of fork-shaped polygons of various scales. The fork-shaped polygon consists of more concave segments than the T-shape and the cross-shaped polygons. For scales $40 \times 40$ and $60 \times 60$, the WKP based approximation recovers the spatial structures of the fork-shaped polygon, whereas the DTPs result in excessively smoothened reconstruction. At a higher scale of $80 \times 80$, the concavities are recovered well by the Krawtchouk moments but their performance is limited due to their compact spatial support at lower orders. From the values of SSIM index and the MHD in shown Figure 3.17(c), it is clear that the order of DTPs required for accurate reconstruction has increased in comparison to the T-shape and the cross-shaped polygons.

From the above analysis, we infer that the performance of the DOPs depends on the scale of the shape and the structural characteristics. Accordingly, the characteristics of the WKPs and the DTPs in representing different shapes can be summarised as follows.

(i) The Krawtchouk moments are efficient when the shape region is sufficiently spanned by the corresponding WKPs. The WKPs have compact supports at lower orders and behave as spatially localised functions. Further, as explained in Section 3.7, the peak frequencies '$\omega_p$' of the lower order WKPs is higher than the peak frequencies of the DTPs. Therefore, the lower order Krawtchouk moments are comparatively more efficient in approximating regions with high spatial frequencies and smaller spatial supports.

(ii) The DTPs have wider support and for any order the support is equal to the size of the image. This implies that the Tchebichef moments are global functions. Hence, the DTPs are better than the WKPs in approximating shapes composed of wide regions of low spatial frequencies such as the shapes composed of convex segments and shallow concavities. For complex shapes composed of several high frequency structures, the DTPs result in excessive smoothing.

(iii) In terms of the data compaction, we can infer that for approximating shapes at lower scales, the WKPs require less order than the DTPs. As the scale increases, the WKPs require higher orders than the DTPs. However, it should be noted that the optimal choice of the order of DTPs in approximating shapes at higher scales is greatly influenced by the structural characteristics of the shape. When the shape is composed of high spatial frequency structures, the WKPs are superior to the DTPs even if the scale of the shape is high.

Thus, we can infer that the WKPs offer better data compaction at lower scales and at these scales, the performance of the WKPs is consistently superior irrespective of the structural characteristics of the shapes. At higher scales, the WKPs offer better data compaction in the case of shapes with high spatial frequencies. Conversely, at higher scales, the data compaction capability of the DTPs is high for shapes with less structural variations.

#### 3.8.2.4 Noise versus reconstruction accuracy

During the binarisation of an image, segmentation errors such as isolated pixels within a uniform region occur due to the presence of the acquisition noise in the gray-scale image and improper threshold selection. These pixels appear as extraneous foreground pixels in the background and extraneous background pixels in the foreground. This results in a noisy binary shape and the resulting binary noise is known as the *salt and pepper noise*. Therefore, noise removal is an essential task in shape representation.

The noise pixels in an image are randomly distributed and they exhibit higher spatial frequencies than the image structures. The study on the spectral characteristics of the WKPs and the DTPs suggests that the polynomials up to certain order may behave like smoothing functions and result in noise removal. The shapes reconstructed from the corresponding moment based approximations can be expected to be denoised.

The objective of this set of experiments is to study the performance of the DOPs in accurately reconstructing shapes that are degraded by different levels of noise. The noisy shape $f_{noisy}$ is obtained by allowing a fixed percentage of randomly selected pixel values to be altered to zero or one with equal probabilities. In this experiment, the robustness of the DOPs is verified by the varying the noise level $p_n$ between 0.05 to 0.6.

Based on the results in Section 3.8.2.3, the size of the shape is fixed at $60 \times 60$ and the image grid size is fixed at $90 \times 90$. The order of the WKPs and the DTPs is chosen as $(n + m) = 60$. The parameters $p_1$ and $p_2$ of the WKPs are fixed at 0.5. The reconstruction accuracy of the DOMs is evaluated in terms of the SSIM index

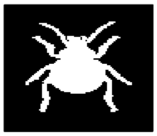


(a)

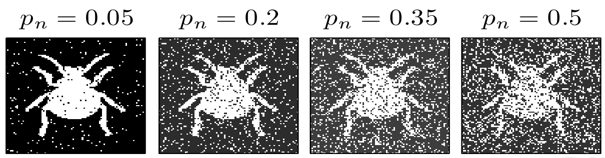


(b) Noisy samples of the original shape in Figure 3.18(a).

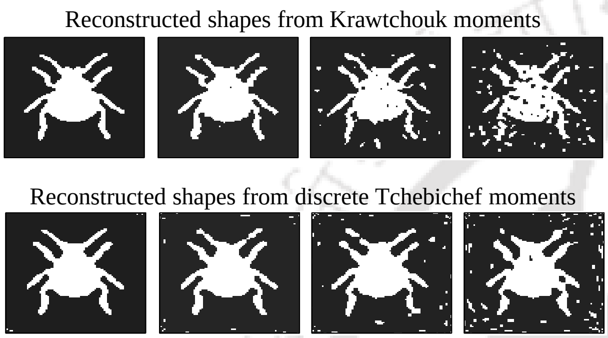


(c) Results of shapes reconstructed from the DOM based approximations of the noisy samples illustrated in Figure 3.18(b). The order of the moments is chosen as $(n + m) = 60$.

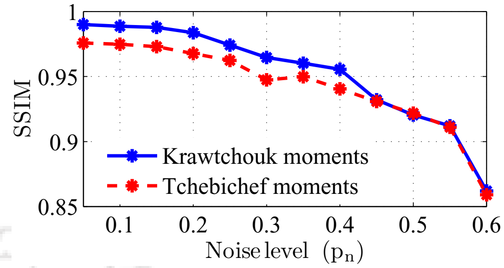


(d) Plot of the SSIM index values obtained for the shapes reconstructed with respect to varying $p_n$.

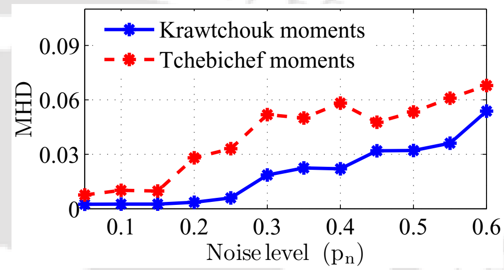


(e) Plot of the MHD values obtained for different values of noise levels ($p_n$).

**Figure 3.18:** Illustration of the reconstruction accuracy of the DOMs with respect to a beetle shape that is degraded by binary noise of level $p_n$. For different values of $p_n$, the shapes reconstructed from the Krawtchouk moments are more accurate than those reconstructed from the discrete Tchebichef moments. The high spatial frequency regions in the beetle shape are efficiently recovered by the Krawtchouk moments. For high noise levels, the significant noise pixels in the foreground region are not sufficiently denoised in WKP based approximation. The discrete Tchebichef moments results in over-smoothening of the structural features and a few noise pixels are retained in the background region of the reconstructed shape. The values of the SSIM index and the MHD suggest that the Krawtchouk moments perform better than the discrete Tchebichef moments at lower noise levels. As the noise level increases, the number of noise pixels retained in DOP based approximation increases.

and the MHD. Different sets of shapes with various curvature properties are used and the results are discussed as below.

The illustrations in Figure 3.18 demonstrate the noise sensitivity of the DOMs in the case of the beetle shape shown in Figure 3.18(a). The samples of beetle shape corrupted by noise of different levels are shown in Figure 3.18(b). The shapes reconstructed from the Krawtchouk and the discrete Tchebichef moments based approximation of the noisy shapes are given in Figure 3.18(c). From the results, it is observed that the shape reconstructed from the Krawtchouk moments is perceptually closer to the original shape in comparison to the discrete Tchebichef moment based approximations. The high spatial frequency structures in the beetle shape are properly recovered by the Krawtchouk moments. The reconstruction accuracy of the DOMs in terms of the SSIM index and the MHD is shown in Figure 3.18(d) and Figure 3.18(e). For low noise levels, the Krawtchouk

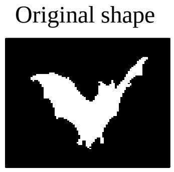


(a)

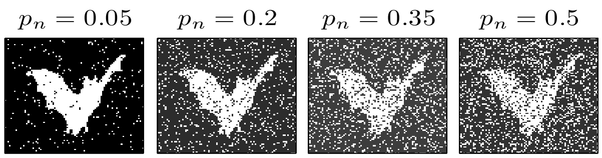


(b) Noisy samples of the bird shape in Figure 3.19(a).

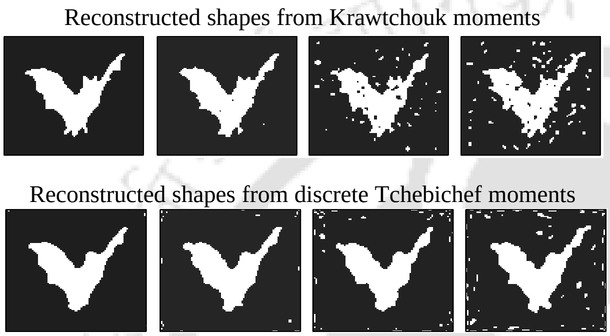


(c) Results of shapes reconstructed from the DOM based approximations of the noisy samples illustrated in Figure 3.19(b).

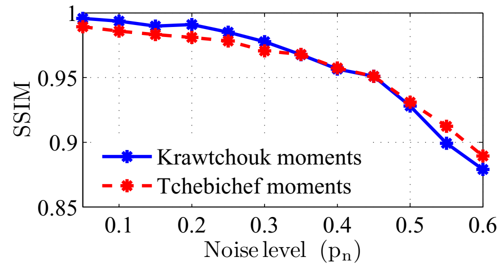


(d) Plot of the SSIM index values obtained for the shapes reconstructed with respect to different levels of $p_n$.

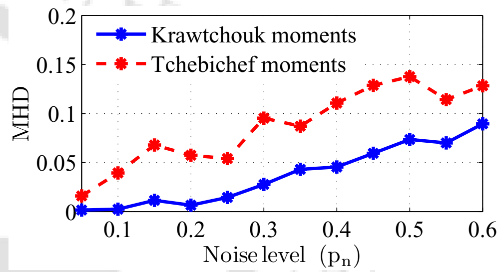


(e) Plot of the MHD values obtained with respect to varying levels of noise ($p_n$).

**Figure 3.19:** Illustration of the noise sensitivity of the DOMs with respect to a bird shape. The order of the moments is chosen as $(n + m) = 60$. The shapes reconstructed from the Krawtchouk moments based approximation exhibit comparatively higher perceptual similarity to the original shape. The values of the SSIM index and the MHD suggest that for $p_n \leq 0.35$, the Krawtchouk moments are more robust to noise than the discrete Tchebichef moments and result in high reconstruction efficiency. As $p_n$ increases, both the moments result in poor denoising efficiency. The discrete Tchebichef moments exhibit sensitivity to noise along the image border and the Krawtchouk moments are sensitive to noise around the centre the image.

moments exhibit denoising efficiency higher than that of the discrete Tchebichef moments. With the increase in the noise levels, the WKP based approximation becomes sensitive to the noise pixels that lie within and around the neighbourhood of the centre of the image. The DTP based reconstruction results in excessively smoothened shapes. As the level of noise increases, the discrete Tchebichef moments become sensitive to the noise pixels that lie along the image borders.

Figure 3.19 presents the results obtained for the shape of a bird. The original and the noisy shapes are shown in Figure 3.19(a) and Figure 3.19(b) respectively. The reconstructed shapes given in Figure 3.19(c) indicate that the Krawtchouk moments are efficient in restoring the shape. The minute structural features on the shape boundary are efficiently recovered from the noisy shape. The plots of the SSIM index and the MHD are shown in Figure 3.19(d) and Figure 3.19(e) respectively. With the increase in the noise levels, the object region becomes more degraded in the WKP based approximation resulting in a low SSIM index. On the contrary, the boundary of the shapes reconstructed from the discrete Tchebichef moments are excessively smoothened

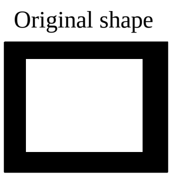


(a)

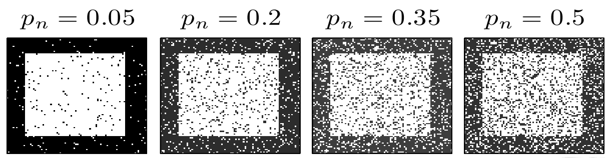


(b) Noisy samples of the original shape in Figure 3.20(a).

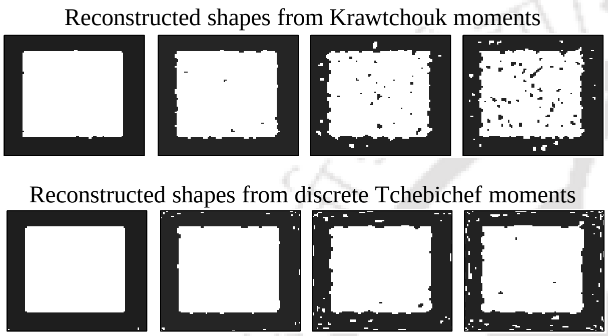


(c) Shapes reconstructed from the DOM based approximations of the noisy samples illustrated in Figure 3.20(b). The order of the moments are chosen as $(n + m) = 60$.

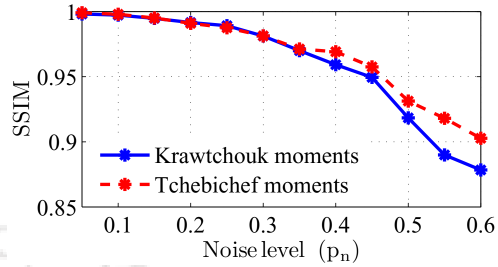


(d) Plot of the SSIM index values obtained with respect to different levels of noise ($p_n$).

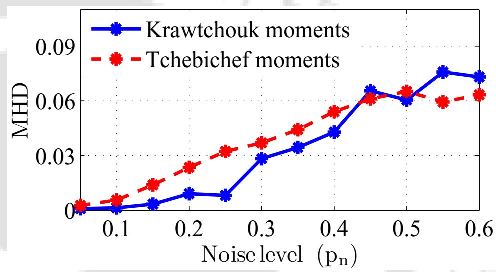


(e) Plot of the MHD values obtained for different values of $p_n$.

**Figure 3.20:** Illustration of the denoising efficiency of the DOMs with respect to the square shape. The shape reconstructed from the Krawtchouk and the discrete Tchebichef moments exhibits similar perceptual quality with respect to the original shape. Hence, the corresponding SSIM values are almost similar for lower $p_n$. With the increase in $p_n$, the number of noise pixels are more in the background region for discrete Tchebichef moments based approximation and noise occurs in the foreground region for Krawtchouk moments based approximation. The values of the SSIM index and the MHD indicate that the performance of the WKP based approximation is comparatively poor for higher noise levels.

resulting in lower MHD values. As the noise level increases, the noise pixels present in the background region and along the image borders are retained in DTP based approximation.

The experimental results obtained for the square shape is presented in Figure 3.20. The original shape and the noisy samples simulated for varying levels of noise are shown in Figure 3.20(a) and Figure 3.20(b) respectively. The shapes reconstructed from the Krawtchouk and the discrete Tchebichef moments are shown in Figure 3.20(c). The plots of the SSIM index and the MHD are given in Figure 3.20(d) and 3.20(e) respectively. From the results, it is evident that the performances of the WKP based and the DTP based reconstructions are similar at lower noise levels. As the noise level increases, the degradations in the WKP based reconstruction is more in the DTP based reconstruction.

From the above results on noise sensitivity, it is evident that the performance of the DOPs is significantly better for $p_n \leq 0.3$. It is inferred that the WKPs are efficient in discriminating the high spatial frequency structures of the shape from the noise pixels. As a result, the reconstruction accuracy is comparatively higher for

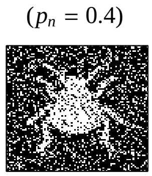


(a) Noisy shape

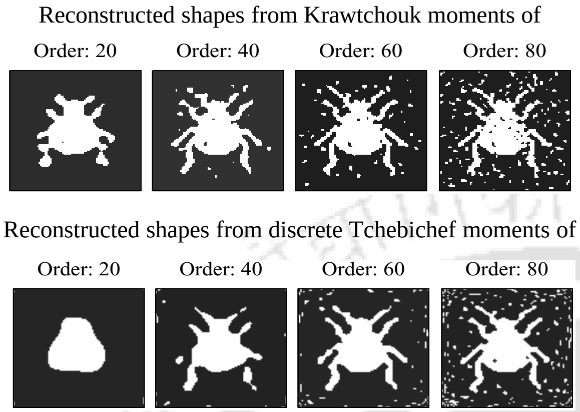


(b) Shapes reconstructed from the DOM based approximation of the noisy sample in Figure 3.21(a).

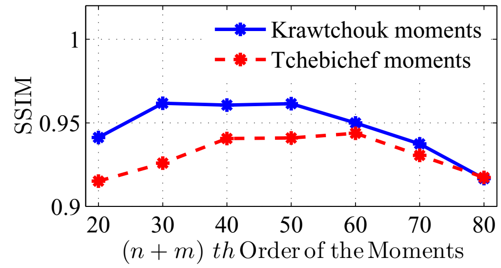


(c) Plot of the SSIM index values versus the order of the moments.

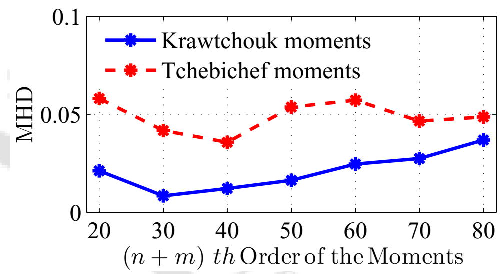


(d) Plot of the MHD values versus the order of the moments.

**Figure 3.21:** Illustration of the robustness of the DOMs to noise with respect to varying orders of DOPs based approximation of the beetle shape. With the increase in order, most of the noise pixels are recovered in reconstruction. Particularly, the Krawtchouk moments exhibit more sensitivity towards noise in the foreground region. As the order increases, the discrete Tchebichef moments result in better reconstruction of the high spatial frequency structures in the beetle shape. Simultaneously, the reconstruction quality gets degraded due to the recovery of more noise pixels in the background region. The SSIM index and the MHD suggest that the Krawtchouk moments exhibit better performance than the discrete Tchebichef moments in most of the orders.

the WKP based approximation. At these noise levels, the DTP based approximation results in over-smoothening of shapes.

It is observed that the robustness of the DOPs decreases at higher noise levels and they exhibit varied behaviour. For $0 \leq x \leq N$, the STFT plots in Figure 3.7 and Figure 3.8 have shown that the frequency response of the DOPs varies as the value of $x$ deviate from $x = N/2$. The WKPs exhibit higher frequency response at the data points around $x = N/2$ and the frequency response decreases as the value of $x$ gets close to 0 and $N$. As a result, the WKPs are more sensitive to the high spatial frequency structures that lie around the centre of the image. Unlike the WKPs, the DTPs exhibit lower frequency response at the data points around $x = N/2$ and the frequency response increases as the value of $x$ gets close to 0 and $N$. Therefore, the DTPs are more sensitive to the high spatial frequency components lying along the image borders.

Considering that the DOMs are computed with respect to the centre of the shape, it can be inferred that the robustness of the WKPs to significant noise pixels around the centre of the image decreases at higher noise levels. On the other hand, the DTPs result in smoothening of the pixels around the centre of the image and are more sensitive to the noise pixels in the background region that lie along the image borders.

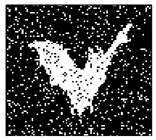


(a) Noisy shape

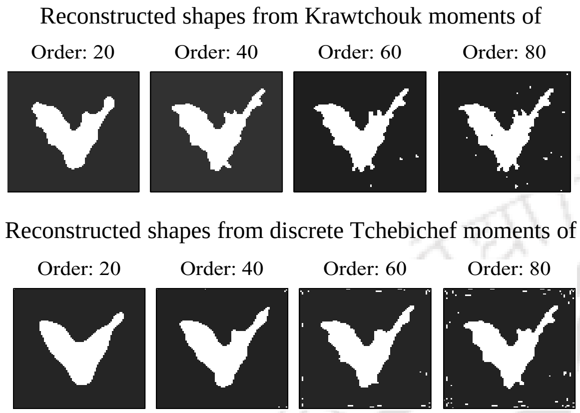


(b) Results of the shapes reconstructed from DOMs of various orders.

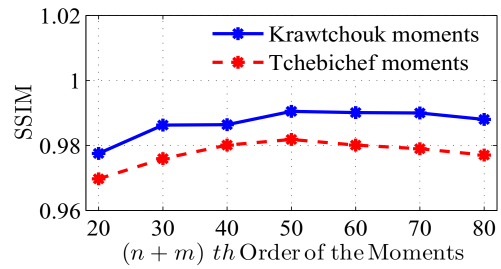


(c) Plot of the SSIM index values versus order of the moments.

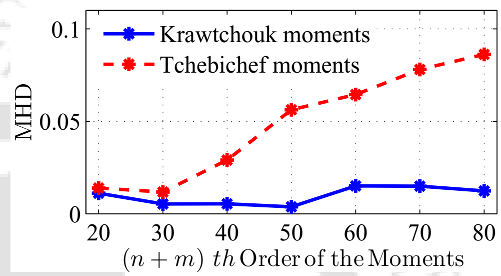


(d) Plot of the MHD values versus order of the moments.

**Figure 3.22:** Illustration of noise sensitivity of the different orders of DOM based reconstruction of the bird shape. With the increase in the order, the moments exhibit more sensitivity to noise. The higher order discrete Tchebichef moments offer better reconstruction of the high spatial frequency structures in the bird shape. However, the reconstruction quality is affected due to the recovery of more noise pixels in the background region. The shapes reconstructed from the Krawtchouk moments exhibit noise in the foreground as well as the background region. The performance in terms of the SSIM index and the MHD indicates that the Krawtchouk moments are better than the discrete Tchebichef moments upto certain orders.

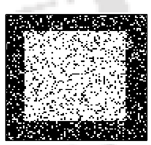


(a) Noisy shape

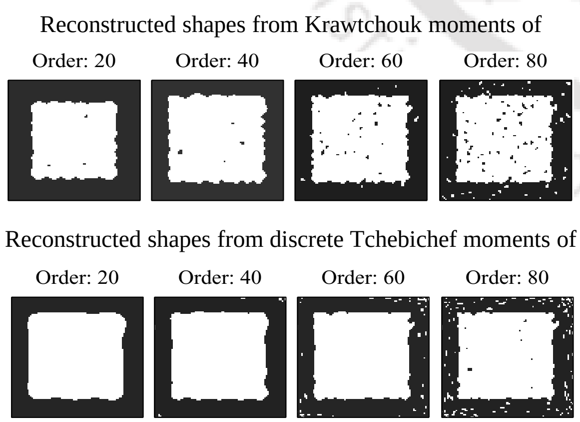


(b) Results of shape reconstruction from the higher order DOMs computed from the noisy shape in Figure 3.23(a).

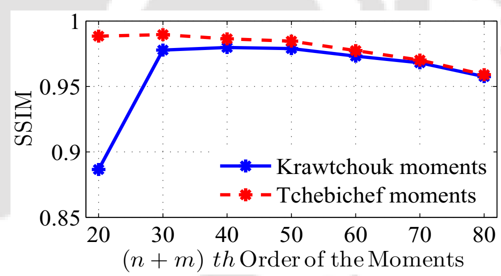


(c) Plot of the SSIM index values versus order of the moments.

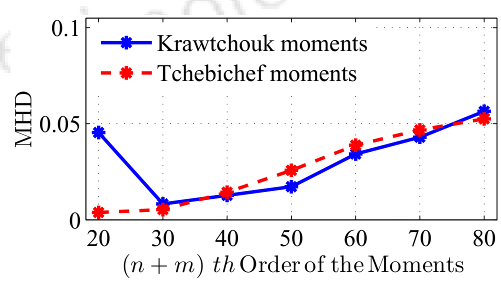


(d) Plot of the MHD values versus order of the moments.

**Figure 3.23:** Illustration of noise sensitivity of DOM based approximation of the square shape at various orders. The values of SSIM index and MHD indicate that up to $(n+m) = 50$, the discrete Tchebichef moments exhibit better performance than the Krawtchouk moments.

Similar experiments were performed in order to evaluate the noise sensitivity of the DOMs at different orders of approximation. Hence, the performance of the DOMs in recovering the shape from a noisy sample is tested by varying the order of the approximation. The experimental results obtained for the beetle, bird and the square shapes corrupted by different noise levels are presented in Figure 3.21, Figure 3.22 and Figure 3.23 respectively.

From the results, it is clear that at higher orders, the polynomials tend to behave like all-pass functions. Therefore, as the order increases the number of noise pixels in the recovered shapes also increases. The plots of the SSIM index and MHD in Figure 3.21, Figure 3.22 and Figure 3.23 show an increase in the reconstruction error with the increase in the order of the moments.

In Figure 3.21 and Figure 3.22, it is noticed that the structural degradation in the shapes reconstructed from the Krawtchouk moments is less than in the shapes reconstructed from the discrete Tchebichef moments. It is also observed that for higher order DTPs, the high spatial frequency structures of the shape are efficiently reconstructed. Despite this improvement, the performance of the discrete Tchebichef moments is marked by the large number of noise pixels left in the background region of the reconstructed shape. The denoising results obtained for the square shape are shown in Figure 3.23. From the plots of the SSIM index and the MHD, it is observed that the reconstruction error for the WKP based approximation is high at the lower orders. As the order increases, the performance of the Krawtchouk moments and the discrete Tchebichef moments becomes almost similar.

By consolidating the results in Figure 3.21, Figure 3.22 and Figure 3.23, it is observed that the reconstruction error for the WKP based approximation reaches its minimum approximately for $(n + m) = 50$. At this order, the spatial structures constituting the shape are effectively recovered and hence, they do not require higher order approximations. The DTPs require higher orders for recovering the high spatial frequency structures of the shapes. Even as the order increases, the noise sensitivity of the discrete Tchebichef moments increases, thus degrading the quality of the reconstructed shape.

### 3.8.3 Experiments on shape classification

The purpose of this study is to demonstrate the capability of the DOMs as features for shape classification.

The experiment is conducted on a dataset collected from the MPEG-7 (CE Shape-1, Part-B) database. The dataset consists of 400 samples of 20 different shape classes with 20 samples per shape class. Out of these, 40 samples are used for training and 360 samples are used for testing. Of the 40 training samples, 20 samples are undistorted shapes and the remaining 20 samples are distorted shapes.

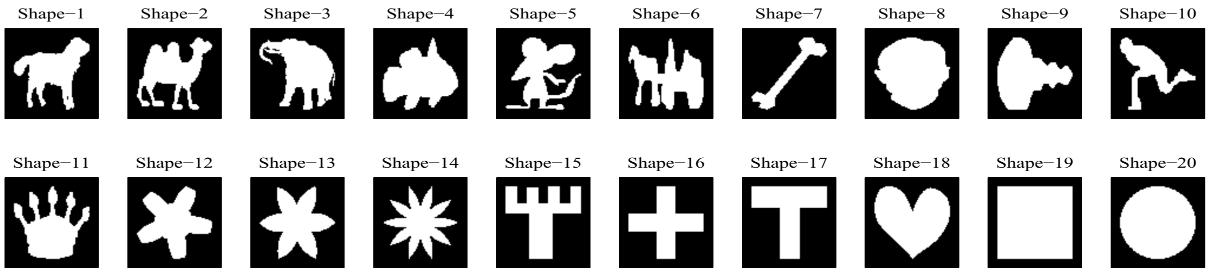


**Figure 3.24:** Illustration of undistorted training sample per shape class constituting the reference dataset.

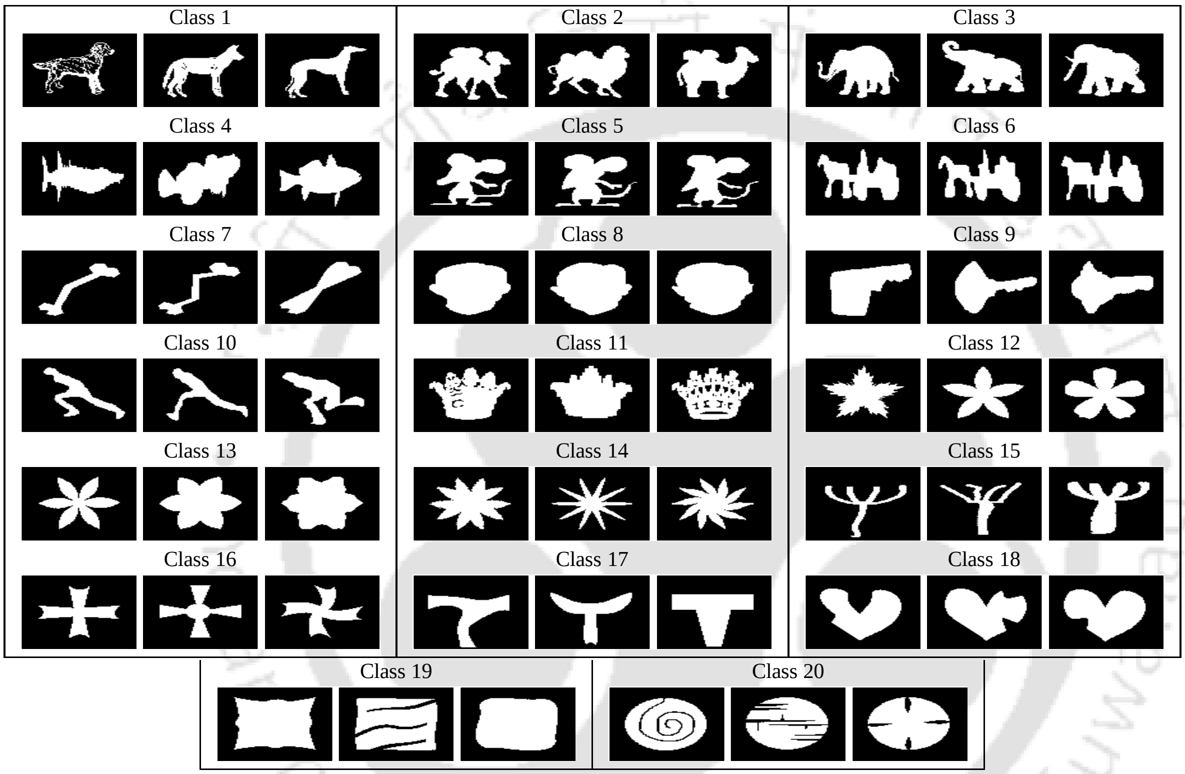


**Figure 3.25:** Examples of test samples contained in each shape class. The figure illustrates the shape defection in the test samples that are caused due to boundary distortion and segmentation errors.

Two sets of experiments are performed on shape classification. The first experiment is performed by using the 20 undistorted shapes for forming training set. Therefore, we have 1 training sample and 18 testing samples for each shape class. In the second experiment, the size of the training set is increased by including the remaining 20 samples of the undistorted shapes in the training set. Thus, the extended training set consists of 2 training samples per shape class.

The training samples used in the first experiment for shape classes are shown in Figure 3.24. The shape classes in the training set are labeled as Shape 1, Shape 2, Shape 3, $\cdots$, Shape 20. A few examples of the test samples for different shape classes are given in Figure 3.25. The shape classes belonging to the test data are labeled as Class 1, Class 2, $\cdots$, Class 20. It can be observed that the test dataset consists of shapes that

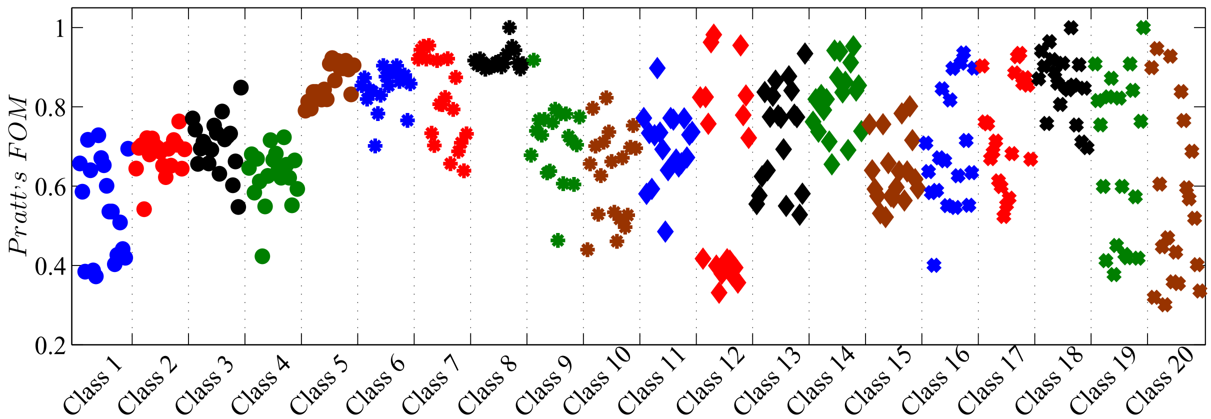


**Figure 3.26:** Plot of the Pratt's FOM values of the test samples with respect to the reference dataset. The measure indicates the deviation in the edge characteristics of the test sample in each class from the corresponding sample in the training set. The illustration signifies the intraclass distance between the test and the reference shapes.

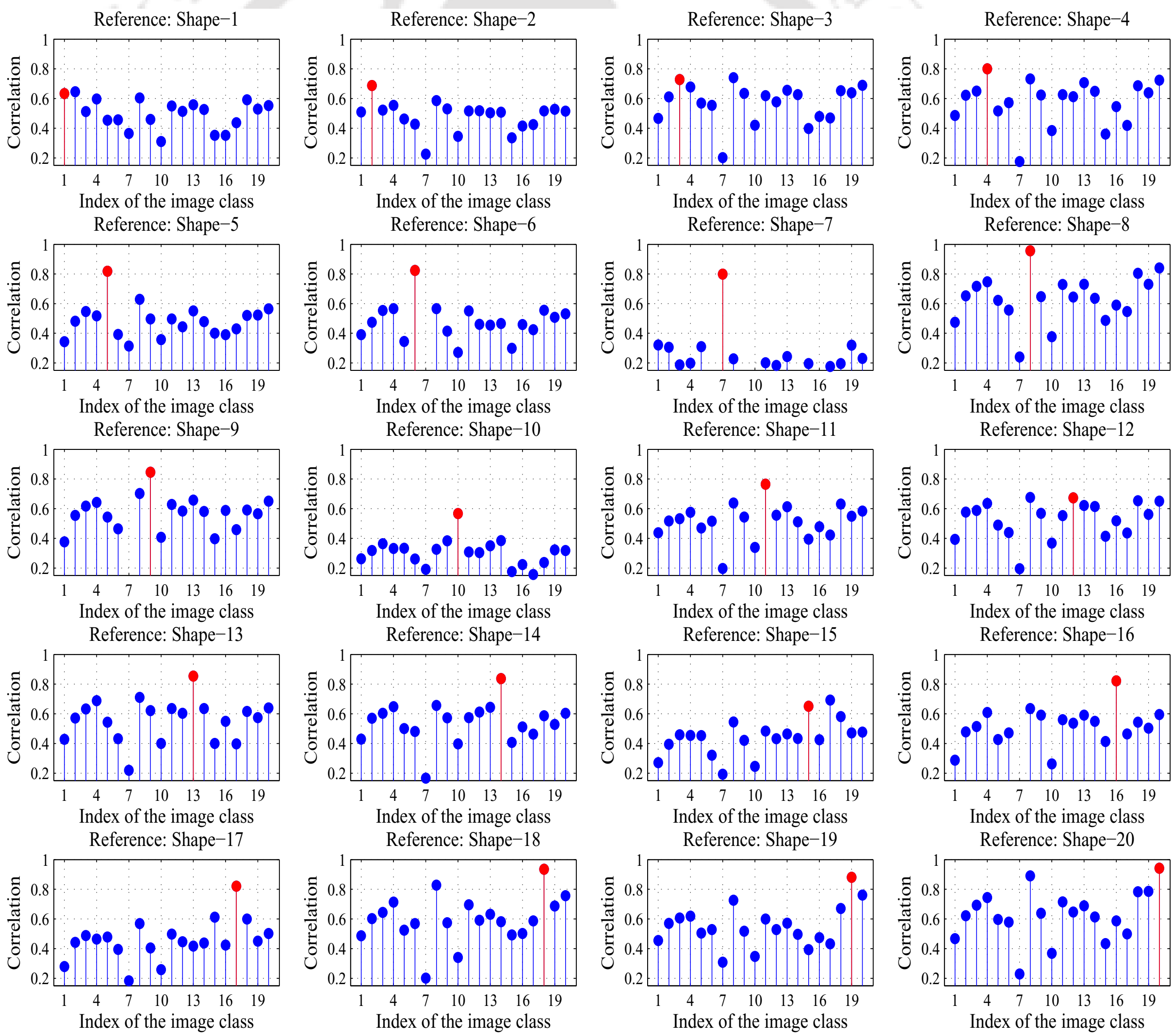


**Figure 3.27:** Illustration comparing the intraclass and the interclass distances between the samples in the database. The distance is measured in terms of the similarity in the spatial distribution of pixels. Hence, the correlation is used as the metric. The values of the correlation signify the similarity between the shapes.

are severely distorted due to shape defections such as segmentation errors and boundary distortion. It is quite evident that the shapes of the objects belonging to a class are perceptually similar but exhibit large differences in terms of structural features. Therefore, the intraclass distance between the samples is measured using the Pratt's figure-of-merit (FOM). The FOM is computed as [170, 171]

$$Pratt's\, FOM = \frac{1}{max\left\{N_s, N_v\right\}} \sum_{j=1}^{N_s} \frac{1}{1 + \alpha D_E\left(j\right)} \tag{3.85}$$

where, $N_v$ and $N_s$denote the number of edge pixels in the reference shape and the test shape respectively, $\alpha$ is the scaling constant and $D_E(j)$ is the distance from the $j^{th}$ edge pixel of the reference shape to the corresponding edge pixel in the test shape. In our experiments, $\alpha$ is chosen as $1/9$ in accordance with [171].

The plot illustrating the Pratt's FOM value obtained for each sample in the test dataset is given in Figure 3.26. The plot shows that most of the test samples belonging to class $5, 6, 7, 8$ and 18 exhibit similar edge characteristics with respect to the corresponding reference shape. In the case of samples belonging to other classes, the FOM value implies that the difference in terms of the edge characteristics is significant. The difference occurs due to shape defections as mentioned earlier.

Similarly, the intraclass and interclass distances between the samples belonging to different classes are measured in terms of the correlation coefficient. The correlation coefficient between the test $f_{test}$ and the reference $f_{ref}$ shapes is computed as

$$\frac{\sum\limits_{x=0}^{N}\sum\limits_{y=0}^{M}\left(f_{test}\left(x,y\right) - \mu_{f_{test}}\right)\left(f_{ref}\left(x,y\right) - \mu_{f_{ref}}\right)}{\sqrt{\sum\limits_{x=0}^{N}\sum\limits_{y=0}^{M}\left(f_{test}\left(x,y\right) - \mu_{f_{test}}\right)^2 \sum\limits_{x=0}^{N}\sum\limits_{y=0}^{M}\left(f_{ref}\left(x,y\right) - \mu_{f_{ref}}\right)^2}} \tag{3.86}$$

$\mu_{f_{test}}$ and $\mu_{f_{ref}}$ denotes the mean of the test and the reference shapes respectively. For ease, we refer the correlation coefficient as the correlation.

The plots of average correlation values obtained for each shape class with respect to a reference shape are shown in Figure 3.27. From the values of the correlation, we infer that some of the shape classes exhibit high interclass similarity along with the intraclass similarity. For example, the correlation values obtained for the Shape 1 reference class exhibits a high similarity with the test samples in its own group Class 1 and other group Class 2. Similarly, the test samples in Class 12, Class 13 and Class 14 exhibit high similarity to the reference class Shape 12. The test samples in Class 17 has high structural similarity with the reference class Shape 15. Therefore, the evaluation of the database in terms of the correlation implies that some of the shape shapes considered in the experiment are perceptually different but exhibit an intricate correlation in terms of the spatial arrangement of the pixels.

The shapes in the dataset are normalised for scale, translation and orientation changes. Hence, the dataset contains only the samples that are subject to severe shape distortion. The scale of the shape is normalised to $90 \times 90$ through the down-sampling or nearest neighbour interpolation. The translation normalization is achieved by shifting the centroid of the shape to the centre of the shape. Hence, the centroid of all the shapes are fixed at $(45, 45)$. The orientation of the shapes are manually corrected so that the shapes belonging to a class are oriented in the same direction. The shape features are derived by computing the Krawtchouk and the discrete Tchebichef moments of the normalised shapes.

The order of the polynomials for approximation is chosen based on the reconstruction accuracy. The classification is performed using a nearest neighbour classifier. Consider $\eta_s$ and $\eta_v$ as the feature vector of the test shape and the target shape ( in the trained set ) respectively. Then, the classification of $\eta_s$ using the nearest neighbour rule is given as

$$D_v(\eta_s, \eta_v) = \sum_{j=1}^{J} \left(\eta_{sj} - \eta_{vj}\right)^2 \tag{3.87}$$

$$\Omega_{match} = \arg\min_{\{v\}} (D_v) .$$

Here, $v$ denotes the index of shapes in the training set and $J$ is the dimension of a feature vector.

The classification accuracy of the DOM-based method is compared with that of the MHD based matching method. The comprehensive scores of the classification results obtained for each shape class in the test data are given through the plot in Figure 3.28. The classification results obtained for the Krawtchouk and the discrete Tchebichef moments are almost similar and their over-all classification rate is better than that of the MHD matching. Therefore, it is evident that the Krawtchouk and the discrete Tchebichef moments are efficient as features for shape classification.

From the results, we note that most of the mismatch has occurred between the shapes with less interclass distance. For example, the test samples in Class 2 is mismatched with the reference Shape 1. Similar correlation in terms of the correlation in Figure 3.27 can be observed between the mismatched shapes in Classes 3, 4, 12 and 15. The mismatched samples in Class 13 are perceptually more similar to the training sample of Shape 8 rather than that of Shape 13. In the case of Class 1, the mismatch is due to severe segmentation error. The mismatch in Class 11 has occurred because, the misclassified test samples exhibit large deviations in the edge characteristics with respect to its reference sample Shape 11. It can be observed that the shape boundaries of

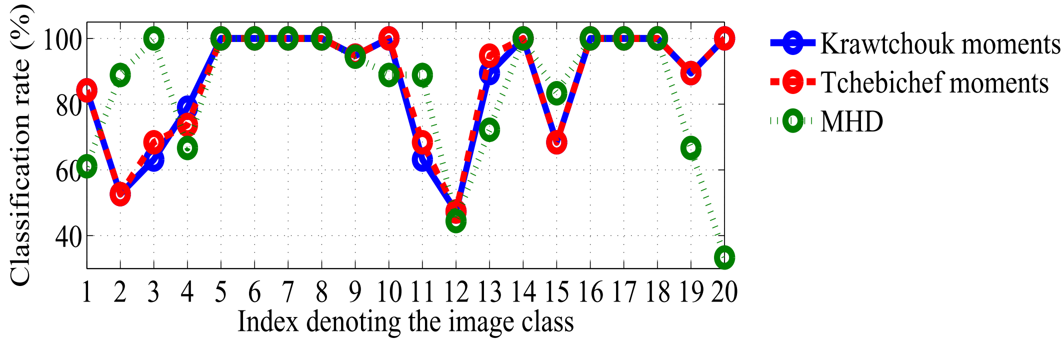


**Figure 3.28:** Comparison of the consolidated classification results obtained with respect to each class. The results are obtained for 1 training sample per shape class and 18 testing samples per shape class. The overall classification rate obtained for discrete Tchebichef moments as features is 87.11%. The overall classification rate for Krawtchouk moments as features is 86.58%. The overall classification rate for MHD matching is 86%.

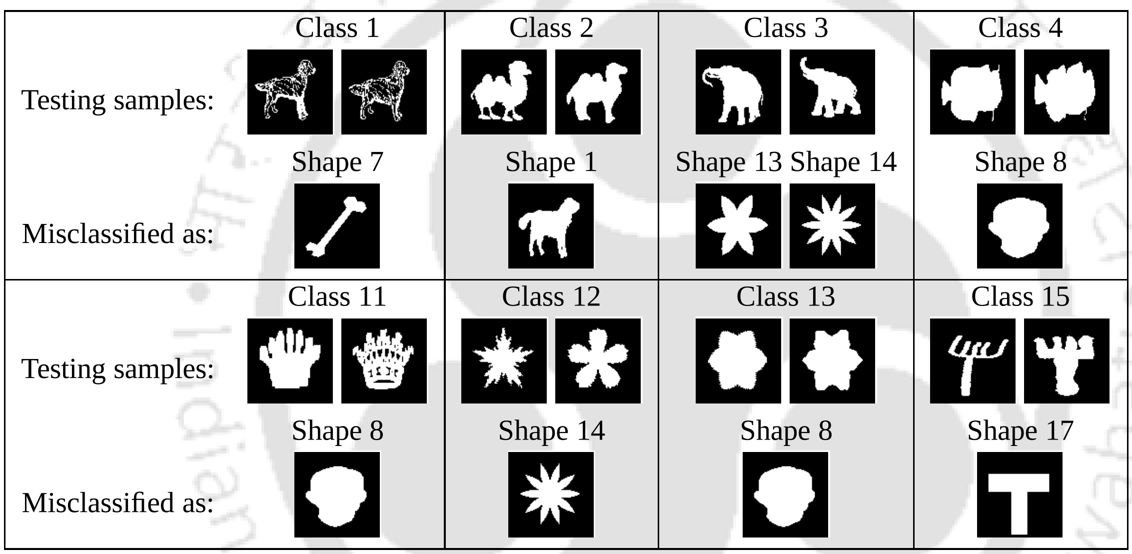


**Figure 3.29:** Results from the experiment on shape classification using 1 training sample per shape class. Examples of the testing samples exhibiting higher misclassification with respect to both the Krawtchouk and the discrete Tchebichef moments as features. It is observed that most of the mismatches have occurred between the shape classes with less interclass distances. The spatial similarity between the misclassified test sample and the corresponding match in the reference set can be obtained from the respective plots in Figure 3.27.

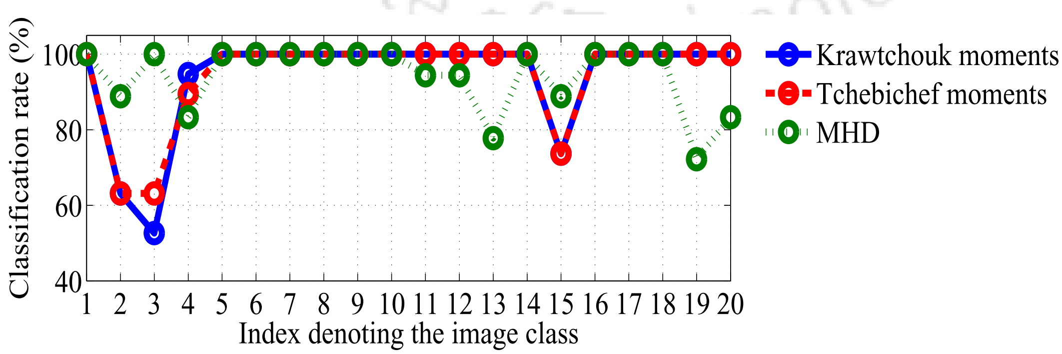


**Figure 3.30:** Comparison of the comprehensive scores of the classification results obtained with respect to each class. The results are obtained for 2 training samples per shape class and 18 testing samples per shape class. The overall classification rate obtained for discrete Tchebichef moments as features is 94.17%. The overall classification rate for Krawtchouk moments as features is 94.44%. The overall classification rate for MHD matching is 94.16%. The number of classes misclassified is comparatively higher in MHD matching.

the misclassified test samples in Class 11 and the reference Shape 8 are almost similar. Hence, the test samples of Class 11 shown in Figure 3.27 can be perceived as the distorted forms of Shape 8.

Despite these misclassifications, it has to be noted that the DOMs exhibit higher classification accuracy for several other test samples that are subject to severe structural distortions. For example, the test samples of Classes 18, 19 and 20 as shown in Figure 3.25 exhibit variations due to segmentation errors. However, the shapes belonging to these classes have higher classification accuracies. The structural variations in these shape classes can be verified from the plot of Pratt's FOM values in Figure 3.26. Similarly, the test samples in Classes 7, 9, 10, 16 and 17 illustrated in Figure 3.25 exhibit significant deviations in the structural characteristics and the corresponding values of intraclass distance can be known from Figure 3.26. The test samples belonging to these classes are accurately classified.

Based on the above discussion, it can be inferred that the DOMs exhibit robustness to deviations in the structural characteristics and to some extent they are insensitive to segmentation errors. Hence, we can expect to increase the classification accuracies of some of the shape classes by increasing the number of training samples. In order to improve the classification results, the experiment on shape classification is repeated by taking an extended training set with 2 training samples per shape class, out of which 1 training sample per shape class has structural distortion. The evaluation is performed on the 360 testing samples used in the previous experiment on classification.

The consolidated plot of the classification results obtained for each shape class with respect to the extended training set is given in Figure 3.30. As expected, the test samples in Classes 1, 4, 11, 12 and 13 show higher classification accuracies. However, there is no significant improvement in the classification accuracies of Classes 2, 3 and 15. Similar to the previous classification results, the test samples of Class 2 is misclassified as Shape 1. The test samples of Class 3 is misclassified as Shape 13 and Class 15 as Shape 17. These results imply that the performance of the DOMs in shape classification depends mainly on the spatial distribution of the pixels. Under such cases, the number of training samples may be increased in order to improve the classification accuracy. The performance of MHD based classification has also improved with the increase of the training set. However, the number of shape classes misclassified in MHD based matching is higher than that in the DOM based matching.

The experiments for evaluating the capability of the DOMs as features for shape classification confirm the Krawtchouk and the discrete Tchebichef moments as robust features for efficient classification of shapes under shape defections such as segmentation errors and boundary deviations.

## 3.9 Summary

This chapter has presented studies on the characteristics of the WKPs and the DTPs in representing shapes. It is shown that for any given order, the WKPs and the DTPs behave like band-pass functions. Accordingly, the polynomials exhibits varied characteristics in representing different shapes.

The first empirical study is on the accuracy of the Krawtchouk and the discrete Tchebichef moments in shape representation. The efficiency of the DOMs is studied with respect to the changes in the shape scale and different structural characteristics. It has been shown that the performance of these moments significantly differs for lower order approximations. The discrete Tchebichef moments are superior to the Krawtchouk moments in accurately representing shapes with low structural variations. On the contrary, the Krawtchouk moments offer representation accuracy higher than that of the discrete Tchebichef moments in approximating shapes containing high spatial frequency structures. Particularly, the discrete Tchebichef moments require higher orders to efficiently reconstruct high spatial frequency structures of the shapes. From this analysis on the shape representation accuracy, it is inferred that the WKPs offer comparatively more data compaction in representing shapes at lower scales. At higher scales, the data compaction of WKPs is more for shapes with more structural variations. The data compaction capability of DTPs is significant only for low spatial frequency shapes at higher scale.

Similar experiments on the noise sensitivity have shown that for low levels of noise, the Krawtchouk moments are comparatively more robust to noise and capable of efficiently recovering the shape from the noisy shape. The discrete Tchebichef moments result in excessively smoothened reconstruction of shapes. As the noise level increases, the robustness of the WKPs and the DTPs to noise decreases resulting in poor denoising efficiency.

The second empirical study is on the applicability of the Krawtchouk and the discrete Tchebichef moments as features in shape classification. The experiment is performed on 400 samples of 20 shape classes taken from the MPEG-7 (CE Shape 1, Part-B) database. The study confirms that the Krawtchouk and the discrete Tchebichef moments are potential features for shape classification and are robust to shape defections caused by segmentation errors and structural deviations.

The empirical studies and the results obtained on shape analysis suggests the DOMs as potential feature descriptors for representing the different shapes. This implies that the DOMs can be employed as a silhouette based feature descriptor for classifying the hand postures based on their silhouette.

## 3.10 Appendix : Proof for the QMF property of WKP basis

Let us write the weighted Krawtchouk polynomial in (3.49) as

$$\overline{K}_n(x;p) = \frac{1}{\sqrt{w(x;p)}\sqrt{\rho(n;p)}} w(x;p) K_n(x;p) \tag{3.88}$$

The objective is to find the frequency domain representation of the term $w(x;p) K_n(x;p)$ in the above equation.

Let us assume $\psi_n(x) = w(x;p) K_n(x;p)$ and $z = e^{\left(\frac{j\omega}{N+1}\right)}$ in (3.73). Accordingly, we get the Z-transform of $\psi_n(x)$ as

$$\psi_n(\omega) = \sum_{x=0}^{N} w(x;p) K_n(x;p) z^{-x} \tag{3.89}$$

The Rodrigues type formula associated with the Krawtchouk polynomial $w(x;p) K_n(x;p)$ can be written as

$$\begin{pmatrix} N \\ x \end{pmatrix} \left(\frac{p}{q}\right)^x K_n(x;p) = \Delta^n \left[ \begin{pmatrix} N-n \\ x \end{pmatrix} \left(\frac{p}{q}\right)^x \right] \tag{3.90}$$

Therefore,

$$\psi_n(z) = \sum_{x=0}^{N} \Delta^n \left[ \begin{pmatrix} N-n \\ x \end{pmatrix} \left(\frac{p}{q} z^{-1}\right)^x \right] \tag{3.91}$$

Using the properties of Z-transform, we can obtain the solution

$$\psi_n(z) = \left(1 - \frac{p}{q} z^{-1}\right)^n \left(1 + \frac{p}{q} z^{-1}\right)^{N-n} \tag{3.92}$$

From (3.92), we can infer

$$\psi_n(z) = \psi_{N-n}(-z) \tag{3.93}$$

Substituting $z = e^{j\omega}$ in the above equation gives

$$\psi_n\left(e^{j\omega}\right) = \psi_{N-n}\left(e^{j(\omega+\pi)}\right) \tag{3.94}$$

On substituting $\omega = \omega - \frac{\pi}{2}$ in (3.94), we obtain [172]

$$\left|\psi_n\left(e^{j\left(\omega-\frac{\pi}{2}\right)}\right)\right| = \left|\psi_{N-n}\left(e^{j\left(\omega+\frac{\pi}{2}\right)}\right)\right| \tag{3.95}$$

Therefore, the quadrature mirror property of $\left|\psi_n\left(e^{j(\omega)}\right)\right|$ and $\left|\psi_{N-n}\left(e^{j(\omega)}\right)\right|$ about $\omega = \frac{\pi}{2}$ is proved.

# 4

# Robust Hand Posture Recognition Using Geometry-based Normalisation and DOM based Shape Description

**Contents**

The empirical study in Chapter 3 has shown the DOMs as efficient descriptors for representing shapes of different structural complexity and the analysis of the experiments on the MPEG-7 shape database suggests the DOMs as potential features for shape classification. This encourages to employ the DOMs as features for shape based hand posture description and classification.

The objective of this work is to propose a hand posture recognition technique based on the DOMs and experimentally validate the efficiency of DOMs as hand shape descriptors. This work also presents a rule-based method for automatically extracting the hand from the forearm region. The technique developed in this work provides a framework for hand posture based interactive tabletop applications. This chapter presents the proposed method and the experimental studies that comparatively validates the DOMs as hand posture features.

## 4.1 Introduction

Vision based interactive tabletops are surface computing systems that create a virtual environment for users based on hand posture interactions. They perform the operations of the conventional devices that include the mouse and the keyboard.

These tabletops are typically constructed using a single desktop computer linked to a projector and a camera. The projector is rear or front-mounted to display the content on the surface of the table. The camera is used to capture the hand postures performed on the tabletop surface. The acquired images are processed by the hand posture recognition system in order to detect the hand posture and interpret the underlying information. The retrieved information is passed to the computer as input commands for interaction. The position of the camera and the projector units vary depending upon the type of application. Similarly, the projection and the acquisition surfaces are either different or coupled together depending on the ease of the application. The schematic representation of a typical vision based tabletop interface system using a front-projected display is shown in Figure 4.1.

The hand posture recognition system developed in this work is aimed to find applicability in vision based tabletop interactions and hence, the experimental setup employed is designed to be in accord with the configuration of hand posture based tabletop interfaces. The proposed system is a monocular vision based system using shape based methodologies for interpreting the hand postures. The acquired hand posture images are modeled using the binary silhouettes. The hand posture recognition system developed in this work addresses the three major issues in hand shape interpretation. They are:

- segmentation of the forearm and extraction of hand region.

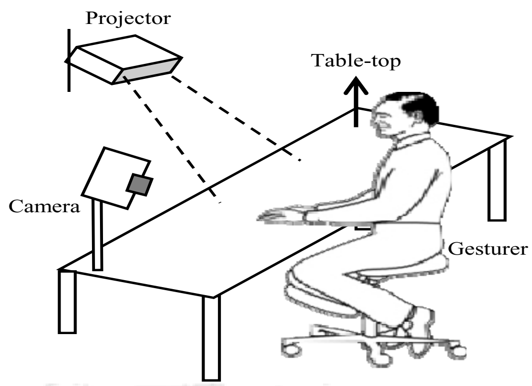


**Figure 4.1:** Illustration of a tabletop user interface setup using a top-mounted camera for natural human-computer interaction through hand postures.

- orientation normalization of the hand postures.
- accurate recognition of postures in the presence of view-angle and the user variations.

The identification of the hand region involves separating the hand from the forearm. The lack of posture information in the forearm makes it redundant and its presence increases the data size. In most of the previous works, the forearm region is excluded by either making the gesturers to wear full arm clothing or by limiting the forearm region into the scene while acquisition. However, such restrictions are not suitable in real-time applications. The orientation of the acquired posture changes due to the angle made by the gesturer with respect to the camera and vice-versa.

This research work proposes novel methods based on the anthropometric measures to automatically identify the hand and its constituent regions. The geometry of the posture is characterized in terms of the abducted fingers. This posture geometry is used to normalize for the orientation changes. These proposed normalization techniques are robust to similarity and perspective distortions. The main contributions reported in this chapter are:

(i) A rule based technique using the anthropometric measures of the hand is devised to identify the forearm and the hand regions.

(ii) A rotation normalization method based on the protruded\abducted fingers and the longest axis of the hand is devised.

(iii) A static hand posture database consisting of 10 posture classes and $4,230$ samples is constructed.

(iv) DOMS are introduced as user and view-invariant hand posture descriptors. In comparison to DOMs, some of the state-of-the art shape descriptors, namely the Fourier descriptors, the geometric moments, the Zernike moments, the Gabor wavelets and the PCA descriptors are also studied for user and view invariant hand posture recognition.

The proposed posture recognition framework is explained by dividing the system development into three sections, namely,

1. Hand posture acquisition and database development
2. System implementation
3. Experimental studies and results

The posture acquisition and the database development section explains the experimental setup used for acquiring the hand postures and the construction of the hand posture database required for the experimental studies. The section also includes a quantitative analysis on the variations in the shape of the hand postures in order validate the database for usability in the experimental studies on user and view independent hand posture description. The section on system implementation presents the procedures and the techniques involved in realising the hand posture recognition system. The section on experimental studies and the results discusses the experiments performed to comparatively evaluate the efficiency of the proposed system with respect to the DOMs and the other shape features. The results of user invariant and view invariant recognition are independently presented.

## 4.2 Hand posture acquisition and database development

The acquisition of hand posture images is the first step towards implementing a hand posture recognition system. The experimental setup employed for posture acquisition consists of a monocular camera that is interfaced to a computer. The two important factors to be considered while setting up the camera for posture acquisition are the

(i) Position of the camera

(ii) View-angle of the camera

The position of the camera specifies the camera's location with respect to the object of focus. The view-angle specifies the angle between the camera and the object of focus. Choosing the optimal position and the view-angle of the camera is an important task in image acquisition.

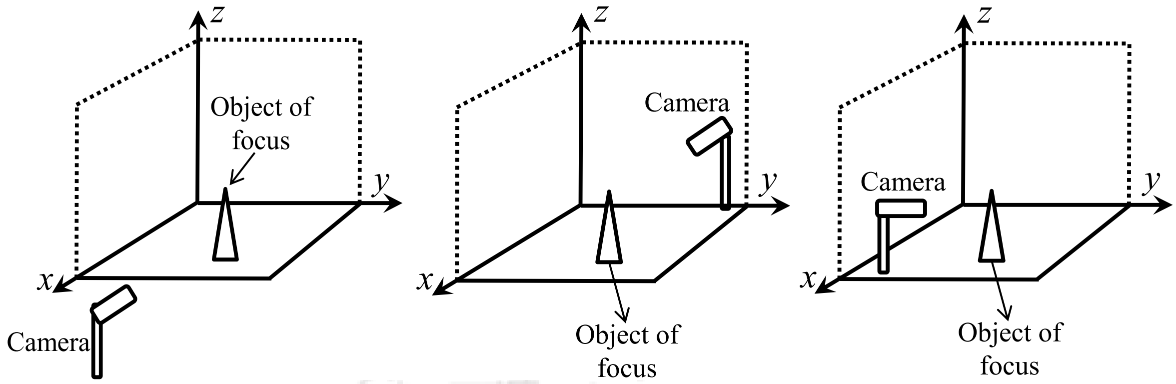


(a) Low-angle position (b) High-angle position (c) Normal-angle position

**Figure 4.2:** Illustration of different camera positions with respect to the object of focus in a 3*D* cartesian space.

### 4.2.1 Determination of camera position

The position of the camera with respect to the object of focus influences the object details that are being efficiently captured by the camera. The three types of camera locations generally used while image acquisition are the [173].

- Low-angle position
- High-angle position
- Normal-angle position

In the **low-angle position**, the camera is placed below the object such that the camera lens has to be titled upwards for focussing. The **high-angle position** occurs when the camera is placed above the object and the camera is lens is titled downwards for focussing the object. The **normal-angle position** has the camera at the same height from the ground as the object of focus. The normal angle position is also known as the eye-level position. Figure 4.2 illustrates the variation in the camera position with respect to the object of focus in a 3D cartesian coordinate system.

The position of the camera for image acquisition must be chosen such that the desired object region is completely within the focus of the camera. In realtime, the optimal position of the camera for acquiring the hand posture depends on the application. In applications like table-top interaction, the postures are performed on the surface of the table [95, 101, 104, 174]. Hence, the camera has to be mounted in the high-angle position such that the entire posture space lie within the focus of the camera. In such systems, the dorsal surface of the hand is focussed by the camera. In the case of table-top interfaces using the glass table tops for interaction, the camera is mounted at low-angle position such that the palmar surface is focussed while acquiring the hand

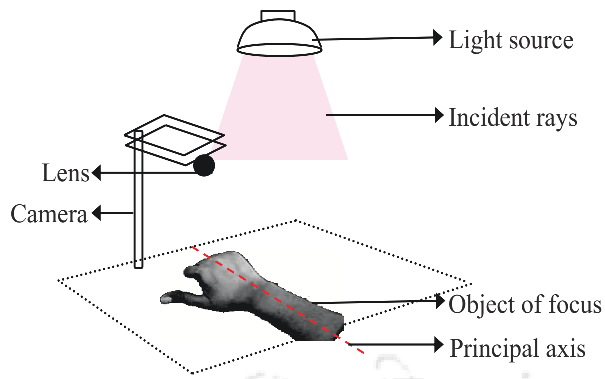


**Figure 4.3:** A schematic representation of the experimental setup employed for acquiring the hand posture images.

postures [175]. In some of the posture based interface systems [2, 94, 133], the camera is placed at the normal-angle position focussing the palmar surface of the hand posture.

### 4.2.2 Determination of view-angle

As mentioned in Section 1.5.2.3 of Chapter 1, the view-angle refers to the angle made by the camera with respect to the object of focus [69]. The optimal choice of viewing angle is determined by the amount of *perspective distortion*. Perspective distortion is caused if the focal plane is not parallel to the object's surface and/or not in level with the center of the object. Hence, the optimum view-angle is assumed to be the angle for which the camera is parallel to the object of focus i.e., the image plane must be parallel to the object plane.

### 4.2.3 System setup

The setup for image acquisition consists of a tabletop and a RGB Frontech e-cam mounted on an adjustable stand with an view of the tabletop. The postures are performed on the surface of the table such that the dorsal side of the hand posture is captured by the camera. The camera has a resolution of $1280 \times 960$ and is connected to an Intel core-II duo 2GB RAM processor. The schematic representation of the acquisition setup is shown in Figure 4.3.

The table surface constitutes the object plane and the length $\times$ width of the tabletop used for the setup is $83\,\text{cm} \times 96\,\text{cm}$. The distance between the table surface and the camera ($C_h$) is experimentally chosen such that the object plane is entirely focussed by the camera. Accordingly, the e-cam is placed at a height of $C_h = 30\,cm$ from the table surface.

In the context of our experiment, we define the viewing angle ($C_\theta$) as the angle made by the camera with the longest axis or the principal axis of the hand. Hence, the viewpoint is assumed to be optimum if the camera is placed parallel to the surface of the hand. For our experimental setup, the optimum viewing angle is

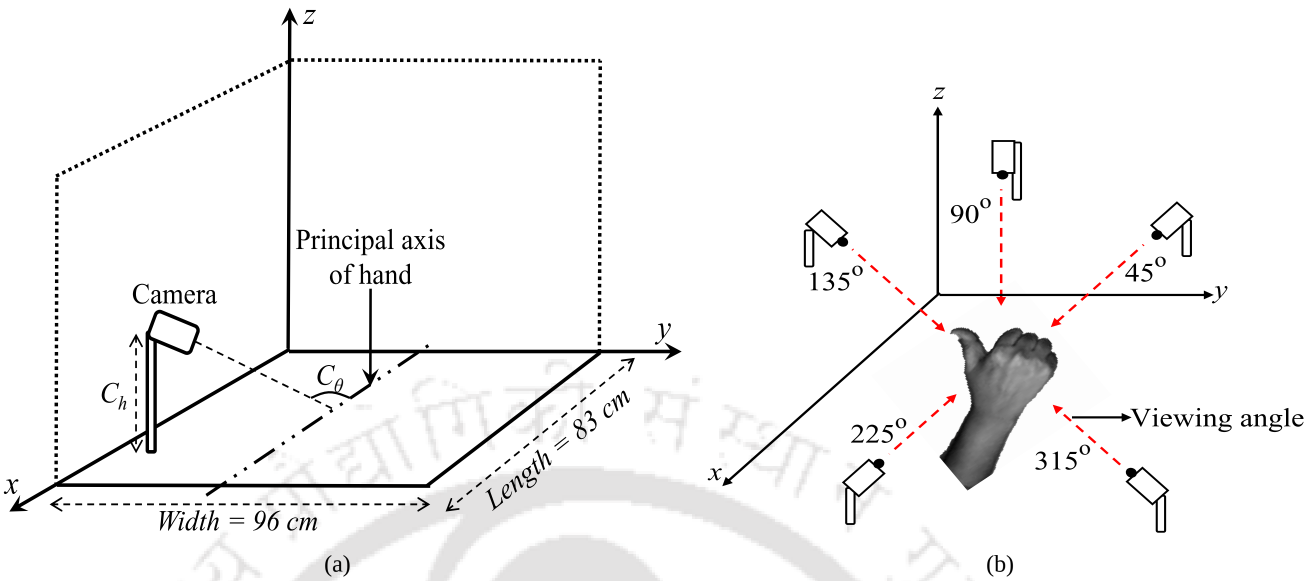


**Figure 4.4:** Illustrations of (a) the estimation of camera position and the view angle using a 3$D$ cartesian coordinate system. The object is assumed to lie on the $x-y$ plane and the camera is mounted along the $z$ axis. $C_h$ denotes the distance between the camera and the table surface and is experimentally chosen as 30 $cm$. The view angle ($C_\theta$) is measured with respect to the $x-y$ plane. (b) the view angle variation between the camera and the object of focus.

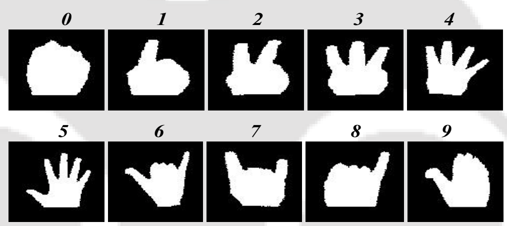


**Figure 4.5:** Posture signs in database.

determined to be 90°. Figure 4.4(a) illustrates the estimation of camera position and the view angle with respect to the principal axis of the hand using a 3$D$ cartesian coordinate system. The $x-y$ plane is the object plane constituting the hand posture. The variations in the viewpoint of the camera with respect to the hand region are illustrated through Figure 4.4(b).

In our experiment, the segmentation overload is simplified by capturing the images under uniform background. However, the foreground is cluttered with other objects and the hand is ensured as the largest skin color object within the FOV. Except for the size, there were no restrictions imposed on the color and texture of the irrelevant cluttered objects. Also, the FOV was sufficiently large enabling the users to perform postures more naturally without interfering their gesturing styles.

### 4.2.4 Development of Hand posture database

The hand posture images required for the experiment are collected from several users at different view angles. The hand posture database is developed in order to evaluate the robustness of several hand posture features for user and view invariant hand posture recognition.

The hand posture database is constructed out in two phases. In the first phase, the hand posture data are acquired at an optimum view angle of $C_\theta = 90°$. During the second phase, the hand postures images are captured at different view angles. The database consists of a total of $4,230$ postures collected from 23 users. The data contains 10 posture signs with 423 samples for each user. The posture signs taken for evaluation are shown in Figure 4.5. The images are collected under three different scales, seven orientations and the view angles at $45°, 90°, 135°, 225°$ and $315°$.

The scale variations are achieved by varying the optical zoom of the camera during each session of image acquisition. The orientation change is achieved by orbiting the camera around the object of focus. However, the view angle is maintained at $90°$. In the second phase of data collection, changing the viewpoint automatically causes the change in the orientation of acquired image.

## 4.3 System Implementation

The proposed hand posture recognition system is developed by broadly dividing the procedure into three phases. They are: (1) hand detection and segmentation, (2) normalization and (3) feature extraction and classification. A description of these tasks are presented below. Figure 4.6 shows a schematic representation of the proposed posture recognition system.

### 4.3.1 Hand detection and segmentation

This phase detects and segments the hand data from the captured image. The hand regions are detected using the skin color pixels. The background is restricted such that the hand is the largest object with respect to the skin color.

Teng *et al* [62] have given a simple and effective method to detect skin color pixels by combining the features obtained from the YCbCr and the YIQ color spaces. The hue value $H_\theta$ is estimated from the Cb-Cr chromatic components by

$$H_\theta = \tan^{-1}\left(\frac{Cr}{Cb}\right) \tag{4.1}$$

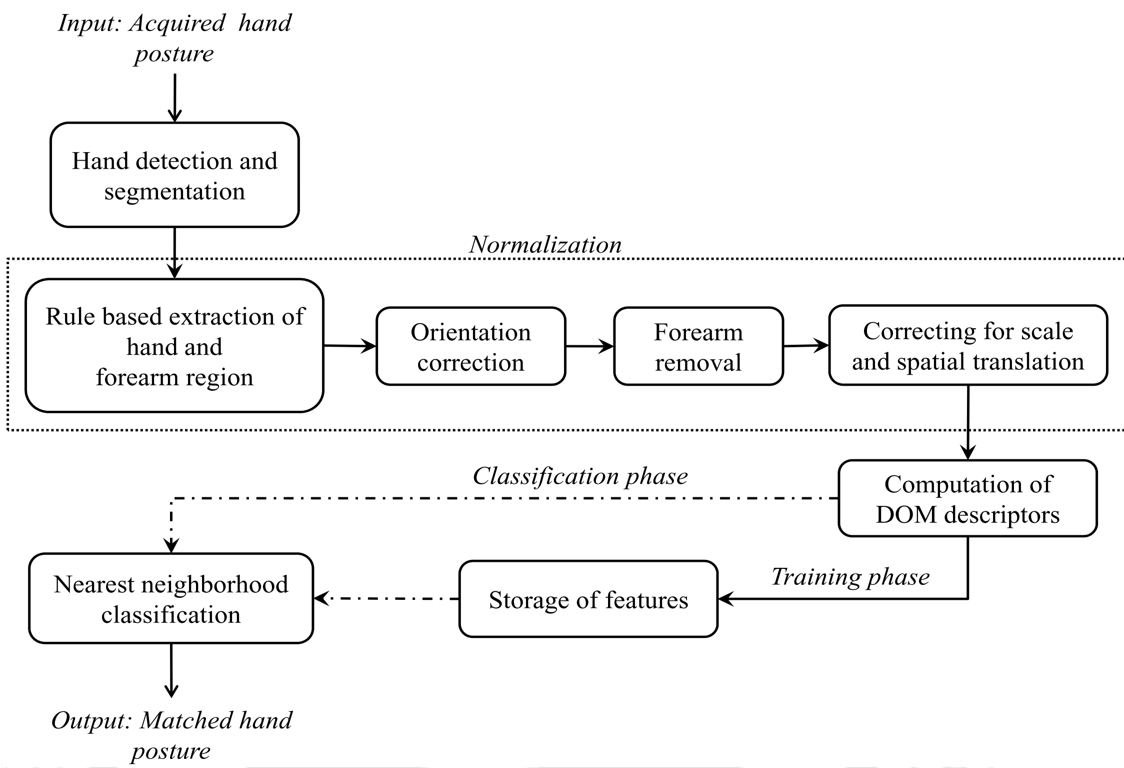


**Figure 4.6:** Schematic representation of the proposed hand posture recognition technique.

The in-phase color component $C_{phase}$ is calculated from the $RGB$ components as

$$C_{phase} = 0.596R - 0.274G - 0.322B \tag{4.2}$$

Their experiments conclude about the ranges of $H_\theta$ and the in-phase color component $C_{phase}$ for Asian and European skin tones. The pixels are grouped as skin color pixels if $105^\circ \leq H_\theta \leq 150^\circ$ and $30 \leq \mathrm{C}_{\mathrm{phase}} \leq 100$.

Figure 4.7(b) illustrates the skin color detection using this method for the hand posture images shown in Figure 4.7(a). The detection results in a binary image which may also contain other objects not belonging to the hand. Since, the hand is assumed to be the largest skin color object, the other components are filtered by comparing the area of the detected binary objects. The resultant is subjected to *morphological closing* operation with a disk-shaped structuring element in order to obtain a well defined segmented posture image.

For a binary image $f(x, y)$ defined on a discrete grid $\mathbb{G} = \{0, 1, \cdots N\} \times \{0, 1, \cdots M\}$ and the structuring element $s_l$, the morphological closing operation denoted by $f \bullet s_l$ is defined as

$$f \bullet s_l = (f \oplus s_l) \ominus s_l \tag{4.3}$$

$f \oplus s_l$ and $f \ominus s_l$ denotes *dilation* and *erosion* operations respectively [176]. The disk-shaped structuring element used for morphological closing operation is shown in Figure 4.8.

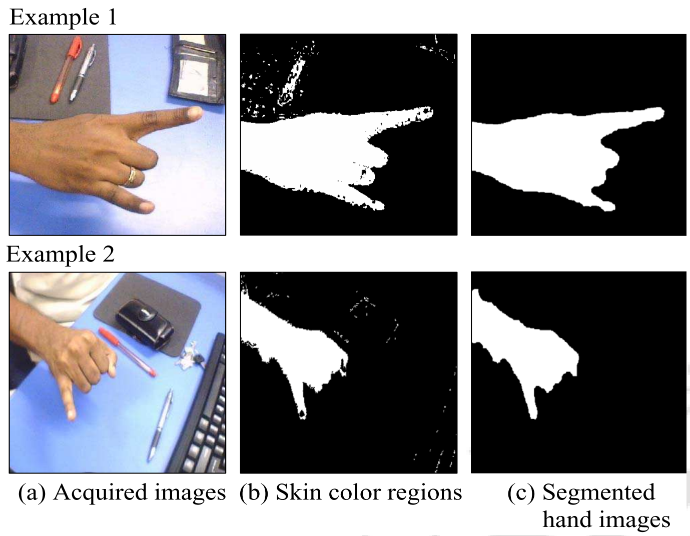


**Figure 4.7:** Results of hand segmentation using skin colour detection.

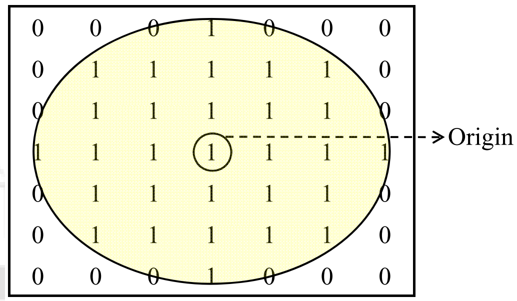


**Figure 4.8:** Illustration of the disk-shaped structuring element used for morphological closing. The radius of the element is 3.

### 4.3.2 Normalization techniques

This is an essential phase in which the segmented image is normalized for any geometrical variations in order to obtain the desired hand posture. The important factors to be compensated in this step are

(i) the presence of forearm region.

(ii) the orientation of the object.

The recognition efficiency can be improved through proper normalization of the hand posture image. Hence, a robust normalization method based on the posture geometry is proposed for extracting the hand region and correcting the orientation.

#### 4.3.2.1 Proposed method for rule based hand extraction

Consider a binary image $f$ defined over a grid $\mathbb{B}$ of size $(N+1)\times(M+1)$. $\mathbb{B}$ is composed of two complementary regions $R$ and $\overline{R}$ representing the hand (object) and the background respectively. Thus,

$$R = \left\{(x,y) \;\middle|\; (x,y) \in \mathbb{B} \text{ and } f(x,y) = 1\right\} \tag{4.4}$$

and the complementary region $\overline{R}$ is given by

$$\overline{R} = \mathbb{B}\backslash R \tag{4.5}$$

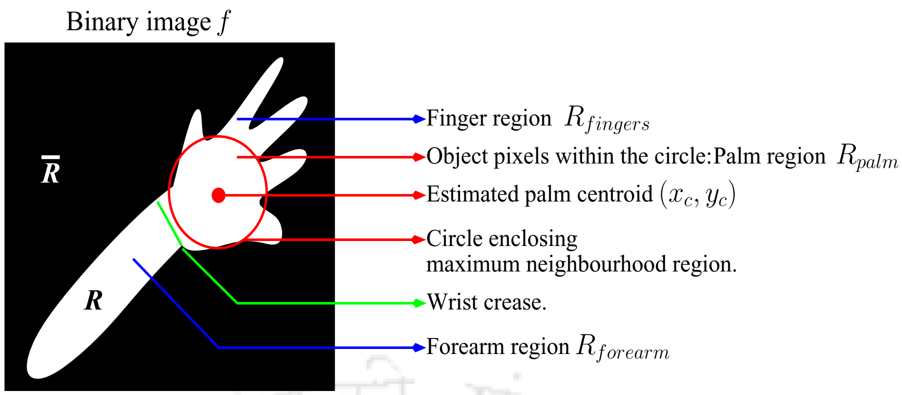


**Figure 4.9:** Pictorial representation of the regions composing the binary image $f$. $R$ denotes the hand region and $\overline{R}$ denotes the background region.

The boundary $\delta R$ of the hand region is defined by the set of pixels in $R$ that are adjacent to at least one pixel in the region $\overline{R}$. It is represented as

$$\delta R = \left\{ (x,y) \middle| (x,y) \in R \text{ and } (x,y) \text{ is adjacent to a pixel in } \overline{R} \right\} \tag{4.6}$$

The hand region R can be partitioned in to three subregions. They are (a) $R_{fingers}$ (fingers), (b) $R_{palm}$ (palm) and (c) $R_{forearm}$ (forearm). Hence

$$R = R_{fingers} \cup R_{palm} \cup R_{forearm} \tag{4.7}$$

such that

$$\begin{aligned} R_{fingers} \cap R_{palm} &= \emptyset \\ R_{fingers} \cap R_{forearm} &= \emptyset \\ R_{palm} \cap R_{forearm} &= \emptyset. \end{aligned} \tag{4.8}$$

Figure 4.9 illustrates these elementary regions comprising the hand object R. Based on the anatomy, the palm and the forearm can be considered as continuous smooth regions. *The forearm extends outside the palm and its width is less than that of the palm region. Conversely, the region containing the fingers is discontinuous under abduction. Also, the width of a finger is much smaller than that of the palm and the forearm. Therefore, the geometrical variations in the* width *and the* continuity *of these subregions in the hand image are used as cues for detection.*

(a) *Computation of width*

The variation in the width along the longest axis of the hand image is calculated from the distance map obtained using the Euclidean distance transform (EDT). The EDT gives the minimum distance of an object pixel to any pixel on the boundary set $\delta R$. The Euclidean distance between a boundary pixel $(x_b, y_b) \in \delta R$ and an object pixel $(x, y) \in R$ is defined as

$$d_{(x_b,y_b),(x,y)} = \sqrt{(x - x_b)^2 + (y - y_b)^2} \tag{4.9}$$

The value of the EDT, $D_{(x,y)}$ for the object pixel $(x, y)$ is computed as

$$D_{(x,y)} = \min_{(x_b,y_b)\in\delta R} d_{(x_b,y_b),(x,y)} \tag{4.10}$$

The values of $D_{(x,y)}$ at different $(x, y)$ are used to detect the subregions of $R$.

The straightforward implementation of EDT defined through (4.9) and (4.10) is computationally expensive. Therefore, the conventional approach to fast EDT based on the Voronoi decomposition of the image proposed in [177] is employed. A study on the several other algorithms proposed for reducing the computational complexity of EDT is discussed in [178].

(b) *Verification of region continuity*

The continuity of the subregions after detection is verified through connected component labelling preceded by morphological erosion. The erosion operation with a small structuring element is performed to disconnect the weakly connected object pixels. The structuring element considered is a disk operator with radius 3. The resultant is verified to be a continuous region if there is only one connected component. If there is more than one connected component, the detected region is verified as discontinuous.

The geometrical measurements along the finger region vary with the users and they get altered due to geometric distortions. However, the measures across the palm and the forearm can be generalized and their ratios are robust to geometric distortions. *The palm is an intactly acquired part that connects the fingers and the forearm.* Since $R_{palm}$ lies as an interface between $R_{fingers}$ and $R_{forearm}$, the separation of palm facilitates the straightforward detection of the other two regions. Hence, the anthropometry of palm is utilized for detecting the regions in the hand image.

**4.3.2.1.1 Anthropometry based palm detection** The parameters of the hand considered for palm detection are the hand length, palm length and the palm width as illustrated in Figure 4.10(a). The anthropometric studies in [179–181] present the statistics of the above mentioned hand parameters. From these studies, we infer that the minimum value of the ratio of palm length ($L_{palm}$) to palm width ($W_{palm}$) is approximately 1.322 and its maximum value is 1.43. Similar observations were made from our photometric experiments. Figure 4.10(b)

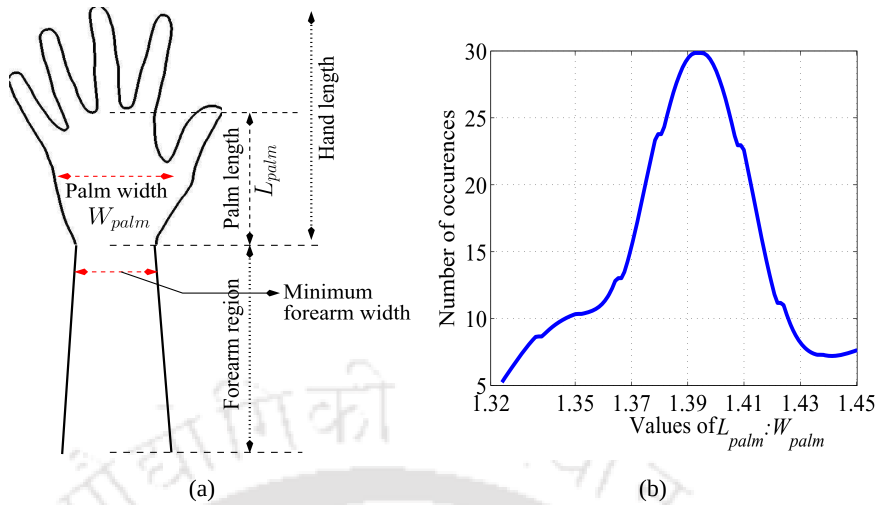


**Figure 4.10:** (a) Hand geometry and (b) Histogram of the experimental values of palm length ($L_{palm}$) to palm width ($W_{palm}$) ratio calculated for 140 image samples taken from 23 persons.

gives the histogram of the $\frac{L_{palm}}{W_{palm}}$ values obtained through our experimentation. This ratio will be utilized to approximate the palm region as an ellipse. Considering all the variations of this ratio, we take

$$L_{palm} = 1.5 \times W_{palm} \tag{4.11}$$

Based on the geometry, we approximate the palm region $R_{palm}$ as an elliptical region with

$$\text{Major axis length} = 1.5 \times \text{minor axis length} \tag{4.12}$$

Assuming $a_{palm}$ as the semi-major axis length and $b_{palm}$ as the semi-minor axis length, we can write

$$a_{palm} = \frac{L_{palm}}{2} \tag{4.13}$$

$$b_{palm} = \frac{W_{palm}}{2} \tag{4.14}$$

Therefore,

$$a_{palm} = 1.5 \times b_{palm} \tag{4.15}$$

From (4.15), it can be inferred that all the pixels constituting $R_{palm}$ will lie within the ellipse of semi-major axis length $a_{palm}$. Therefore, the palm centre and the value of $a_{palm}$ have to be estimated for detecting the palm region.

**a) Computing the palm centre** Given that the boundary of $R_{palm}$ is an ellipse, its centre is known to have the maximum distance to the nearest boundary. Therefore, the centre of $R_{palm}$ is computed using the EDT in (4.10). The pixels $(x, y)$ with EDT values $D_{(x,y)}$ greater than a threshold $\zeta$ are the points belonging to the neighborhood of the centre of the palm. This neighborhood is defined as

$$C = \left\{(x,y) \in R | \, D_{(x,y)} > \zeta\right\} \tag{4.16}$$

The centre $(x_c, y_c)$ is defined as the palm centroid and given by

$$(x_c, y_c) = \left(\lfloor \overline{X} \rceil, \lfloor \overline{Y} \rceil\right) \tag{4.17}$$

where

$$\overline{X} = \frac{1}{|C|} \sum_{(x_i,y_i)\in C} x_i \quad , \quad \overline{Y} = \frac{1}{|C|} \sum_{(x_i,y_i)\in C} y_i,$$

$|C|$ is the cardinality of $C$ and $\lfloor \rceil$ denotes rounding off to the nearest integer.

The threshold $\zeta$ is selected as $max(D_{(x,y)}) - \tau$. The offset $\tau$ is considered to compensate for the inaccuracies due to the viewing angles. For small values of $\tau$, the centroid may not correspond to the exact palm centre and large values of $\tau$ will tend to deviate the centroid from the palm region. The optimal value of $\tau$ is experimentally chosen as 2.

**b) Computing the semi-major axis length** From the geometry, it can be understood that the nearest boundary points from the palm centroid correspond to the end points of the minor axis. Hence, the EDT value at $(x_c, y_c)$ is the length of the semi-minor axis and therefore,

$$b_{palm} = D_{(x_c,y_c)} \tag{4.18}$$

From (4.15), it follows that the length of the semi-major axis can be given as

$$a_{palm} = 1.5 \times D_{(x_c,y_c)} \tag{4.19}$$

**c) Detecting the palm** In order to ensure proper detection of the palm, the finger regions ($R_{fingers}$) are sheared from the segmented object through the morphological opening operation. The structuring element is a disk with radius $d_r$ empirically chosen as

$$d_r = \frac{b_{palm}}{1.5} \tag{4.20}$$

The resultant is considered as the residual and will be referred as the ***oddment***. The oddment is generally composed of the palm region and may or may not contain the forearm. This implies $A \subseteq R$. Therefore, the

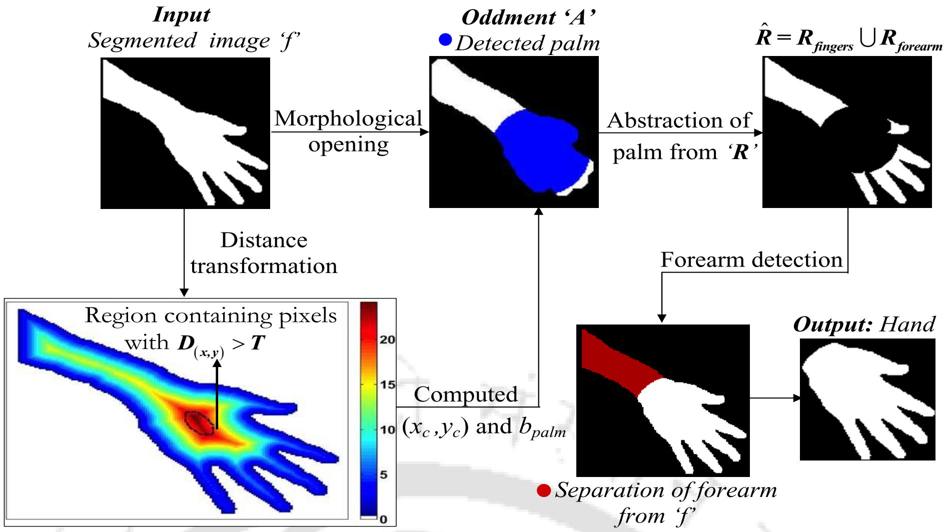


**Figure 4.11:** Illustration of the rule based region detection and separation of the hand from the acquired posture image $f$. The intensity of the background pixels is assigned a 0 and the object pixels are assigned the maximum intensity value 1.

oddment $A$ can be defined as

$$A = R_{palm} \cup R_{forearm}$$

For $R$ with no forearm region, $R_{forearm} = \emptyset$ and $A = R_{palm}$. $R_{palm}$ is a part of $A$ that is approximated as an elliptic region. Thus,

$$R_{palm} = \left\{ (x_{\mathbf{o}}, y_{\mathbf{o}}) \middle| \begin{array}{l} (x_{\mathbf{o}}, y_{\mathbf{o}}) \in A \quad and \\ \left(\dfrac{x_{\mathbf{o}} - x_c}{a_{palm}}\right)^2 + \left(\dfrac{y_{\mathbf{o}} - y_c}{b_{palm}}\right)^2 \leqslant 1 \end{array} \right\} \tag{4.21}$$

**d) Detection of forearm** The forearm is detected through the abstraction of the palm region $R_{palm}$ from the posture image $R$. The abstraction separates the forearm and the finger regions, such that $R$ is modified as

$$\hat{R} = R \backslash R_{palm} = R_{fingers} \cup R_{forearm} \tag{4.22}$$

As in the case of palm detection, the finger region is removed from $\hat{R}$ through the morphological opening operation. The structuring element is a disk with its radius calculated from (4.20). The resultant is a forearm region and has the following characteristics:

(i) The resultant $R_{forearm} \subseteq A$ and the region enclosing $R_{forearm}$ is continuous.

(ii) The width of the wrist crease is considered as the minimum width of the forearm region. From the anthropometric measures in [180], the minimum value of the ratio of the palm width to wrist breadth is obtained as 1.29 and the maximum value is computed as 1.55. Using this statistics, the empirical value for the width of the forearm should satisfy the relation

$$W_{forearm} > \frac{2b_{palm}}{1.29} \tag{4.23}$$

**e) Identifying the finger region** Having detected the palm and the forearm, the remaining section of the hand image $R$ will contain the finger region if it satisfies the following conditions,

- $R_{fingers} \nsubseteq A$.
- The region enclosing $R_{fingers}$ is marked by irregular boundary, if more than one finger is abducted.
- The width of a finger (maximum EDT value in this section) is much less than that of the palm and the forearm. Experimentally,

$$W_{finger} \leq \frac{b_{palm}}{2} \tag{4.24}$$

A procedural illustration of the proposed rule-based method for detecting the hand region from the input image is shown in Figure 4.11. After detecting the hand region, the pixels belonging to the forearm $R_{forearm}$ are assigned with zero values, thus including $R_{forearm}$ in the background.

#### 4.3.2.2 Proposed approach to orientation correction

The orientation of the hand can be assumed to imply the orientation of the hand posture. In a hand posture based system, the information is conveyed through the finger configurations. Since the human hand is highly flexible, it is natural that the orientation of the oddment might not be the orientation of the fingers. Hence, the major axis of the hand posture is not sufficient to estimate the angular deviation that is caused by the fingers. Therefore, in order to align a posture class uniformly, the orientation with respect to the abducted fingers is utilized. If the number of abducted fingers is less than 2, the orientation correction is achieved using the oddment.

**a) Orientation correction using finger configuration** The normalization of rotation changes based on the finger configuration is achieved by detecting the tip of the abducted fingers. For this purpose, the boundary points $(x_b, y_b)$ are ordered as a contiguous chain of coordinates using the 8-connectivity. Any one of the boundary pixels that is not enclosed within the region containing fingers is used as the starting point and the ordering is performed in the clockwise direction.

Suppose, $z$ is the length of the boundary measured in the number of pixels. A distance curve $g(z)$ is generated by computing the Euclidean distances between the palm centroid $(x_c, y_c)$ and the boundary pixel $(x_b, y_b)$ at $z$ using (4.9).

The curve $g$ is smoothed using cubic-spline smoothing [182]. The resultant is a smooth curve consisting of peaks that correspond to the finger tips of the hand posture. These peaks are detected by computing the first and the second order derivatives of $g$ using the finite difference approximations. Thus, $g(z)$ is considered to be a peak if

$$\left|g'(z)\right| < \xi \text{ and } g''(z) < 0 \tag{4.25}$$

where $\xi$ is the user defined minimum permissible difference. The finite difference approximations,

$$g'(z) \simeq \frac{g(z+1) - g(z-1)}{2} \tag{4.26}$$

and

$$g''(z) \simeq \frac{g(z+1) + g(z-1) - 2g(z)}{4} \tag{4.27}$$

are used to implement (4.25). In some cases, a few peaks may correspond to the palm region. These points are easily eliminated by verifying their presence in the oddment $A$. The $2D$ coordinate positions of the detected peaks are utilized to find a representative peak for each abducted finger. The distance curve corresponding to a posture and the detected finger tips are shown in Figure 4.12.

Let $L$ be the total number of detected peaks and $\gamma_i$, $i = 1, \ldots, L$ define the position vectors of the detected points with respect to $(x_c, y_c)$, indexed from left to right. These vectors $\gamma_i$s are referred as the *finger vectors* and the central finger vector $\hat{\gamma}$ is computed from

$$\hat{\gamma} = \begin{cases} \gamma_{\frac{L+1}{2}} & if\, L\, is\, odd \\ \frac{\gamma_{\frac{L}{2}} + \gamma_{\frac{L}{2}+1}}{2} & otherwise \end{cases} \tag{4.28}$$

The postures are assumed to be perfectly aligned if the vector $\hat{\gamma}$ is at $90^\circ$ with respect to the horizontal axis of the image. Otherwise, the segmented hand posture image is to be rotated by $90^\circ - \angle\hat{\gamma}$.

**b) Orientation correction using the oddment** The geometry of the oddment $A$ is utilized to correct the orientation of the hand postures with only one abducted finger and the postures like the *fist*. The shape of the oddment can be well approximated by an ellipse and hence, the orientation of its major axis with respect to the horizontal axis of the image gives the approximate rotation angle of the hand posture.

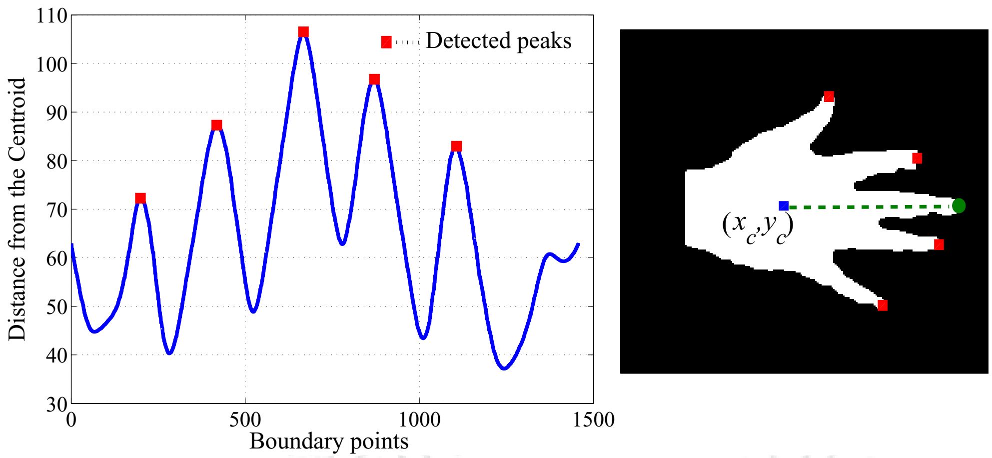


**Figure 4.12:** Description for finger tip detection using the peaks in the distance curve. - - - - - denotes $\hat{\gamma}$.

#### 4.3.2.3 Normalization of scale and spatial translation

The scale of the rotation corrected posture region is normalized and fixed to a pre-defined size through the nearest neighbor interpolation \ down sampling technique. The resolution of the segmented posture image is fixed at $104 \times 104$ with the scale of the hand object normalized to $64 \times 64$.

The spatial translation is corrected by shifting the palm centroid $(x_c, y_c)$ to the centre of the image. Accordingly, the centroids of the hand posture images are shifted to $(52, 52)$.

Therefore, the resultant is the segmented hand posture image that is normalized for transformations due to rotation, scaling and translation.

### 4.3.3 Feature Extraction

The shape of the normalized hand posture images are represented using the proposed DOM based shape descriptors proposed in Chapter 3. The shape descriptors constitute the unique features extracted from the hand posture. Thus, the first set of features extracted are the Krawtchouk and the discrete Tchebichef moments based features.

Based on the review of several shape features presented in Chapter 2, the other robust hand posture descriptors considered along with the DOMs for comparative evaluation are the (a) Fourier descriptors (FDs); (b) geometric moments; (c) Zernike moments; (d) Gabor wavelets and the (e) PCA based features.

Given the normalized hand posture shape $f(x,y)$, the extraction of the shape features are explained as follows.

#### 4.3.3.1 Extraction of moment shape descriptors

The moment based shape descriptors that include the geometric, the Zernike, the Krawtchouk and the discrete Tchebichef moments are region based descriptors. Proper choice of the order of the moments is an important factor in deriving the moment features. The order of the orthogonal moments are chosen based on the reconstruction accuracy.

**a) Extracting the proposed DOM based shape descriptors** The DOPs namely the WKPs and the DTPs required for approximating the function $f(x, y)$ are derived from (3.50) and (3.64) respectively. The corresponding Krawtchouk and the discrete Tchebichef moment features are computed using (3.71) and (3.72) respectively. For the Krawtchouk and the discrete Tchebichef moments computed up to order $(n + m)$, the number of moment features obtained are $(n + 1)(m + 1)$.

**b) Extracting the geometric and the Zernike moment descriptors** The non-orthogonal geometric moments of order $(n + m)$ representing $f(x, y)$ are derived using (2.11). The order of the geometric moments is chosen experimentally as 14 ($n = 7$ and $m = 7$).

The continuous orthogonal Zernike moment features are computed using the formulation given through (2.12) and (2.13). In the case of Zernike moments, the repetition $m$ is chosen to take only positive integer values. For order up to $n$ and $m \geq 0$, the number of Zernike moment features obtained can be easily verified to be $\left(\frac{n}{2} + 1\right)^2$ if $n$ is *even* and $\frac{(n+1)(n+3)}{4}$ if $n$ is *odd*.

An example illustrating the reconstruction accuracy of the Zernike, the Krawtchouk and the discrete Tchebichef moments for various choice of number of moment features is shown in Figure 4.13. The images reconstructed from the moments based approximations at various order are shown in Figure 4.13(b). The reconstruction error computed in terms of the SSIM index and the MHD values are shown in Figure 4.13(c) and 4.13(d) respectively. From the plots, we infer that for the given order, the Krawtchouk moments exhibit comparatively higher reconstruction accuracy. The results in Figure 4.13(b) show that the images reconstructed using the Zernike moments are comparatively not well defined. It is noted that the concavities are better defined in Krawtchouk based approximation and the rate of convergence towards the optimal value is faster in the case of Krawtchouk moments. For higher orders, the Zernike moments become numerically unstable resulting in higher reconstruction errors. However, at lower orders, the performance of the Zernike moments is almost close to that of the discrete Tchebichef moments. As the order increases, the performance of the discrete Tchebichef moments is close to that of the Krawtchouk moments.

Based on the analysis on reconstruction error, the order $n$ of the Zernike moments is chosen as 29. Be-

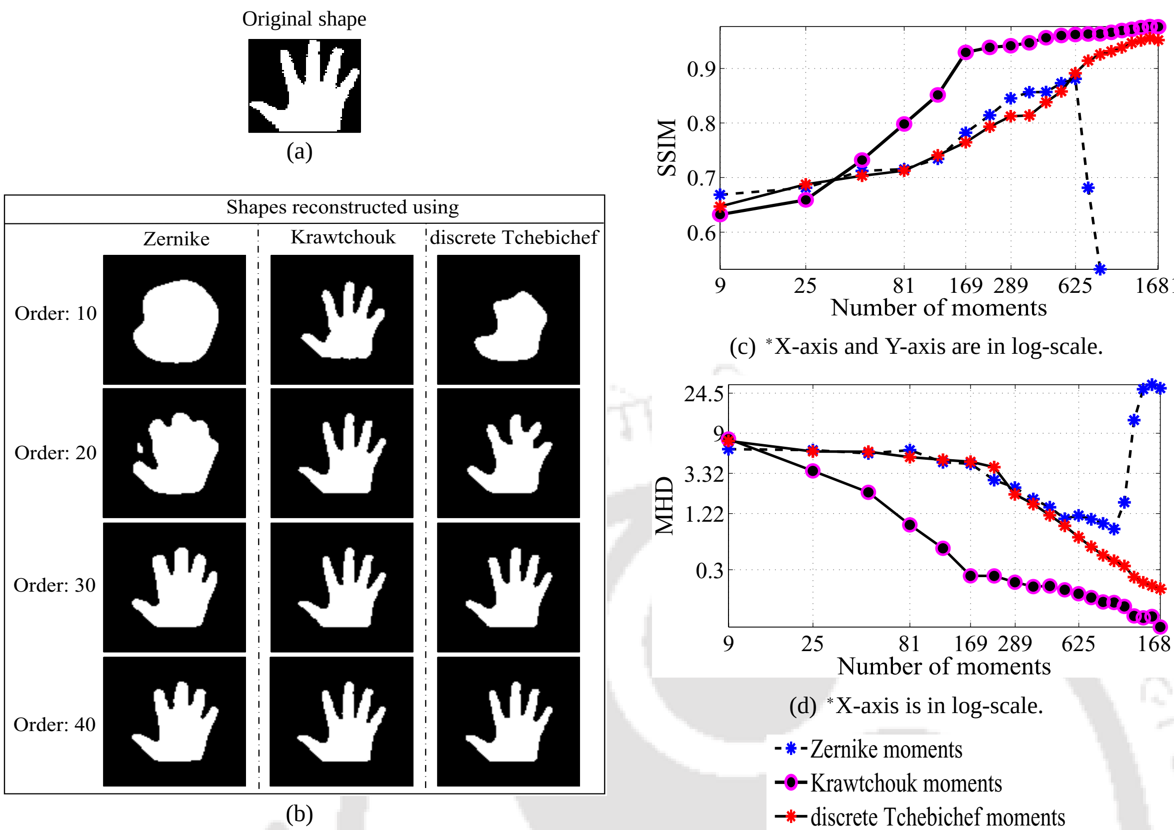


**Figure 4.13:** Illustration of reconstruction of the hand posture shape for different orders of orthogonal moments. (a) Original hand posture shape; (b) Shape reconstructed from orthogonal moments. Comparative plot of (c) SSIM index vs number of moments and (d) MHD vs number of moments.

yond this order, there is only marginal improvement in the reconstruction accuracy. Also, it is known that the computational complexity of the Zernike moments increases with the order. Therefore, as a trade-off between the computational time and the reconstruction accuracy, the order is chosen as $n = 29$. The optimal choice of the order $(n + m)$ for the Krawtchouk and the discrete Tchebichef moments are chosen as 80 such that $n = 40$ and $m = 40$. At this order, we observed that both the moments exhibit similar performance with higher reconstruction accuracy.

#### 4.3.3.2 Extraction of non-moment shape descriptors

**a) Extracting FDs** The FDs representing the hand postures are derived from the boundary of the hand posture images. The number of boundary points representing the shape boundary are normalized to a fixed value. The points on the shape boundary for efficiently representing the hand postures are chosen at uniform intervals and the number of boundary points is experimentally chosen as 255. For these points $(x, y) \in \mathbb{B}$, the FDs are computed using (2.9) and (2.10).

**b) Deriving Gabor wavelet features** The Gabor wavelet features are derived from the normalized hand posture images using the formulation given in (2.26). The number of scales and the orientations are experimentally chosen as 8 and 10 respectively. As per the experimental studies in [4], the optimal value of width of the Gaussian function is chosen as $\sigma = \pi$ and the center frequency is chosen as $\omega_{\max} = \frac{\pi}{2}$.

**c) Computing PCA features** Similar to the moments based approach, the PCA based method is a region based shape descriptor. The PCA based shape features are computed through the steps explained in Section 2.3.2.2. The PCA features are estimated using the definitions in (2.14) to (2.16) and the projected images are computed using (2.17).

The number of eigen components required for computing the transformation matrix is experimentally chosen based on the reconstruction accuracy. Given the eigen values $\{\lambda_1, \lambda_2, \cdots, \lambda_k\}$ , the eigen values to be retained is computed from the ratio [183],

$$\chi_{eigen} = \frac{\sum\limits_{i=1}^{l} \lambda_i}{\sum\limits_{i=1}^{k} \lambda_i} \; ; \; l < k \tag{4.29}$$

The number of eigenvalues $l$ for which the ratio $\chi_{eigen}$ is atleast 0.95 are chosen to form the projection matrix. This ratio implies that 95% of the variance present in the data are retained by the first $l$ number of eigenvalues that are arranged in decreasing order.

Based on (4.29), the number of eigen components representing 99% of the data variance is obtained as 130. Therefore, the eigenvectors corresponding to the first 130 eigenvalues can be used to form the transformation matrix $W_{pca}$. However, the experiments on reconstruction accuracy with respect to the varying $l$ have shown that the number of eigen components required for accurately reconstructing the image from the PCA projections is only 30. An example, illustrating the shape reconstruction accuracy of the PCA projections for varying choice of number of eigen components is shown in Figure 4.14. The reconstruction accuracy is computed using the SSIM index and the MHD value. The results show that for $l = 30$, the reconstruction accuracy in terms of the SSIM index is around 0.99 and the MHD value is around 0.3. Beyond $l = 30$, the improvement is not very significant and hence, it suggests that the eigenvectors corresponding to the first 30 eigenvalues are sufficient for forming the transformation matrix. For $l = 30$, the ratio $\chi_{eigen}$ is 0.78 implying that 78% of the data variance are represented by the first 30 eigenvalues.

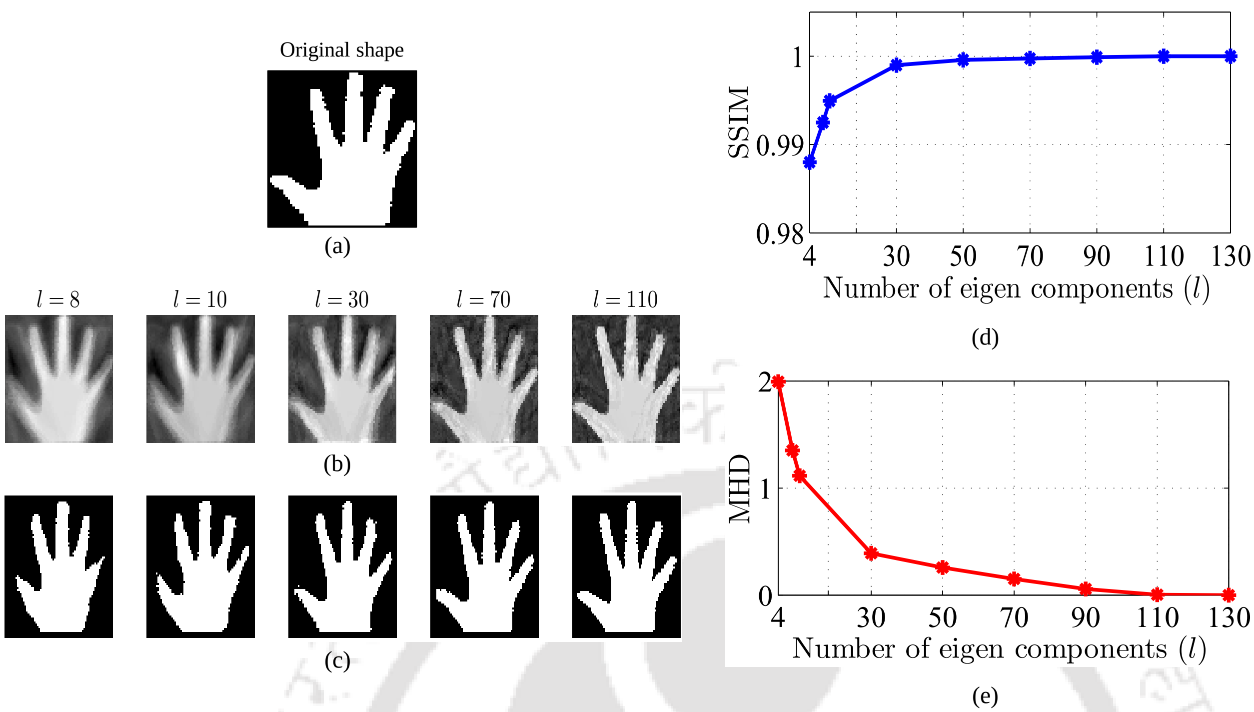


**Figure 4.14:** Illustration of shape reconstruction with respect to varying number of eigen components (a) Original shape; (b) Shapes reconstructed from the PCA projections for different number of eigenvalues and (c) the results of binarisation of the reconstructed shapes in (b). The threshold for binarisation is uniformly chosen as 120. Comparative plots of (d) SSIM index vs number of eigenvalues and (e) MHD vs number of eigenvalues, computed between the shape in (a) and the reconstructed binary shapes in (c).

### 4.3.4 Classification

Consider $z_s$ and $z_t$ as the feature vectors of the test and the target shapes ( in the reference set ) respectively. Then, the classification of $z_s$ is done using the minimum distance classifier defined as

$$d_t\left(z_s, z_t\right) = \sum_{j=1}^{T} \left(z_{sj} - z_{tj}\right)^2 \tag{4.30}$$

$$Match = \underset{\{t\}}{\arg\min}\left(d_t\right)$$

where $t$ is the index of signs in the reference set and $T$ is the dimension of the feature vectors.

## 4.4 Experimental Studies and Results

The performance of the proposed DOM descriptors in comparison with the other shape descriptors discussed above is verified through two different experiments on hand posture shapes. The first experiment studies the user independence characteristics of the shape descriptors. The second experiment is for verifying the robustness of the shape features in view invariant hand posture representation.

Of the 4,230 hand posture images corresponding to 10 posture classes, 2,260 are collected during the first phase at a view angle of 90° and the remaining 1,970 are collected during the second phase by varying the view angles. We refer the dataset taken at 90° as *Dataset 1* and the remaining data as *Dataset 2*. The 10 postures classes in the database are labeled from 0 to 9.

The Dataset 1 consists of postures that vary due to similarity transformations of rotation and scaling. Dataset 2 consists of postures that are taken at different view angles and scales. Due to the viewing angles, the postures undergo perspective distortions and the view angle variation also imposes orientation changes. Thus, the postures in Dataset 2 accounts for both perspective (view angle) and similarity (orientation and scale) distortions. Also, the postures in Dataset 1 are collected cautiously such that there is no self-occlusion between the fingers. But, while collecting the samples in Dataset 2 the precautions were not taken to control self-occlusion which might occur due to either the user's flexibility or the view angle variation. Therefore, it can be expected that the hand posture shapes in the Dataset 2 are more distorted than those in Dataset 1. The variations in the hand posture shapes caused due to user and viewpoint changes are quantitatively analyzed using the Pratt's FOM and the correlation coefficient.

### 4.4.1 Quantitative analysis of hand posture variations

The structural variations between the hand posture images of each class are verified from the intraclass and the interclass distances among the hand posture images. The intraclass and the interclass distances are computed using the Pratt's FOM and the correlation coefficient. The samples required for this analysis are randomly chosen from Dataset 1 and Dataset 2. The reference set required for computing the distances are taken from Dataset 1 and there are 23 samples per hand posture class comprising of data collected from 23 users. Similarly, the query set is formed by collecting 69 samples per posture class from each of Dataset 1 and Dataset 2.

Figure 4.15 illustrates the intraclass distances computed in terms of the Pratt's FOM. By comparing the plots in Figure 4.15(a) and Figure 4.15(b), we can infer that most of the samples in Dataset 1 exhibits comparatively higher values of FOM. Further, it is also evident that the range of variation in the FOM values corresponding to the samples from Dataset 2 is more than that of the samples from Dataset 1. The standard deviation plot of the intraclass FOMs shown in Figure 4.16 shows the variability in the values of Pratt's FOM with respect to each class . By comparing the standard deviation values obtained for each class, it is observed that the intraclass distance is comparatively less only for the samples from posture classes 6, 7 and 9.

The plots illustrating the comparison between the intraclass and the interclass distances for hand posture

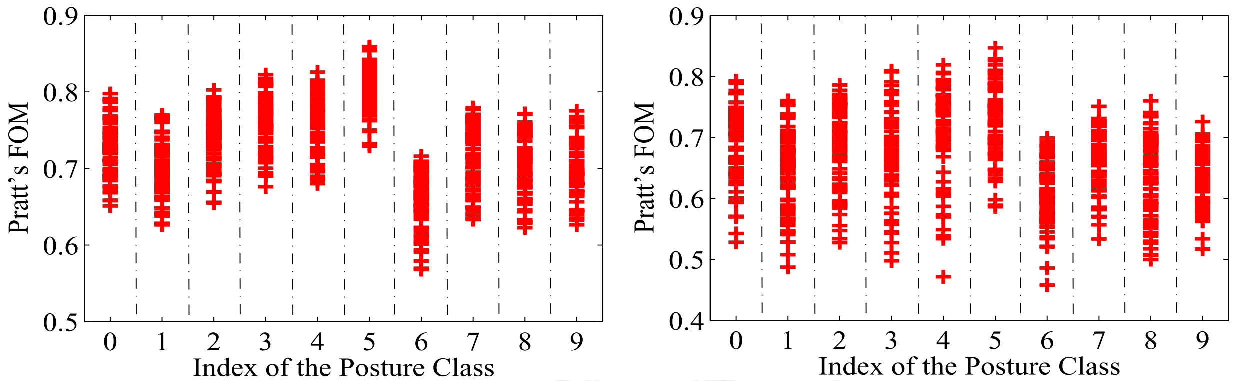


(a) (b)

**Figure 4.15:** Intraclass distance measured in terms of Pratt's FOM for samples in (a) Dataset 1 and (b) Dataset 2. The reference set is taken from Dataset 1. There are 690 testing samples with 69 samples \ posture sign in each of the dataset and 230 samples in the reference set with 23 samples \ posture sign.

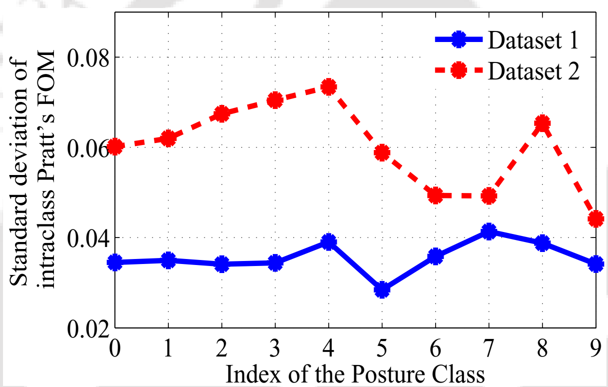


(a)

**Figure 4.16:** Illustration of variability in the intraclass FOM values with respect to samples in each posture class.

images in Dataset 1 and Dataset 2 are shown in Figure 4.17. The plots are generated by computing the average of the correlation values obtained with respect to the samples in each posture class. From the distance values, it is evident that the intraclass samples exhibit higher similarity than the interclass samples. This implies that the posture signs comprising the database are structurally distinct shapes.

As we examine the correlation values in Figure 4.17 obtained for Dataset 1 and Dataset 2, it is observed that the correlation values with respect to the interclass samples are over 0.55. Further, the maximum difference between the intraclass and the interclass correlation values is approximately around 25%. Despite the structural distinctiveness, these values indicate that the samples corresponding to any class exhibit approximately 50% structural similarity with respect to the samples in every other class. Therefore, it is clear that the hand posture shapes of different classes consist of overlapping regions.

It is known that the hand is composed of the palm and the finger regions. Of these, the fingers move at different degrees in order to constitute different hand postures. The palm region is a static region and the hand

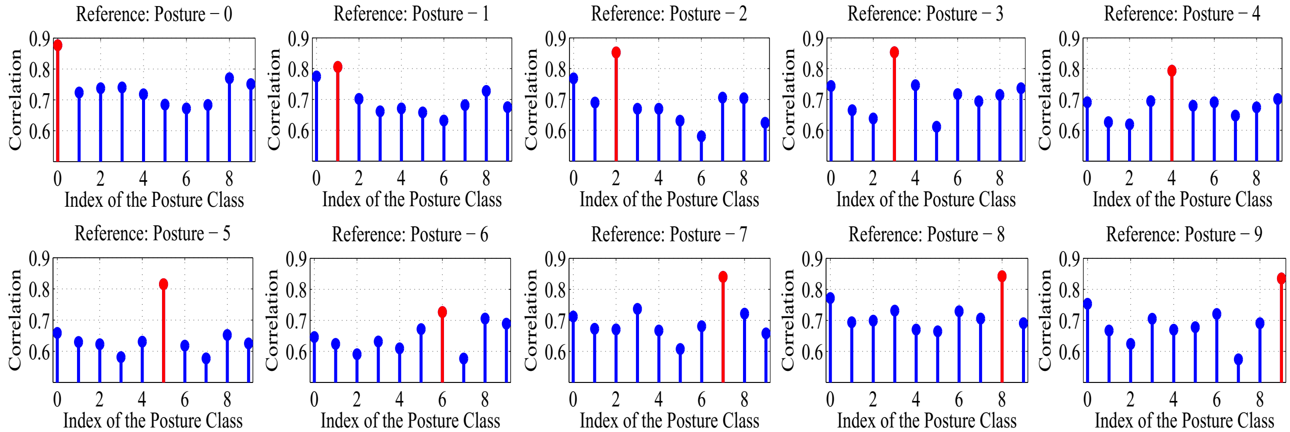


(a)

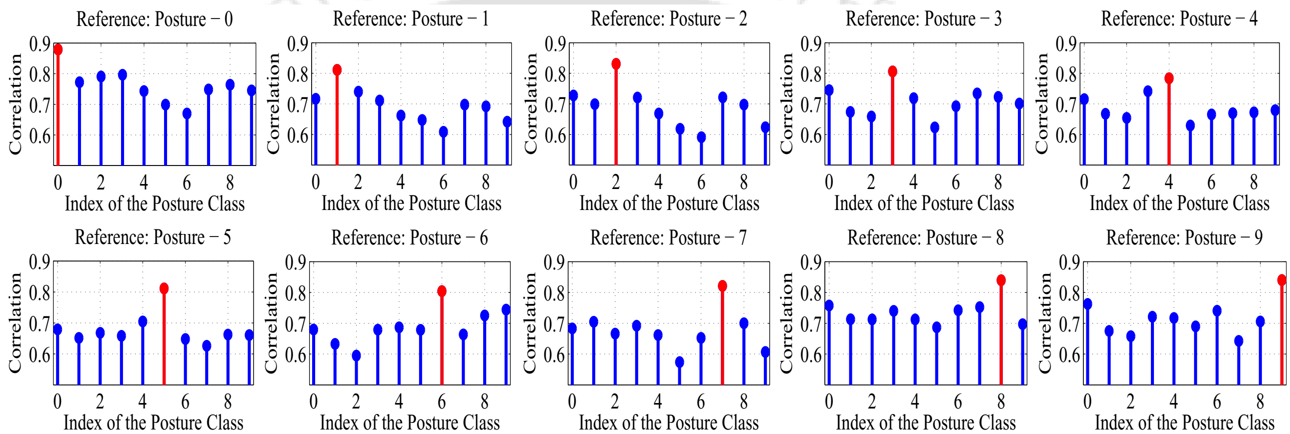


(b)

**Figure 4.17:** Illustration comparing the intraclass and the interclass variability of the samples in (a) Dataset 1 and (b) Dataset 2 based on the correlation measure. The correlation values exhibits the region based similarity between the samples.

postures considered in this work are such that the orientation of palm is uniform for all the hand postures. Therefore, with respect to shape, the overlapping regions in different posture classes mainly comprise of the palm region. Along with the palm region, it is also observed that in some of the posture signs the finger regions also overlap such that some of the posture shapes in the database can be considered as the subsets of other posture shapes in the context of finger configuration.

The illustration of hand posture shapes that constitute the subset of other posture classes due to overlapping finger configurations is shown in Figure 4.18. Among the posture shapes, the shape of posture ‘5’ can be considered as a superset with respect to which the finger configurations of all the other posture classes for the subset. Since, the palm region is uniformly present over all the posture shapes, posture ‘0’ forms the subset of all the posture signs in the database.

Due to these associations between the hand postures, the interclass correlations between the hand posture

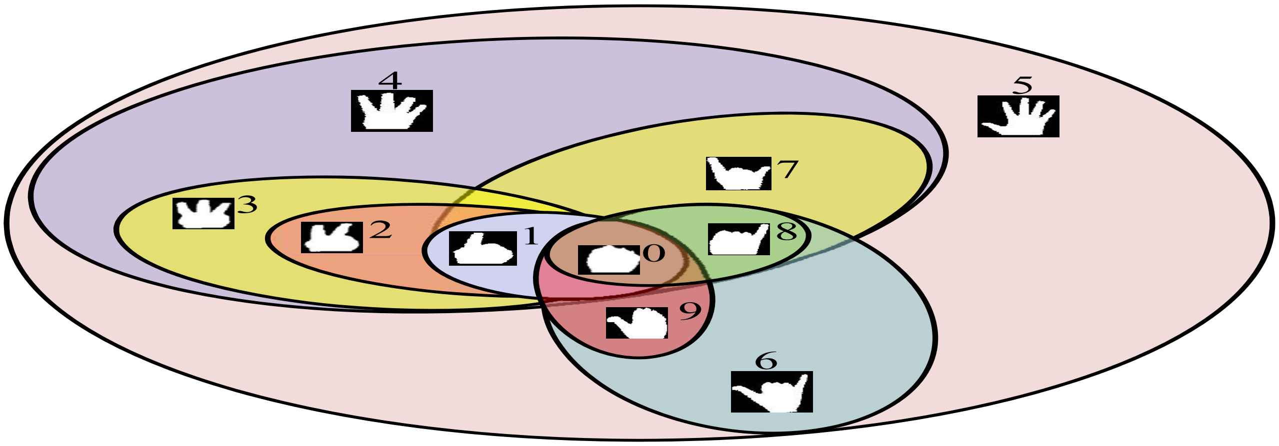


**Figure 4.18:** Illustration of the classes of the hand posture shapes that form the subsets of other posture class in the context of finger configuration.

shapes illustrated through Figure 4.17 are high. On comparing the correlation values obtained for Dataset 1 and Dataset 2, it is clear that the intraclass correlation and the difference between the intraclass and the interclass correlation values decreases for the samples in Dataset 2. Further, due to viewpoint changes the interclass correlation between the posture classes that form the set and the postures contained in the corresponding subsets is observed to increase.

The above analysis on the hand posture variations in terms of the intraclass and the interclass distances suggests that the database is composed of hand posture images with more structural deviations indicating the effects of user variations and the viewpoint changes. Therefore, the above analysis validates the applicability of the developed hand posture database for experiments on user and view invariant hand posture classification.

### 4.4.2 Experiments on hand posture classification

In this study, two sets of experiments are performed to analyze the efficiency of the proposed DOM based hand posture recognition technique. The first experiment studies the user independent characteristics of the DOM features. The second experiment concentrates on studying the view invariant classification accuracy of the DOM features. The performance of the DOM features in both the experiments is verified in comparison with the hand posture descriptors obtained using other state-of-the art features discussed in Section 4.3.3. The details of the experiment and the results obtained for user independent and view invariant hand posture classification are discussed as follows.

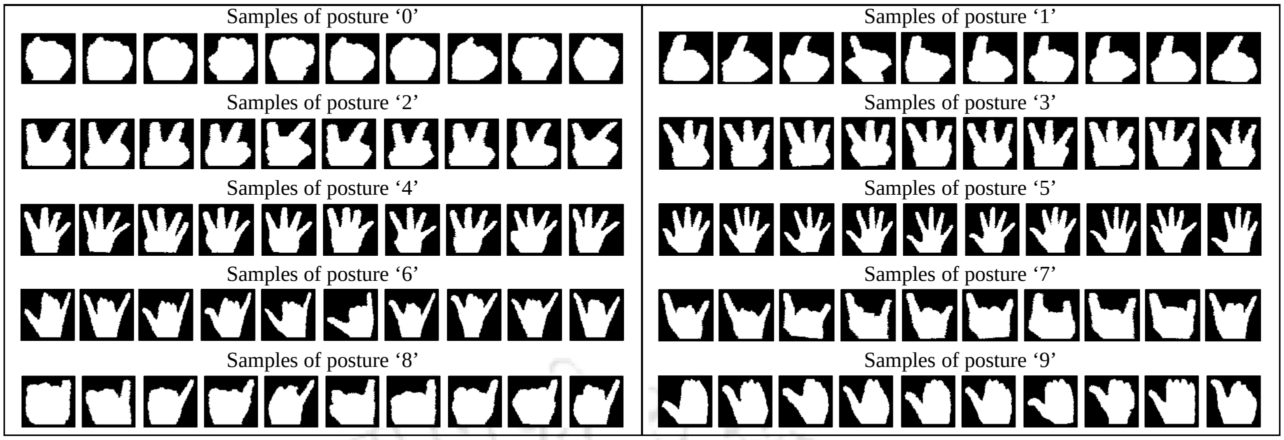


**Figure 4.19:** Examples of the hand postures taken from Dataset 1 to form the training set.

#### 4.4.2.1 Verification of user independence

In order to perform the experiment, the training and the testing samples are taken from Dataset 1. As stated earlier, the hand postures in Dataset 1 are collected at the optimum view angle such that they do not undergo perspective distortions. Therefore, the variations among the hand posture samples in Dataset 1 are only due to the user variations. For this reason, the experiments for verifying the user-invariance are performed using only the samples in Dataset1.

The user independence of the shape descriptors is verified by varying the number of users considered while training. The number of users considered in forming the training set for experimentation are varied as 23, 15, 7 and 1. Thus, the largest training dataset consists of 230 samples with 23 training samples per class. Some examples of the hand postures contained in the training set are shown in Figure 4.19. The classification is performed on $2,030$ testing samples that are collected from 23 users.

The consolidated classification results for different feature descriptors are given in Table 4.1 and the posture wise overall classification rates are shown in the plots in Figure 4.20. The confusion matrices with respect to the classification results in Table 4.1, obtained for each shape descriptor are given in Tables 4.2 - 4.8. From the consolidated scores in Table 4.1, it can be observed that the Krawtchouk moments, the discrete Tchebichef moments and the PCA technique exhibit almost similar performance and they offer high classification accuracies for varying number of users in the training set. Particularly, the DOMs offer high classification accuracy than the PCA method as the number of users in training is reduced to 1. The Zernike moments and the Gabor wavelets offer better results than the geometric moments and the FDs. The geometric moments exhibit the poor performance in terms of the classification rate. The confusion matrices corresponding to the FD based classification results are given in Tables 4.6(a) - 4.6(c). From the posture wise classification results obtained

**Table 4.1:** Comparison of classification results obtained for varying number of users in the training set. The number of testing samples in Dataset 1 is 2030. (% of CC- Percentage of correct classification )

| | | CLASSIFICATION RESULTS FOR THE TESTING SAMPLES FROM DATASET 1 BASED ON | | | | | | |
|---|---|---|---|---|---|---|---|---|
| No. of users in the Training set | No. of Training samples per gesture | Krawtchouk moments | discrete Tchebichef moments | Geometric moments | Zernike moments | FDs | Gabor wavelets | PCA |
| | | % of CC | % of CC | % of CC | % of CC | % of CC | % of CC | % of CC |
| 23 | 23 | 95.22 | 95.47 | 82.07 | 91.87 | 88.08 | 92.81 | 95.37 |
| 15 | 15 | 94.98 | 95.12 | 78.47 | 90.44 | 86.01 | 91.23 | 94.83 |
| 7 | 7 | 91.97 | 92.25 | 72.66 | 86.11 | 82.71 | 87.24 | 92.27 |
| 1 | 1 | 82.12 | 82.27 | 59.16 | 68.13 | 65.52 | 73.65 | 78.87 |

for varying number of users during training, it can be observed that the misclassifications in FD based representation have occurred for samples with almost similar boundary profiles. The posture classes 1, 2, 8 and 9 exhibit higher misclassifications as the number of users in the training set vary. Similarly, posture 6 is mostly mismatched with posture 7 and the misclassification increases for decreasing number of users while training. Apart from these, the samples belonging to other posture classes exhibit almost similar classification rates for varying number of users.

In the case of geometric moments, the rate of misclassification increases considerably as the number of users in the training set decreases. Further, the decline in the classification accuracies indicates that the geometric moments provide the least user independence. The posture-wise classification results of the geometric moments obtained for varying number of users in the training set are tabulated in Tables 4.4(a) - 4.4(c). From these results, it is observed that most of the mismatches have occurred among the postures that are geometrically close. For example, posture 3 is mostly misclassified as posture 2, posture 1 is misidentified as posture 7, posture 2 is recognized as either posture 1 or posture 3 and posture 7 is matched as posture 2. It is also observed that in the case of geometric moments there is poor perceptual correspondence between the mismatched postures. This is because the geometric moments are global features and they only represent the statistical attributes of a shape.

The Zernike moments offer better classification rate than the geometric moments even as the number of users considered for training decreases. From the comprehensive scores of the classification results given in Tables 4.5(a) - 4.5(c), it is understood that the accuracy of Zernike moments is mainly reduced due to the confusion among the postures 1, 8 and 9. Since the Zernike polynomials are defined in the polar domain, the magnitude of the Zernike moments for shapes with almost similar boundary profile will also be approximately same. Hence, similar to the FDs, the misclassification in the case of Zernike moments occurred between the postures that have almost similar boundary profiles. From the samples shown in Figure 4.19, it can be noted that the postures 1, 8 and 9 have almost same boundary profiles and hence, are frequently mismatched.

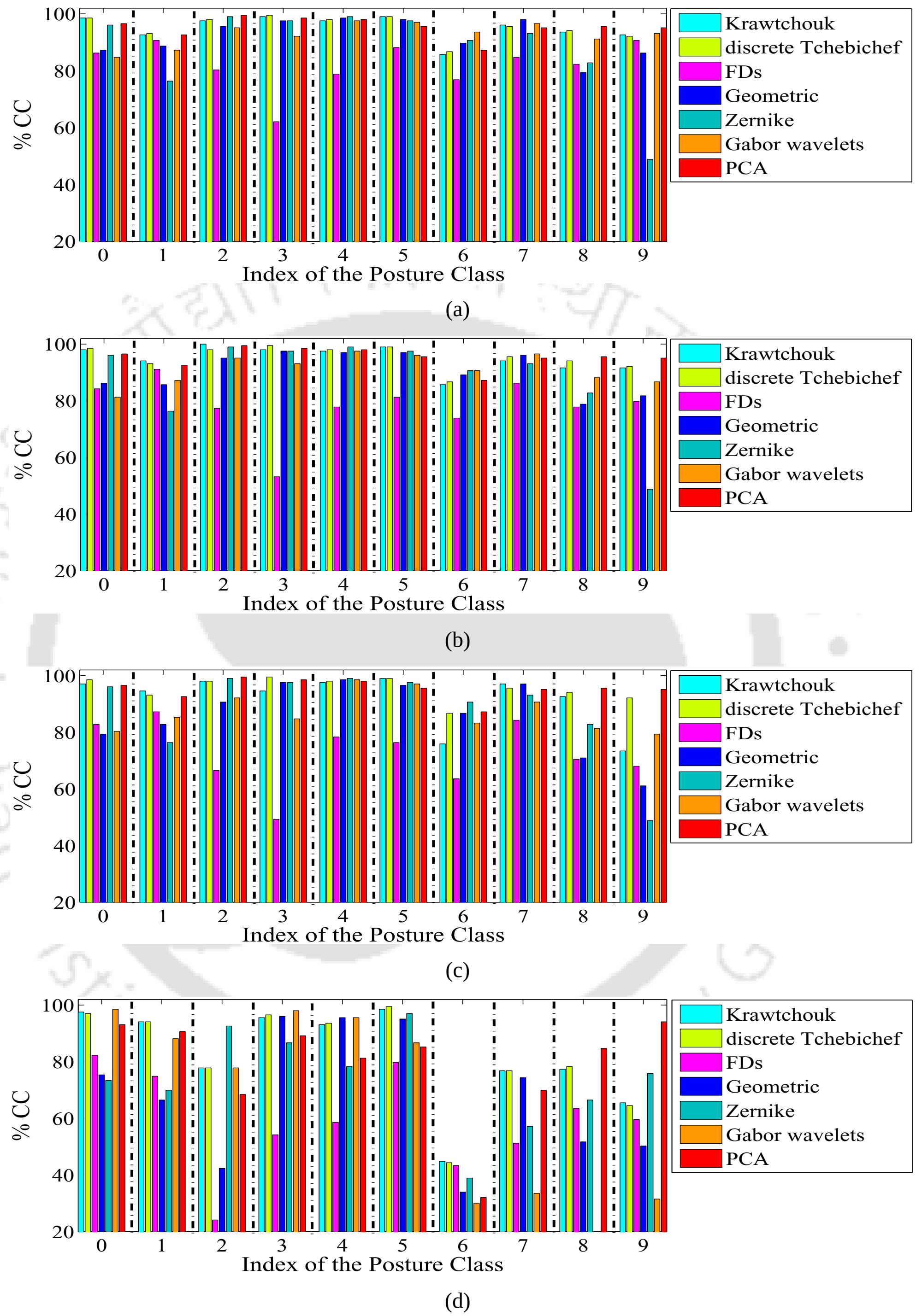


(a)

(b)

(c)

(d)

**Figure 4.20:** Plots of the posture wise classification results for (a) 23 users; (b) 15 users; (c) 7 users and (d) 1 user in the training set.

**Table 4.2:** Confusion matrix corresponding to the results in Table 4.1 for Krawtchouk moment features with respect to varying number of users in the training set and 203 testing samples\gesture.

(a) 23 training samples\gesture.

| O/P I/P | | 1 | 2 | 3 | 4 | 5 | 6 | 7 | 8 | 9 |
|---|---|---|---|---|---|---|---|---|---|---|
| 0 | 200 | 1 | | | | | | | 2 | |
| 1 | | 188 | | | | | | 15 | | |
| 2 | | 2 | 198 | | | | | 3 | | |
| 3 | 1 | | | 201 | | 1 | | | | |
| 4 | 2 | | | 2 | 198 | 1 | | | | |
| 5 | | | | | | 201 | | | | 2 |
| 6 | | | | | 3 | | 174 | 25 | | 1 |
| 7 | | 1 | 1 | | | | 1 | 195 | 5 | |
| 8 | 4 | 3 | | | 2 | | 1 | 3 | 190 | |
| 9 | 3 | | | | | | 6 | 6 | | 188 |

(b) 15 training samples\gesture.

| O/P I/P | 0 | 1 | 2 | 3 | 4 | 5 | 6 | 7 | 8 | 9 |
|---|---|---|---|---|---|---|---|---|---|---|
| 0 | 199 | 1 | | | | | | | 3 | |
| 1 | | 191 | | | | | | 12 | | |
| 2 | | | 203 | | | | | | | |
| 3 | 2 | | | 199 | | 1 | | 1 | | |
| 4 | 2 | | | 2 | 198 | 1 | | | | |
| 5 | | | | | | 201 | | | | 2 |
| 6 | | | | | 5 | | 174 | 23 | | 1 |
| 7 | | 2 | 1 | | | | 3 | 191 | 6 | |
| 8 | 7 | 2 | | | 4 | | 1 | 3 | 186 | |
| 9 | 5 | | | | | | 5 | 7 | | 186 |

(c) 7 training samples\gesture.

| O/P I/P | 0 | 1 | 2 | 3 | 4 | 5 | 6 | 7 | 8 | 9 |
|---|---|---|---|---|---|---|---|---|---|---|
| 0 | 197 | 1 | | | | | | | 5 | |
| 1 | | 192 | | | | | | 11 | | |
| 2 | | 4 | 199 | | | | | | | |
| 3 | 1 | | | 192 | 1 | 1 | | 7 | 1 | |
| 4 | 2 | | | | 198 | 2 | 1 | | | |
| 5 | | | | | | 201 | | | | 2 |
| 6 | | | | | 8 | | 154 | 41 | | |
| 7 | | 1 | 3 | | | | 1 | 197 | 1 | |
| 8 | 4 | 5 | | | 4 | | 1 | 1 | 188 | |
| 9 | 1 | | | 4 | 3 | | 23 | 23 | | 149 |

(d) 1 training samples\gesture.

| O/P I/P | 0 | 1 | 2 | 3 | 4 | 5 | 6 | 7 | 8 | 9 |
|---|---|---|---|---|---|---|---|---|---|---|
| 0 | 198 | 4 | | 1 | | | | | | |
| 1 | 1 | 191 | 1 | | | | 1 | 7 | 1 | 1 |
| 2 | 2 | 43 | 158 | | | | | | | |
| 3 | | | | 194 | 1 | 1 | | 6 | 1 | |
| 4 | 5 | 2 | | 4 | 189 | 2 | | | | 1 |
| 5 | | | | | | 200 | 3 | | | |
| 6 | | | | | 18 | | 91 | 81 | 11 | 2 |
| 7 | | 2 | 42 | 3 | | | | 156 | | |
| 8 | 12 | 3 | 15 | 1 | 1 | | 12 | 2 | 157 | |
| 9 | 5 | | | 2 | 21 | | 12 | 30 | | 133 |

**Table 4.3:** Comprehensive scores of the classification results in Table 4.1 for discrete Tchebichef moments based features with respect to different number of users in the training set and 203 testing samples\gesture.

(a) 23 training samples\gesture.

| O/P I/P | 0 | 1 | 2 | 3 | 4 | 5 | 6 | 7 | 8 | 9 |
|---|---|---|---|---|---|---|---|---|---|---|
| 0 | 200 | 1 | | | | | | | 2 | |
| 1 | | 189 | | | | | | 14 | | |
| 2 | | 1 | 199 | | | | | 3 | | |
| 3 | | | | 202 | | 1 | | | | |
| 4 | 2 | | | 2 | 199 | | | | | |
| 5 | | | | | | 201 | | | | 2 |
| 6 | | | | | 3 | | 176 | 23 | | 1 |
| 7 | | 1 | 1 | | | | 1 | 194 | 6 | |
| 8 | 3 | 3 | | | 2 | | 1 | 3 | 191 | |
| 9 | 3 | | | | | | 8 | 5 | | 187 |

(b) 15 training samples\gesture.

| O/P I/P | 0 | 1 | 2 | 3 | 4 | 5 | 6 | 7 | 8 | 9 |
|---|---|---|---|---|---|---|---|---|---|---|
| 0 | 199 | 1 | | | | | | | 3 | |
| 1 | | 191 | | | | | | 12 | | |
| 2 | | | 203 | | | | | | | |
| 3 | 2 | | | 200 | | 1 | | | | |
| 4 | 2 | | | 1 | 199 | 1 | | | | |
| 5 | | | | | | 201 | | | | 2 |
| 6 | | | | | 6 | | 174 | 22 | | 1 |
| 7 | | 2 | 1 | | | | 3 | 190 | 7 | |
| 8 | 4 | 2 | | | 4 | | 1 | 3 | 189 | |
| 9 | 4 | | | | 1 | | 6 | 7 | | 185 |

(c) 7 training samples\gesture.

| O/P I/P | 0 | 1 | 2 | 3 | 4 | 5 | 6 | 7 | 8 | 9 |
|---|---|---|---|---|---|---|---|---|---|---|
| 0 | 197 | 1 | | | | | | | 5 | |
| 1 | | 192 | | | | | | 11 | | |
| 2 | | 4 | 199 | | | | | | | |
| 3 | 1 | | | 193 | 1 | 1 | | 6 | 1 | |
| 4 | 2 | | | | 199 | 1 | 1 | | | |
| 5 | | | | | | 201 | | | | 2 |
| 6 | | | | | 9 | | 155 | 39 | | |
| 7 | | 1 | 3 | | | | 1 | 197 | 1 | |
| 8 | 4 | 4 | | | 4 | | 1 | 1 | 189 | |
| 9 | 1 | | | 3 | 3 | | 26 | 22 | | 148 |

(d) 1 training samples\gesture.

| O/P I/P | 0 | 1 | 2 | 3 | 4 | 5 | 6 | 7 | 8 | 9 |
|---|---|---|---|---|---|---|---|---|---|---|
| 0 | 197 | 5 | | 1 | | | | | | |
| 1 | 1 | 191 | 1 | | | | 1 | 7 | 1 | 1 |
| 2 | 2 | 43 | 158 | | | | | | | |
| 3 | | | | 196 | 1 | 1 | | 4 | 1 | |
| 4 | 5 | 2 | | 3 | 190 | 2 | | | | 1 |
| 5 | | | | | | 202 | 1 | | | |
| 6 | | | | | 29 | | 90 | 71 | 12 | 1 |
| 7 | | 2 | 42 | 3 | | | | 156 | | |
| 8 | 9 | 3 | 15 | 1 | 2 | | 12 | 2 | 159 | |
| 9 | 5 | | | 2 | 23 | 1 | 12 | 29 | | 131 |

**Table 4.4:** Confusion matrix corresponding to the results in Table 4.1 for geometric moments based features with respect to different number of users in the training set and 203 testing samples\gesture.

(a) 23 training samples\gesture.

| O/P I/P | 0 | 1 | 2 | 3 | 4 | 5 | 6 | 7 | 8 | 9 |
|---|---|---|---|---|---|---|---|---|---|---|
| 0 | 175 | | 1 | 8 | 1 | | | 1 | 8 | 9 |
| 1 | | 184 | | | | | | 19 | | |
| 2 | | 18 | 163 | 13 | 4 | 2 | | 1 | 1 | 1 |
| 3 | 4 | 1 | 53 | 126 | 12 | | | 1 | | 6 |
| 4 | 1 | 1 | 12 | 18 | 160 | 5 | 2 | | 3 | 1 |
| 5 | | | | | 13 | 179 | 7 | | | 4 |
| 6 | | 1 | | 1 | 10 | 5 | 156 | 27 | | 3 |
| 7 | | 1 | 17 | 2 | 3 | | 3 | 172 | 5 | |
| 8 | 9 | 3 | 3 | 5 | 13 | | 2 | 1 | 167 | |
| 9 | | | 1 | 4 | | | 2 | 12 | | 184 |

(b) 15 training samples\gesture.

| O/P I/P | 0 | 1 | 2 | 3 | 4 | 5 | 6 | 7 | 8 | 9 |
|---|---|---|---|---|---|---|---|---|---|---|
| 0 | 171 | 5 | 1 | 12 | 3 | | | 1 | 7 | 3 |
| 1 | | 185 | | | | | 1 | 17 | | |
| 2 | | 18 | 157 | 19 | 6 | | | 1 | 1 | 1 |
| 3 | 5 | 1 | 65 | 108 | 19 | | | | | 5 |
| 4 | 1 | 1 | 15 | 15 | 158 | 5 | 3 | | 2 | 3 |
| 5 | | | | | 22 | 165 | 13 | | | 3 |
| 6 | | 5 | | | 16 | 6 | 150 | 23 | 1 | 2 |
| 7 | | 1 | 10 | 2 | 3 | | 5 | 175 | 7 | |
| 8 | 11 | 2 | 4 | 2 | 22 | | 3 | 1 | 158 | |
| 9 | 3 | 2 | 1 | 8 | | | 2 | 25 | | 162 |

(c) 7 training samples\gesture.

| O/P I/P | 0 | 1 | 2 | 3 | 4 | 5 | 6 | 7 | 8 | 9 |
|---|---|---|---|---|---|---|---|---|---|---|
| 0 | 168 | 4 | 1 | 14 | 4 | | | 1 | 8 | 3 |
| 1 | | 177 | | | | | 1 | 25 | | |
| 2 | | 26 | 135 | 29 | 8 | | | 2 | 1 | 2 |
| 3 | 19 | | 54 | 100 | 20 | | 1 | 1 | | 8 |
| 4 | 1 | 2 | 2 | 19 | 159 | 5 | 10 | | 2 | 3 |
| 5 | | 2 | | | 22 | 155 | 21 | | | 3 |
| 6 | | 1 | | 2 | 30 | 1 | 129 | 38 | 1 | 1 |
| 7 | | 1 | 15 | 2 | 4 | | 4 | 171 | 6 | |
| 8 | 13 | 4 | 3 | 2 | 34 | | 4 | | 143 | |
| 9 | 2 | 2 | 2 | 9 | 4 | | 5 | 41 | | 138 |

(d) 1 training samples\gesture.

| O/P I/P | 0 | 1 | 2 | 3 | 4 | 5 | 6 | 7 | 8 | 9 |
|---|---|---|---|---|---|---|---|---|---|---|
| 0 | 167 | | | 33 | | | | | 1 | 2 |
| 1 | | 152 | | 2 | 9 | 5 | 4 | 26 | 5 | |
| 2 | | 111 | 49 | 34 | 2 | | | | 7 | |
| 3 | 16 | 6 | 20 | 110 | 12 | | 1 | | 3 | 35 |
| 4 | 1 | 26 | | 8 | 119 | 13 | 1 | | 16 | 19 |
| 5 | | | | | 36 | 162 | | | 1 | 4 |
| 6 | | | | | 45 | 18 | 88 | 48 | 1 | 3 |
| 7 | | 14 | 65 | 12 | 3 | | 1 | 104 | 2 | 2 |
| 8 | 15 | 2 | 24 | 16 | | | 10 | 1 | 129 | 6 |
| 9 | 1 | 1 | | 11 | 16 | | 3 | 47 | 3 | 121 |

**Table 4.5:** Confusion matrix corresponding to the results in Table 4.1 for Zernike moment features under varying number of users in the training set and 203 testing samples\gesture.

(a) 23 training samples\gesture.

| O/P I/P | 0 | 1 | 2 | 3 | 4 | 5 | 6 | 7 | 8 | 9 |
|---|---|---|---|---|---|---|---|---|---|---|
| 0 | 177 | 4 | | | | | | | 18 | 4 |
| 1 | | 180 | | | | | | 5 | 3 | 15 |
| 2 | | 4 | 194 | | | | | | | 5 |
| 3 | | | 1 | 198 | 3 | | | 1 | | |
| 4 | | | | 1 | 200 | 1 | | | | 1 |
| 5 | | | | | | 199 | 4 | | | |
| 6 | | | | | | | 182 | 17 | 1 | 3 |
| 7 | | | 3 | | | | | 199 | 1 | |
| 8 | | 18 | | | | | | 2 | 161 | 22 |
| 9 | | 8 | | | | | | 1 | 19 | 175 |

(b) 15 training samples\gesture.

| O/P I/P | 0 | 1 | 2 | 3 | 4 | 5 | 6 | 7 | 8 | 9 |
|---|---|---|---|---|---|---|---|---|---|---|
| 0 | 175 | 6 | | | | | | | 17 | 5 |
| 1 | | 174 | | | | | | 4 | 6 | 19 |
| 2 | | 4 | 193 | | | | | | | 6 |
| 3 | | | 1 | 198 | 3 | | | 1 | | |
| 4 | | | | 2 | 197 | 2 | | | 2 | |
| 5 | | | | | | 197 | 6 | | | |
| 6 | | | | | | | 181 | 17 | 1 | 4 |
| 7 | | 2 | 3 | | | | 1 | 195 | 2 | |
| 8 | | 17 | | | | | | 2 | 160 | 24 |
| 9 | | 17 | | | | | 1 | 4 | 15 | 166 |

(c) 7 training samples\gesture.

| O/P I/P | 0 | 1 | 2 | 3 | 4 | 5 | 6 | 7 | 8 | 9 |
|---|---|---|---|---|---|---|---|---|---|---|
| 0 | 161 | 12 | | | | | | | 16 | 14 |
| 1 | | 168 | | | | | 3 | 14 | 3 | 15 |
| 2 | | 5 | 184 | | | | | | | 14 |
| 3 | | | | 198 | 3 | | | 1 | | 1 |
| 4 | | | | 1 | 200 | | | | 2 | |
| 5 | | | | | 1 | 196 | 6 | | | |
| 6 | | | | | | | 176 | 26 | | 1 |
| 7 | | 2 | 3 | | | | | 197 | | 1 |
| 8 | | 32 | | | | | 1 | 12 | 144 | 14 |
| 9 | | 17 | | | | | 5 | 25 | 32 | 124 |

(d) 1 training samples\gesture.

| O/P I/P | 0 | 1 | 2 | 3 | 4 | 5 | 6 | 7 | 8 | 9 |
|---|---|---|---|---|---|---|---|---|---|---|
| 0 | 153 | 12 | | | | | | | | 38 |
| 1 | | 135 | | | | | 4 | 36 | | 28 |
| 2 | | 7 | 86 | 20 | | | 1 | | | 89 |
| 3 | | | | 195 | | | | 6 | | 2 |
| 4 | | | | 9 | 194 | | | | | |
| 5 | | | | | 5 | 193 | 5 | | | |
| 6 | | 1 | | | 1 | | 69 | 130 | 1 | 1 |
| 7 | | | 24 | 1 | | | | 151 | 1 | 26 |
| 8 | | 25 | 3 | 5 | | | 3 | 16 | 105 | 46 |
| 9 | | 30 | | | | | 9 | 48 | 14 | 102 |

**Table 4.6:** Confusion matrix corresponding to the results in Table 4.1 for FD based representation with respect to varying number of users in the training set and 203 testing samples\gesture.

(a) 23 training samples\gesture.

| I/P \ O/P | 0 | 1 | 2 | 3 | 4 | 5 | 6 | 7 | 8 | 9 |
|---|---|---|---|---|---|---|---|---|---|---|
| 0 | 195 | 2 | | | | | | | 6 | |
| 1 | | 155 | | | | | | | 41 | 7 |
| 2 | | 2 | 201 | | | | | | | |
| 3 | | | 1 | 198 | 2 | | 1 | | | 1 |
| 4 | | | | 2 | 201 | | | | | |
| 5 | | | | | 5 | 198 | | | | |
| 6 | | 3 | | | | | 184 | 14 | 1 | 1 |
| 7 | | 2 | 1 | | | | 4 | 189 | 2 | 5 |
| 8 | | 20 | | | | | | 1 | 168 | 14 |
| 9 | | 41 | | | | | | | 63 | 99 |

(b) 15 training samples\gesture.

| I/P \ O/P | 0 | 1 | 2 | 3 | 4 | 5 | 6 | 7 | 8 | 9 |
|---|---|---|---|---|---|---|---|---|---|---|
| 0 | 193 | 4 | | | | | | | 6 | |
| 1 | | 144 | | | | | | | 47 | 12 |
| 2 | | 2 | 201 | | | | | | | |
| 3 | | | 1 | 198 | 2 | | 1 | | | 1 |
| 4 | | | | 2 | 201 | | | | | |
| 5 | | | | | 5 | 198 | | | | |
| 6 | | 6 | | | | | 177 | 19 | 1 | |
| 7 | | | 2 | | | | 4 | 185 | 3 | 9 |
| 8 | | 21 | | | | | | 2 | 166 | 14 |
| 9 | | 47 | | | | | | | 73 | 83 |

(c) 7 training samples\gesture.

| I/P \ O/P | 0 | 1 | 2 | 3 | 4 | 5 | 6 | 7 | 8 | 9 |
|---|---|---|---|---|---|---|---|---|---|---|
| 0 | 191 | 12 | | | | | | | | |
| 1 | | 153 | | | | | | 1 | 36 | 13 |
| 2 | | | 200 | | | | 1 | | 1 | 1 |
| 3 | | | | 198 | 2 | | 1 | | | 2 |
| 4 | | | | 2 | 201 | | | | | |
| 5 | | | | | 10 | 193 | | | | |
| 6 | | 4 | | | | | 151 | 48 | | |
| 7 | | | 5 | | | | 1 | 188 | 5 | 4 |
| 8 | | 37 | | | | | | 5 | 143 | 18 |
| 9 | | 62 | | | | | | | 80 | 61 |

(d) 1 training samples\gesture.

| I/P \ O/P | 0 | 1 | 2 | 3 | 4 | 5 | 6 | 7 | 8 | 9 |
|---|---|---|---|---|---|---|---|---|---|---|
| 0 | 200 | 3 | | | | | | | | |
| 1 | | 179 | | | | | 13 | 1 | 4 | 6 |
| 2 | | | 158 | 6 | | | | | | 39 |
| 3 | | | | 199 | | | | 1 | | 3 |
| 4 | | | | 4 | 194 | 5 | | | | |
| 5 | | | | | 25 | 176 | | | 2 | |
| 6 | | 14 | | | | | 61 | 126 | | 2 |
| 7 | | | 47 | | | | 4 | 68 | 22 | 62 |
| 8 | | 89 | | | | | 50 | | 31 | 33 |
| 9 | | 80 | | | | | 48 | | 11 | 64 |

**Table 4.7:** Confusion matrix corresponding to the results in Table 4.1 for Gabor wavelets based features under varying number of users in the training set and 203 testing samples\gesture.

(a) 23 training samples\gesture.

| I/P \ O/P | 0 | 1 | 2 | 3 | 4 | 5 | 6 | 7 | 8 | 9 |
|---|---|---|---|---|---|---|---|---|---|---|
| 0 | 172 | 7 | | | | | | | 5 | 19 |
| 1 | 2 | 177 | | | | | | 2 | 11 | 11 |
| 2 | | | 193 | | | | | 3 | 7 | |
| 3 | | | | 187 | 1 | | | 10 | 2 | 3 |
| 4 | | | | 1 | 198 | | 1 | 3 | | |
| 5 | | | | | | 197 | 6 | | | |
| 6 | 1 | 3 | | | 1 | | 190 | 8 | | |
| 7 | | 1 | 1 | 3 | | | 1 | 196 | 1 | |
| 8 | 8 | 5 | | | | | | 4 | 185 | 1 |
| 9 | 4 | 1 | | | | | 1 | 8 | | 189 |

(b) 15 training samples\gesture.

| I/P \ O/P | 0 | 1 | 2 | 3 | 4 | 5 | 6 | 7 | 8 | 9 |
|---|---|---|---|---|---|---|---|---|---|---|
| 0 | 165 | 10 | | | | | | | 6 | 22 |
| 1 | 2 | 177 | | | | | | 2 | 11 | 11 |
| 2 | | | 193 | | | | | 3 | 7 | |
| 3 | | | | 189 | 1 | | | 9 | 2 | 2 |
| 4 | | | | 1 | 198 | | | 2 | 2 | |
| 5 | | | | | | 195 | 8 | | | |
| 6 | 7 | 4 | | | 1 | | 184 | 6 | | 1 |
| 7 | | 1 | 1 | 3 | | | 1 | 196 | 1 | |
| 8 | 10 | 9 | | | | | | 4 | 179 | 1 |
| 9 | 6 | 1 | | | | | 14 | 6 | | 176 |

(c) 7 training samples\gesture.

| I/P \ O/P | 0 | 1 | 2 | 3 | 4 | 5 | 6 | 7 | 8 | 9 |
|---|---|---|---|---|---|---|---|---|---|---|
| 0 | 163 | 14 | | | | | | | 7 | 19 |
| 1 | 9 | 173 | | | | | 1 | 5 | 5 | 10 |
| 2 | | 1 | 187 | | | | | 5 | 10 | |
| 3 | | | 16 | 172 | 1 | | | 7 | 5 | 2 |
| 4 | | | | 1 | 200 | | | 2 | | |
| 5 | | | | | | 197 | 6 | | | |
| 6 | 11 | 10 | | | 1 | | 169 | 9 | | 3 |
| 7 | 1 | 1 | 15 | | | | 1 | 184 | 1 | |
| 8 | 15 | 13 | | | | | | 9 | 165 | 1 |
| 9 | 5 | 3 | | | | | 26 | 8 | | 161 |

(d) 1 training samples\gesture.

| I/P \ O/P | 0 | 1 | 2 | 3 | 4 | 5 | 6 | 7 | 8 | 9 |
|---|---|---|---|---|---|---|---|---|---|---|
| 0 | 149 | 36 | | | | | | 2 | 2 | 14 |
| 1 | 42 | 142 | | | | | 4 | 2 | 1 | 12 |
| 2 | | 3 | 188 | 1 | | | | 4 | 7 | |
| 3 | | 1 | 10 | 176 | | | | 13 | 1 | 2 |
| 4 | | | | 3 | 159 | | 1 | 19 | 21 | |
| 5 | | | | | | 197 | 6 | | | |
| 6 | 29 | 1 | | | 11 | 19 | 79 | 63 | | 1 |
| 7 | | 1 | 52 | 33 | | | 1 | 116 | | |
| 8 | 1 | 46 | 1 | | | | | 18 | 135 | 2 |
| 9 | 4 | | | | | | 36 | 9 | | 154 |

**Table 4.8:** Confusion matrix corresponding to the results in Table 4.1 for PCA based description with different number of users in the training set and 203 testing samples\gesture.

(a) 23 training samples\gesture.

| I/P \ O/P | 0 | 1 | 2 | 3 | 4 | 5 | 6 | 7 | 8 | 9 |
|---|---|---|---|---|---|---|---|---|---|---|
| 0 | 196 | 3 | | | | | | 1 | 3 | |
| 1 | | 188 | | | | | | 14 | | 1 |
| 2 | | 1 | 202 | | | | | | | |
| 3 | 2 | | | 200 | 1 | | | | | |
| 4 | 4 | | | | 199 | | | | | |
| 5 | | | | | | 194 | 3 | | | 6 |
| 6 | | | | | 1 | | 177 | 24 | | 1 |
| 7 | | 4 | 1 | | | | | 193 | 5 | |
| 8 | 2 | 3 | | | 1 | | 1 | 2 | 194 | |
| 9 | 4 | 1 | 1 | 2 | | | | 2 | | 193 |

(b) 15 training samples\gesture.

| I/P \ O/P | 0 | 1 | 2 | 3 | 4 | 5 | 6 | 7 | 8 | 9 |
|---|---|---|---|---|---|---|---|---|---|---|
| 0 | 195 | 4 | | | | | | 1 | 3 | |
| 1 | | 186 | 2 | | | | | 14 | | 1 |
| 2 | | 1 | 202 | | | | | | | |
| 3 | 2 | | | 200 | | | 1 | | | |
| 4 | 4 | | | 1 | 197 | | | | 1 | |
| 5 | | | | | | 193 | 4 | | | 6 |
| 6 | | | | | 1 | | 179 | 22 | | 1 |
| 7 | | 5 | 1 | | | | 3 | 186 | 8 | |
| 8 | 3 | 2 | | | 1 | | 1 | 1 | 195 | |
| 9 | 4 | 2 | | 2 | | | | 3 | | 192 |

(c) 7 training samples\gesture.

| I/P \ O/P | 0 | 1 | 2 | 3 | 4 | 5 | 6 | 7 | 8 | 9 |
|---|---|---|---|---|---|---|---|---|---|---|
| 0 | 193 | 5 | | | | | | | 4 | 1 |
| 1 | | 186 | 2 | | | | | 15 | | |
| 2 | | 4 | 199 | | | | | | | |
| 3 | 3 | 2 | | 184 | 3 | | | 8 | 3 | |
| 4 | 4 | | | | 197 | | | | 2 | |
| 5 | | | | | | 193 | 5 | | | 5 |
| 6 | | | | | 3 | | 152 | 47 | | 1 |
| 7 | | 3 | 2 | | | | 2 | 195 | 1 | |
| 8 | 2 | 1 | 7 | | | | 2 | 1 | 190 | |
| 9 | 3 | | | 7 | | | | 9 | | 184 |

(d) 1 training samples\gesture.

| I/P \ O/P | 0 | 1 | 2 | 3 | 4 | 5 | 6 | 7 | 8 | 9 |
|---|---|---|---|---|---|---|---|---|---|---|
| 0 | 189 | 10 | | 3 | | | | | | 1 |
| 1 | 1 | 184 | 10 | | | | | 7 | 1 | |
| 2 | 2 | 62 | 139 | | | | | | | |
| 3 | 1 | 2 | 1 | 181 | 1 | | | 14 | 3 | |
| 4 | 4 | 10 | | 1 | 165 | | | | 23 | |
| 5 | | | | | 4 | 173 | 20 | | 2 | 4 |
| 6 | | | | | 29 | | 65 | 87 | 20 | 2 |
| 7 | 2 | 5 | 52 | 2 | | | | 142 | | |
| 8 | 3 | | 10 | 4 | | | 13 | 1 | 172 | |
| 9 | 3 | | | 1 | | | 1 | 6 | 1 | 191 |

In the case of Krawtchouk moments, the mismatch has occurred between the postures with coinciding regions. As per the results in Tables 4.2(a) - 4.2(c), the postures 1, 6 and 9 exhibit higher misclassifications. Further, it is observed that the posture classes 6 and 9 show significant improvement in the classification accuracy as the number of users in the training set increases. It can be noticed that posture classes 1 and 6 are frequently mismatched with posture class 7 and posture class 9 is mismatched with posture classes 6 and 7. Similar observations can be made from the results obtained for discrete Tchebichef moment based features. From the confusion matrices given in Tables 4.3(a) - 4.3(c), it is clear that the misclassifications in the case of discrete Tchebichef moment features are similar to the Krawtchouk moments.

The misclassifications in DOM based representations occur when the hand posture images consist of overlapping regions. With respect to the shape, some posture signs in the dataset can be considered as the subsets of other signs in the context of spatial distribution of their pixels. To show that, in DOMs based representation

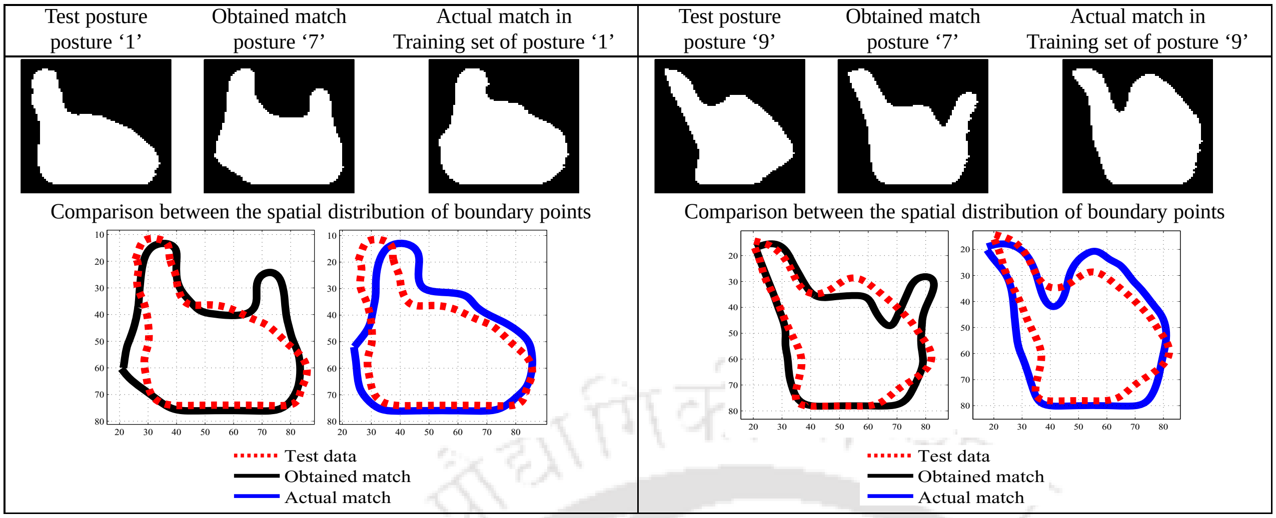


**Figure 4.21:** Examples of results from DOM based classification. The illustration is presented to show that the DOM depend on the similarity between the spatial distribution of the pixels within the posture regions. The spatial correspondence between the postures is analyzed based on the shape boundary. It can be observed that the maximum number of boundary pixels from the test sample coincide more with the obtained match rather than the actual match.

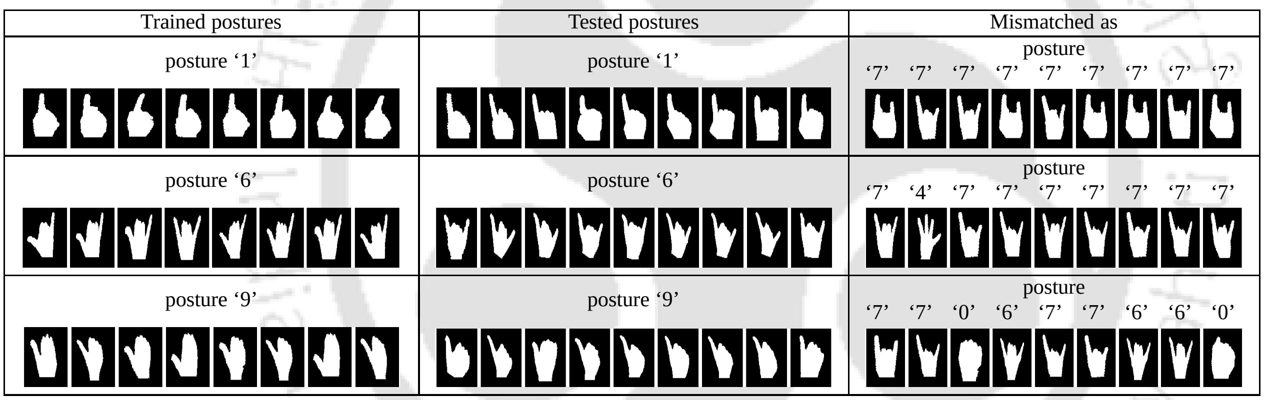


**Figure 4.22:** Results from the experiment on user invariance. Examples of the testing samples that are misclassified in DOMs based method. The correspondence of the test posture can be observed to be high with respect to the mismatched posture rather than the trained postures within the same class.

the confusion has occurred between the postures with almost same spatial distribution of the pixels, a simple analysis is performed by comparing the spatial distribution of the boundary pixels. If the boundary pixels exhibit higher correspondence, so will be the regions within the boundaries will exhibit similar correspondence. Figure 4.21 illustrates a few examples from the misclassifications in posture classes 1 and 9. It can be verified that the spatial distribution of the pixels in the test postures coincides highly with the matches obtained through Krawtchouk moments based classification. Some examples of these misclassifications along with the corresponding training postures are shown in Figure 4.22.

The comprehensive scores of the classification results obtained for Gabor wavelet based hand posture description are given in Table 4.7(a) and Table 4.7(c). It is seen that more misclassification occurs due to the

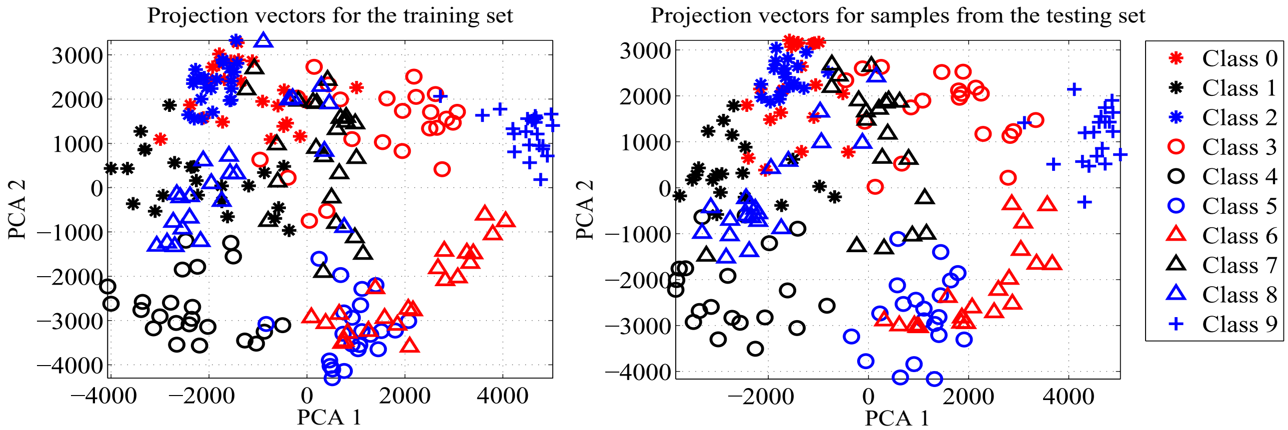


**Figure 4.23:** Illustration of separation between the hand posture classes in PCA projection space.

posture classes 0, 1, 3, 6, 8 and 9. The mismatch in Gabor wavelets based description occurs between the samples with similar edge magnitudes and the orientations. For example, the posture class 9 is mostly mismatched with posture class 6. In Section 4.4.1, it has been shown that the posture sign 9 can be considered as a subset of posture sign 6. The coinciding thumb finger region in both these posture classes have same orientation and hence, these postures are matched. From Table 4.1, it can be observed that the rate of misclassification in Gabor wavelets based classification drastically increases when the number of users in training is decreased to 7. As we examine the confusion matrix in Table 4.7(c), it is evident that the misclassification has increased for all the posture classes.

The confusion matrices for the PCA based classification results are given in Tables 4.8(a) - 4.8(c). By comparing the posture wise classification results, it can be understood that the performance of the PCA technique is consistent with the varying number of users in training. More misclassification has occurred in the posture classes 1 and 6. In the case of PCA projections, the between-class separation is not considered and hence, the projections corresponding to different image classes largely overlap. The plot illustrating the projection on the first two PCA components is shown in Figure 4.23. The misclassification occurs when the projection corresponding to the test sample fall within the overlapping region.

The observations from the experimental results on user invariance can be summarized as follows.

1] The Krawtchouk and the discrete Tchebichef moments offer high classification accuracies. Even as the number of users decreases during training, the classification scores are almost similar. This shows that the DOMS are user invariant features. Particularly, the discrete Tchebichef moments offer slightly better performance in comparison to Krawtchouk moments.

2] The geometric moments offer low classification accuracies and the misclassifications increases for decreasing number of users. This implies that the geometric moments are sensitive to user variations and they exhibit poor user invariance.

3] The FDs and the Zernike moments fail in efficiently discriminating hand posture shapes with almost similar boundary profile. The FDs are derived from the frequency description of $1D$ boundary profile and hence, the information on spatial localization is lost. In the case of Zernike moments, the information about spatial localization in preserved in the polar domain representation. However, even small boundary deviations in the spatial domain may cause large shifts in the polar domain due to which misclassifications occur between samples with similar boundary profiles.

From the plot of the intraclass distance based on Pratt's FOM as shown in Figure 4.15, it can be noted that the boundary distortion between the intraclass samples is comparatively more for posture classes 1, 6, 8 and 9. As a result, the misclassifications in FDs and Zernike moments are mainly due to postures 1, 6, 8 and 9. Except for these postures, the FDs and the Zernike moments exhibit consistently high classification accuracies for other posture classes. Hence, the FDs and the Zernike moments are robust to user variations in classifying hand postures with distinct boundary profile.

4] The Gabor wavelets offer better classification accuracy when the number of users in the training is more. As the number of users decreases to 7, the performance of the Gabor wavelets decreases by almost 4%. This implies that the Gabor wavelets based description requires large number of training samples for achieving user independence.

5] From the results obtained for the PCA, we infer that the performance efficiency of the PCA is similar to that of the Krawtchouk features and PCA offers high classification accuracy exhibiting more robustness to user variations. However, as the number of user is reduced to 1, the performance of PCA is significantly less than the DOMs.

#### 4.4.2.2 Verification of view invariance

The view angle variations during hand posture acquisition lead to perspective distortions and may sometimes cause self-occlusion. The self-occlusion can also be due to the poor flexibility of the postures. The study on view invariance verifies the robustness of the methods towards the effects of viewpoint changes.

In order to study the view invariance property of the considered methods, the initial experiment is performed by considering the training set taken from Dataset 1. We refer the training samples from Dataset 1 as *Training set-I*. The testing set consists of 3,600 samples that include 2,030 samples from Dataset 1 and 1,570 samples from Dataset 2. The classification results obtained using the Training set-I are tabulated in Table 4.9. The comprehensive posture-wise classification scores are given in Table 4.10(a) - 4.10(g).

**Table 4.9:** Experimental validation of view invariance. Comparison of classification results obtained for Training set-I and II. The training set includes hand postures collected from 23 users. The number of testing samples in Dataset 1 and Dataset 2 is 2,030 and 1,570 respectively. (% CC- percentage of correct classification. )

| Methods | Training set-I | | | Training set-II | | |
|---|---|---|---|---|---|---|
| | % CC for Dataset 1 | % CC for Dataset 2 | Overall % CC | % CC for Dataset 1 | % CC for Dataset 2 | Overall % CC |
| Krawtchouk moments | 95.22 | 87.90 | 92.03 | 97.93 | 95.73 | 96.97 |
| discrete Tchebichef moments | 95.47 | 88.79 | 92.55 | 97.83 | 96.24 | 97.14 |
| Geometric moments | 82.07 | 71.4 | 77.42 | 87.39 | 80.57 | 84.42 |
| Zernike moments | 90.89 | 75.48 | 84.17 | 94.83 | 90.32 | 92.86 |
| FDs | 88.08 | 70.57 | 80.44 | 90.15 | 85.99 | 88.33 |
| Gabor wavelets | 92.81 | 73.12 | 84.22 | 95.52 | 88.47 | 92.44 |
| PCA | 95.37 | 88.79 | 91.38 | 97.93 | 96.24 | 97.19 |

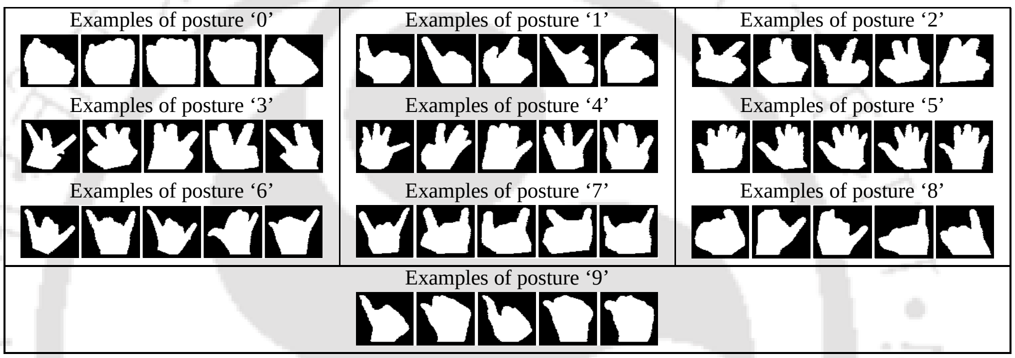


**Figure 4.24:** Samples of the test postures from Dataset 2 that has less recognition accuracy with respect to all the methods.

From the results in Table 4.9, it is evident that among the considered methods, the Krawtchouk moments, the discrete Tchebichef moments and the PCA technique offer better classification accuracy. The performance efficiency of other methods that includes FDs, Zernike moments and Gabor wavelets mainly degrades for samples from Dataset 2. This implies that the DOMs and the PCA based descriptors exhibit more robustness to view angle variations. It should be noted that the discrete Tchebichef moments

By comparing the classification results given in the Tables 4.9, it is observed that the number of misclassifications is notably more for almost all the postures in Dataset 2. It is known that the perspective distortion affects the boundary profile and the geometric attributes of a shape. Hence, the FDs and the geometric moments are insufficient for recognizing the postures under view angle variations. From the detailed scores in Tables 4.10(e), we infer that the number of classes misclassified in FD based technique is more than in the case of user independence and it is difficult to establish the perceptual correspondence between the mismatched samples.

From the comprehensive scores for the geometric moments based features given in Table 4.10(c), it is understood that performance of the geometric moments becomes unstable for structural distortions due to view

**Table 4.10:** Confusion Matrix for the classification results given in Table 4.9 for Training set-I with 23 training samples\gesture sign and 360 testing samples\gesture sign. Detailed scores for

(a) Krawtchouk moments based features

| I/P \ O/P | 0 | 1 | 2 | 3 | 4 | 5 | 6 | 7 | 8 | 9 |
|---|---|---|---|---|---|---|---|---|---|---|
| 0 | 355 | 3 | 0 | 0 | 0 | 0 | 0 | 0 | 2 | 0 |
| 1 | 0 | 323 | 1 | 0 | 0 | 0 | 0 | 34 | 0 | 2 |
| 2 | 6 | 17 | 334 | 0 | 0 | 0 | 0 | 3 | 0 | 0 |
| 3 | 18 | 1 | 10 | 317 | 1 | 1 | 0 | 0 | 2 | 10 |
| 4 | 12 | 0 | 0 | 7 | 331 | 3 | 0 | 3 | 3 | 1 |
| 5 | 1 | 0 | 0 | 0 | 0 | 337 | 4 | 0 | 3 | 15 |
| 6 | 0 | 0 | 0 | 0 | 4 | 0 | 304 | 39 | 9 | 4 |
| 7 | 0 | 1 | 2 | 0 | 0 | 0 | 2 | 346 | 9 | 0 |
| 8 | 13 | 5 | 0 | 0 | 6 | 0 | 1 | 5 | 329 | 1 |
| 9 | 6 | 0 | 0 | 0 | 0 | 0 | 8 | 9 | 0 | 337 |

(b) discrete Tchebichef moment based features

| I/P \ O/P | 0 | 1 | 2 | 3 | 4 | 5 | 6 | 7 | 8 | 9 |
|---|---|---|---|---|---|---|---|---|---|---|
| 0 | 355 | 3 | 0 | 0 | 0 | 0 | 0 | 0 | 2 | 0 |
| 1 | 0 | 324 | 1 | 0 | 0 | 0 | 0 | 32 | 0 | 3 |
| 2 | 5 | 16 | 336 | 0 | 0 | 0 | 0 | 3 | 0 | 0 |
| 3 | 16 | 1 | 10 | 320 | 1 | 1 | 0 | 0 | 1 | 10 |
| 4 | 9 | 0 | 0 | 8 | 335 | 2 | 0 | 3 | 2 | 1 |
| 5 | 1 | 0 | 0 | 0 | 0 | 341 | 4 | 0 | 2 | 12 |
| 6 | 0 | 0 | 0 | 0 | 4 | 0 | 310 | 36 | 6 | 4 |
| 7 | 0 | 1 | 2 | 0 | 0 | 0 | 1 | 346 | 10 | 0 |
| 8 | 12 | 5 | 0 | 0 | 6 | 0 | 1 | 5 | 330 | 1 |
| 9 | 6 | 0 | 0 | 0 | 1 | 0 | 10 | 8 | 0 | 335 |

(c) Geometric moments based features

| I/P \ O/P | 0 | 1 | 2 | 3 | 4 | 5 | 6 | 7 | 8 | 9 |
|---|---|---|---|---|---|---|---|---|---|---|
| 0 | 306 | 3 | 1 | 14 | 1 | 0 | 0 | 1 | 17 | 17 |
| 1 | 1 | 309 | 0 | 0 | 0 | 4 | 0 | 45 | 0 | 1 |
| 2 | 0 | 39 | 277 | 22 | 10 | 2 | 0 | 1 | 2 | 7 |
| 3 | 24 | 3 | 90 | 203 | 21 | 0 | 0 | 1 | 2 | 16 |
| 4 | 6 | 2 | 23 | 35 | 272 | 10 | 2 | 0 | 6 | 4 |
| 5 | 0 | 0 | 0 | 1 | 39 | 274 | 25 | 0 | 1 | 20 |
| 6 | 0 | 2 | 0 | 5 | 37 | 6 | 259 | 39 | 4 | 8 |
| 7 | 0 | 10 | 38 | 13 | 3 | 0 | 7 | 276 | 11 | 2 |
| 8 | 21 | 4 | 7 | 7 | 28 | 0 | 4 | 1 | 285 | 3 |
| 9 | 1 | 0 | 1 | 13 | 1 | 0 | 2 | 16 | 0 | 326 |

(d) Zernike moments based features

| I/P \ O/P | 0 | 1 | 2 | 3 | 4 | 5 | 6 | 7 | 8 | 9 |
|---|---|---|---|---|---|---|---|---|---|---|
| 0 | 320 | 9 | 0 | 0 | 0 | 0 | 0 | 0 | 25 | 6 |
| 1 | 0 | 293 | 0 | 0 | 0 | 0 | 0 | 9 | 18 | 40 |
| 2 | 0 | 41 | 303 | 0 | 0 | 0 | 0 | 0 | 0 | 16 |
| 3 | 5 | 1 | 7 | 317 | 16 | 0 | 0 | 2 | 0 | 12 |
| 4 | 0 | 1 | 0 | 6 | 334 | 1 | 3 | 0 | 2 | 13 |
| 5 | 0 | 3 | 0 | 0 | 2 | 332 | 11 | 0 | 0 | 12 |
| 6 | 0 | 26 | 0 | 0 | 0 | 0 | 283 | 35 | 5 | 11 |
| 7 | 0 | 3 | 17 | 0 | 0 | 0 | 0 | 327 | 6 | 7 |
| 8 | 2 | 43 | 0 | 0 | 0 | 0 | 0 | 4 | 277 | 34 |
| 9 | 0 | 25 | 0 | 0 | 0 | 0 | 0 | 1 | 43 | 291 |

(e) FD based representation

| I/P \ O/P | 0 | 1 | 2 | 3 | 4 | 5 | 6 | 7 | 8 | 9 |
|---|---|---|---|---|---|---|---|---|---|---|
| 0 | 350 | 2 | 0 | 0 | 0 | 0 | 0 | 0 | 8 | 0 |
| 1 | 0 | 265 | 0 | 0 | 0 | 0 | 0 | 0 | 83 | 12 |
| 2 | 0 | 11 | 341 | 0 | 0 | 0 | 0 | 1 | 6 | 1 |
| 3 | 4 | 2 | 13 | 297 | 17 | 0 | 2 | 4 | 1 | 20 |
| 4 | 1 | 5 | 0 | 9 | 338 | 0 | 0 | 0 | 0 | 7 |
| 5 | 1 | 3 | 1 | 0 | 34 | 320 | 0 | 0 | 0 | 1 |
| 6 | 0 | 36 | 0 | 0 | 0 | 0 | 286 | 20 | 6 | 12 |
| 7 | 0 | 4 | 27 | 0 | 0 | 0 | 6 | 285 | 12 | 26 |
| 8 | 0 | 58 | 0 | 0 | 0 | 0 | 0 | 1 | 277 | 24 |
| 9 | 3 | 103 | 0 | 0 | 0 | 0 | 1 | 1 | 115 | 137 |

(f) Gabor wavelets based descriptors

| I/P \ O/P | 0 | 1 | 2 | 3 | 4 | 5 | 6 | 7 | 8 | 9 |
|---|---|---|---|---|---|---|---|---|---|---|
| 0 | 310 | 10 | 0 | 0 | 0 | 0 | 1 | 0 | 8 | 31 |
| 1 | 12 | 298 | 0 | 0 | 0 | 0 | 0 | 9 | 19 | 22 |
| 2 | 7 | 6 | 285 | 0 | 0 | 0 | 1 | 33 | 28 | 0 |
| 3 | 3 | 0 | 7 | 255 | 3 | 0 | 2 | 51 | 21 | 18 |
| 4 | 1 | 0 | 0 | 3 | 314 | 1 | 3 | 19 | 18 | 1 |
| 5 | 4 | 0 | 0 | 0 | 2 | 315 | 30 | 0 | 0 | 9 |
| 6 | 19 | 23 | 0 | 0 | 1 | 0 | 281 | 25 | 11 | 0 |
| 7 | 1 | 3 | 6 | 3 | 0 | 0 | 4 | 334 | 2 | 7 |
| 8 | 21 | 9 | 0 | 0 | 0 | 0 | 0 | 11 | 316 | 3 |
| 9 | 23 | 4 | 0 | 0 | 0 | 0 | 1 | 8 | 0 | 324 |

(g) PCA based description

| I/P \ O/P | 0 | 1 | 2 | 3 | 4 | 5 | 6 | 7 | 8 | 9 |
|---|---|---|---|---|---|---|---|---|---|---|
| 0 | 352 | 4 | 0 | 0 | 0 | 0 | 0 | 1 | 3 | 0 |
| 1 | 1 | 319 | 1 | 0 | 0 | 0 | 0 | 35 | 0 | 4 |
| 2 | 7 | 16 | 337 | 0 | 0 | 0 | 0 | 0 | 0 | 0 |
| 3 | 26 | 1 | 8 | 310 | 2 | 0 | 0 | 0 | 7 | 6 |
| 4 | 16 | 0 | 0 | 9 | 334 | 1 | 0 | 0 | 0 | 0 |
| 5 | 2 | 0 | 0 | 0 | 0 | 319 | 19 | 0 | 0 | 20 |
| 6 | 0 | 0 | 0 | 0 | 1 | 0 | 303 | 48 | 5 | 3 |
| 7 | 1 | 11 | 3 | 0 | 0 | 0 | 0 | 334 | 10 | 1 |
| 8 | 8 | 4 | 0 | 0 | 3 | 0 | 1 | 3 | 341 | 0 |
| 9 | 7 | 3 | 1 | 4 | 0 | 0 | 0 | 4 | 0 | 341 |

angle variation. Similarly, the Zernike moments are sensitive to boundary distortions and as a result the performance of the Zernike moments is low for the posture samples from Dataset 2. From the detailed scores in Table 4.10(d), it is observed that the maximum misclassification in Zernike moments based method is again due to the confusion among the postures 1, 8, and 9. Similarly, posture 7 is confused with posture 2 and posture 6 is misclassified as posture 7. Unlike FDs and the geometric moments, the Zernike moments exhibit some correspondence between the mismatched samples.

The detailed scores of the classification results of Gabor wavelet based description is given in Table 4.10(f). From the table, it is evident that samples in most of the posture classes show misclassification. The perspective distortion caused by the view angle variations affects the orientation of contours and it can be observed that most of the mismatched samples are from the posture classes 0, 1, 7, 8 and 9.

The Krawtchouk and the discrete Tchebichef moments have higher recognition rates for the testing samples from Dataset 1 and 2. Particularly, in the case of Dataset 2, the improvement is almost by 11% for *Training set-I* and it indicates that the DOMs are robust to the view angle variations. The PCA based description method exhibits similar performance as the DOMs. From the detailed scores in Tables 4.10(a), 4.10(b) and 4.10(g), it is observed that the misclassifications in the case of DOMs and the PCA occur with respect to similar samples. Accordingly, the maximum misclassification has occurred for posture classes 1 and 6. The samples in both of these posture classes are mismatched with posture 7.

From Table 4.9 it should be noted that the classification accuracy is better for the testing samples from Dataset 1. The samples of some of the postures from Dataset 2 with higher misclassification rates are shown in Figure 4.24. It can be understood that the recognition efficiency is reduced mainly due to the self-occlusion between the fingers and the boundary deviations. This is because the *Training set-I* is constructed using the samples taken from Dataset 1. This indicates that the performance for Dataset 2 can be improved if the training set also includes samples taken at varied view angles.

#### 4.4.2.3 Improving view invariant recognition

In order to improve the view invariant classification rate, the experiments are repeated by including the postures taken at different view angles in the training set. The extended training set consists of 630 posture samples that are collected from 23 users. Among those, 230 samples are taken from Dataset 1 and 400 samples from Dataset 2. We refer the extended training set as *Training set-II*. The classification results are obtained for 3600 samples that contain 2030 samples from Dataset 1 and 1570 samples from Dataset 2. The results are consolidated in Table 4.9. As expected, the improvement in recognition accuracies for Dataset 2 is higher for

**Table 4.11:** Confusion Matrix for the classification results given in Table 4.9 for Training set-II with 23 training samples\gesture sign and 360 testing samples\gesture sign. Detailed scores for

(a) Krawtchouk moments based features

| I/P \ O/P | 0 | 1 | 2 | 3 | 4 | 5 | 6 | 7 | 8 | 9 |
|---|---|---|---|---|---|---|---|---|---|---|
| 0 | 355 | 2 | 0 | 0 | 0 | 0 | 0 | 0 | 0 | 3 |
| 1 | 0 | 354 | 0 | 0 | 0 | 0 | 0 | 2 | 0 | 4 |
| 2 | 0 | 0 | 357 | 0 | 0 | 0 | 0 | 3 | 0 | 0 |
| 3 | 5 | 0 | 2 | 346 | 0 | 0 | 0 | 1 | 0 | 6 |
| 4 | 0 | 0 | 0 | 8 | 345 | 4 | 0 | 1 | 2 | 0 |
| 5 | 1 | 0 | 0 | 0 | 0 | 358 | 0 | 0 | 0 | 1 |
| 6 | 0 | 0 | 0 | 0 | 0 | 0 | 327 | 21 | 6 | 6 |
| 7 | 0 | 3 | 1 | 0 | 0 | 0 | 5 | 350 | 1 | 0 |
| 8 | 4 | 2 | 0 | 0 | 3 | 0 | 7 | 2 | 342 | 0 |
| 9 | 2 | 1 | 0 | 0 | 0 | 0 | 0 | 0 | 0 | 357 |

(b) discrete Tchebichef moments based features

| I/P \ O/P | 0 | 1 | 2 | 3 | 4 | 5 | 6 | 7 | 8 | 9 |
|---|---|---|---|---|---|---|---|---|---|---|
| 0 | 354 | 2 | 0 | 0 | 0 | 0 | 0 | 0 | 1 | 3 |
| 1 | 0 | 353 | 0 | 0 | 0 | 0 | 0 | 3 | 0 | 4 |
| 2 | 0 | 0 | 357 | 0 | 0 | 0 | 0 | 3 | 0 | 0 |
| 3 | 5 | 0 | 2 | 347 | 0 | 0 | 0 | 1 | 0 | 5 |
| 4 | 0 | 0 | 0 | 8 | 347 | 3 | 0 | 1 | 1 | 0 |
| 5 | 1 | 0 | 0 | 0 | 0 | 359 | 0 | 0 | 0 | 0 |
| 6 | 0 | 0 | 0 | 0 | 0 | 0 | 330 | 21 | 4 | 5 |
| 7 | 0 | 3 | 1 | 0 | 0 | 0 | 4 | 351 | 1 | 0 |
| 8 | 3 | 2 | 0 | 0 | 2 | 1 | 7 | 3 | 342 | 0 |
| 9 | 2 | 1 | 0 | 0 | 0 | 0 | 0 | 0 | 0 | 357 |

(c) Geometric moments based features

| I/P \ O/P | 0 | 1 | 2 | 3 | 4 | 5 | 6 | 7 | 8 | 9 |
|---|---|---|---|---|---|---|---|---|---|---|
| 0 | 323 | 5 | 2 | 12 | 5 | 0 | 0 | 0 | 6 | 7 |
| 1 | 0 | 328 | 4 | 2 | 3 | 1 | 1 | 19 | 1 | 1 |
| 2 | 0 | 19 | 305 | 24 | 6 | 1 | 0 | 4 | 1 | 0 |
| 3 | 14 | 1 | 60 | 246 | 27 | 0 | 1 | 1 | 2 | 8 |
| 4 | 1 | 2 | 11 | 62 | 264 | 11 | 2 | 2 | 4 | 1 |
| 5 | 0 | 0 | 1 | 2 | 14 | 330 | 4 | 0 | 0 | 9 |
| 6 | 0 | 0 | 0 | 4 | 9 | 6 | 286 | 42 | 8 | 5 |
| 7 | 0 | 13 | 10 | 7 | 0 | 0 | 5 | 322 | 2 | 1 |
| 8 | 4 | 3 | 0 | 13 | 20 | 0 | 3 | 5 | 310 | 2 |
| 9 | 1 | 3 | 0 | 12 | 2 | 5 | 8 | 4 | 0 | 325 |

(d) Zernike moments based features

| I/P \ O/P | 0 | 1 | 2 | 3 | 4 | 5 | 6 | 7 | 8 | 9 |
|---|---|---|---|---|---|---|---|---|---|---|
| 0 | 341 | 1 | 0 | 0 | 0 | 0 | 0 | 0 | 4 | 14 |
| 1 | 0 | 331 | 0 | 0 | 0 | 0 | 1 | 0 | 13 | 15 |
| 2 | 0 | 0 | 353 | 0 | 0 | 0 | 0 | 7 | 0 | 0 |
| 3 | 0 | 0 | 2 | 350 | 1 | 0 | 1 | 0 | 0 | 6 |
| 4 | 0 | 0 | 0 | 4 | 351 | 4 | 0 | 0 | 0 | 1 |
| 5 | 0 | 0 | 0 | 0 | 1 | 359 | 0 | 0 | 0 | 0 |
| 6 | 0 | 3 | 0 | 0 | 0 | 0 | 342 | 9 | 6 | 0 |
| 7 | 0 | 1 | 4 | 0 | 0 | 0 | 6 | 349 | 0 | 0 |
| 8 | 1 | 36 | 0 | 0 | 0 | 0 | 7 | 3 | 289 | 24 |
| 9 | 1 | 12 | 0 | 0 | 0 | 0 | 1 | 0 | 25 | 321 |

(e) FD based representation

| I/P \ O/P | 0 | 1 | 2 | 3 | 4 | 5 | 6 | 7 | 8 | 9 |
|---|---|---|---|---|---|---|---|---|---|---|
| 0 | 351 | 1 | 0 | 0 | 0 | 0 | 0 | 0 | 3 | 5 |
| 1 | 1 | 265 | 0 | 0 | 0 | 0 | 1 | 1 | 53 | 39 |
| 2 | 0 | 0 | 342 | 6 | 0 | 0 | 0 | 9 | 3 | 0 |
| 3 | 0 | 0 | 9 | 341 | 2 | 0 | 2 | 1 | 1 | 4 |
| 4 | 0 | 0 | 3 | 9 | 346 | 1 | 1 | 0 | 0 | 0 |
| 5 | 0 | 0 | 0 | 0 | 2 | 358 | 0 | 0 | 0 | 0 |
| 6 | 0 | 5 | 0 | 0 | 0 | 0 | 317 | 32 | 3 | 3 |
| 7 | 0 | 1 | 8 | 0 | 0 | 0 | 14 | 325 | 8 | 4 |
| 8 | 0 | 47 | 1 | 0 | 0 | 0 | 3 | 6 | 278 | 25 |
| 9 | 4 | 66 | 0 | 0 | 0 | 0 | 0 | 0 | 33 | 257 |

(f) Gabor wavelets based descriptors

| I/P \ O/P | 0 | 1 | 2 | 3 | 4 | 5 | 6 | 7 | 8 | 9 |
|---|---|---|---|---|---|---|---|---|---|---|
| 0 | 322 | 3 | 0 | 0 | 0 | 0 | 0 | 0 | 4 | 31 |
| 1 | 6 | 327 | 0 | 0 | 0 | 0 | 0 | 1 | 9 | 17 |
| 2 | 3 | 0 | 342 | 1 | 0 | 0 | 0 | 8 | 6 | 0 |
| 3 | 1 | 0 | 12 | 325 | 3 | 0 | 1 | 9 | 2 | 7 |
| 4 | 0 | 0 | 4 | 19 | 331 | 0 | 1 | 4 | 1 | 0 |
| 5 | 0 | 0 | 0 | 0 | 1 | 358 | 1 | 0 | 0 | 0 |
| 6 | 5 | 4 | 0 | 0 | 0 | 0 | 338 | 9 | 2 | 2 |
| 7 | 0 | 0 | 3 | 3 | 0 | 0 | 10 | 339 | 0 | 5 |
| 8 | 17 | 18 | 1 | 0 | 0 | 0 | 8 | 4 | 311 | 1 |
| 9 | 15 | 1 | 0 | 1 | 0 | 0 | 3 | 3 | 2 | 335 |

(g) PCA based description

| I/P \ O/P | 0 | 1 | 2 | 3 | 4 | 5 | 6 | 7 | 8 | 9 |
|---|---|---|---|---|---|---|---|---|---|---|
| 0 | 353 | 4 | 0 | 0 | 1 | 0 | 0 | 0 | 1 | 1 |
| 1 | 0 | 352 | 1 | 0 | 0 | 1 | 0 | 2 | 0 | 4 |
| 2 | 0 | 0 | 360 | 0 | 0 | 0 | 0 | 0 | 0 | 0 |
| 3 | 4 | 1 | 3 | 344 | 1 | 0 | 0 | 1 | 1 | 5 |
| 4 | 0 | 0 | 0 | 8 | 352 | 0 | 0 | 0 | 0 | 0 |
| 5 | 0 | 0 | 0 | 0 | 1 | 358 | 0 | 0 | 0 | 1 |
| 6 | 0 | 0 | 0 | 0 | 0 | 1 | 334 | 21 | 2 | 2 |
| 7 | 0 | 5 | 0 | 0 | 0 | 0 | 10 | 344 | 1 | 0 |
| 8 | 1 | 1 | 0 | 0 | 6 | 0 | 2 | 3 | 347 | 0 |
| 9 | 2 | 1 | 0 | 2 | 0 | 0 | 0 | 0 | 0 | 355 |

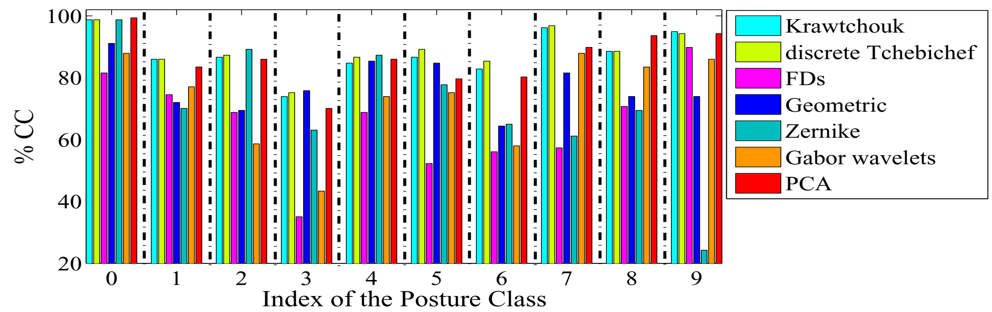


(a)

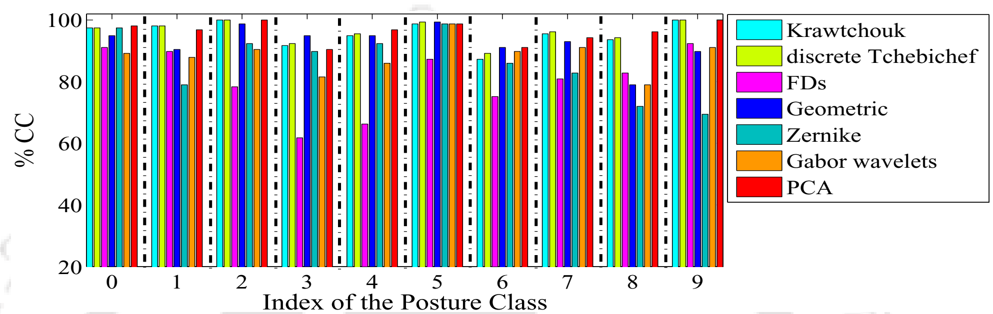


(b)

**Figure 4.25:** Plots of consolidated values of posture wise classification results for samples in Dataset 2 with respect to (a) Training set-I and (b) Training set-II. The plots illustrate the improvement in the classification results with respect to the extended training set, Training set-II.

Training set-II. The performances of the DOMs and the PCA based features are consistently superior to that of the other considered methods for both the training sets.

The comprehensive scores for the results obtained using *Training set-II* is given in Table 4.11. It is evident that including more samples from different view points to the training set has improved the distinctness of the postures. The results in Table 4.11(e) show that the FDs exhibit good classification accuracy for most of the posture classes. Similar to the user independence case, the misclassifications have occurred between samples with similar boundary profiles. From the results for geometric moments in Table 4.11(c), it is observed that more misclassifications have occurred for postures 2, 3, 4 and 6. In the case of Zernike moments, the results in Table 4.11(d) show that postures 6, 8 and 9 have less classification rates. Similarly, the detailed scores for the Gabor wavelets in Table 4.11(f) show good correspondence between the mismatched classes. The posture class 3 is mismatched with 2 and posture class 4 is mismatched with 3. Also, more misclassifications have occurred between posture classes 0 and 9.

The plots in Figure 4.25 illustrate the posture wise classification accuracies obtained for Dataset 2 with respect to the Training set-I and Training set-II. By comparing the plots in Figure 4.25a and 4.25b, it can be inferred that the classification accuracies of the different feature descriptors increase and show significant improvement for classification using Training set-II. The performances of the Krawtchouk moments, the discrete

Tchebichef moments and the PCA technique are consistently superior and they are more robust features for view invariant posture classification.

## 4.5 Summary

This chapter has presented a hand posture recognition technique using geometry based normalizations and DOM based features for classifying the simple single-hand postures. The proposed technique is robust to similarity transformations and projective variations. A rule based normalization method utilizing the anthropometry of hand is formulated for separating the hand region from the forearm. The method also identifies the finger and the palm regions of the hand. An adaptive rotation normalization procedure based on the abducted fingers and the major axes of the hand is proposed. The $2D$ DOMs are used to represent the hand posture shape. The classification is performed using a minimum distance classifier. The experiments are aimed towards analyzing the accuracy of the DOMs as descriptors in user and view invariant hand posture classification.

The experiments are conducted on a large database consisting of 10 posture classes and $4,230$ hand posture samples. The analysis on the intraclass and the interclass similarities of the hand posture shapes in the database is quantified using Pratt's FOM and correlation coefficient. The analysis has shown that the database exhibits more structural deviations in the hand posture shape that are caused due to user and view-angle variations.

A detailed study on the DOM based classification is conducted in comparison with the geometric moments, the Zernike moments, the Fourier descriptors, the Gabor wavelets and the PCA based methods. The results show that the DOMs are robust features for achieving user independent and view invariant recognition of hand postures. It is also observed that the discrete Tchebichef moments offer marginally better performance than the Krawtchouk moments.

# 5

# DOM based Recognition of Asamyuta Hastas



**Contents**

This research work is motivated towards developing CBA systems like content-based annotation and retrieval of Bharatanatyam dance videos. As a first step, the DOM based hand posture recognition technique developed in Chapter 4 is applied for robust recognition of the Asamyuta hastas in Bharatanatyam. This chapter presents in detail the development of the Asamyuta hasta database, the system implementation strategies and the experimental studies on the automatic recognition of hand postures constituting the Asamyuta hastas in Bharatanatyam.

## 5.1 Introduction

Dance is a remarkable art form that involves body movements and facial expressions to portray human emotions insync with the music. The intelligence level in a dance form can be either high so as to depict the vocal information or subtle as just movements in accord with the rhythm. The artistic features in the dance genre offer insight into the ethnicity, geography, dress, and the religious nature of a particular populace [184]. With the effort to conserve and pass on the culture, the dance styles are documented using the notation systems. These notation systems are symbolic representations of movement that are used for individual interpretation and learning [185]. The widely employed dance notation system is the Labanotation [185–187].

The first instance of technology in dance is the use of computers to compose and edit the dance notation scores. Eventually, the developments in the computer and the imaging technologies have facilitated CBA systems in dance. These systems include dance partner robots [188], interactive dance games [189], automated dance training and evaluation systems [190, 191], dance synthesis [192], and dancing avatar animation [193].

A few works [194–199] have concentrated in developing computer vision based markerless motion-capture methods for dance technology. Some of the dance forms for which vision based gesture representation algorithms are explored include the modern or free style dance [190, 194, 197, 200, 201], ballet [198, 202, 203], ballroom dance [188] and Japanese traditional dances [204–206]. Other applications of computer vision techniques for dance includes retrieval systems [207, 208] and dance video annotations [209–211]. However, only very few works have concentrated on developing intelligent algorithms for Indian classical dances like Bharatanatyam. Mamania et al. [195], have used some basic movements in Bharatanatyam for their work on developing markerless motion-capture method from monocular videos. In [212], Bharatanatyam is considered for developing concept based video annotation. The technique relied on specific body movements, body postures and music for annotation. Recently, vision based techniques for recognising the hand postures in Bharatanatyam are developed. In [213], edge orientation histograms were employed as features for representing the single-hand postures in Bharatanatyam. Their work is aimed at facilitating E-learning tools for Bharatanatyam. Similar technique was used in [214] for recognising the two-hand postures in Bharatanatyam. Their work combined the edge orientation histogram features and the skeleton based matching technique for classifying the hand postures.

From the literature, it is evident that the CBA systems are yet to be adopted to different classical dance genres around the world. Particularly, the Indian classical dance forms are yet to advance even to the level of automated notation systems. The Indian classical dance, Bharatanatyam is an intricate dance form that comprises of hand postures, facial expressions and different movements with respect to each part of the body. Hence, developing CBA systems for Bharatanatyam is a challenge.

The integral meaning of a Bharatanatyam dance performance is conveyed through the hand postures. Unlike the simple hand postures that involve basic movements like abduction/adduction and extension/flexion of fingers, the hand postures in Bharatanatyam involve complex movements in which the configuration at every finger joint varies resulting in variegated hand postures. Therefore, for successful realisation of a vision based CBA system for Bharatanatyam, it is crucial to develop image processing techniques for efficient description and classification of the hand postures in Bharatanatyam. It is also essential that the technique must be robust to the user and the view-angle variations.

In a Bharatanatyam dance video, the frames containing the hand postures will be considered as the key frames. The key frames and the order in which these frames occur within the shots can be used to characterise a video segment. Eventually, the descriptions of the shots will represent the entire video. Thus, it can be understood that the primary factor in developing a vision-based CBA system for Bharatanatyam is the recognition of the hand postures in the key frames. Some of the major issues in developing the vision-based CBA system for recognizing the hand postures in a Bharatanatyam dance video are:

(i) Segmentation of the hand from the dance video.

(ii) Variations in the scale, the orientation and the spatial position of the hand postures.

(iii) Structural variations due to variabilities in the hand geometry and the gesturing style of the dancers.

(iv) Structural distortions due to varying view-angles that occur while capturing the dance video.

This research is focussed towards developing techniques that are robust to variations in the shape of the hand posture caused by user and viewpoint changes.

In Chapter 4, a DOM based hand posture recognition technique is proposed for the description of simple hand postures. The experimental studies have confirmed DOMs as robust and efficient descriptors for user and view invariant representation of simple hand postures formed by simple finger configurations. This work aims at employing DOMs for the description of hand postures in Bharatanatyam and experimentally verify the robustness of DOMs in uniquely representing these complex hand postures.

The rest of the chapter is divided into four broad sections. The first section gives an brief introduction to Bharatanatyam, emphasizing the role of hand postures in representing the content of a Bharatanatyam dance. The second section explains the posture acquisition and the database development procedures. The system implementation strategies and the experimental studies are presented in the third and the fourth sections respectively.

## 5.2 Bharatanatyam and its gestures

In the world of dance, the Indian classical dance forms are unique for their intricate styles through the combination of facial expressions, body poses and the hand gestures. The classical dances of India are Bharatanatyam, Kathak, Kathakali, Kuchipudi, Manipuri, Mohiniyattam, Odissi and Sattriya [215]. These dances derived their form and meaning from the books of arts, the *Natyashastra* and the *Abhinayadarphana* [216]. Bharatanatyam is one of the ancient and most widely practised dance forms in India. It is believed to be created by Bharata, the saint author of Natyashastra. The dancers consider the practice of Bharatanatyam to be the high form of *yoga* and as a way of spiritual elevation that goes beyond mere entertainment [215].

Bharatanatyam is composed of three basic units known as the *hastas*, the *adavus* and the *bhedas* [6]. Each of these units stipulates the movements with respect to a particular part of the body and is described as follows:

(i) Hastas: *The hastas refer to hand postures and are descriptively defined in [217] as "the fingers in Bharatanatyam speak an eloquent language of their own. They stretch, fold, raise, lower, close, open, separate and join to create variegated hand patterns known as the hastas or mudras". The hand postures in Bharatanatyam are used to denote a lot of emotions, nouns, verbs , adverbs and adjectives [218].*

(ii) Adavus: *The word "adavu" means "basic step". It denotes the combination of position of the legs, standing posture, walking movement and hand postures insync with the rhythm.*

(iii) Bhedas: *In the context of dance, the word "bheda" refers to movement. This specifies the neck movements, eye movements and the head movements. These Bhedas form the integral part of Bharatanatyam and are used to improve the quality of expression.*

Clearly, these basic units can be considered as the gesturing entities. Among these three entities, hastas or the hand postures are the most essential features that depict or communicate the essence of vocals. The hastas are considered as individual words that combine appropriately to form a sentence, thus, forming the dance phonemics [219]. The hastas are basically divided into two groups. They are (i) Asamyuta hastas (*single-hand postures*) and (ii) Samyuta hastas (*two-hand postures*). The Samyuta hastas can be perceived as postures formed by the combination of two Asamyuta hastas in such a way to portray different meanings. Therefore, sufficient information about the different hand symbols in Bharatanatyam can be derived from the Asamyuta hastas.

In general, a Bharatanatyam dance comprises of three aspects, namely, the *Nritta*, the *Nritya* and the *Natya* [220, 221]. The Nritta of Bharatanatyam is an abstract style of dance in which the body movements and the postures are performed rhythmically and they do not convey any meaning. The Nritya aspect of Bharatanatyam is an interpretative dance style accompanied by the music and song. The mood of the music and the information in the song are conveyed through facial expressions, hand postures and body movements. The Natya corresponds to the drama representation and it is a composite form that encompasses, the Nritta and the Nritya. Natya is accompanied by entities including music, song and speech. The postures and the body movements in Natya represent the meaning of the song and the speech accompanying the dance. Particularly, the hastas are the real language of the Nritya and the Natya conveying literal word meanings and they can be used as cues for the description of an entire dance performance.

The hand postures in the form of hastas occur in all the three aspects of a Bharatanatyam dance and therefore, they can be considered as the key elements in developing CBA systems for Bharatanatyam.

### 5.2.1 Asamyuta hastas - the single-hand postures

The Asamyuta hastas are the single-hand postures in Bharatanatyam in which the fingers are bent at different angles to form patterns leading to visually distinct hand postures. The occurrence of Asamyuta hastas in Nritta does not convey any meaning and they are used to accentuate the beauty of the dance. In Nritya, the hastas are used as narrative elements to indicate different characters, objects and emotions associated with the story narrated through the dance.

According to Natyashastra and the Abhinayadarphana, there are 28 Asamyuta hastas [216] of which 27 hastas are static signs and one corresponds to a dynamic hand gesture, namely, the *samdamsha* which is composed of a sequence of two hand postures belonging to Asamyuta hastas. The contemporary form of Bharatanatyam defines 32 Asamyuta hastas by including four other hastas from the *Angika Abhinaya*. In Natyashastra, Angika Abhinaya is a detailed study on the possible gestures, postures and movements of every part of the body. The study states the use of total body to express certain meaning [6].

Excluding the samdamsha hand gesture, the other 31 Asamyuta hastas used in Bharatanatyam are illustrated in Figure 5.1. The slight variations in practising these hastas are also included in the illustration. For example, in Figure 5.1, the Bhramaram posture in 22($b$) is the variation of the original posture in 22($a$) and it is used in the Samyuta hastas to convey a different meaning. The meaning of the hastas and some of the representations emoted through them are given in [6, 222, 223].

From the illustration of the Asamyuta hastas, it can be observed that each Asamyuta hasta is formed by obeying certain rules associated with the spatial localisation of the fingers and bending angles at the finger joints. However, the values of the joint angles are not precisely defined and to certain extent, variations in the joint angles depending on the convenience of the dancer and the dancer's hand geometry are allowed. These variations will neither be perceivable nor large in such a way to alter the appearance of the posture. Unlike the simple hand postures that are formed by either complete extension/flexion or abduction/adduction of fingers, the Asamyuta hastas are formed by bending the fingers at intermediate angles and varying the spatial position of each finger. Since, the hand postures are formed by complex finger configurations, the Asamyuta hastas in Bharatanatyam are considered as complex hand postures.

## 5.3 Hand posture acquisition and database development

The images of the Asamyuta hastas are captured using a monocular camera that is interfaced to a computer. As explained in Section 4.2, the position and the view-angle of the camera are important factors to be considered while acquisition. The choice of the optimal camera position and the view-angle to capture the hand postures in Bharatanatyam is discussed as follows.

### 5.3.1 Determination of camera position

The optimal position of the camera for acquiring the Asamyuta hastas is chosen based on the spatial arrangement between the dancer and the audience in a Bharatanatyam recital. In a Bharatanatyam recital, the audience is positioned in front of the stage in such a way that they do not surround the performance space and so, are able to gain a frontal view of the dancers body at all times [224]. Therefore, while recording the dance video, the camera must be placed at a position to capture the frontal view of the dancer and the dancer must be completely within the focus of the camera. The camera position with respect to the dancer in a 3D space is illustrated using the 3D cartesian coordinate system as shown in Figure 5.2(a). The dancer is the object of focus and the frontal view of the dancer is its projection onto the $y-z$ plane. Thus, in order to acquire the frontal view


**Figure 5.1:** Illustration of different Asamyuta hastas. The indexing as (a) and (b) represents the variations in postures as adapted by different dancers. Images are taken from: [5] and [6].

TH-1228_06610210

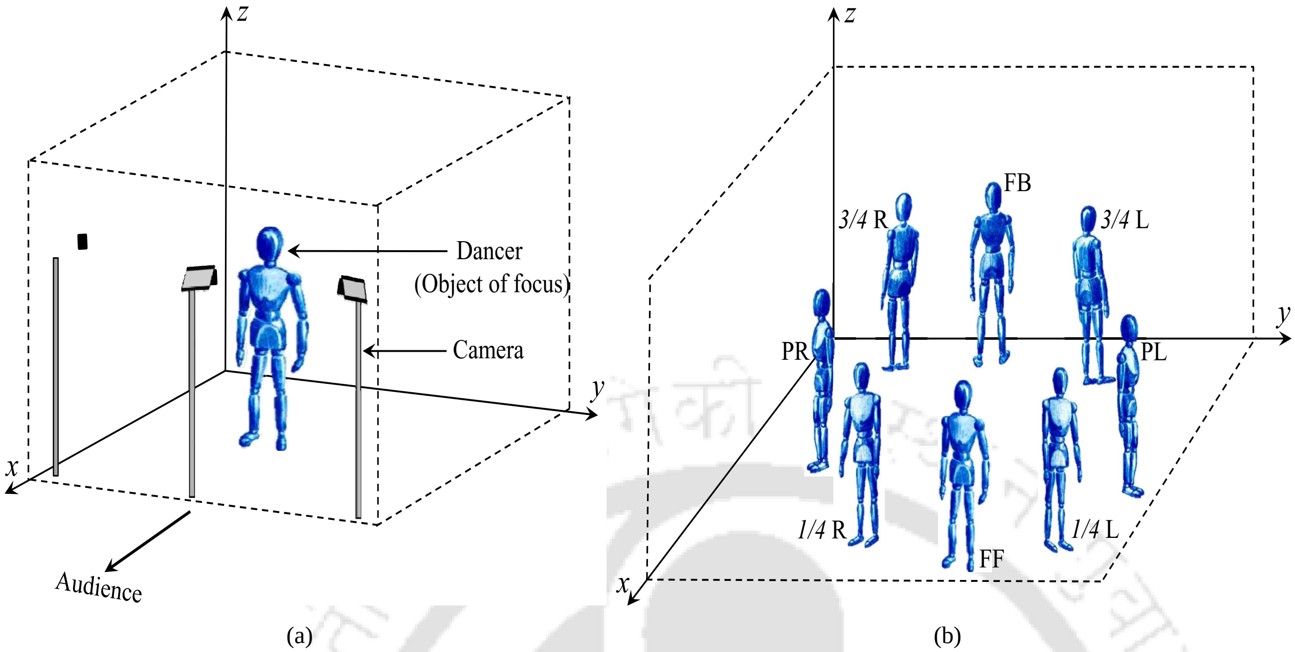


**Figure 5.2:** Schematic representation of the (a) camera at normal-angle position with respect to the dancer and (b) different types of body positions the dancer exhibit while performing on the stage. The illustration in (a), also shows the spatial arrangement between the dancer and the audience.

of the dancer, the camera must be placed at the normal-angle position, in which the camera and the object of focus are at the same height from the ground. The image acquired at the normal-angle position is also known as the *eye-level shot*.

### 5.3.2 Determination of view-angle

For illustration in Figure 5.2(a), the view-angle refers to the angle made by the camera with respect to the $y - z$ plane. Therefore, at the normal-angle position, the structural variations occur due to the movement of the dancer along the $x - y$ plane. As the dancer moves, the camera should pan such that it stays intact with the object of focus. Pivoting the camera horizontally from left to right or right to left is known as the *panning*.

The movement along the $x$ direction causes variation in the distance between the camera and the dancer, resulting in the variation in the scale of the acquired object. The movement along the $x$ axis does not cause view-angle changes. The angle of view between the camera and the dancer varies, when the dancer moves and the camera pans along the horizontal direction. As the dancer moves, he/she exhibits different body positions on stage that influences the range up to which the camera can be panned.

Like in any theatrical performance, the body position of the dancer on stage can be categorised into eight types [225]. They are

**Full front (FF)**: The position in which the dancer faces the audience.

**Profile left (PL)**: The dancer turns 90° to left, such that the right profile is towards the audience.

**Profile right (PR)**: The dancer turns 90° to right, so that the left profile is towards the audience.

**One-quarter left (**1/4**L)**: The dancer is in a position halfway between the FF and the PL position.

**One-quarter right (**1/4**R)**: The dancer is in a position halfway between the FF and the PR position.

**Full back (FB)**: The dancer's back is towards the audience.

**Three-quarter left (**3/4**L)**: The dancer is in a position halfway between the FB and the PL position.

**Three-quarter right (**3/4**R)**: The dancer is in a position halfway between the FB and the PR position.

The illustration of body positions on a stage using the 3D Euclidean coordinate system is shown in Figure 5.2(b). As mentioned earlier, in Bharatanatyam the communication with the audience is mainly through facial expressions and hand postures. Hence, it requires that the dancer's face and the body must be open to the audience in order to gain better visibility. Therefore, during the Nritya aspect of a Bharatanatyam recital, the frequently occurring body positions on stage are the FF, PL, PR, 1/4L and 1/4R. The FB and the three-quarter positions (3/4L, 3/4R) mainly occur during the Nritta aspect. If the hand postures are used as significant elements in the FB and three-quarter positions, the postures are formed by stretching the hands away from the body in such a way that they are visible to the audience. This ensures that the projection of the hand postures onto the $y-z$ plane occur at all the body positions and hence, camera panning can be limited only along the $y$ direction.

While acquiring the video of a Bharatanatyam recital, the reference spatial position of the camera can be fixed as the position at which the optical axis intersects the centre of the object of focus. At this position, the image plane is parallel to the object plane and the angle of view corresponds to the optimum view-angle. The image acquired at optimum view-angle corresponds to the front view of the object of focus. Panning the camera along the $y$ direction, results in oblique view-angles for which the right or the left side view of the object of focus is acquired.

When the camera pans from the reference position to the right, the acquired image corresponds to the right side view of the object. Similarly, as the camera pans towards the left, the resultant image corresponds to the left side view of the object. Since the camera is at normal-angle position and not tilted upwards or downwards, the perspective distortion is minimised for camera panning [226]. As the view-angle varies along the horizontal direction, the structural variation in the acquired images occurs due to the variation in the side view profile of the object and the self-occlusion between the fingers at oblique angle of views.

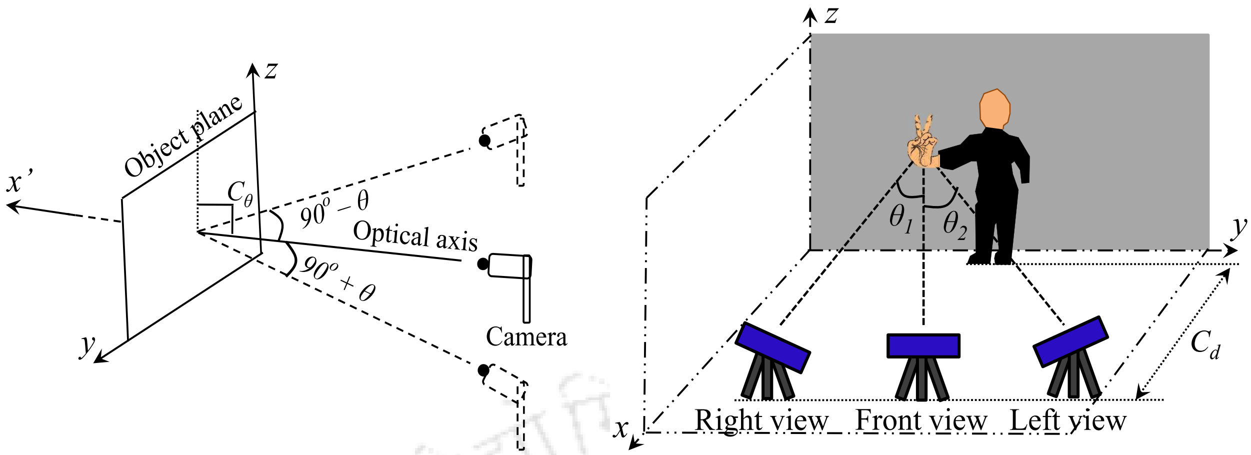


(a) (b)

**Figure 5.3:** (a) Illustration of camera alignment with respect to the hand; (b) A schematic representation of the setup created for database development. The angle $\theta_1 = 90 - \theta$ and $\theta_2 = 90 + \theta$.

### 5.3.3 System setup

The postures in the database are captured using a RGB Frontech e-cam under varying light conditions. The camera has a resolution of $1280 \times 960$ and is connected to a Intel core-II duo 2GB RAM processor. The images are collected in a black background and the subjects are made to wear a black suit. Therefore, hand is ensured as the only skin colour object contained within the FOV.

The subjects perform the hastas by holding the hand in front of their body. Thus the dancer is in the FF position with respect to the audience. The camera is mounted on a tripod in such a way that the optical axis of the camera passes through the centre of the object plane as illustrated in Figure 5.3(a). In this experiment, the viewing angle ($C_\theta$) is measured as the angle made by the camera with respect to the $y - z$ plane. The viewpoint is assumed to be optimum if the camera is placed parallel to the hand making the posture. The $y - z$ plane comprises of the object plane and the optimal view-angle is determined to be $C_\theta = 90°$. The camera is kept at a distance $C_d$ from the gesturer. The distance $C_d$ is chosen such that the entire hand posture lies within the FOV.

The schematic representation of the studio set up employed for acquiring the hastas is given in Figure 5.3(b).

## 5.4 Development of Asamyuta hasta database

The database is collected from 6 female subjects. Among these, 3 subjects are well trained in Bharatanatyam and the remaining received training on the hastas in order to participate in database development. The hand postures are made with the right hand and the hand is extended outwards and placed approximately at the chest level.


**Figure 5.4:** Illustration of Asamyuta hastas acquired for the database. The figure illustrates the variation in the usage of some of the hastas, namely, the Padmakosam, the Kangulam and the Katakamukham 2. These variations are also included in the database. The number indicates the posture index.

Among the hand postures shown in Figure 5.1, 29 Asamyuta hastas that occur in the contemporary form of Bharatanatyam are chosen for constructing the database. The usage of each hand posture changes according to the context of dance and it continues to evolve with the progress in Bharatanatyam. By including the variations in the usage of some of the hastas, this database includes 32 hand postures under the group of Asamyuta hasta.

The hand postures are collected by varying the view-angle $C_\theta$. The Asamyuta hastas are sensitive to view-angles and they adopt different shape profiles with the change in the angle of view. The other major issue that accompanies view-angle is the self-occlusion between the fingers. The degree of occlusion completely depends on the angle of view. To take these distortions into account, the images are acquired at 3 viewing directions: the *front view*, the *right view* and the *left view* as illustrated in Figure 5.3.

The front view of the hand posture is obtained at the optimal angle of view $C_\theta = 90°$. The right and the left views of the hand postures are obtained by panning the camera to the right and the left respectively of the object of focus. Therefore, the right and the left views respectively are the directions in which the optical axis of the camera is at angle $90° - \theta$ and $90° + \theta$ with respect to the object plane. The angle $\theta$ is chosen such that there is no severe occlusion among the fingers and is fixed at 30° by trial and error.

The postures are collected by allocating 14 sessions for each subject. In 7 sessions, the data were collected by fixing the distance $C_d$ approximately to $1\,meter$. For the other 7 sessions, the distance between the gesturer and the camera is fixed approximately as $C_d = 0.6\,meter$. The images are acquired under uncontrolled illumination conditions.

At a session, 96 hand postures (32 postures per view) corresponding to the 3 viewing directions are acquired. Therefore, the database consists of $8,064$ images of 32 Asamyuta hastas with 252 samples for each hasta. The images in the database are 24 bit colour images with the maximum spatial resolution of $1280 \times 960$ and are saved as JPEG files.

Figure 5.4 illustrates samples of hastas acquired for the Asamyuta hasta database. As shown in this figure, the 32 hand posture classes in the Asamyuta hasta database are labelled from 1 to 32.

## 5.5 System implementation

The block diagram representation of the hand posture recognition technique proposed for classifying the postures in the Asamyuta hasta database is shown in Figure 5.5. The procedure is broadly divided into four phases. They are: (1) hand segmentation, (2) normalisation of scale and translation changes, (3) feature extraction and (4) classification. A description of these tasks are presented below.

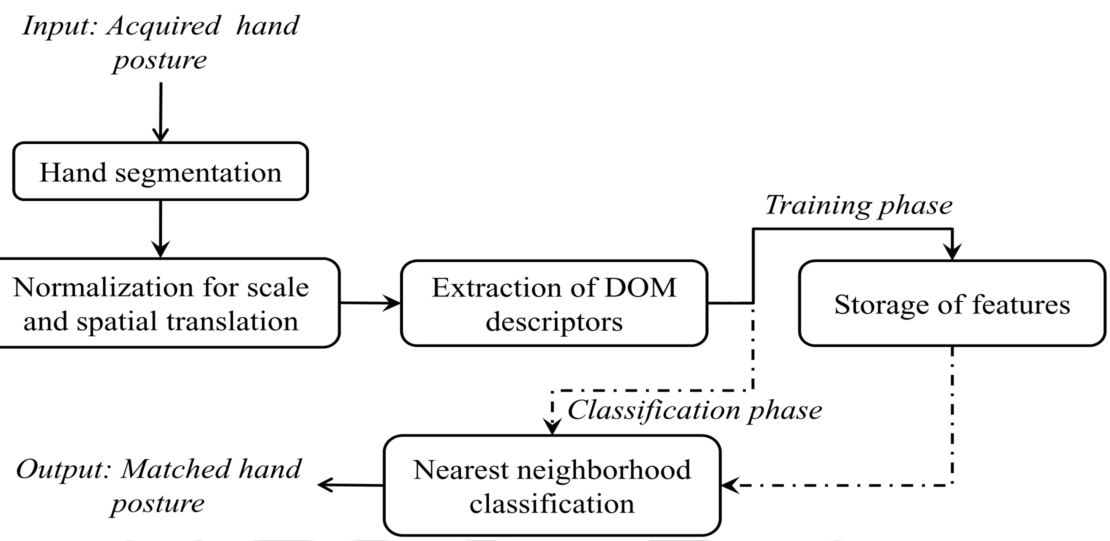


**Figure 5.5:** Schematic representation of the proposed hand posture recognition system.

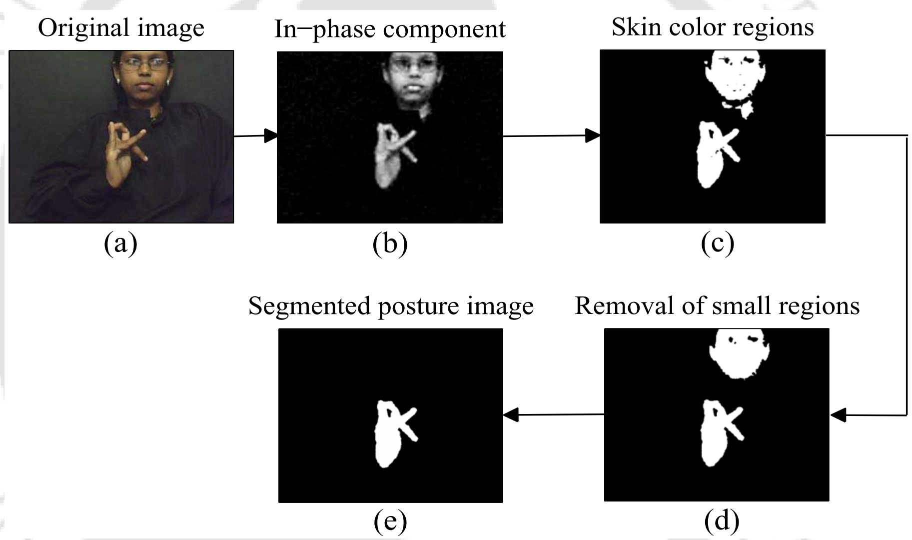


**Figure 5.6:** Illustration of hand posture segmentation through thresholding the in-phase colour component.

### 5.5.1 Hand segmentation

The hand postures were acquired in uniform, uncluttered background and hence, the face and the hand are the only contrasting objects present in the acquired image. Therefore, the segmentation is achieved simply by thresholding the image at a particular intensity level. Since the illumination conditions are uncontrolled, it is difficult to determine a global threshold based on the *RGB* values. Therefore, the skin colour detection method based on the hue and the in-phase colour component, as explained in Section 4.3.1 can be used for segmenting the hand postures. In this experiment, the background is uncluttered and hence, it is not necessary to employ the hue component. The threshold can be derived by using only the in-phase colour component defined in (4.2). The threshold is experimentally chosen as 10 and the pixels are grouped as skin colour pixels if $C_{phase} \geq 10$.

The in-phase colour component of an acquired hand posture image in Figure 5.6a is shown in Figure 5.6b and Figure 5.6(c) illustrates the result of skin colour detection through thresholding the in-phase colour component. The detection results in a binary image which may also contain other regions not belonging to the hand. The unwanted regions are mostly pixels belonging to the face and the neck part of the gesturer.

Among the detected regions, the hand and the face regions have large areas and hence, the other small regions are removed by comparing the area of the detected regions. The hand and the face regions are differentiated based on their spatial localisations. The postures are performed by extending the hand outwards at the chest level or lower than the face level. Therefore, in the acquired image, the hand is spatially separated from the face and the desired hand region is easily segmented by comparing the spatial coordinates of the detected regions. Figure 5.6 illustrates the segmentation of the desired hand posture from the acquired image. The segmented image is the binary silhouette of the hasta, as shown in Figure 5.6(e).

### 5.5.2 Orientation normalisation

In Bharatanatyam, the orientations of the hand postures vary widely depending on the context of their occurrences. In order to achieve rotation invariant classification, the hand postures belonging to each class must be aligned such that the orientation of the postures remain uniform. A method based on the geometry of the hand postures is proposed in Section 4.3.2.2, for orientation alignment of the simple hand postures. The method is based on the abducted fingers that comprise the geometry of the posture and is experimentally verified to be efficient for uniquely aligning the simple hand postures of each class.

The results suggest that the orientation of the binary silhouettes of the hand postures in the Asamyuta hasta database can be normalised using the geometry based orientation correction method explained in Section 4.3.2.2. The illustration in Figure 5.7 presents a few examples of the result of orientation alignment based on the geometry of the segmented hand postures. It is observed that the approach leads to unstable results and the segmented hand postures are not aligned uniformly when there are structural deviations due to the user and the view-angle changes.

Unlike the simple hand postures employed in Chapter 4, the orientation of the palm surface in the hand postures of Asamyuta hasta database varies for each posture class and in some posture classes like posture 15, the palm region does not constitute the frontal plane of the hand posture. As a result, the centre of the palm cannot be accurately estimated from the segmented hand posture and it is difficult to separate the palm and the finger regions. Additionally, the user and the view-angle variations result in self-occlusion of the fingers leading to variations in the shape of the hand posture. This leads to errors in orientation normalisation.

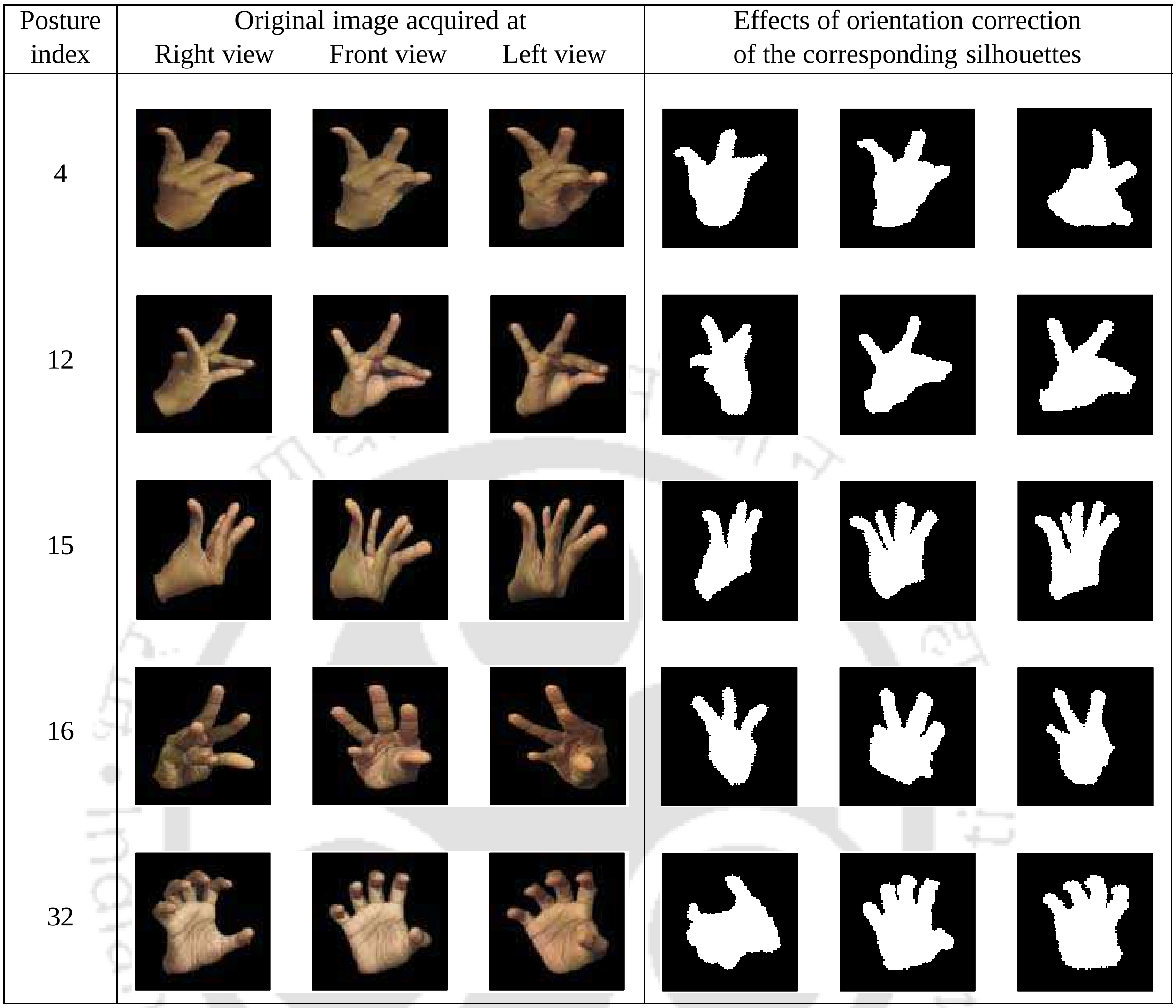


**Figure 5.7:** Examples to illustrate the effect of orientation correction using the posture geometry based approach. The illustration shows that the orientation normalisation leads to unstable results and it is due to the variation in the shape of the posture caused by self-occlusion of fingers and different view-angles.

This work employs an alternative technique to achieve rotation invariant classification. The orientation normalisation is achieved by including the rotated samples of the binary silhouette of the hastas in the training set. Given the binary silhouette $f(x, y)$ of the hand posture, the rotated samples $f(x', y')$ are generated using the coordinate transformation defined as

$$[x' \; y' \; 1] = [x \; y \; 1] \begin{bmatrix} \cos\theta & \sin\theta & 0 \\ -\sin\theta & \cos\theta & 0 \\ 0 & 0 & 1 \end{bmatrix} \quad (5.1)$$

The angle $\theta$ is varied between $0°$ and $350°$ in steps of $10°$. The rotated samples corresponding to each hand posture shape constitute the reference training set for classification.

### 5.5.3 Normalisation for scale and translation changes

The resolutions of the rotated hand posture silhouettes are normalised to $104 \times 104$ through the nearest neighbourhood interpolation \ down sampling technique. The scale of the silhouette is normalised to $64 \times 64$. The spatial translation is normalised by shifting the centroid of the silhouette to the centre $(52, 52)$ of the image.

### 5.5.4 Extraction of DOM features

The DOM based descriptors are derived as features for representing the shape of the hand postures in the Asamyuta hasta database. The parameter to be determined is the order of the DOMs required for representing the hand postures. Experiments have been already performed in Chapter 3 and Chapter 4 to study the optimal choice of the order of DOMs for representing different shapes. The results in Chapter 3 and Chapter 4 suggest that at higher orders the DOMs give accurate reconstruction. Accordingly, for representing the shape of the hand posture of scale $64 \times 64$, the order of the DOMs is chosen as 80 ($n = 40$ and $m = 40$). At this order, it is shown in Chapter 3 and 4 that both Krawtchouk and discrete Tchebichef moments exhibit similar performance with high reconstruction accuracy.

#### 5.5.4.1 Comparison with other descriptors

The results in Chapter 4 have demonstrated the DOMs and the PCA based features as comparatively efficient shape descriptors for user and view invariant classification of the simple hand postures. Therefore, based on the experimental studies presented in Section 4.4.2, the other feature descriptor used for comparatively validating the efficiency of the DOMs is the PCA based method. The number of eigen features for computing the transformation matrix $W_{pca}$, is chosen based on the reconstruction accuracy.

Using (4.29), it is determined that 90% of the data variance corresponding to each sample in the database is represented by the first $l = 180$ eigen components. The number of eigen components for which the shapes are efficiently represented is determined by verifying the reconstruction accuracies for different values of $l$. The reconstruction accuracy is computed using the SSIM index and the MHD value. From the experiments performed on the normalized silhouettes of the hand postures in the Asamyuta hasta database, the value of $l$ for which the reconstruction accuracy is sufficiently high is determined as 100. The experiments on the reconstruction accuracy with respect to different values of $l$ for a hasta shape is illustrated in Figure 5.8. The results show that for $l > 90$, the shapes are efficiently reconstructed and the accuracy in terms of the SSIM index and the MHD value are significantly high. The transformation matrix $W_{pca}$ is formed using the eigen vectors corresponding to the first $l = 100$ eigen values. Therefore, if there are $I$ number of training samples, the

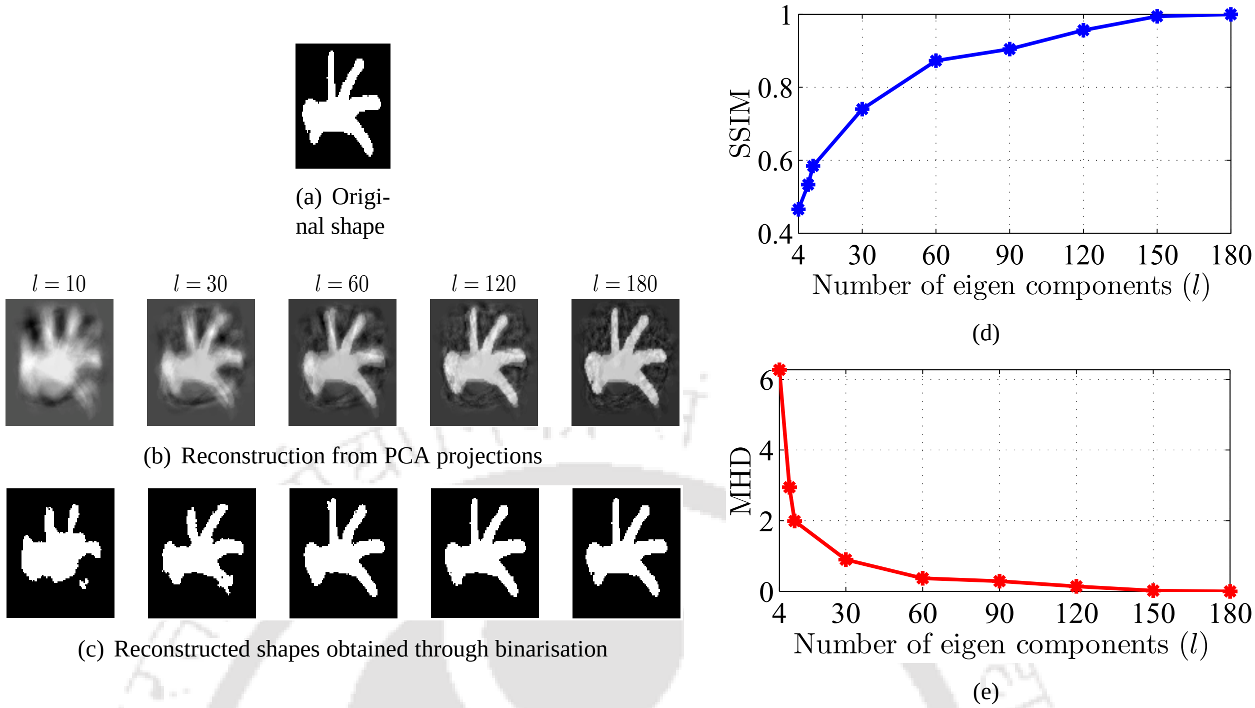


**Figure 5.8:** Illustration of shape reconstruction from PCA projection on different number of eigen components (a) Original hasta shape; (b) Reconstruction of (a) from the PCA projections for different values of $l$; (c) Binarisation of the images in (b) to obtain the reconstructed shapes. The threshold for binarisation is uniformly chosen as 120. Comparative plot of (c) SSIM index vs number of eigenvalues and (d) MHD vs number of eigenvalues computed between the image in (a) and the reconstructed shapes in (c).

total number of feature vectors obtained after projection into eigen space is $100 \times I$. For the selected number of eigen values, the ratio $\chi_{eigen}$ in (4.29) is 0.85.

### 5.5.5 Classification

Let $z_s$ be the feature vector of the test image of unknown orientation and $z_t^{\theta}$ the feature vector of the target image of orientation $\theta$ contained in the reference set. The classification of $z_s$ is done using the minimum distance classifier defined in (4.30). Considering the training samples at different orientations, the distance can be calculated as

$$d_t^{\theta}(z_s, z_t) = \sum_{j=1}^{T} (z_{sj} - z_{tj}^{\theta})^2 \qquad (5.2)$$

$$Match = \underset{\{t,\theta\}}{argmin} \left( d_t^{\theta} \right)$$

## 5.6 Experimental studies and results

The experiments presented in this section verify the efficiency of the proposed DOM based hand posture recognition technique in classifying the hand posture shapes in the Asamyuta hasta database. The robustness of the DOM descriptors to the user and the view-angle distortions in the hand posture shapes is investigated. The classification accuracy of the DOM descriptors is compared with that of the PCA based description.

The $8,064$ hand posture images in the Asamyuta hasta database is divided into three equal datasets based on the angle of view employed for posture acquisition. Accordingly, the three datasets are referred as the *Right view*, the *Front view* and the *Left view*. Each of these datasets consists of $2,688$ samples of the 32 hand postures, thereby containing 84 samples per hand posture.

The hand posture shapes in all the 3 datasets exhibit user variations and orientation and scale changes. The hand postures in Front view are acquired at the optimum view-angle $C_\theta = 90^\circ$ and hence, these samples are not subject to distortions that occur at oblique angles of view. The Right view and the Left view datasets are composed of hand posture images acquired at $C_\theta = 60^\circ$ and $C_\theta = 120^\circ$ respectively. Therefore, the images in the Right view and the Left view datasets exhibit shape variations caused by self-occlusion of fingers and variations in the perceived hand posture shapes due to different view-angles. Examples of the hand postures in the Asamyuta hasta database obtained at three different view-angles and the corresponding binary shapes are illustrated in Figure 5.9. From this figure, the structural difference between the hand posture shapes of each class contained in the three datasets can be observed. These variations in the hand posture shapes are quantitatively analysed to corroborate the robustness of the DOM descriptors in classifying hand postures under several structural variations.

### 5.6.1 Quantitative analysis on hand posture variations

The structural variations in the hand posture shapes are represented by computing the intraclass and the interclass distances between the shapes in each dataset. The intraclass distance in terms of the boundary similarity is measured using the Pratt's FOM. The interclass and the intraclass distances based on region similarity between the samples are measured using the correlation coefficient. The reference samples for computing these measures are taken from the Front view dataset.

The plots of the Pratt's FOM values obtained for the hand posture shapes in the Right view, the Front view and the Left view datasets are given in Figure 5.10. The intraclass FOM values obtained for the Front view dataset as shown in Figure 5.10(b), represent the structural changes in the hand posture shapes that occur due


**Figure 5.9:** Illustration of samples of hand posture images and the corresponding shapes in the Asamyuta hasta database. The illustration shows the variations in the hand postures when acquired at different view-angles.

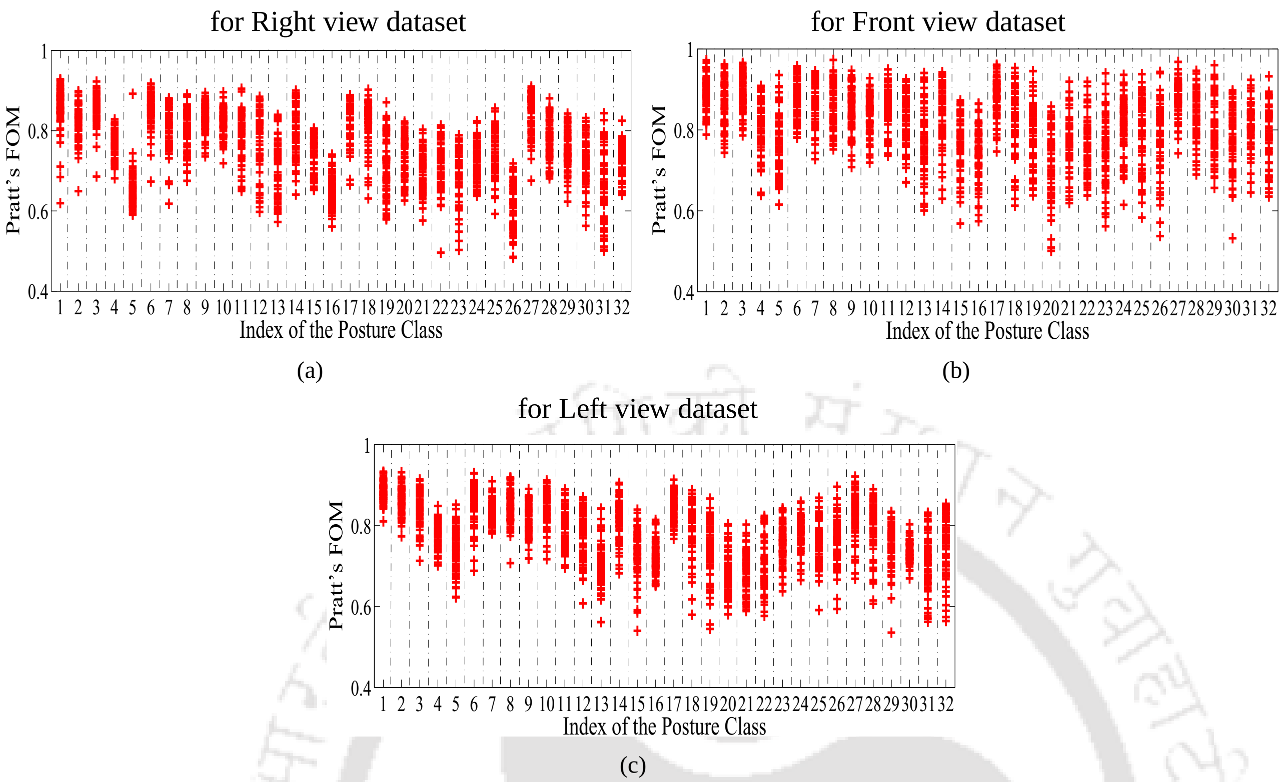


**Figure 5.10:** Plots illustrating the intraclass variability of the hand posture shapes in the hastas of (a) Right view dataset; (b) Front view dataset and (c) Left view dataset. The intraclass FOMs are measured with reference to the samples taken from Front view.

to user variations in the gesturing style. The user variations in the gesturing style correspond to the changes in the silhouette of the hand posture due to small variations in the angular displacements at the finger joints and the self-occlusions caused by it.

The intraclass FOMs corresponding to the Front view dataset represent the user variations and the FOM values corresponding to the Right view and the Left view datasets include both the user and the view-angle variations. From the values of the intraclass FOMs, it can be inferred that the hand posture shapes in the Asamyuta hasta database exhibit at least 20% deviation in the structural characteristics. The plots of intraclass FOMs of the samples in the the Right view and the Left view datasets are given in Figure 5.10(a) and Figure 5.10(c) respectively. The values in Figure 5.10(a) signify the similarities between the Right view and the Front view samples. Similarly, Figure 5.10(c) represents the similarities between the hand posture shapes in the Left view and the Front view datasets.

The plot comparing the posture wise mean of the intraclass FOM values obtained for the three datasets is shown in Figure 5.11(a). From the plot, it is evident that the hand posture shapes in the Right view and the Left view samples exhibit lower intraclass similarities with the reference samples in Front view. The decrease in the intraclass FOM values quantifies the structural changes that occur at different view-angles. Employing

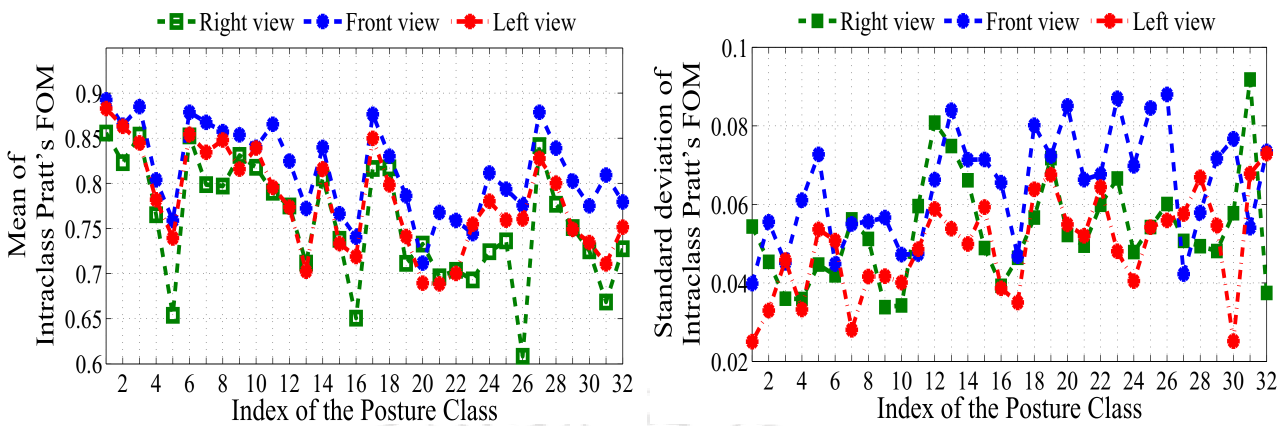


(a) (b)

**Figure 5.11:** Plots illustrating the postures with high intraclass variations and intraclass similarities using the (a) mean and the (b) standard deviation of the intraclass FOM values respectively. The plots are obtained for the posture classes in the Right view, the Front view and the Left view datasets.

different view-angles in the horizontal direction acquires the variation in the side profile of the hand postures. For different view-angles along the horizontal direction, the variations in the side profile of the hand postures are acquired. These variations may cause notable changes in the silhouette of the hand postures. Therefore, the intraclass FOMs of the Right view and the Left view samples are less in comparison to the Front view samples.

Particularly, Figure 5.11(a) shows that the Right view samples exhibit less FOM values than the Left view samples. For the given experimental setup, it should be noted that the view-angles for which the structural variations are more is based on the hand used for performing the postures. The posture classes in the Right view dataset with less intraclass FOM values are the postures 5, 16, 26 and 31. The variations in the shapes of these postures with respect to the view-angles can be inferred from the examples illustrated in Figure 5.9.

As we observe the FOM values in the plots shown in Figure 5.10, it is evident that the variations in the range of the FOM values obtained for the Right view and the Left view datasets are less than that of the Front view dataset. This suggests that the effect of user variations on the hand posture shape is comparatively less, when the hand postures are acquired from the right and the left views. However, these variations may cause significant changes in the hand posture shape when acquired from the front view. Further, it is also known that the perspective distortion due to the view-angle changes gets minimised when the camera is placed at a normal-angle position [226]. Due to these factors, the variation in the intraclass FOM values are comparatively less for the Right view and the Left view datasets. This can also be confirmed by analyzing the standard deviations of the intraclass FOM values for each dataset. The plots comparing the standard deviation of the posture wise FOM values in the datasets are given in Figure 5.11(b). It is evident that the variability in the intraclass samples is comparatively more for the Front view dataset. Examples of the hand posture shapes in the Front view dataset


**Figure 5.12:** Illustration of a few examples of hand posture images from the Front view dataset, exhibiting more intraclass variations. The shape of a hand posture varies due to structural changes caused by variations in the gesturing style of the gesturers.

with more variations in the intraclass FOM values are shown in Figure 5.12.

The region based similarities between the interclass samples in comparison to the intraclass similarities are measured using the correlation coefficient. The plots of the interclass correlation values computed with respect to each posture class in the datasets are shown in Figure 5.13 and Figure 5.14. The plots comparatively illustrate the interclass correlation values obtained with respect to each dataset. It shows that the hand posture shapes in all the datasets exhibit approximately similar interclass correlation characteristics.

As we examine the plots, the minimum difference between the intraclass and the interclass correlation values can be observed to be approximately around 10%. Similarly, the maximum difference between the intraclass and the interclass correlation values is approximately 50%. This implies that the Asamyuta hasta database is composed of different hand posture shapes with distinct as well as overlapping regions.

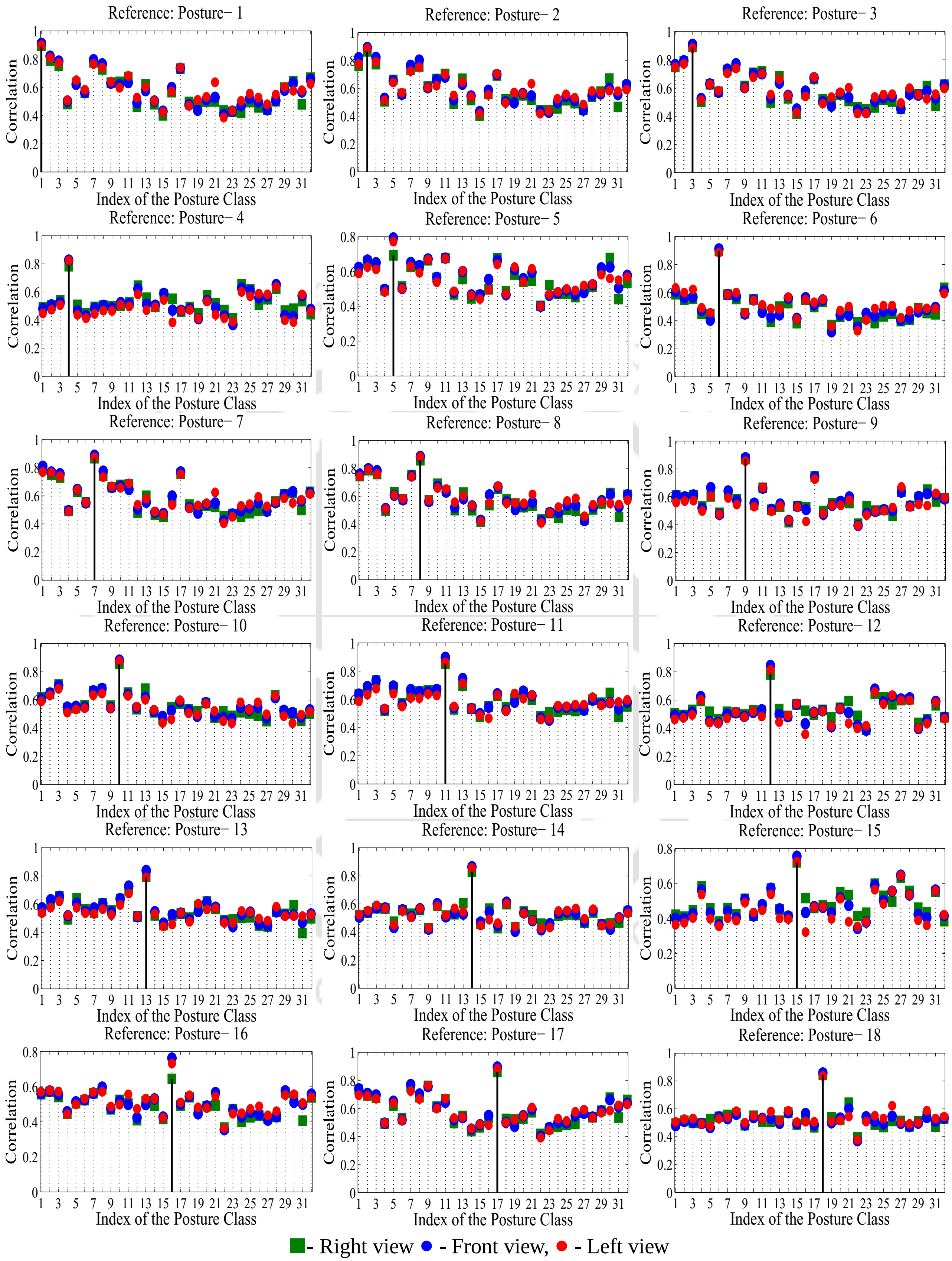


**Figure 5.13:** Illustration comparing the intraclass and the interclass correlations between the hand posture samples. The reference samples for comparison are taken from the Front view dataset. The plots show the correlation values computed with respect to reference postures from class 1 to class 18.

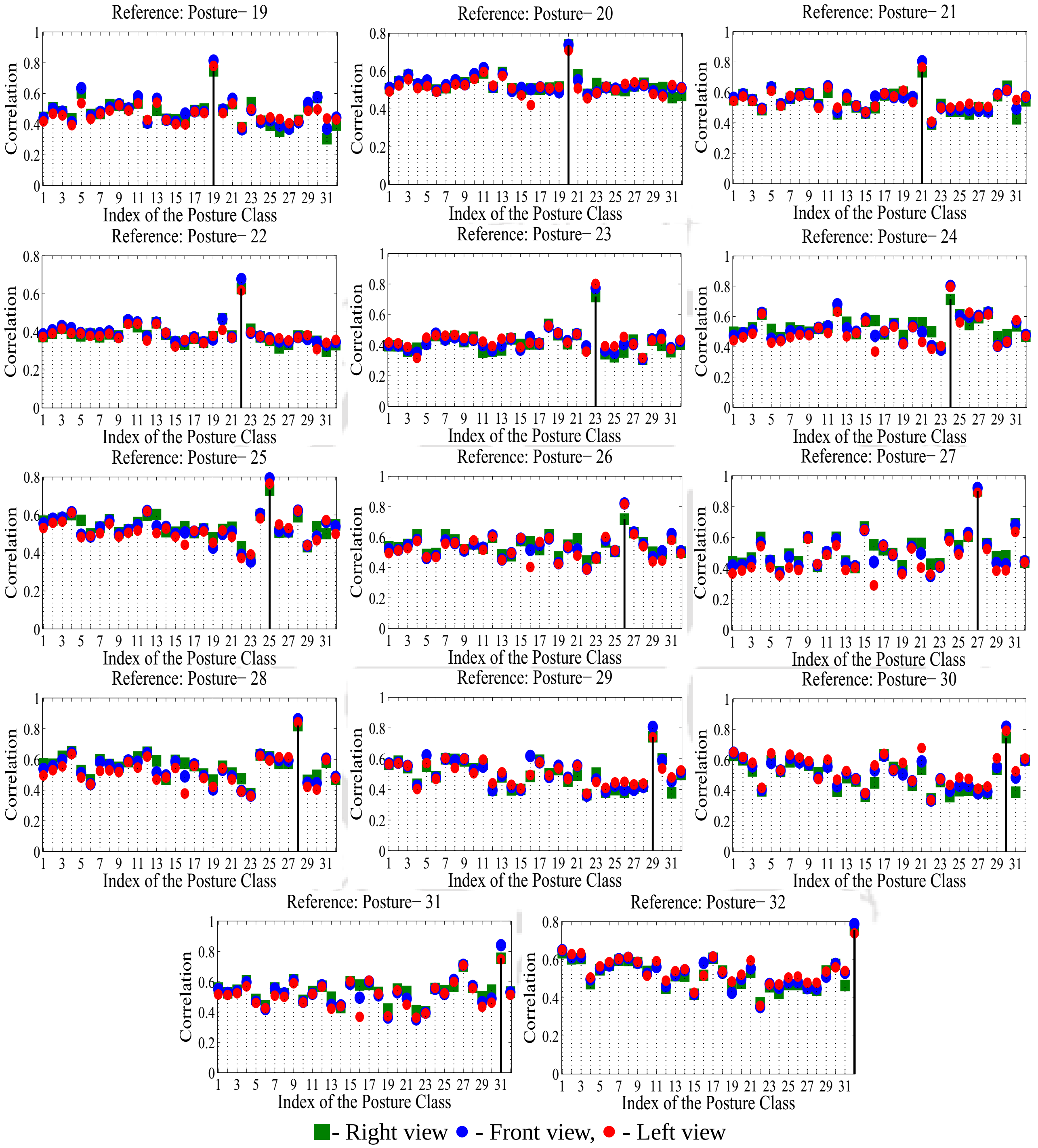


**Figure 5.14:** Illustration comparing the intraclass and the interclass correlations between the hand posture samples. The reference samples for comparison are taken from the Front view dataset. The plots show the correlation values computed with respect to reference postures from class 19 to class 32.

TH-1228_06610210

From the plots obtained with respect to different reference posture classes, as shown in Figure 5.13 and Figure 5.14, we can infer that the posture classes 6, 14, 18, 22, 23, 27 and 28 exhibit high intraclass correlation values in comparison to the respective interclass correlations. The minimum difference between the intraclass correlation and the interclass correlation values corresponding to these posture classes is over 21%. Therefore, they constitute the comparatively distinct hand posture shapes in the Asamyuta hasta database. The examples of the hand posture shapes belonging to these classes are shown in Figure 5.9.

The hand posture classes with interclass correlations as high as the intraclass correlation values are the samples belonging to classes 1, 2, 3, 5, 7, 8, 13, 15, 17 and 21. The minimum difference between the intraclass and the interclass correlation values for these posture classes is less than 12%. Among these, the interclass correlation is high between the posture shapes in the classes 1, 2, 3, 5, 7 and 8. This implies that these hand postures exhibit almost similar structural characteristics with more overlapping regions. Few examples of the shapes of these posture classes are illustrated in Figure 5.9.

From the mean of intraclass FOM values shown in Figure 5.11(a), it is known that the posture classes 5, 16, 24, 26 and 31 in the Right view dataset show less intraclass similarity with respect to the samples in the Front view dataset. This suggests that these hand posture classes may exhibit high interclass correlations when acquired from the right view direction. This can be verified from the plots in Figure 5.13 and Figure 5.14 that illustrate the correlation values obtained for the samples in the Right view dataset with respect to the reference posture classes 5, 16, 24, 26 and 31.

The analysis on the structural variations in the hand posture shapes in terms of the intraclass and the interclass distances confirms that the Asamyuta hasta database consists of hand posture images with more structural deviations indicating the effects of user variations and the view-angle changes. Therefore, the above analysis validates the applicability of the developed Asamyuta hasta database for experiments on user and view invariant hand posture classification.

### 5.6.2 Experiments on posture classification

The efficiency of the proposed DOM based descriptors for user and view invariant classification of the hand posture shapes in the Asamyuta hasta database are empirically studied in this section. The performance of the DOM descriptors is verified in comparison with the PCA based description method discussed in Section 5.5.4. The details of the experiment and the results obtained for user independent and view invariant recognition of the postures in the Asamyuta hasta database are discussed as follows.

In this work, the Asamyuta hasta database is developed by collecting the hand postures from 6 users and

**Table 5.1:** Consolidated classification results of DOM based features in comparison to the PCA method. The values are sorted with respect to the Right view, Front view and the Left view datasets. The training set contained 1, 152 samples of 32 hand postures taken from the Front view dataset. Considering rotation invariance, there are 41, 472 samples generated by rotating the 1, 152 samples in the training set. The number of testing samples in each dataset is 1, 536 and hence, the total number of testing samples is 4, 608. (% CC- Percentage of correct classification. )

| **Methods** | Classification results obtained for test samples from | | | **Overall %CC** |
|---|---|---|---|---|
| | Right view | Front view | Left view | |
| Krawtchouk moments | 81.12 | 94.34 | 81.97 | 85.81 |
| discrete Tchebichef moments | 85.09 | 96.16 | 86.26 | 89.17 |
| PCA based description | 81.64 | 95.44 | 83.07 | 86.72 |

the analysis on the hand posture variations has shown that the postures in the three datasets of Asamyuta hasta database represent more variations pertaining to the changes in the gesturing style of the users. Since the observed variations are more in comparison to the number of users, verifying user independence by varying the number of users in the training set will only lead to unstable results. Further, it is known that all the three datasets exhibit more intraclass variations due to the intra-user changes in the gesturing style. Therefore, the classification accuracies obtained with respect to these datasets will inherently quantify the user invariance characteristics of the feature descriptors. The robustness of the methods to view-angle variations is analysed by training the system only with the samples taken from the Front view dataset containing hand posture images acquired at the viewing angle of 90°.

The training set consists of 1,152 samples of 32 hand posture shapes taken from the Front view dataset. Therefore, there are 36 training samples per posture. In order to achieve rotation invariance, the samples in the training set are rotated in steps of 10° between 0° to 350°. Therefore, along with the rotated samples, the training set consists of totally 41, 472 samples. The testing set consists of 4, 608 samples constituting 1, 536 samples per dataset (representing the viewing direction).

The consolidated classification results comparing the performance of the proposed DOM features are given in Table 5.1 and the posture wise classification rates are shown in the plots in Figure 5.15. It is evident that the performance of the discrete Tchebichef moments is superior to that of the Krawtchouk moments and the PCA based method. The performance of the Krawtchouk moments is slightly poorer but comparable to that of the PCA based classification. The inferences on the user and view-angle invariance are discussed next.

#### 5.6.2.1 Verification of user invariance

As discussed earlier, the front view is the optimum viewing direction and hence, the Front view dataset will only represent the user variations and it does not include distortions that occur due to view-angle changes.

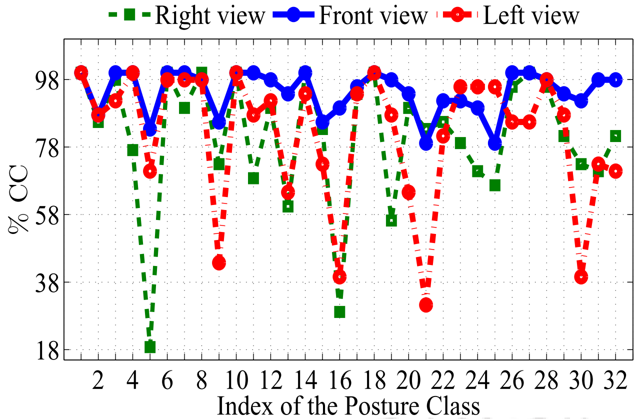


(a) Krawtchouk moments based features

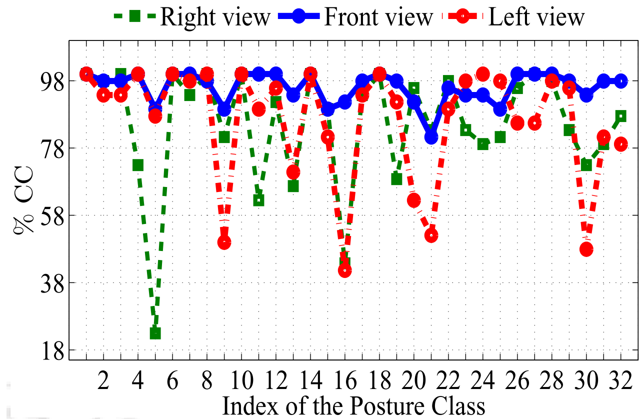


(b) discrete Tchebichef moments based features

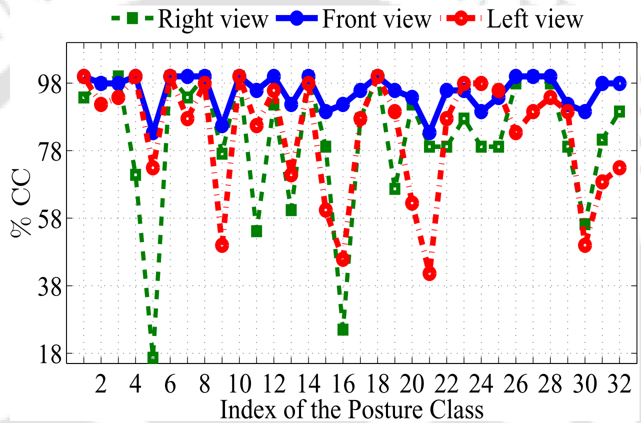


(c) PCA based description

**Figure 5.15:** Illustration comparing the posture wise classification results obtained for the Right view, Front view and the Left view datasets. The classification accuracies obtained for (a) Krawtchouk moments based features; (b) discrete Tchebichef moments based features and (c) PCA based hand posture description.

Therefore, the user invariance efficiency of the descriptors can be studied by analyzing the classification results obtained on the Front view dataset.

The results in Table 5.1 show that the discrete Tchebichef moments offer around 3% increase in the classification accuracy and hence, it implies that the discrete Tchebichef moments exhibit better user invariance characteristics. The response of the DOM descriptors with respect to each posture class can be inferred from the plots in Figure 5.15(a) and Figure 5.15(b). From the plot of the posture wise classification values corresponding to the Front view dataset, it is evident that most of the posture classes are correctly classified and only the posture classes 5, 9, 15, 21 and 25 attain classification accuracies less than 85%. The samples of these posture classes that are misclassified in DOM based description are illustrated in Figure 5.16. From the illustration it is evident that the misclassification has occurred when the shapes of the postures change due to self-occlusion between the fingers which takes place as the effect of user variations. The change in the posture shape is in such a way that it matches with the shape of a different posture class leading to classification errors. The overlap

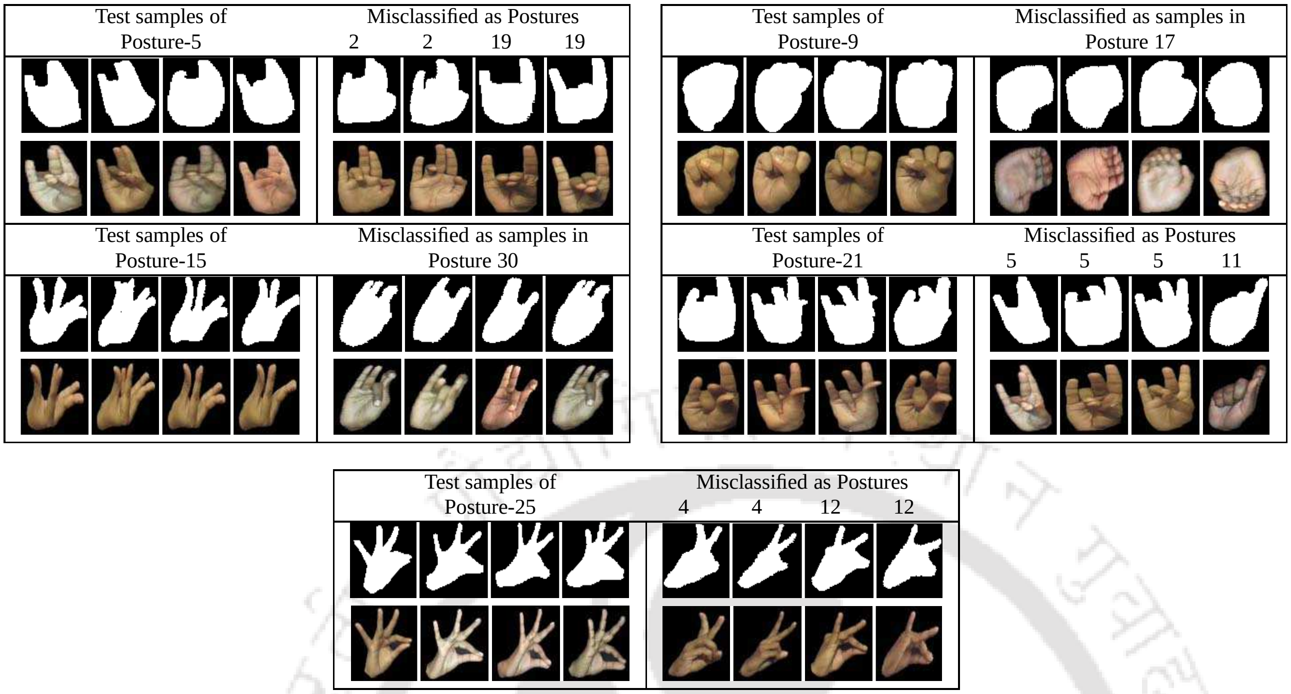


**Figure 5.16:** Examples of the hand posture classes in the Front view dataset of the Asamyuta hasta database exhibiting higher misclassification rate.

between the regions of the two hand posture shapes also occurs as the orientations of the hand posture vary. As a result, two different hand posture classes exhibiting overlapping regions at different orientations are also mismatched. For example, as shown in Figure 5.16, the samples of posture 15 are mismatched with the samples in posture 30. The mismatch has occurred for a particular orientation of the samples in posture 30. The study on intraclass variations in Section 5.6.1 has shown that the hand posture shapes in the Asamyuta hasta database exhibit at least 20% structural deviation and shapes belonging to classes 13, 18, 20, 23 and 26 have shown utmost 40% intraclass variations. Despite of high intraclass variations, the classification accuracies for these classes are higher than 90%. Further, the analysis on interclass correlation in Section 5.6.1 has shown that, except the posture classes 6, 14, 18, 22, 23, 27 and 28, all the other posture classes exhibit interclass correlations comparably high as the intraclass correlations. For example, the posture classes 1, 2, 3, 7 and 8 show interclass correlations almost similar to the intraclass correlation value. As we examine the classification results in Figure 5.15(a) and Figure 5.15(b), it can be known that these posture classes offer classification accuracies around 98%. These observations on the misclassified samples and the analysis on the classification accuracies with respect to intraclass variations confirm that the DOM based descriptors are efficient as user invariant features.

The posture wise classification results of the Front view dataset obtained with respect to the PCA based description is shown in Figure 5.15(c). From the results, it is observed that the PCA based classification results

**Table 5.2:** Confusion matrix corresponding to the results in Table 5.1 for Krawtchouk moments based description of testing samples in the Front view dataset. The total number of testing samples per posture is 48 with a total of 1,536 testing samples.

| I/P \ O/P | 1 | 2 | 3 | 4 | 5 | 6 | 7 | 8 | 9 | 10 | 11 | 12 | 13 | 14 | 15 | 16 | 17 | 18 | 19 | 20 | 21 | 22 | 23 | 24 | 25 | 26 | 27 | 28 | 29 | 30 | 31 | 32 |
|---|---|---|---|---|---|---|---|---|---|---|---|---|---|---|---|---|---|---|---|---|---|---|---|---|---|---|---|---|---|---|---|---|
| 1 | 48 | | | | | | | | | | | | | | | | | | | | | | | | | | | | | | | |
| 2 | | 42 | 6 | | | | | | | | | | | | | | | | | | | | | | | | | | | | | |
| 3 | | | 48 | | | | | | | | | | | | | | | | | | | | | | | | | | | | | |
| 4 | | | | 48 | | | | | | | | | | | | | | | | | | | | | | | | | | | | |
| 5 | 1 | 2 | | | 40 | | | | 1 | | | | | | | | 1 | | 3 | | | | | | | | | | | | | |
| 6 | | | | | | 48 | | | | | | | | | | | | | | | | | | | | | | | | | | |
| 7 | | | | | | | 48 | | | | | | | | | | | | | | | | | | | | | | | | | |
| 8 | | 1 | | | | | | 47 | | | | | | | | | | | | | | | | | | | | | | | | |
| 9 | | | | | | | | | 41 | | | | | | | | 7 | | | | | | | | | | | | | | | |
| 10 | | | | | | | | | | 48 | | | | | | | | | | | | | | | | | | | | | | |
| 11 | | | | | | | | | | | 48 | | | | | | | | | | | | | | | | | | | | | |
| 12 | | | | | | | | | | | | 47 | | | | | | | | | | | | 1 | | | | | | | | |
| 13 | | | 1 | | | | | | | | 2 | | 45 | | | | | | | | | | | | | | | | | | | |
| 14 | | | | | | | | | | | | | | 48 | | | | | | | | | | | | | | | | | | |
| 15 | 1 | | | | 1 | | | | | | | | | | 41 | | | | | | | | | | | 1 | | | | 4 | | |
| 16 | | | | | | | | | | | 2 | | | | | 43 | | | | 1 | | | | | | | | | 2 | | | |
| 17 | | | | | | | | | 2 | | | | | | | | 46 | | | | | | | | | | | | | | | |
| 18 | | | | | | | | | | | | | | | | | | 48 | | | | | | | | | | | | | | |
| 19 | | | | | | | | | | | | | | | | | | | 47 | | 1 | | | | | | | | | | | |
| 20 | | | | | 1 | | | | | | | | | | | | | | | 45 | | | | | | | | | | 1 | 1 | |
| 21 | | | | | 3 | | | | | | 6 | | | | | | | | | | 38 | | | | | | | | | 1 | | |
| 22 | | | | | | | | | | | | | | | | | | 1 | | | | 44 | | | 3 | | | | | | | |
| 23 | | | | 1 | | | | | | | 1 | | | 2 | | | | | | | | | 44 | | | | | | | | | |
| 24 | | | | 1 | | | | | | | | 3 | | | | | | | | | | | | 43 | | | | | | 1 | | |
| 25 | | | | 6 | | | | | | | | 3 | | | | | | | | | | | | | 38 | | | 1 | | | | |
| 26 | | | | | | | | | | | | | | | | | | | | | | | | | | 48 | | | | | | |
| 27 | | | | | | | | | | | | | | | | | | | | | | | | | | | 48 | | | | | |
| 28 | | | | | | | | | 1 | | | | | | | | | | | | | | | | | | | 47 | | | | |
| 29 | | | | | 1 | | 1 | | | | | | | | | | | | | | | | | | | | | | 45 | 1 | | |
| 30 | | | | | | | | | 1 | | | | | | | | 1 | | | | | | | 1 | | 1 | | | | 44 | | |
| 31 | | | | | | | | | 1 | | | | | | | | | | | | | | | | | | | | | | 47 | |
| 32 | | | | | | | | | | | | | | | | | | | | | | | | | | | | | 1 | | | 47 |

**Table 5.3:** Confusion matrix corresponding to the results in Table 5.1 for discrete Tchebichef moments based description of testing samples in the Front view dataset. The total number of testing samples per posture is 48 with a total of 1,536 testing samples.

| I/P \ O/P | 1 | 2 | 3 | 4 | 5 | 6 | 7 | 8 | 9 | 10 | 11 | 12 | 13 | 14 | 15 | 16 | 17 | 18 | 19 | 20 | 21 | 22 | 23 | 24 | 25 | 26 | 27 | 28 | 29 | 30 | 31 | 32 |
|---|---|---|---|---|---|---|---|---|---|---|---|---|---|---|---|---|---|---|---|---|---|---|---|---|---|---|---|---|---|---|---|---|
| 1 | 48 | | | | | | | | | | | | | | | | | | | | | | | | | | | | | | | |
| 2 | | 47 | 1 | | | | | | | | | | | | | | | | | | | | | | | | | | | | | |
| 3 | | 1 | 47 | | | | | | | | | | | | | | | | | | | | | | | | | | | | | |
| 4 | | | | 48 | | | | | | | | | | | | | | | | | | | | | | | | | | | | |
| 5 | | 2 | | | 43 | | | | | | | | | | | | 1 | | 2 | | | | | | | | | | | | | |
| 6 | | | | | | 48 | | | | | | | | | | | | | | | | | | | | | | | | | | |
| 7 | | | | | | | 48 | | | | | | | | | | | | | | | | | | | | | | | | | |
| 8 | | 1 | | | | | | 47 | | | | | | | | | | | | | | | | | | | | | | | | |
| 9 | | | | | | | | | 43 | | | | | | | | 5 | | | | | | | | | | | | | | | |
| 10 | | | | | | | | | | 48 | | | | | | | | | | | | | | | | | | | | | | |
| 11 | | | | | | | | | | | 48 | | | | | | | | | | | | | | | | | | | | | |
| 12 | | | | | | | | | | | | 48 | | | | | | | | | | | | | | | | | | | | |
| 13 | | | 1 | | | | | | | | 2 | | 45 | | | | | | | | | | | | | | | | | | | |
| 14 | | | | | | | | | | | | | | 48 | | | | | | | | | | | | | | | | | | |
| 15 | 1 | | | | 1 | | | | | | | | | | 43 | | | | | | | | | | | | | | | 3 | | |
| 16 | | | | | | | | | | | 1 | | | | | 44 | | | | | | | | | | | | | 2 | 1 | | |
| 17 | | | | | | | | | 1 | | | | | | | | 47 | | | | | | | | | | | | | | | |
| 18 | | | | | | | | | | | | | | | | | | 48 | | | | | | | | | | | | | | |
| 19 | | | | | | | | | | | | | | | | | | | 47 | | 1 | | | | | | | | | | | |
| 20 | | | | | 1 | | | | | | | | | | | | | | | 44 | | | | | | | | 1 | | 1 | 1 | |
| 21 | | | | | 3 | | | | | | 4 | | 1 | | | | | | 1 | | 39 | | | | | | | | | | | |
| 22 | | | | | | | | | | | | | | | | 1 | | | | | | 46 | | | 1 | | | | | | | |
| 23 | | | | | | | | | | | | | 1 | 2 | | | | | | | | | 45 | | | | | | | | | |
| 24 | | | | 1 | | | | | | | | 2 | | | | | | | | | | | | 45 | | | | | | | | |
| 25 | | | | 3 | | | | | | | | 2 | | | | | | | | | | | | | 43 | | | | | | | |
| 26 | | | | | | | | | | | | | | | | | | | | | | | | | | 48 | | | | | | |
| 27 | | | | | | | | | | | | | | | | | | | | | | | | | | | 48 | | | | | |
| 28 | | | | | | | | | | | | | | | | | | | | | | | | | | | | 48 | | | | |
| 29 | | | | | 1 | | | | | | | | | | | | | | | | | | | | | | | | 47 | | | |
| 30 | | | | | | | | | | | | | | | | | 1 | | | | | | | 1 | | | | | | 45 | 1 | |
| 31 | | | | | | | | | 1 | | | | | | | | | | | | | | | | | | | | | | 47 | |
| 32 | | | | | | | | | | | | | | | | | | | | | | | | | | | | | 1 | | | 47 |

**Table 5.4:** Confusion matrix corresponding to the results in Table 5.1 for PCA based description of testing samples in the Front view dataset. The total number of testing samples per posture is 48 with a total of 1,536 testing samples.

| I/P \ O/P | 1 | 2 | 3 | 4 | 5 | 6 | 7 | 8 | 9 | 10 | 11 | 12 | 13 | 14 | 15 | 16 | 17 | 18 | 19 | 20 | 21 | 22 | 23 | 24 | 25 | 26 | 27 | 28 | 29 | 30 | 31 | 32 |
|---|---|---|---|---|---|---|---|---|---|---|---|---|---|---|---|---|---|---|---|---|---|---|---|---|---|---|---|---|---|---|---|---|
| 1 | 48 | | | | | | | | | | | | | | | | | | | | | | | | | | | | | | | |
| 2 | | 47 | 1 | | | | | | | | | | | | | | | | | | | | | | | | | | | | | |
| 3 | | 1 | 47 | | | | | | | | | | | | | | | | | | | | | | | | | | | | | |
| 4 | | | | 48 | | | | | | | | | | | | | | | | | | | | | | | | | | | | |
| 5 | | 2 | | | 40 | | | | 1 | | | | | | | | 2 | | 2 | | 1 | | | | | | | | | | | |
| 6 | | | | | | 48 | | | | | | | | | | | | | | | | | | | | | | | | | | |
| 7 | | | | | | | 48 | | | | | | | | | | | | | | | | | | | | | | | | | |
| 8 | | | | | | | | 48 | | | | | | | | | | | | | | | | | | | | | | | | |
| 9 | | | | | | | | | 41 | | | | | | | | 7 | | | | | | | | | | | | | | | |
| 10 | | | | | | | | | | 48 | | | | | | | | | | | | | | | | | | | | | | |
| 11 | | | | | | | 1 | | 1 | | 46 | | | | | | | | | | | | | | | | | | | | | |
| 12 | | | | | | | | | | | | 48 | | | | | | | | | | | | | | | | | | | | |
| 13 | | | 3 | | | | | | | | 1 | | 44 | | | | | | | | | | | | | | | | | | | |
| 14 | | | | | | | | | | | | | | 48 | | | | | | | | | | | | | | | | | | |
| 15 | 1 | | | | 1 | | | | | | | | | | 43 | | | | | | | | | | | | | | | 3 | | |
| 16 | | | | | | | | | | | 2 | | | | | 44 | | | | | | | | | | | | | 2 | | | |
| 17 | | | | | | | | | 2 | | | | | | | | 46 | | | | | | | | | | | | | | | |
| 18 | | | | | | | | | | | | | | | | | | 48 | | | | | | | | | | | | | | |
| 19 | | | | | | | | | | | | | | | | | | | 46 | | 2 | | | | | | | | | | | |
| 20 | | | | | 1 | | | | | | | | | | | | | | | 45 | | | | | | | | | | 1 | 1 | |
| 21 | | | | | 2 | | | | | | 4 | | | | | | 1 | | 1 | | 40 | | | | | | | | | | | |
| 22 | | | | | | | | | | | | | | | | 1 | | | | | | 46 | | | 1 | | | | | | | |
| 23 | | | | | | | | | | | | | | 2 | | | | | | | | | 46 | | | | | | | | | |
| 24 | | | | 2 | | | | | | | | 2 | | | | | | | | | | | | 43 | | | | | 1 | | | |
| 25 | | | | 1 | | | | | | | | 2 | | | | | | | | | | | | | 45 | | | | | | | |
| 26 | | | | | | | | | | | | | | | | | | | | | | | | | | 48 | | | | | | |
| 27 | | | | | | | | | | | | | | | | | | | | | | | | | | | 48 | | | | | |
| 28 | | | | | | | | | | | | | | | | | | | | | | | | | | | | 48 | | | | |
| 29 | | | | | 1 | | 1 | | | | | | | | | 1 | | | | | | | | | | | 1 | | 44 | | | |
| 30 | | | | | | | | | 3 | | | | | | | | | | | | | | | 1 | | | | | | 43 | 1 | |
| 31 | | | | | | | | | 1 | | | | | | | | | | | | | | | | | | | | | | 47 | |
| 32 | | | | | | | | | | | | | | | | | | | | | | | | | | | | | 1 | | | 47 |

exhibit similar characteristics as the DOM based descriptors. The confusion matrix for classification results of Front view dataset obtained for the DOMs and the PCA are given in Table 5.2 - Table 5.4. It can be observed that the misclassified posture classes and the corresponding mismatched posture classes are almost similar in the DOM and the PCA based descriptions.

#### 5.6.2.2 Verification of view invariance

The efficiency of the DOM based descriptors for view invariant complex hand posture recognition is inferred from the classification results obtained for the hand posture samples in the Right view and the Left view datasets.

From the values in Table 5.1, it is evident that the classification accuracies with respect to the Right view and the Left view datasets are higher for discrete Tchebichef moment based descriptors. In comparison to the discrete Tchebichef moments, the Krawtchouk moments offers around 5% less classification rate. The PCA based method exhibits almost similar performance as the Krawtchouk moments with respect to the Right view dataset. In the case of Left view dataset, the PCA offers 2% improvement in the classification accuracy compared to the Krawtchouk moments. The results in Table 5.1 suggest the discrete Tchebichef moments as


**Figure 5.17:** Examples of the hand posture classes in the Right view dataset of the Asamyuta hasta database exhibiting higher misclassification rate.

better feature descriptors for view invariant hand posture classification.

The posture wise classification results for the Right view and the Left view datasets using the DOM based descriptors are shown in Figure 5.15(a) and Figure 5.15(b) respectively. These plots show that almost 38% of the posture classes exhibit classification accuracies less than 80%. Of these, some of the posture classes achieved the lowest classification rate of 30%. The posture classes in the Right view dataset with less classification rates are postures 5, 11 and 16. Similarly, the posture classes in the Left view dataset offering less classification accuracy are the postures 9, 16, 21 and 30.

Figure 5.17 and Figure 5.18 present an illustration of the mismatched posture samples in the Right view and the Left view datasets respectively. The illustrations show that the mismatch occurs between the hand posture samples whose shapes contain more overlapping regions. The variation in shapes is mainly due to the

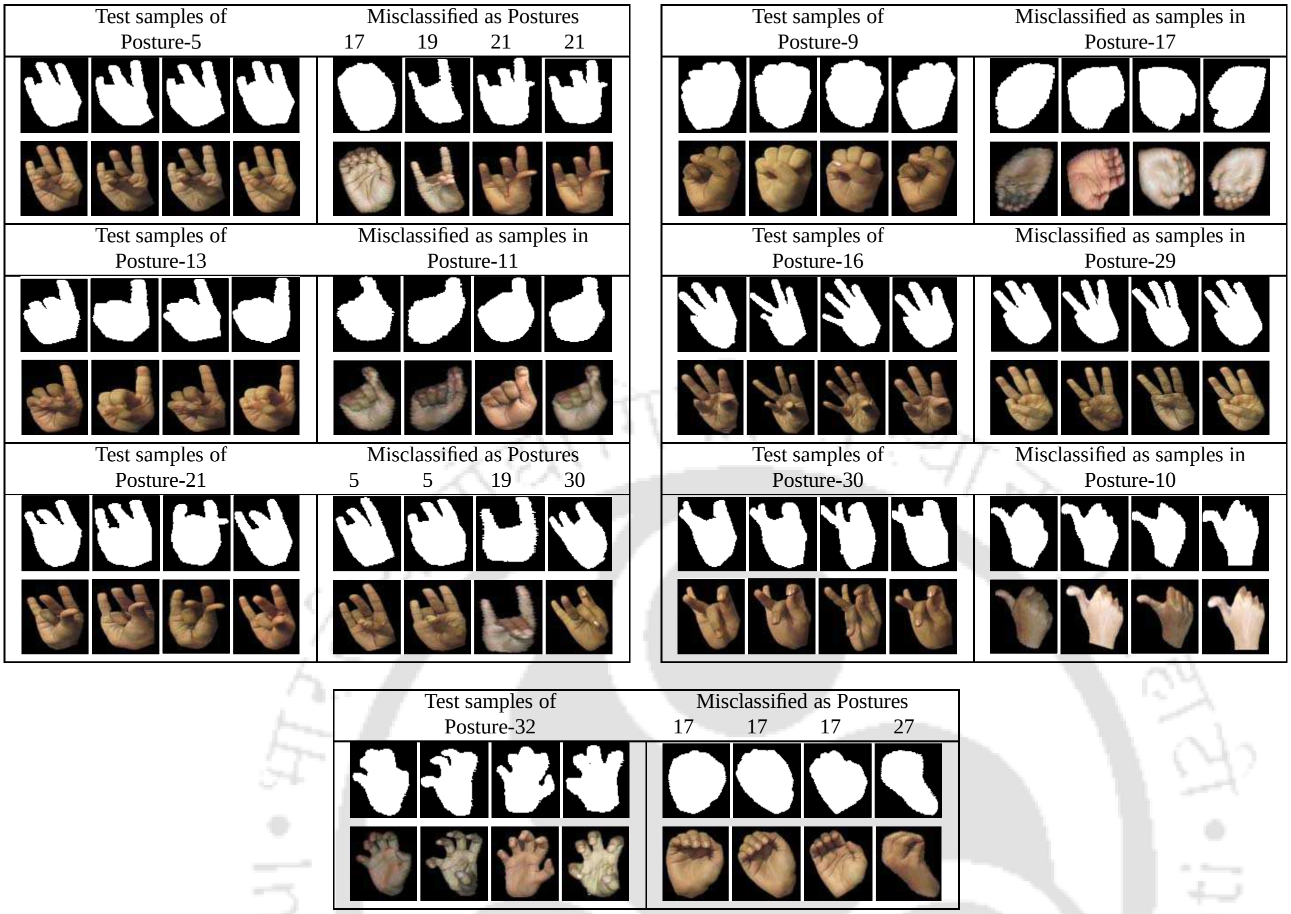


**Figure 5.18:** Examples of the hand posture classes in the Left view dataset of the Asamyuta hasta database exhibiting higher misclassification rate.

self-occlusion of fingers and the variation in the side profiles of the hand postures. It should also be observed that the high correspondence between the mismatched posture classes occurs also due to orientation changes. From Figure 5.11(a), it can be inferred that the samples in the Right view and the Left view datasets with more misclassification rates correspond to the posture classes with less intraclass FOM values.

From the plot in Figure 5.15(c), the posture wise classification results obtained for the PCA method on to the Right view and the Left view datasets can be verified. It can be inferred that the posture wise classification response of PCA is almost similar to that of the Krawtchouk moments.

The detailed scores of the classification results obtained with respect to the Right view dataset are given in Table 5.5-Table 5.7 and the results corresponding to the Left view dataset are given in Table 5.8-Table 5.10. By analyzing the detailed scores of the posture wise classification results, it is observed that the mismatch has occurred between the classes that exhibit more interclass correlations.

**Table 5.5:** Confusion matrix corresponding to the results in Table 5.1 for Krawtchouk moments based description of testing samples in the Right view dataset. The total number of testing samples per posture is 48 with a total of 1, 536 testing samples.

| I/P \ O/P | 1 | 2 | 3 | 4 | 5 | 6 | 7 | 8 | 9 | 10 | 11 | 12 | 13 | 14 | 15 | 16 | 17 | 18 | 19 | 20 | 21 | 22 | 23 | 24 | 25 | 26 | 27 | 28 | 29 | 30 | 31 | 32 |
|---|---|---|---|---|---|---|---|---|---|---|---|---|---|---|---|---|---|---|---|---|---|---|---|---|---|---|---|---|---|---|---|---|
| 1 | 48 | | | | | | | | | | | | | | | | | | | | | | | | | | | | | | | |
| 2 | | 41 | 5 | | 1 | | | 1 | | | | | | | | | | | | | | | | | | | | | | | | |
| 3 | | 1 | 47 | | | | | | | | | | | | | | | | | | | | | | | | | | | | | |
| 4 | | | | 37 | | | | | | | | 4 | | | | | | | | | 7 | | | | | | | | | | | |
| 5 | 1 | 19 | 3 | | 9 | | 2 | 3 | | | 1 | | | | | | | | 6 | | 4 | | | | | | | | | | | |
| 6 | | | | | | 48 | | | | | | | | | | | | | | | | | | | | | | | | | | |
| 7 | | | | | | | 43 | 3 | | | 1 | | | | | | | | | | | | | | | | 1 | | | | | |
| 8 | | | | | | | | 48 | | | | | | | | | | | | | | | | | | | | | | | | |
| 9 | | | | | | | | | 35 | | | | | | | | 13 | | | | | | | | | | | | | | | |
| 10 | | | | | | | | | | 48 | | | | | | | | | | | | | | | | | | | | | | |
| 11 | 11 | | 1 | | | | | | | | 33 | | | | | | 3 | | | | | | | | | | | | | | | |
| 12 | | | | 4 | | | | | | | | 43 | | | | | | | | | | | | | | 1 | | | | | | |
| 13 | | | 3 | | | 1 | | 5 | | | | | 29 | 1 | | 1 | | | | | | | 7 | | | 1 | | | | | | |
| 14 | | | | | | | | | | | | | | 48 | | | | | | | | | | | | | | | | | | |
| 15 | | | | | 1 | | | | | | | | | | 40 | | 1 | | | 1 | | | | | | 2 | | | 1 | | 1 | 1 |
| 16 | | | | 4 | | 6 | | | | | | | | 4 | | 14 | | 2 | | 2 | | | | 3 | 2 | 3 | | | 2 | 1 | | 5 |
| 17 | | | | | | | | | 3 | | | | | | | | 45 | | | | | | | | | | | | | | | |
| 18 | | | | | | | | | | | | | | | | | | 48 | | | | | | | | | | | | | | |
| 19 | | 2 | | | 1 | | | 8 | | | | | 2 | | | | | 2 | 27 | | 6 | | | | | | | | | | | |
| 20 | | | | 2 | 1 | | | | | | | | | | 1 | | | | | 43 | | | 1 | | | | | | | | | |
| 21 | | | 1 | 1 | 1 | | | 2 | | | | | | 1 | | | | | 1 | | 40 | | 1 | | | | | | | | | |
| 22 | | | | 1 | | | | | | | | 2 | | | | 1 | | 1 | | | | 41 | 1 | 1 | | | | | | | | |
| 23 | | | | | | | | | | | 2 | | 1 | 7 | | | | | | | | | 38 | | | | | | | | | |
| 24 | | | | 1 | | | 1 | | | | | 6 | 1 | | | | | | | | 1 | | 2 | 34 | | | | | | 1 | 1 | |
| 25 | | | | 9 | | | | | | | | 6 | | | | | | | | | | | | 1 | 32 | | | | | | | |
| 26 | | | | | | | | | | | 1 | | | | | | | | | | | | | | | 46 | | | | | 1 | |
| 27 | | | | | | | | | | | | | | | | | | | | | | | | | | | 48 | | | | | |
| 28 | | | | | | | | | | | | | | | | | 1 | | | | | | | | | | 1 | 46 | | | | |
| 29 | | | | | | | 1 | | 3 | | | | | | | 3 | | | | | | | | | | | | | 39 | | | 2 |
| 30 | | 1 | | | 2 | | | | 3 | 1 | | | | | | | | | | | 3 | | | | | 2 | | | | 35 | 1 | |
| 31 | | | | | | | | 1 | | | 1 | | 9 | | | | | | | | | | | | | 3 | | | | | 34 | |
| 32 | 4 | | | | | 2 | | | 1 | | | | 1 | | | | 1 | | | | | | | | | | | | | | | 39 |

**Table 5.6:** Confusion matrix corresponding to the results in Table 5.1 for discrete Tchebichef moments based description of testing samples in the Right view dataset. The total number of testing samples per posture is 48 with a total of 1, 536 testing samples.

| I/P \ O/P | 1 | 2 | 3 | 4 | 5 | 6 | 7 | 8 | 9 | 10 | 11 | 12 | 13 | 14 | 15 | 16 | 17 | 18 | 19 | 20 | 21 | 22 | 23 | 24 | 25 | 26 | 27 | 28 | 29 | 30 | 31 | 32 |
|---|---|---|---|---|---|---|---|---|---|---|---|---|---|---|---|---|---|---|---|---|---|---|---|---|---|---|---|---|---|---|---|---|
| 1 | 48 | | | | | | | | | | | | | | | | | | | | | | | | | | | | | | | |
| 2 | | 47 | | | 1 | | | | | | | | | | | | | | | | | | | | | | | | | | | |
| 3 | | | 48 | | | | | | | | | | | | | | | | | | | | | | | | | | | | | |
| 4 | | | | 35 | | | | | | | | 7 | | | | | | | | | 6 | | | | | | | | | | | |
| 5 | | 20 | 1 | | 11 | | | 2 | | | 1 | | | | | | | | 7 | | 5 | | 1 | | | | | | | | | |
| 6 | | | | | | 48 | | | | | | | | | | | | | | | | | | | | | | | | | | |
| 7 | | | | | | | 45 | 1 | | | 1 | | | | | | | | | | | | | | | | 1 | | | | | |
| 8 | | | | | | | | 48 | | | | | | | | | | | | | | | | | | | | | | | | |
| 9 | | | | | | | | | 39 | | | | | | | | 9 | | | | | | | | | | | | | | | |
| 10 | | | | | | | | | | 48 | | | | | | | | | | | | | | | | | | | | | | |
| 11 | 10 | | 2 | | | | | | | | 30 | | | | | | 6 | | | | | | | | | | | | | | | |
| 12 | | | | 3 | | | | | | | | 44 | | | | 1 | | | | | | | | | | | | | | | | |
| 13 | | | 6 | | | 4 | | 2 | | | | | 32 | | | | | | | | | | 2 | | | 2 | | | | | | |
| 14 | | | | | | | | | | | | | | 48 | | | | | | | | | | | | | | | | | | |
| 15 | | | | 1 | 1 | | | | | | | | | | 43 | | | | | 2 | | | | | | | | | | | | 1 |
| 16 | | | | 5 | | 2 | | 2 | | | | | | 3 | | 21 | | 4 | | | 1 | | | 6 | 1 | | | | 2 | 1 | | |
| 17 | | | | | | | | | 3 | | | | | | | | 45 | | | | | | | | | | | | | | | |
| 18 | | | | | | | | | | | | | | | | | | 48 | | | | | | | | | | | | | | |
| 19 | | 2 | | | 1 | | | 6 | | | | | 1 | | | | | | 33 | | 5 | | | | | | | | | | | |
| 20 | | | | 1 | | | | | | | | | | | | | | | | 46 | | | 1 | | | | | | | | | |
| 21 | | | 1 | | 1 | | 1 | 2 | | | | 1 | | | | | | 1 | 1 | | 40 | | | | | | | | | | | |
| 22 | | | | | | | | | | | | | | | | | | 1 | | | | 47 | | | | | | | | | | |
| 23 | | | 1 | | | | | | | | | | | 6 | | | | | | | | | 40 | | | | | 1 | | | | |
| 24 | | | | | 1 | | 1 | | | | | 6 | | | | | | | | | 1 | | | 38 | 1 | | | | | | | |
| 25 | | | | 6 | | | | | | | | 3 | | | | | | | | | | | | | 39 | | | | | | | |
| 26 | | | | | | | | | | | | | | | | | | | | | 1 | | | | | 46 | | | | | 1 | |
| 27 | | | | | | | | | | | | | | | | | | | | | | | | | | | 48 | | | | | |
| 28 | | | | | | | | | | | | | | | | | 1 | | | | | | | | | | | 47 | | | | |
| 29 | | | | | | | 1 | | 1 | | | | | | | 3 | | | | 1 | | | | | | | | | 40 | | | 2 |
| 30 | | | | | 3 | | | | 2 | 1 | | | | | | | | | | | 4 | | | | | 1 | | | 1 | 35 | 1 | |
| 31 | | | | | | | | | | | 1 | 1 | 7 | | | | | | | | | | | | | | 1 | | | | 38 | |
| 32 | 1 | | | | | 3 | | | | | | | | | | | | | 1 | | 1 | | | | | | | | | | | 42 |

**Table 5.7:** Confusion matrix corresponding to the results in Table 5.1 for PCA based description of testing samples in the Right view dataset. The total number of testing samples per posture is 48 with a total of 1, 536 testing samples.

| O/P I/P | 1 | 2 | 3 | 4 | 5 | 6 | 7 | 8 | 9 | 10 | 11 | 12 | 13 | 14 | 15 | 16 | 17 | 18 | 19 | 20 | 21 | 22 | 23 | 24 | 25 | 26 | 27 | 28 | 29 | 30 | 31 | 32 |
|---|---|---|---|---|---|---|---|---|---|---|---|---|---|---|---|---|---|---|---|---|---|---|---|---|---|---|---|---|---|---|---|---|
| 1 | 45 | | | | | | | | | | | | | | | | | | | | | | | | | | 3 | | | | | |
| 2 | | 47 | | | 1 | | | | | | | | | | | | | | | | | | | | | | | | | | | |
| 3 | | | 48 | | | | | | | | | | | | | | | | | | | | | | | | | | | | | |
| 4 | | | | 34 | | | | | | | | 6 | | | | | | | | | 8 | | | | | | | | | | | |
| 5 | | 19 | | | 8 | | | | | | 1 | | | | | | | | 9 | | 5 | | 1 | | | | 5 | | | | | |
| 6 | | | | | | 48 | | | | | | | | | | | | | | | | | | | | | | | | | | |
| 7 | | | | | | | 45 | 1 | | | 1 | | | | | | | | | | | | | | | | 1 | | | | | |
| 8 | | | | | | | | 48 | | | | | | | | | | | | | | | | | | | | | | | | |
| 9 | | | | | | | | | 37 | | | | | | | | 11 | | | | | | | | | | | | | | | |
| 10 | | | | | | | | | | 48 | | | | | | | | | | | | | | | | | | | | | | |
| 11 | 12 | | 2 | | | | | | 5 | | 26 | | | | | | 2 | | | | | | | | | | 1 | | | | | |
| 12 | | | | 3 | | | | | | | | 44 | | | | 1 | | | | | | | | | | | | | | | | |
| 13 | | | 7 | | | 8 | | | | | | | 29 | | | | | | | | | | 4 | | | | | | | | | |
| 14 | | | | | | | | | | | | | | 48 | | | | | | | | | | | | | | | | | | |
| 15 | 1 | | | 1 | 1 | | | | | | | | | | 38 | | | | | 2 | | | | | | 1 | | | 2 | | | 2 |
| 16 | | | | 6 | 1 | 3 | | | | | | | | 1 | | 12 | | 4 | | 5 | | | 2 | 8 | 1 | | | | 3 | 2 | | |
| 17 | | | | | | | | | 5 | | | | | | | | 42 | | | | | | | | | | 1 | | | | | |
| 18 | | | | | | | | | | | | | | | | | | 48 | | | | | | | | | | | | | | |
| 19 | | 3 | | | 1 | | | 3 | | | | | | | | | | | 32 | | 8 | | 1 | | | | | | | | | |
| 20 | | | | | | | | | | | | | | | 1 | | | | | 44 | | | 1 | | | | | | | 2 | | |
| 21 | | 1 | 1 | | 1 | | | 2 | | | | 1 | | | | 1 | | | 1 | | 38 | | | | | | | | | 2 | | |
| 22 | | | | | | | | | | | | 2 | | | | 1 | | 1 | 1 | | 1 | 38 | 2 | | 2 | | | | | | | |
| 23 | | | 1 | | | | | | | | | | | 5 | | | | | | | | | 42 | | | | | | | | | |
| 24 | | | | | 1 | | 3 | 1 | | | | 4 | | | | | | | | | 1 | | | 38 | | | | | | | | |
| 25 | | | | 7 | | | | | | | | 3 | | | | | | | | | | | | | 38 | | | | | | | |
| 26 | | | | | | | | | | | | | | | | | | | | | 1 | | | | | 47 | | | | | | |
| 27 | | | | | | | | | | | | | | | | | | | | | | | | | | | 48 | | | | | |
| 28 | | | | | | | | | | | | | | | | | 1 | | | | | | | | | | | 47 | | | | |
| 29 | | | | | | | 1 | | | | | | | | | 3 | 1 | | | 1 | | | | | | | 2 | | 38 | | | 2 |
| 30 | | 2 | | | 1 | | | | 10 | 5 | | | | | | | | | | | | | | | | 1 | | | 1 | 27 | 1 | |
| 31 | | | | | | 1 | | | | | 1 | | 6 | | | | | | | | | | | | | | 1 | | | | 39 | |
| 32 | | | | | | 3 | | | | | | | | | | | | | 1 | | 1 | | | | | | | | | | | 43 |

**Table 5.8:** Confusion matrix corresponding to the results in Table 5.1 for Krawtchouk moments based description of testing samples in the Left view dataset. The total number of testing samples per posture is 48 with a total of 1, 536 testing samples.

| O/P I/P | 1 | 2 | 3 | 4 | 5 | 6 | 7 | 8 | 9 | 10 | 11 | 12 | 13 | 14 | 15 | 16 | 17 | 18 | 19 | 20 | 21 | 22 | 23 | 24 | 25 | 26 | 27 | 28 | 29 | 30 | 31 | 32 |
|---|---|---|---|---|---|---|---|---|---|---|---|---|---|---|---|---|---|---|---|---|---|---|---|---|---|---|---|---|---|---|---|---|
| 1 | 48 | | | | | | | | | | | | | | | | | | | | | | | | | | | | | | | |
| 2 | 1 | 42 | 5 | | | | | | | | | | | | | | | | | | | | | | | | | | | | | |
| 3 | | 2 | 44 | | | | | | | | 2 | | | | | | | | | | | | | | | | | | | | | |
| 4 | | | | 48 | | | | | | | | | | | | | | | | | | | | | | | | | | | | |
| 5 | 1 | | | | 34 | | | | 2 | | | | | | | | 5 | | 3 | | 2 | | | | | | | | | 1 | | |
| 6 | | | | | | 47 | | | | | | | | | | | | 1 | | | | | | | | | | | | | | |
| 7 | | | | | | | 47 | | | | | | | | | | 1 | | | | | | | | | | | | | | | |
| 8 | | | | | | | | 47 | | | | | | | | | | | | | | | | | | | 1 | | | | | |
| 9 | | | | | | | | | 21 | | | | | | | | 25 | | | | | | | | | | 2 | | | | | |
| 10 | | | | | | | | | | 48 | | | | | | | | | | | | | | | | | | | | | | |
| 11 | 1 | | | | | | 1 | | 3 | | 42 | | | | | | 1 | | | | | | | | | | | | | | | |
| 12 | | | | | | | | | | | | 44 | | | | | | | | 1 | | | | 3 | | | | | | | | |
| 13 | | | 1 | | | 3 | | | | | 12 | | 31 | | | | | | 1 | | | | | | | | | | | | | |
| 14 | | | | | | | | | | | | | | 45 | | | | 1 | | | | | 2 | | | | | | | | | |
| 15 | | | | | 1 | | | | 1 | | | 2 | | | 35 | 1 | 1 | | | 2 | | | | | | 1 | | | 2 | | 2 | |
| 16 | | | | | 3 | | 2 | | | | 1 | | | | | 19 | | | 2 | | 2 | | | | | | | | 14 | 5 | | |
| 17 | | | | | | | | | 1 | | | | | | | | 45 | | | | | | | | | | 2 | | | | | |
| 18 | | | | | | | | | | | | | | | | | | 48 | | | | | | | | | | | | | | |
| 19 | | 1 | | | 1 | | | | | | 1 | | 1 | | | | | | 42 | | 2 | | | | | | | | | | | |
| 20 | | | | | | | | | | | 1 | | | 1 | 8 | 1 | | | 1 | 31 | | | 1 | | | | | | | 1 | | 3 |
| 21 | | | | | 11 | | 1 | | 4 | 1 | | | | | | | 1 | | 8 | | 15 | | | | | | | | | 7 | | |
| 22 | | | | 3 | | | | | | | | 3 | | | | | | 1 | | | | 39 | | | 2 | | | | | | | |
| 23 | | | | | | | | | | | | | | 1 | | | | | | | | | 46 | | | | 1 | | | | | |
| 24 | | | | | | | | | | | | 2 | | | | | | | | | | | | 46 | | | | | | | | |
| 25 | | | | | | | | | | | | 1 | | | | | | | | | | | | 1 | 46 | | | | | | | |
| 26 | | | | | | | | | | 3 | | | | | | | | 1 | | | | | | | | 41 | | 3 | | | | |
| 27 | 1 | | | | | | | | 3 | | | | | | | | 3 | | | | | | | | | | 41 | | | | | |
| 28 | | | | | | | | | | | | | | | | | 1 | | | | | | | | | | | 47 | | | | |
| 29 | | | | | | | | | 1 | | | | | | | 2 | 1 | | 2 | | | | | | | | | | 42 | | | |
| 30 | | | 2 | | 1 | | | | 1 | 18 | | | 2 | | | | | | 1 | | | | | | | 4 | | | | 19 | | |
| 31 | | | | | | | | | 2 | | | 1 | | | | | 3 | | | | 2 | | | | | 1 | 1 | | | 3 | 35 | |
| 32 | | | | | | | | | 6 | 1 | 1 | | | | | | | | | | | | | | | | 5 | 1 | | | | 34 |

**Table 5.9:** Confusion matrix corresponding to the results in Table 5.1 for discrete Tchebichef moments based description of testing samples in the Left view dataset. The total number of testing samples per posture is 48 with a total of 1, 536 testing samples.

| I/P \ O/P | 1 | 2 | 3 | 4 | 5 | 6 | 7 | 8 | 9 | 10 | 11 | 12 | 13 | 14 | 15 | 16 | 17 | 18 | 19 | 20 | 21 | 22 | 23 | 24 | 25 | 26 | 27 | 28 | 29 | 30 | 31 | 32 |
|---|---|---|---|---|---|---|---|---|---|---|---|---|---|---|---|---|---|---|---|---|---|---|---|---|---|---|---|---|---|---|---|---|
| 1 | 48 | | | | | | | | | | | | | | | | | | | | | | | | | | | | | | | |
| 2 | 2 | 45 | 1 | | | | | | | | | | | | | | | | | | | | | | | | | | | | | |
| 3 | | | 45 | | | | | | | | 2 | | 1 | | | | | | | | | | | | | | | | | | | |
| 4 | | | | 48 | | | | | | | | | | | | | | | | | | | | | | | | | | | | |
| 5 | | | | | 42 | | | | | | | | | | | | 3 | | 1 | | | | | | | | | | 1 | 1 | | |
| 6 | | | | | | 48 | | | | | | | | | | | | | | | | | | | | | | | | | | |
| 7 | | | | | | | 47 | | 1 | | | | | | | | | | | | | | | | | | | | | | | |
| 8 | | | | | | | | 48 | | | | | | | | | | | | | | | | | | | | | | | | |
| 9 | | | | | | | | | 24 | | | | | | | | 22 | | | | | | | | | | 2 | | | | | |
| 10 | | | | | | | | | | 48 | | | | | | | | | | | | | | | | | | | | | | |
| 11 | 1 | | | | | | 1 | | 3 | | 43 | | | | | | | | | | | | | | | | | | | | | |
| 12 | | | | | | | | | | | | 46 | | | | | | | | | | | | 1 | 1 | | | | | | | |
| 13 | | | 1 | | | 1 | | | | | 11 | | 34 | | | | | | 1 | | | | | | | | | | | | | |
| 14 | | | | | | | | | | | | | | 48 | | | | | | | | | | | | | | | | | | |
| 15 | | | | | 1 | | | | | | | 1 | | | 39 | 1 | | | | | 1 | | | | | | | | 2 | 3 | | |
| 16 | | | | | 1 | | 1 | | | | 1 | | | | | 20 | | | 1 | | | | | 1 | | | | | 14 | 9 | | |
| 17 | | | | | | | | | 1 | | | | | | | | 45 | | | | | | | | | | 2 | | | | | |
| 18 | | | | | | | | | | | | | | | | | | 48 | | | | | | | | | | | | | | |
| 19 | | 1 | | | 1 | | | | | | | | | | | | | | 44 | | 1 | | | | | | | | | 1 | | |
| 20 | | | | | | | | | | | | | | 2 | 10 | 4 | | | | 30 | | | 1 | | | | | | | | | 1 |
| 21 | | | | | 8 | | | | 2 | | | | | | | | 1 | | 6 | | 25 | | | | | | | | | 6 | | |
| 22 | | | | 3 | | | | | | | | | | | | | | | | | | 43 | | 1 | 1 | | | | | | | |
| 23 | | | | | | | | | | | | | | | | | | | | | | | 47 | | | | 1 | | | | | |
| 24 | | | | | | | | | | | | | | | | | | | | | | | | 48 | | | | | | | | |
| 25 | | | | | | | | | | | | | | | | | | | | | | | | 1 | 47 | | | | | | | |
| 26 | | | | | | | | | | 3 | | | | | | | | | | | | | | | | 41 | | 4 | | | | |
| 27 | | | | | | | | | 4 | | | | | | | | 3 | | | | | | | | | | 41 | | | | | |
| 28 | | | | | | | | | | | | | | | | | 1 | | | | | | | | | | | 47 | | | | |
| 29 | | | | | | | | | | | | | | | | 1 | | | 1 | | | | | | | | | | 46 | | | |
| 30 | | | 1 | | 1 | | | | | 17 | | | 4 | | | | | | | | | | | | | 2 | | | | 23 | | |
| 31 | | | | | | | | | | 2 | | | | | | | 1 | | | | 1 | | | | | | 1 | | | 4 | 39 | |
| 32 | | | | | | | | | 3 | 1 | | | | | | | | | | 1 | | | | | | | 4 | | 1 | | | 38 |

**Table 5.10:** Confusion matrix corresponding to the results in Table 5.1 for PCA based description of testing samples in the Left view dataset. The total number of testing samples per posture is 48 with a total of 1, 536 testing samples.

| I/P \ O/P | 1 | 2 | 3 | 4 | 5 | 6 | 7 | 8 | 9 | 10 | 11 | 12 | 13 | 14 | 15 | 16 | 17 | 18 | 19 | 20 | 21 | 22 | 23 | 24 | 25 | 26 | 27 | 28 | 29 | 30 | 31 | 32 |
|---|---|---|---|---|---|---|---|---|---|---|---|---|---|---|---|---|---|---|---|---|---|---|---|---|---|---|---|---|---|---|---|---|
| 1 | 48 | | | | | | | | | | | | | | | | | | | | | | | | | | | | | | | |
| 2 | 3 | 44 | 1 | | | | | | | | | | | | | | | | | | | | | | | | | | | | | |
| 3 | | | 45 | | | | | | | | 2 | | 1 | | | | | | | | | | | | | | | | | | | |
| 4 | | | | 48 | | | | | | | | | | | | | | | | | | | | | | | | | | | | |
| 5 | | | | | 35 | | | | 5 | | | | | | | | 6 | | | | | | | | | | | | 1 | 1 | | |
| 6 | | | | | | 48 | | | | | | | | | | | | | | | | | | | | | | | | | | |
| 7 | | | | | | | 42 | | 4 | | | | | | | | 1 | | | | | | | | | | 1 | | | | | |
| 8 | | | | | | | | 47 | | | | | | | | | | | | | | | | | | | 1 | | | | | |
| 9 | | | | | | | | | 24 | | | | | | | | 21 | | | | | | | | | | 3 | | | | | |
| 10 | | | | | | | | | | 48 | | | | | | | | | | | | | | | | | | | | | | |
| 11 | | | | | | | 1 | | 6 | | 41 | | | | | | | | | | | | | | | | | | | | | |
| 12 | | | | | | | | | | | | 46 | | | | | | | | 1 | | | | 1 | | | | | | | | |
| 13 | 1 | | 1 | | | 2 | | | | | 10 | | 34 | | | | | | | | | | | | | | | | | | | |
| 14 | | | | | | | | | | | | | | 47 | | | | | | | | | 1 | | | | | | | | | |
| 15 | | | | | 2 | | | | 1 | 1 | | | 1 | | 29 | 1 | | | | 2 | 2 | | | | | | | | 1 | 5 | 1 | 2 |
| 16 | | | | | | | | | 2 | | | | | | | 22 | 2 | | | | 2 | | | 1 | | | | | 11 | 8 | | |
| 17 | | | | | | | | | 4 | | | | | | | | 42 | | | | | | | | | | 2 | | | | | |
| 18 | | | | | | | | | | | | | | | | | | 48 | | | | | | | | | | | | | | |
| 19 | | 1 | | | | | | | | | | | | | | | | | 43 | | 3 | | | | | | | | | 1 | | |
| 20 | | | | | | | | | | 2 | | | | 1 | 5 | 3 | | | | 30 | | | 1 | | | | 4 | | | | | 2 |
| 21 | | | | | 8 | | | | 2 | | | | | | | | 5 | | 5 | | 20 | | | | | | | | | 8 | | |
| 22 | | | | 3 | | | | | | | | 1 | | | | | | | | | | 42 | | | 2 | | | | | | | |
| 23 | | | | | | | | | | | | | | | | | | | | | | | 47 | | | | 1 | | | | | |
| 24 | | | | | | | | | | | | | | | | | | | | 1 | | | | 47 | | | | | | | | |
| 25 | | | | | | | | | | | | | | | | 1 | | | | | | | | 1 | 46 | | | | | | | |
| 26 | | | | | | | | | | 4 | | | | | | | | | | | | | | | | 40 | | 4 | | | | |
| 27 | | | | | | | | | 1 | | | | | | | | 4 | | | | | | | | | | 43 | | | | | |
| 28 | | | | | | | | | | | | | | | | | 1 | | | | | | | | | | 2 | 45 | | | | |
| 29 | | | | | | | | | 1 | | | | | | | 3 | 1 | | | | | | | | | | | | 43 | | | |
| 30 | | | 2 | | | | | | | 16 | | | 3 | | | | | | | | | | | | | 2 | 1 | | | 24 | | |
| 31 | | | | | | | | 3 | 4 | 2 | | 1 | | | | | | | | | 1 | | | | | | 1 | | | 3 | 33 | |
| 32 | | | | | | | | | 5 | 3 | | | | | | | | | | 1 | | | | | | | 3 | | 1 | | | 35 |

**Table 5.11:** Consolidated values of the classification results comparing the DOM based descriptors with the PCA. The training set contained 3, 456 samples of 32 hand postures taken from the all the three datasets. For rotation invariance, the each training samples is rotated between 0° to 350° in steps of 10°. The total number of testing samples is 4, 608 with 1, 536 samples per dataset.
(% CC- Percentage of correct classification. )

| **Methods** | Classification results obtained for test samples from | | | **Overall % CC** |
|---|---|---|---|---|
| | Right view | Front view | Left view | |
| Krawtchouk moments | 96.16 | 96.09 | 94.01 | 95.42 |
| discrete Tchebichef moments | 97.27 | 97.53 | 96.48 | 97.09 |
| PCA based description | 96.61 | 96.35 | 94.92 | 95.96 |

#### 5.6.2.3 Improving view invariant classification

The study on the view-angle invariance has shown that the training set consisting of samples taken only from the Front view dataset are not sufficient to conceal the structural variations in the hand postures that occur due to view-angle changes. Though, the performance offered by the DOM based descriptors, particularly, the discrete Tchebichef moments are comparatively better, the efficiency of these descriptors can be further improved by adding hand posture samples taken from the right and the left viewing directions to the training set. Accordingly, the experiment for view invariance is repeated by increasing the number of samples in the training set.

The size of the training set is increased by adding 1, 152 samples from each of the Right view and the Left view dataset to the training set. Therefore, the extended training set consists of 3, 456 samples of 32 hand posture shapes in the Asamyuta hasta database. As in the previous studies, the number of testing samples used for the experiment is 4, 608. In order to achieve rotation invariant recognition, the samples in the training set are rotated in steps of 10° between 0° to 350°.

The classification results obtained with respect to the extended training set are given in Table 5.11 and the posture wise classification accuracies are shown in the plots in Figure 5.19. Clearly, the performance of the feature descriptors with respect to the Right view and the Left view dataset has increased. The efficiency of the Krawtchouk moments has improved by approximately 14% and they exhibit similar performance as the PCA based method.

The posture wise classification results obtained for the extended training set are shown in Figure 5.19. From the plots obtained for the DOM descriptors, as shown in Figure 5.19(a) and Figure 5.19(b), we can infer that the samples with classification accuracies less than 80% belong to the posture classes 5 and 9. Among these, posture 9 exhibits classification accuracy over 80% in discrete Tchebichef moments based description. Similar to the results in Figure 5.16, Figure 5.17 and Figure 5.18, we observed that the the samples of posture 5 are

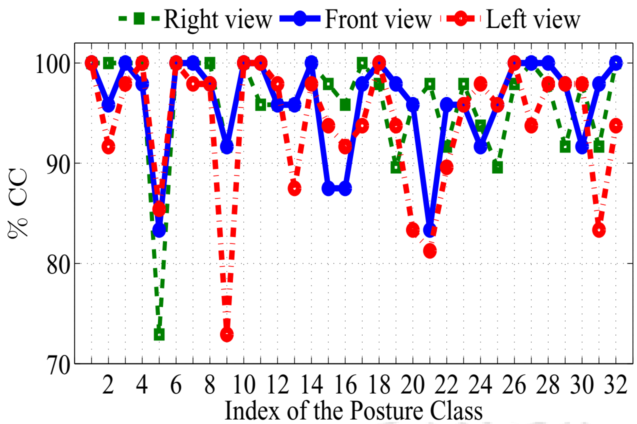


(a) Krawtchouk moments based features

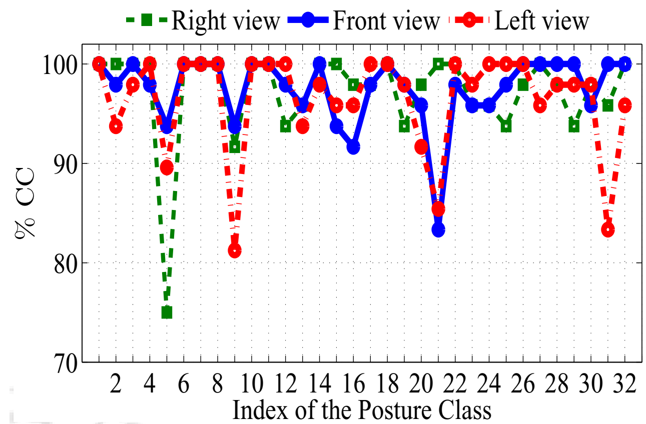


(b) discrete Tchebichef moments based features

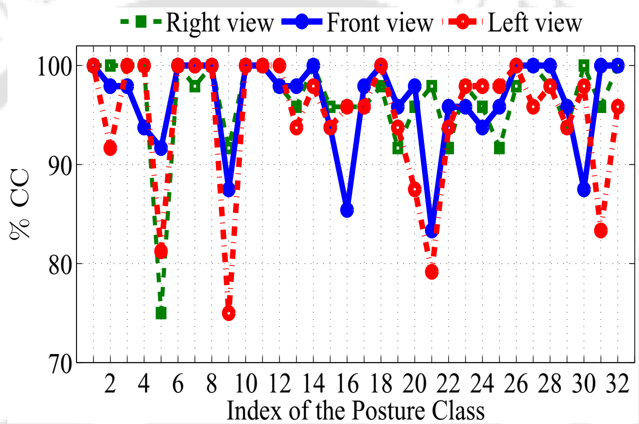


(c) PCA based hand posture description

**Figure 5.19:** Illustration comparing the posture wise classification results obtained for the Right view, Front view and the Left view datasets with respect to the extended training set. The classification accuracies obtained for (a) Krawtchouk moments based features (b) discrete Tchebichef moments based features and (c) PCA based hand posture description.

mostly misclassified with postures 2 and 21. The samples of posture 9 are mostly misclassified as posture 17. In some cases, the shapes of these mismatched posture classes are not visually distinguishable and they exhibit more overlapping regions.

From the results obtained in this experiment, it is evident that the DOMs are robust features for view invariant hand posture recognition. The discrete Tchebichef moments offer comparatively higher classification accuracies exhibiting better view invariance characteristics.

## 5.7 Summary

This work has presented a novel DOM based hand posture recognition technique for representation and description of Asamyuta hastas in Bharatanatyam. The proposed technique is robust to similarity transformations, user variations and view-angle changes along the horizontal direction. A database, namely, the Asamyuta hasta database, consisting of $8,064$ samples of the 32 hand postures in Bharatanatyam is developed for conducting the experiments. The database is collected from 6 users and it contains samples acquired at 3 viewing directions- the Right view, the Front view and the Left view.

The hand region is segmented through skin colour detection and the DOMs are used to represent the segmented binary hand postures. The classification is performed using a minimum distance classifier. The experiments are aimed towards analyzing the accuracy of the DOMs as features in user and view invariant classification of the hand postures in the Asamyuta hasta database.

The structural variations in the hand posture shapes in Asamyuta hasta database are studied by computing the intraclass and interclass distances in terms of the Pratt's FOM and the correlation coefficient. A detailed study on the DOM based classification is conducted in comparison with the PCA based descriptor. Based on the results, the performance of the DOMs are comparable to the PCA based method. Especially the discrete Tchebichef moments offer better performance than the PCA method.

# 6 Conclusions and Future Work

Contents

This chapter summarizes the conclusions derived from the main contributions of this thesis. Also, it provides a direction into few areas that may be explored for further research.

## 6.1 Concluding remarks

The objective of this research has been to explore the two DOMs, namely the Krawtchouk and the discrete Tchebichef moments as shape descriptors for hand posture recognition. The proposed DOM based hand posture recognition technique is intended to find applicability in hand posture based HCI for tabletop interfaces and data cues for automatic annotation and retrieval of Bharatanatyam dance videos. In this context, we have tested the efficiency of the proposed DOM based shape descriptors in representing two different classes of hand postures. They are the simple hand postures that are suitable for HCI and the complex hand postures in Bharatanatyam, known as the Asamyuta hastas.

This thesis studied the characteristics of the Krawtchouk and the discrete Tchebichef polynomials and empirically inferred that the Krawtchouk and the discrete Tchebichef moments are efficient descriptors in representing shape under structural deformations. The DOMs are employed for robustly representing the hand posture shapes in the presence of structural distortions caused by the user and the view-angle variations. The conclusions of the work reported in this dissertation are presented chapter wise.

(i) In the **Introduction**, we presented the scope of hand gestures in CBA systems and stated the significance of hand postures as user interface data in HCI and as data cues for content-based image/video analysis. Based on the angular positions of the finger joints, the hand postures are categorised as simple and complex hand postures. The advantages of the monocular vision based approaches to hand posture recognition in CBA systems are discussed. The general outline of vision based hand posture recognition techniques and the major issues to be addressed by the method are elaborated. It is shown that the variations in the hand posture parameters (angular position of the finger joints) and the view-angle while image acquisition are the major issues that cause structural distortions in the hand posture image that is to be used as input for the hand posture recognition technique. Based on the general outline, the problems to be explored were defined.

(ii) A review on the feature descriptors used for representing the hand postures in vision-based hand posture recognition was presented in **Chapter 2**. From this chapter,it is understood that the shape based methods for hand posture representation are computationally less demanding and they offer good classification accuracies. Some of the important shape based descriptors identified are, the geometric moments, the

Zernike moments, the Fourier descriptors, the Gabor wavelets and the PCA. In comparison to some of these methods, the DOMs have the prospects to be efficient in terms of accurate representation in image analysis. Unlike the Zernike class of moments, DOMs do not involve numerical approximations. Unlike the PCA, the basis functions do not vary for different images. As a result, the computations involved in deriving the DOM features are less than that of the PCA method. This suggested the applicability of DOMs for shape description.

(iii) The DOMs are derived from the DOPs. Particularly, the Krawtchouk and the discrete Tchebichef moments are derived from the WKPs and the DTPs respectively. The formulations of these DOPs and their characteristics were presented in **Chapter 3**. It is shown that for any given order, the WKPs and the DTPs behave like band-pass functions and hence, they exhibit varied characteristics in representing different shapes.

The chapter studied the efficiency of the Krawtchouk and the discrete Tchebichef moments in shape representation in the presence of different shape defections. It established that at lower scales, the Krawtchouk moments are superior to the discrete Tchebichef moments in accurately representing the shapes. With the increase in scale, the performance of these moments varies at lower orders according to the structural characteristics of the shapes. At the lower orders, the discrete Tchebichef moments are superior to the Krawtchouk moments in accurately representing shapes with low structural variations. On the contrary, the Krawtchouk moments offer representation accuracy higher than that of the discrete Tchebichef moments in approximating shapes containing high spatial frequency structures. Particularly, the discrete Tchebichef moments require higher orders to efficiently reconstruct high spatial frequency structures of the shapes. The study on the shape representation accuracy has shown that the WKPs offer comparatively more data compaction in representing shapes at lower scales. At higher scales, the data compaction of WKPs is more for shapes with more structural variations. The data compaction capability of DTPs is found to be significant only for low spatial frequency shapes at higher scales. Similar experiments were performed to verify the robustness of the DOMs in shape representation in the presence of noise. The experiments suggested that both the moments are robust up to 35% noise level.

The second empirical study verified the applicability of the Krawtchouk and the discrete Tchebichef moments as shape descriptors for classification. The experiment was performed on 400 samples of 20 shape classes taken from the MPEG-7 (CE Shape 1, Part-B) database. The database consisted of samples subject to various structural distortions. The study suggested the Krawtchouk and the discrete

Tchebichef moments as potential features for robust shape classification against shape defections caused by segmentation errors and structural deviations.

The empirical studies and the results obtained in this chapter have shown that the DOMs are potential feature descriptors for representing different shapes. Therefore, it is concluded that the DOMs can be employed as feature descriptors for classifying the hand postures based on their shapes.

(iv) **Chapter 4** presented the proposed hand posture recognition technique using geometry based normalizations and DOM based features for classifying the simple single-hand postures. The hand postures are formed by the flexion/extension and abduction/adduction movements of fingers to their maximum range. The hand postures and the experimental setup employed in this work are chosen to suit the framework of tabletop interfaces. In this chapter, two major issues of the separation of the forearm and the orientation alignment of the hand postures are investigated. The methods based on the anthropometric dimensions of the hand and the geometry of the hand postures are proposed to address these issues.

The experiments are conducted on a large database consisting of 10 posture classes and $4,230$ hand posture samples acquired at varying view-angles and orientations. The hand postures images are collected from 23 users. For the experimental setup used in this work, the images are acquired from the high-angle position. Hence, varying the view-angles while acquisition, resulted in more perspective distortions and the effect like self-occlusion of fingers is minimised. The structural variations in the hand posture samples of each class are analyzed using the Pratt's FOM and the correlation coefficient. The analysis has shown that the database exhibits more structural deviations in the hand posture shapes that are caused due to user and view-angle variations. The comparison of the interclass and intraclass correlations of the hand posture shapes has shown that the database constitutes of visually distinct hand posture shapes. However, the hand posture shapes of different classes consist of overlapping regions such that some of the hand posture classes form a subset of the other hand posture classes. A detailed study on the DOM based classification is conducted in comparison with the geometric moments, the Zernike moments, the Fourier descriptors, the Gabor wavelets and the PCA based methods. The user invariance is verified by varying the number of users considered for forming the training dataset. The view invariance is verified by examining the classification accuracies obtained for the hand posture samples that are acquired at different view-angles. The results established that the DOMs are comparatively robust features for achieving user independent and view invariant recognition of simple hand postures. The classification accuracies of the DOMs are comparable to the PCA method. In some cases, the discrete Tchebichef moments offer marginally better performance than the Krawtchouk moments and the PCA. The experimental results obtained in this work suggest that the proposed hand posture recognition technique using geometry based normalizations and DOM based features is robust to the similarity transformations (scale, translation and orientation changes), the user variations and the projective distortions caused by the view-angle changes.

(v) A novel DOM based hand posture recognition technique for representation and description of Asamyuta hastas in Bharatanatyam was proposed in **Chapter 5**. The Asamyuta hastas are complex hand postures in which the angular positions of each finger joint are varied to form a hand posture. The hand posture images for the database are acquired at normal-angle position and the hand postures are performed by extending the hand outwards, in front of the body. Therefore, for this setup the view-angle is changed along the horizontal direction in such a way that the front profile and the right and the left profiles of the hand postures are acquired. The developed Asamyuta hasta database consists of $8,064$ samples of the 32 hand postures in Bharatanatyam. The database is collected from 6 users and it contains samples acquired at 3 viewing directions- the Right view, the Front view and the Left view. In this setup, the view-angle changes result in minimised perspective distortions and the structural variations are mainly due to the self-occlusion of fingers and the variations in the right and the left side profiles of the hand postures. The structural variations in the hand posture shapes in Asamyuta hasta database are studied by computing the intraclass and interclass distances in terms of the Pratt's FOM and the correlation coefficient. The samples in the Asamyuta hasta database have shown comparatively less intraclass variations for the samples in the Right view and the Left view dataset. Also, samples of some of the hand posture classes have shown high interclass correlations. Unlike the hand posture database in Chapter 4, the Asamyuta hasta database consists of both structurally distinct as well as overlapping hand posture samples. The variations in the side profiles and the self-occlusion of fingers have resulted in structural distortions such that the hand posture shapes are structurally overlapping in nature.

The analysis on intraclass variations has shown that the samples exhibit at least 20% structural deviations. The deviations are the result of intra-user as well as the inter-user variabilities. It is obvious that the inter-user variability will be comparatively more due to the variations in the hand geometry. Hence, establishing user invariance by varying the number of users in the training set will only lead to more misclassifications. However, the user invariance with respect to the intra-user variations in the gesturing style can be easily verified. Therefore, the user invariance efficiency of the DOMs is inferred from the classification results obtained for the samples in the Front view dataset. The view invariance is studied from the results obtained for the Right view and the Left view datasets. The discrete Tchebichef moments offered higher performance efficiency than the Krawtchouk moments and the PCA. The classification accuracies of the Krawtchouk moments are comparable to that of the PCA method.

The results in Chapter 4 and Chapter 5 have shown that, of the two DOMs considered, the discrete Tchebichef moments are better than the Krawtchouk moments in classifying the hand posture shapes. Particularly, for the hand posture shapes in the Asamyuta hasta database, the performance of the Krawtchouk moments is significantly poorer than that of the discrete Tchebichef moments. The possible reason for the reduced efficiency of Krawtchouk moments, may be the localised support of the lower order WKPs, due to which the lower order Krawtchouk moments cannot represent the variations in the entire hand posture shape. Therefore, if the structural variations in the regions of different shape classes that lie within the localised supports of the lower order WKPs are less, it may lead to more misclassifications. Considering that the lower order WKPs are capable of accurately representing the shapes of low spatial scales, we can expect to achieve better performance by either reducing the scale of the shape or by increasing the size of the image grid on which the shape is defined. Practically, these approaches may not be advantageous, because, reducing the scale of the shape through down sampling may result in losing the structural features and increasing the size of the image grid will unnecessarily increase the computational load.

Our study shows the discrete Tchebichef moment based shape descriptor proves to be a suitable alternative for hand posture recognition.

## 6.2 Suggestions for future research

The research of the thesis points to some interesting extensions.

(i) The WKPs offer some interesting properties such as varying the spatial support of the polynomials by controlling parameters $p_1$ and $p_2$ and localization at the lower orders. These properties can be explored to derive the local description of shapes, such that the local variations in the structural characteristics of the shapes of different classes are efficiently represented for improving the shape classification accuracies. This may be useful in hand posture classification, because the hand posture shapes consists of more overlapping regions due to which the misclassifications occur.

(ii) The other DOMs, namely the discrete Hahn moments and the discrete Racah moments may be explored for shape description.

(iii) Further work may also concentrate on verifying the inter-user variabilities in performing the Asamyuta hastas. An improved Asamyuta hasta database can be developed by collecting the hastas from more number of persons. The inter-user variabilities can be analysed and the efficiency of the DOMs in classifying the hastas can be verified by varying the number of persons included in the training.

(iv) The proposed hand posture recognition technique for Asamyuta hastas can be extended for classifying the Samyuta hastas, the two-hand postures in Bharatanatyam.

(v) The proposed DOM based hand posture recognition technique can be extended to develop content-based annotation and retrieval systems for Bharatanatyam dance videos. The block diagram representations of the models for the content-based annotation and the retrieval systems are illustrated in Figure 6.1.

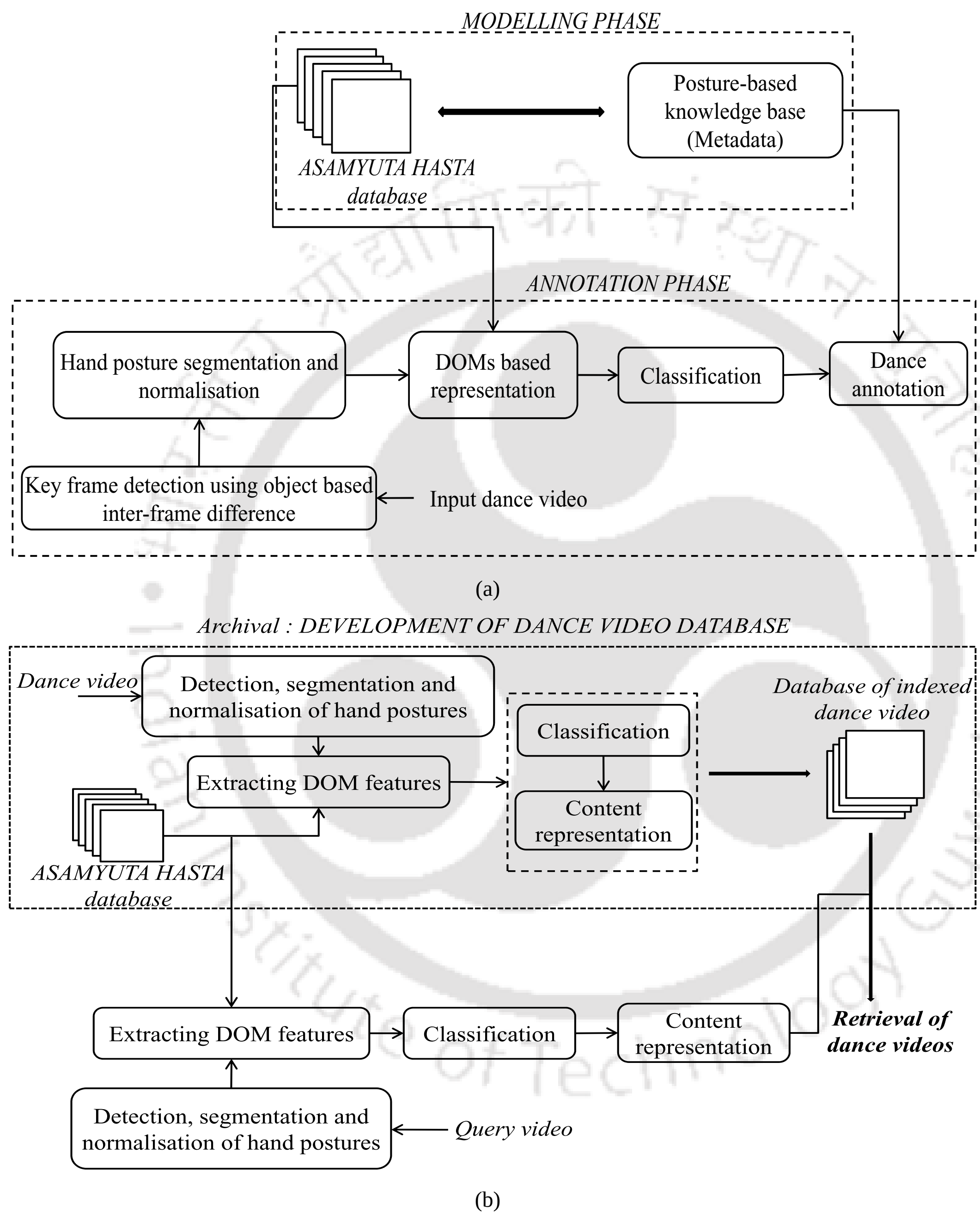


**Figure 6.1:** Block diagram representation of the model for the content-based (a) annotation system and (b) retrieval system for Bharatanatyam dance videos.

# References


[1] [Online]. Available: http://en.wikipedia.org/wiki/Gesture_recognition

[2] J. Triesch and C. von der Malsburg, "Robust classification of hand postures against complex backgrounds," in *Proc. of the 2nd International conference on automatic face and gesture recognition*. IEEE Computer society press, October 1996, pp. 170–175.

[3] A. Barczak, N. Reyes, M. Abastillas, A. Piccio, and T. Susnjak, "A new 2D static hand gesture colour image dataset for ASL gestures," *Research letters in the information and mathematical sciences*, vol. 15, pp. 12–20, 2011.

[4] M. Lades, J. C. Vorbrüggen, J. Buhmann, J. Lange, C. v.d. Malsburg, R. P. Würtz, and W. Konen, "Distortion invariant object recognition in the dynamic link architecture," *IEEE Trans. on Computers*, vol. 42, no. 3, pp. 300–311, March 1993.

[5] [Online]. Available: http://www.gauri-dance.narod.ru/Hastas.pdf

[6] Anjali Nandan. [Online]. Available: http://onlinebharatanatyam.com/

[7] D. C. Schoen, *Adult orthopaedic nursing*. Philadelphia: Lippincott, 2000.

[8] S. Goldin-Meadow, "The role of gesture in communication and thinking," *Trends in cognitive sciences*, vol. 3, no. 11, pp. 419–429, November 1999.

[9] D. McNeill, Ed., *Language and Gesture*, ser. Language, culture and cognition ; 2. Cambridge university press, 2000.

[10] K. Emmorey, *Language, cognition, and the brain: Insights From sign language research*. Lawrence Erlbaum Associates Inc., 2002.

[11] M. Nielsen, T. B. Moeslund, M. Storring, and E. Granum, *HCI beyond the GUI:Design for haptic, speech, olfactory and other nontraditional interfaces*. Morgan Kauffman, Elsevier, 2008, ch. Gesture Interfaces, pp. 75–106.

[12] R.-D. Vatavu, "Interfaces that should feel right: Natural interaction with multimedia information," in *Recent advances in multimedia signal processing and communications*, M. Grgic, K. Delac, and M. Ghanbari, Eds. Springer-Berlin Heidelberg, 2009, vol. 231, pp. 145–170.

[13] A. A. Argyros and M. I. Lourakis, "Vision-based interpretation of hand gestures for remote control of a computer mouse," in *Computer Vision in Human-Computer Interaction*, ser. Lecture notes in computer science, vol. 3979. Springer-Verlag, 2006, pp. 40–51.

[14] R. A. Bolt, "Put-that-there: Voice and gesture at the graphics interface," *ACM Siggraph Computer Graphics*, vol. 14, no. 3, pp. 262–270, July 1980.

[15] T. B. Moeslund, M. Strring, and E. Granum, "Pointing and command gestures for augmented reality," in *Proceedings of International Workshop on Visual Observation of Deictic Gestures (Pointing 2004)*, Cambridge, U.K, August 2004.

[16] D. Stein, P. Dreuw, H. Ney, S. Morrissey, and A. Way, "Hand in Hand: Automatic sign language to English translation," in 11th *Conference on theoretical and methodological issues in machine translation*, Skvde, Sweden, September 2007, pp. 214–220.

[17] P. Dreuw, D. Stein, and H. Ney, "Enhancing a sign language translation system with vision-based features," in *Gesture-Based Human-Computer Interaction and Simulation*, ser. Lecture Notes in Computer Science, vol. 5085. Springer-Verlag, 2009, pp. 108–113.

[18] I. Singh, *Text book of anatomy with colour atlas*. Jaypee Brothers Medical Publishers (P) Limited, 2008.

[19] G. A. Malanga and S. Nadler, *Musculoskeletal Physical Examination: An Evidence-Based Approach*. Elsevier Health Sciences, 2006.

[20] P. Cavanagh, "Reconstructing the third dimension: Interactions between color, texture, motion, binocular disparity, and shape," *Computer vision, Graphics and Image processing*, vol. 37, pp. 171–195, 1987.

[21] F. Parvini, D. McLeod, C. Shahabi, B. Navai, B. Zali, and S. Ghandeharizadeh, "An approach to glove-based gesture recognition," in 13$^{th}$ *International conference on human-computer interaction. Part II: Novel interaction methods and techniques*. Springer-Verlag, 2009, pp. 236–245.

[22] L. Dipietro, A. M. Sabatini, and P. Dario, "A survey of glove-based systems and their applications," *IEEE trans. on systems, man and cybernatics - Part C: Applications and reviews*, vol. 38, no. 4, pp. 461–482, July 2008.

[23] G. D. Kessler, L. F. Hodges, and N. Walker, "Evaluation of the CyberGlove as a whole-hand input device," *ACM trans. on computer-human interaction*, vol. 2, no. 4, pp. 263–283, December 1995.

[24] D. J. Sturman and D. Zeltzer, "A survey of glove-based input," *IEEE computer graphics and applications*, vol. 14, no. 1, pp. 30–39, January 1994.

[25] M. Bhuiyan and R. Picking, "Gesture-controlled user interfaces, what have we done and whats next?" in *Proc. of 5th collaborative reserach symposium on security, E-learning, internet and networking*. University of Plymoth, Darmstadt, Germany, November 2009, pp. 59–69.

[26] G. J. Grimes, "Digital data entry glove interface device," U.S. Patent 4 414 537, November 8, 1983. [Online]. Available: http://www.google.com/patents/US4414537

[27] T. G. Zimmerman, J. Lanier, C. Blanchard, S. Bryson, and Y. Harvill, "A hand gesture interface device," in *Proceedings of the SIGCHI/GI conference on Human factors in computing systems and graphics interface*. ACM, 1987, pp. 189–192.

[28] J. P. Kramer, P. Lindener, and W. R. George, "The talking glove an expressive and receptive verbal communication aid for the deaf, deaf-blind, and non-vocal," U.S. Patent 5 047 952, September 10, 1991. [Online]. Available: http://www.freepatentsonline.com/5047952.html

[29] [Online]. Available: http://www.cyberglovesystems.com/sites/default/files/CyberGloveII_Brochure_2009.pdf

[30] [Online]. Available: http://www.5dt.com

[31] [Online]. Available: www.5dt.com/downloads/dataglove/old/5DTDataGlove5Manual.pdf

[32] [Online]. Available: http://www.hmw.it

[33] [Online]. Available: http://www.fakespacelabs.com

[34] L. Dipietro, A. M. Sabatini, and P. Dario, "Evaluation of an instrumented glove for hand-movement acquisition," *Journal of Rehabilitation Research and Development*, vol. 40, no. 2, pp. 179–190, 2003.

[35] S. S. Fels and G. E. Hinton, "Glove-Talk II - a neural-network interface which maps gestures to parallel formant speech synthesizer controls," *IEEE trans. on neural networks*, vol. 9, no. 1, pp. 205–212, January 1998.

[36] J. L. Hernandez-Rebollar, N. Kyriakopoulos, and R. W. Lindeman, "A new instrumented approach for translating American sign language into sound and text," in *Proc. of the 6th IEEE International conference on automatic face and gesture recognition*. IEEE, May 2004, pp. 547–552.

[37] Y. Kitamura, T. Higashi, T. Iida, and F. Kishino, "Interactive computer animation of hand gestures using status estimation with multiple regression analysis," *Computer Graphics Forum*, vol. 20, no. 3, pp. 251–259, September 2001.

[38] J. Steffen, J. Maycock, and H. Ritter, "Robust dataglove mapping for recording human hand postures," in *Intelligent Robotics and Applications*, ser. Lecture Notes in Computer Science, S. Jeschke, H. Liu, and D. Schilberg, Eds. Springer Berlin / Heidelberg, 2011, vol. 7102, pp. 34–45. [Online]. Available: http://dx.doi.org/10.1007/978-3-642-25489-5_4

[39] H. Du, W. Xiong, and Z. Wang, "Modeling and interaction of virtual hand based on Virtools," in *International conference on multimedia technology (ICMT)*. IEEE, July 2011, pp. 416–419.

[40] T. P. Bednarz, C. Caris, J. Thompson, C. Wesner, and M. Dunn, "Human-computer interaction experiments - Immersive virtual reality applications for the mining industry," in *24th IEEE International conference on advanced information networking and applications*. IEEE, April 2010, pp. 1323–1327.

[41] N. I. N. Ismail and M. Oshita, "Motion selection and motion parameter control using data gloves," in *IEEE International Games Innovation Conference (IGIC)*. IEEE, 2011, pp. 113–114.

[42] H. Teleb and G. Chang, "Data glove integration with 3D virtual environments," in *2012 International conference on systems and informatics (ICSAI)*. IEEE, May 2012, pp. 107–112.

[43] M. Porta, "Vision-based user interfaces: methods and applications," *International Journal of Human-Computer Studies, Elsevier*, vol. 57, no. 1, pp. 27–73, July 2002.

[44] J. J. L. Jr., "A survey of hand posture and gesture recognition techniques and technology," Brown University, Providence, RI,USA, Tech. Rep., 1999.

[45] E. Ueda, Y. Matsumoto, M. Imai, and T. Ogasawara, "A hand-pose estimation for vision-based human interfaces," *IEEE trans. on industrial electronics*, vol. 50, no. 4, pp. 676–684, August 2003.

[46] G. Bebis, F. Harris, A. Erol, B. Yi, J. Martinez, J. Hernandez-Usabiaga, and S. Fritzinger, "Development of a nationally competitive program in computer vision technologies for effective human-computer interaction in virtual environments," BioVIS Lab. in BioVIS Technology Center of NASA Ames Research Center, Tech. Rep., 2002.

[47] A. Erol, G. Bebis, M. Nicolescu, R. D. Boyle, and X. Twombly, "Vision-based hand pose estimation: A review," *Computer Vision and Image Understanding, Elsevier*, vol. 108, no. 1-2, pp. 52–73, January 2007.

[48] R. Hartley and A. Zisserman, *Multiple View Geometry in Computer Vision*. Cambridge university press, 2003.

[49] H. Y. Guan, C. S. Chua, and Y. K. Ho, "Hand posture estimation from 2D monocular image," in *Proc. of second International conference on 3-D digital Imaging and modeling*. IEEE, 1999, pp. 424–429.

[50] N. Shimada, K. Kimura, and Y. Shirai, "Real-time 3D hand posture estimation based on 2D appearance retrieval using monocular camera," in *Proc. of IEEE ICCV Workshop on Recognition, Analysis, and Tracking of Faces and Gestures in Real-Time Systems*. IEEE, 2001.

[51] C.-S. Chua, H. Guan, and Y.-K. Ho, "Model-based 3D hand posture estimation from a single 2D image," *Image and vision computing, Elsevier*, vol. 20, pp. 191–202, 2002.

[52] A. Thayananthan, "Template-based pose estimation and tracking of 3D hand motion," Ph.D. dissertation, University of Cambridge, 2005.

[53] M. de La Gorce, D. J. Fleet, and N. Paragios, "Model-based 3D hand pose estimation from monocular video," *IEEE trans. on pattern analysis and machine intelligence*, vol. 33, no. 9, pp. 1793–1805, September 2011.

[54] M. Vaezi and M. A. Nekouie, "3D human hand posture reconstruction using a single 2D image," *International journal of human computer interaction*, vol. 1, no. 4, pp. 83–94, 2011.

[55] R. Y. Wang and J. Popovic, "Real-time hand-tracking with a color glove," *ACM trans. on Graphics*, vol. 28, no. 3, Article No.63, pp. 63:1–63:8, August 2009.

[56] B. Dorner, "Chasing the colour glove: Visual hand tracking," Master's thesis, Simon Fraser University, June 1994.

[57] F.-S. Chen, C.-M. Fu, and C.-L. Huang, "Hand gesture recognition using a real-time tracking method and hidden Markov models," *Image and Vision Computing*, vol. 21, no. 8, pp. 745–758, August 2003.

[58] A. Ogihara, H. Matsumoto, and A. Shiozaki, "Hand region extraction by background subtraction with renewable background for hand gesture recognition," in *International symposium on intelligent signal processing and communications*. IEEE, December 2006, pp. 227–230.

[59] J. christophe Terrillon, A. Pilpr, Y. Niwa, and K. Yamamoto, "Robust face detection and Japanese sign language hand posture recognition for human-computer interaction," in $5^{th}$ *International conference on vision interface*, 2002.

[60] S. C. Ong and S. Ranganath, "Automatic sign language analysis: A survey and the future beyond lexical meaning," *IEEE trans. on pattern analysis and machine intelligence*, vol. 27, no. 6, pp. 873–891, June 2005.

[61] V. I. Pavlovic, R. Sharma, and T. S. Huang, “Visual interpretation of hand gestures for human-computer interaction: A Review,” *IEEE trans. on pattern analysis and machine intelligence*, vol. 19, no. 7, pp. 677–695, July 1997.

[62] X. Teng, B. Wu, W. Yu, and C. Liu, “A Hand Gesture Recognition based on Local Linear Embedding,” *Journal of Visual Languages and Computing*, vol. 16, pp. 442–454, April 2005.

[63] D. Zhang and G. Lu, “Review of shape representation and description techniques,” *Pattern Recognition*, vol. 37, no. 1, pp. 1–19, 2004.

[64] J.-L. Coatrieux, “Moment-based approaches in imaging. Part 2: Invariance,” *IEEE engineering in medicine and biology magazine*, vol. 27, no. 1, pp. 81–83, 2008.

[65] A. Chalechale, F.Safaei, G.Naghdy, and P.Premaratne, “Hand posture analysis for visual based human machine interface,” in *Proc. of the APRS Workshop on Digital image Computing*, B. C. Lovell and A. J. Maeder, Eds. Brisbane, Australia: The Australian Pattern Recognition Society, February 2005, pp. 91–96.

[66] C.-C. Chang, J. J. Chen, W.-K. Tai, and C.-C. Han, “New approach for static gesture recognition,” *Journal of Information Science and Engineering*, vol. 22, pp. 1047–1057, January 2006.

[67] L. Gu and J. Su, “Natural hand posture classification based on Zernike moments and hierarchial classifier,” in *Proc. of the International Conference on Robotics and Automaton*. CA, USA: IEEE, May 2008, pp. 3088–3093.

[68] B. Buchholz, “A kinematic model of the human hand to evaluate its prehensile capabilities,” *Journal of Biomechanics*, vol. 25, no. 2, pp. 149–162, 1992.

[69] F. Hunter and P. Fuqua, *Light Science and Magic: An Introduction to Photographic Lighting*, 2nd ed. Elsevier, 1997.

[70] K. Milburn, *Digital Photography Expert Techniques*. O’Reilly Media, March 2004.

[71] R. Mukundan, S. H. Ong, and P. A. Lee, “Image analysis by Tchebichef moments,” *IEEE Trans. on Image Processing*, vol. 10, no. 9, pp. 1357–1364, September 2001.

[72] P. T. Yap, R. Paramesran, and S. H. Ong, “Image analysis by Krawtchouk moments,” *IEEE Trans. on Image Processing*, vol. 12, no. 11, pp. 1367–1376, November 2003.

[73] B. Bayraktar, T. Bernas, J. Robinson, and B. Rajwa, “A numerical recipe for accurate image reconstruction from discrete orthogonal moments,” *Pattern Recognition*, vol. 40, no. 2, pp. 659–669, February 2007.

[74] A. Sinha, *Let’s know Dances of India*. Star publications Pvt Ltd., 2006.

[75] C. A. Jones and J. D. Ryan, *Encyclopedia of Hinduism*, J. G. Melton, Ed. Infobase publications, 2007.

[76] S. Loncaric, “A survey of shape analysis techniques,” *Pattern Recognition*, vol. 31, no. 8, pp. 983–1001, 1998.

[77] H.-K. Kim and J.-D. Kim, “Region-based shape descriptor invariant to rotation, scale and translation,” *Signal Processing: Image Communication*, vol. 16, no. 12, pp. 87–93, 2000.

[78] J. Lee, Y. Lee, E. Lee, and S. Hong, “Hand region extraction and gesture recognition from video stream with complex background through entropy analysis,” in *Proc. of the 26th Annual International Conference of the IEEE EMBS*. San Francisco, CA, USA: IEEE, September 2004, pp. 1513–1516.

[79] H. Jag, J.-H. Do, J. Jung, K.-H. Park, and Z. Z. Bien, “View-invariant hand-posture recognition method for Soft-Remocon system,” in *Proc. of 2004 IEEE/RSJ lnternatlonal Conference on Intelligent Robots and Systems*. Sendal, Japan: IEEE, September 2004, pp. 295–300.

[80] A. Malima, E. Özgür, and M. Çetin, “A fast algorithm for vision-based hand gesture recognition for robot control,” in *14th IEEE Conference on Signal Processing and Communications Applications*. Turkey: IEEE, April 2006, pp. 1–4.

[81] K. Fujimura and X. Liu, “Sign recognition using depth image streams,” in *Proc. of the 7th International Conference on Automatic Face and Gesture Recognition*. Southampton, United Kingdom: IEEE, April 2006, pp. 381–386.

[82] X. Yin and M. Xie, “Finger identification and hand posture recognition for human–robot interaction,” *Image and Vision Computing*, vol. 25, no. 8, pp. 1291–1300, August 2007.

[83] E. Stergiopoulou and N. Papamarkos, "Hand gesture recognition using a neural network shape fitting technique," *Engineering Applications of Artificial Intelligence*, vol. 22, no. 8, pp. 1141–1158, December 2009.

[84] D. Dahmani and S. Larabi, "User independent system of hand postures recognition using part-based shape representation," in *7th International Conference on Signal-Image Technology and Internet-Based Systems*. Dijon, France: IEEE, November-December 2011, pp. 366–373.

[85] M. Flasiński and S. Myśliński, "On the use of graph parsing for recognition of isolated hand postures of Polish sign language," *Pattern Recognition*, vol. 43, no. 6, pp. 2249–2264, June 2010.

[86] J. M. S. Dias, P. Nande, N. Barata, and A. Correia, "O.G.R.E.-Open Gesture Recognition Engine, A platform for gesture based communication and interaction," *Lecture Notes in Artificial Intelligence, Springer-Verlag*, vol. 3881, pp. 129–132, March 2006.

[87] F. Mokhtarian and A. Mackworth, "A theory of multiscale, curvature-based shape representation for planar curves," *IEEE Trans. on Pattern Analysis and Machine Intelligence*, vol. 4, no. 8, pp. 789–805, August 1992.

[88] S. Kopf, T. Haenselmann, and W. Effelsberg, "Shape-based posture and gesture recognition in videos," in *Proc. of IS&T/SPIE Electronic Imaging*, vol. 5682, San Jose, CA, USA, 2005, pp. 114–124.

[89] C.-C. Chang, "Adaptive multiple sets of CSS features for hand posture recognition," *Neurocomputing*, vol. 69, no. 16-18, pp. 2017–2025, October 2006.

[90] C.-C. Chang, C.-Y. Liu, and W.-K. Tai, "Feature alignment approach for hand posture recognition based on curvature scale space," *Neurocomputing*, vol. 71, p. 1947 1953, 2008.

[91] M. pierre Dubuisson and A. K. Jain, "A modified Hausdorff distance for object matching," in *Proceedings of the 12th IAPR International Conference on Pattern Recognition, Conference A: Computer Vision and Image Processing*, vol. 1. IEEE, October 1994, pp. 566–568.

[92] E. Sánchez-Nielsen, L. Antón-Canalís, and M. Hernández-Tejera, "Hand gesture recognition for human-machine interaction," *Jounal of WSCG*, vol. 12, no. 1-3, 2003.

[93] V.S.Rao and C.Mahanta, "Gesture based robot control," in *4th International Conference on Intelligent Sensing and Information Processing*. Bangalore, India: IEEE, December 2006, pp. 145–148.

[94] A. Licsár and T. Szirányi, "User-adaptive hand gesture recognition system with interactive training," *Image and Vision Computing*, vol. 23, no. 12, pp. 1102–1114, November 2005.

[95] J. Yang, J. Xu, M. Li, D. Zhang, and C. Wang, "A real-time command system based on hand gesture recognition," in *7th International Conference on Natural Computation*, vol. 3. Shangai, China: IEEE, July 2011, pp. 1588–1592.

[96] S. Bourennane and C. Fossati, "Comparison of shape descriptors for hand posture recognition in video," *Signal, Image and Video Processing, Springer-Verlag*, vol. 6, no. 1, pp. 147–157, March 2012.

[97] R. J. Prokop and A. P. Reeves, "A survey of moment-based techniques for unoccluded object representation and recognition," *CVGIP: Graphical Models and Image Processing*, vol. 54, no. 5, pp. 438–460, 1992.

[98] J. Flusser, T. Suk, and B. Zitov, *Moments and Moment Invariants in Pattern Recognition*. Wiley, 2009.

[99] R.Mukundan and K.R.Ramakrishnan, *Moment Functions in Image Analysis: Theory and Applications*. World Scientific Publishing Co.Pte.Ltd., 1998.

[100] M.-K. Hu, "Visual pattern recognition by moment invariants," *IRE Trans. on Information Theory*, vol. 8, no. 2, pp. 179–187, February 1962.

[101] P. Ziaie, T. Muller, and A. Knoll, "A novel approach to hand-gesture recognition in a human-robot dialog system," in *First International Workshop on Image Processing Theory, Tools and Applications*. Sousse, Tunisia: IEEE, November 2008, pp. 1–8.

[102] G. Tofighi, S. Monadjemi, and N. Ghasem-Aghaee, "Rapid hand posture recognition using adaptive histogram template of skin and hand edge contour," in *6th Iranian Machine Vision and Image Processing*. Isfahan, Iran: IEEE, October 2010, pp. 1–5.

[103] M.R.Teague, "Image analysis via the general theory of moments," *Journal of Optic Society of America*, vol. 70, pp. 920–930, August 1962.

[104] R.G.O'Hagan, A.Zelinsky, and S.Rougeaux, "Visual gesture interfaces for virtual environments," *Interacting with Computers*, vol. 14, no. 3, pp. 231–250, April 2002.

[105] D. Kelly, J. McDonald, and C. Markham, "A person independent system for recognition of hand postures used in sign language," *Pattern Recognition Letters*, vol. 31, no. 11, pp. 1359–1368, August 2010.

[106] N. Liu and B. C. Lovell, "Hand gesture extraction by active shape models," in *Proc. of the Digital Image Computing on Techniques and Applications*. Washington, DC, USA: IEEE, December 2005, p. 10.

[107] Z. Feng, B. Yang, Y. Chen, Y. Zheng, T. Xu, Y. Li, T. Xu, and D. Zhu, "Features extraction from hand images based on new detection operators," *Pattern Recognition*, vol. 44, no. 5, pp. 1089–1105, May 2011.

[108] L. Yun, Z. Lifeng, and Z. Shujun, "A hand gesture recognition method based on multi-feature fusion and template matching," *Procedia Engineering*, vol. 29, pp. 1678–1684, 2012.

[109] P. M. Roth and M. Winter, "Survey of appearance-based methods for object recognition," Inst. for Computer Graphics and Vision, Graw University of Technology, Austria, Technical Report ICG-TR-01/08, January 2008.

[110] William.T.Freeman and M. Roth, "Orientation histogram for hand gesture recognition," in *Proc. of the 1st International Workshop on Automatic Face and Gesture Recognition*. IEEE, June 1995, pp. 296–301.

[111] B. Ionescu, D. Coquin, P. Lambert, and V. Buzuloiu, "Dynamic hand gesture recognition using the skeleton of the hand," *EURASIP Journal on Applied Signal Processing*, vol. 13, p. 21012109, December 2005.

[112] H. Zhou, D. J. Lin, and T. S. Huang, "Static hand gesture recognition based on local orientation histogram feature distribution model," in *Proc.of the IEEE Conference on Computer Vision and Pattern Recognition Workshops*, vol. 10. IEEE, June 2004, p. 161.

[113] L. Sha, G. Wang, A. Yao, X. Lin, and X. Chai, "Hand posture recognition in video using multiple cues," in *IEEE International Conference on Multimedia and Expo*. New York, USA: IEEE, June-July 2009, pp. 886–889.

[114] Q. Munib, M. Habeeb, B. Takruri, and H. A. Al-Malik, "American sign language (ASL) recognition based on Hough transform and neural networks," *Expert Systems with Applications*, vol. 32, no. 1, pp. 24–37, January 2007.

[115] O. Altun and S. Albayrak, "Turkish fingerspelling recognition system using generalized hough transform, interest regions, and local descriptors," *Pattern Recognition Letters*, vol. 32, no. 13, pp. 1626–1632, October 2011.

[116] M. AL-Rousan, K. Assaleh, and A. Talaa, "Video-based signer-independent Arabic sign language recognition using hidden markov models," *Applied Soft Computing*, vol. 9, no. 3, pp. 990–999, June 2009.

[117] P. N. Belhumeur, J. P. Hespanha, and D. J. Kriegman, "Eigenfaces vs. Fisherfaces: Recognition using class specific linear projection," *IEEE Trans. on Pattern Analysis and Machine Intelligence*, vol. 19, no. 7, pp. 711–720, July 1997.

[118] A. M. Martínez and A. C. Kak, "PCA versus LDA," *IEEE Trans. on Pattern Analysis and Machine Intelligence*, vol. 23, no. 2, pp. 228–233, February 2001.

[119] K. Delac, M. Grgic, and S. Grgic, "Independent comparative study of PCA, ICA, and LDA on the FERET data set," *International Journal of Imaging Systems and Technology, Wiley*, vol. 15, no. 5, pp. 252–260, 2005.

[120] J. Martin and J. L. Crowley, "An appearance-based approach to gesture recognition," *Lecture Notes in Computer Science, Springer-Verlag*, vol. 1311, pp. 340–347, 1997.

[121] H. Birk, T. B. Moeslund, and C. B. Madsen, "Real-time recognition of hand alphabet gestures using principal component analysis," in *The 10th Scandinavian Conference on Image Analysis*, Lappeenranta,Finland, June 1997.

[122] S. Malassiotis and M. Strintzis, "Real-time hand posture recognition using range data," *Image and Vision Computing*, vol. 26, no. 7, p. 10271037, July 2008.

[123] N. H. Dardas and E. M. Petriu, "Hand gesture detection and recognition using principal component analysis," in *IEEE International conference on computational intelligence for measurement systems and applications (CIMSA)*. IEEE, September 2011, pp. 1–6.

[124] Y. Cui, D. L. Swets, and J. J. Weng, "Learning-based hand sign recognition using SHOSLF-M," in *International Workshop on Automatic Face and Gesture Recognition*, Zurich, 1995, pp. 631–636.

[125] Y. Cui and J. Weng, “Appearance- based hand sign recognition from intensity image sequences,” *Computer Vision and Image Understanding*, vol. 78, no. 2, pp. 157–176, May 2000.

[126] K. YASUMOTO, J. MIZUNO, and T. KURITA, “Improvement of generalization ability of kernel-based Fisher discriminant analysis for recognition of Japanese sign language hand postures, ”Yubi-Moji”, using K-means method,” in *IAPR Workshop on Machine Vision Applications*, Nara, Japan, December 2002, pp. 269–272.

[127] J. Deng and H. Tsui, “A PCA/MDA scheme for hand posture recognition,” in *Proc. of the 5th IEEE International Conference on Automatic Face and Gesture Recognition*. IEEE, May 2002, pp. 294–299.

[128] M. Amin and H. Yan, “Sign language finger alphabet recognition from Gabor-PCA representation of hand gestures,” in *Proc. of the International Conference on Machine Learning and Cybernatics*, vol. 4. IEEE, August 2007, pp. 2218–2223.

[129] Y. F. Admasu and K. Raimond, “Ethiopian sign language recognition using artificial neural network,” in *10th International Conference on Intelligent Systems Design and Applications*. Cairo, Egypt: IEEE, November 2010, pp. 995–1000.

[130] D.-Y. Huang, W.-C. Hu, and S.-H. Chang, “Gabor filter-based hand pose angle estimation for hand gesture recognition under varying illumination,” *Expert Systems with Applications*, vol. 38, no. 5, pp. 6031–6042, May 2011.

[131] A. Karami, B. Zanj, and A. K. Sarkaleh, “Persian sign language (PSL) recognition using wavelet transform and neural networks,” *Expert Systems with Applications*, vol. 38, no. 3, pp. 2661–2667, March 2011.

[132] D. Conte, P. Foggia, C. Sansone, and M. Vento, “Thirty years of graph matching in pattern recognition,” *International Journal of Pattern Recognition and Artificial Intelligence*, vol. 18, no. 3, pp. 265–298, 2004.

[133] J. Triesch and C. von der Malsburg, “A system for person independent hand posture recognition against complex backgrounds,” *IEEE Trans. on Pattern Analysis and Machine Intelligence*, vol. 23, no. 12, pp. 1449–1453, December 2001.

[134] Y. Ding, H. Pang, X. Wu, and J. Lan, “Recognition of hand gestures using improved local binary pattern,” in *International Conference on Multimedia Technology (ICMT)*. China: IEEE, July 2011, pp. 3171–3174.

[135] Y. Freund and R. E. Schapire, “A decision-theoretic generalization of on-line learning and an application to boosting,” *Journal of System and Computer Sciences*, vol. 55, pp. 119–139, 1997.

[136] B. Fröba and A. Ernst, “Face detection with the modified Census transform,” in *Sixth IEEE International Conference on Automatic Face and Gesture Recognition*. Seoul, Korea: IEEE, May 2004, pp. 91–96.

[137] A. Just, Y. Rodriguez, and S. Marcel, “Hand posture classification and recognition using the modified Census transform,” in *Proc. of the 7th International Conference on Automatic Face and Gesture Recognition*. Southampton, United Kingdom: IEEE, April 2006, pp. 351–356.

[138] P. Viola and M. J. Jones, “Robust real-time face detection,” *International Journal of Computer Vision*, vol. 57, no. 2, pp. 137–154, 2004.

[139] J. Wachs, H. Stern, Y. Edan, M. Gillam, C. Feied, M. Smith, and J. Handler, “A real - time hand gesture system based on evolutionary search,” in *Vision*. Society of Manufacturing Engineers, October 2006, vol. 22, no. 3.

[140] Q. Chen, N. D. Georganas, and E. M. Petriu, “Hand gesture recognition using Haar-like features and a stochastic context-free grammar,” *IEEE Trans. on Instrumentation and Measurement*, vol. 57, no. 8, p. 15621571, August 2008.

[141] T.-T.-H. Tran and T.-T.-M. Nguyen, “Invariant lighting hand posture classification,” in *IEEE International Conference on Progress in Informatics and Computing*, vol. 2. Shanghai, China: IEEE, December 2010, pp. 827–831.

[142] D. G. Lowe, “Object recognition from local scale-invariant features,” in *Proc. of the Seventh IEEE International Conference on Computer Vision*, vol. 2. Corfu, Greece: IEEE, September 1999, pp. 1150–1157.

[143] ——, “Distinctive image features from scale-invariant keypoint,” *International Journal of Computer Vision*, vol. 60, no. 2, pp. 91–110, 2004.

[144] C.-C. Wang and K.-C. Wang, *Hand Posture Recognition Using Adaboost with SIFT for Human Robot Interaction*, ser. Lecture notes in control and information sciences, S. Lee, I. H. Suh, and M. S. Kim, Eds. Springer-Verlag, 2008, vol. 370.

[145] S.S.Ge, Y.Yang, and T.H.Lee, "Hand gesture recognition and tracking based on distributed locally linear embedding," *Journal of Image and Vision Computing*, vol. 26, no. 12, pp. 1607–1620, December 2008.

[146] P. Xiang, C. Qihua, and L. Zhi, "Content-based 3D retreival by Krawtchouk moments," *Lecture Notes in Computer Science, Springer-Verlag*, vol. 4142, pp. 217–224, September 2006.

[147] C.-H. Teh, "On image analysis by the methods of moments," *IEEE Trans. on Pattern Analysis and Machine Intelligence*, vol. 10, no. 4, pp. 496 – 513, 1988.

[148] C. Kan and M. D. Srinath, "Invariant character recognition with Zernike and orthogonal Fourier-mellin moments," *Pattern Recognition*, vol. 35, no. 1, pp. 143–154, 2002.

[149] A. Ono, "Face recognition with Zernike moments," *Systems and Computers in Japan*, vol. 34, no. 10, p. 2635, 2003.

[150] J. Zhou, H. Shu, H. Zhu, C. Toumoulin, and L. Luo, "Image analysis by discrete orthogonal Hahn moments," in *Image Analysis and Recognition*, ser. Lecture Notes in Computer Science, M. Kamel and A. Campilho, Eds. Springer Berlin Heidelberg, 2005, vol. 3656, pp. 524–531.

[151] P.-T. Yap, R. Paramesran, and S.-H. Ong, "Image analysis using Hahn moments," *IEEE Trans. on Pattern Analysis and Machine Intelligence*, vol. 29, no. 11, pp. 2057–2062, 2007.

[152] H. Zhu, H. Shu, J. Liang, L. Luo, and J.-L. Coatrieux, "Image analysis by discrete orthogonal Racah moments," *Signal Processing*, vol. 87, no. 4, p. 687708, 2007.

[153] H. Zhu, M. Liu, H. Shu, H. Zhang, and L. Luo, "General form for obtaining discrete orthogonal moments," *IET Image Processing*, vol. 4, no. 5, pp. 335–352, 2010.

[154] Harry Bateman, *Higher Transcendental Functions*. McGraw-Hill book company, Inc, 1953, vol. II.

[155] G. Szego, *Orthogonal Polynomials*, 4th ed. American Mathematical Society Colloquium Publications, 1975, vol. XXIII.

[156] W. Koepf, *Hypergeometric Summation -An Algorithmic Approach to Summation and Special Function Identities*. Braunschweig, Germany: Vieweg, 1998.

[157] R. Koekoek, P. A. Lesky, and R. F. Swarttouw, *Hypergeometric Orthogonal Polynomials and Their q-Analogues*, ser. Springer monographs in mathematics. Springer, 2010.

[158] R. Beals and R. Wong, *Special Functions : A Graduate Text*, ser. Cambridge Studies In Advanced Mathematics, B. Bollobas, W. Fulton, A. Katok, F. Kirwan, P. Sarnak, B. Simon, and B. Totaro, Eds. Cambridge University Press, 2010.

[159] G. E. Andrews, R. Askey, and R. Roy, *Special Functions*, ser. Encyclopedia Of Mathematics And Its Applications, G.-C. Rota, Ed. Cambridge University Press, 1999, vol. 71.

[160] R. Koekoek and R. Swarttouw, "The Askey-scheme of hypergeometric orthogonal polynomials and its q-analogue," Technische Universiteit Delft Faculty of Technical Mathematics and Informatics Report 98-17, Delft, Netherlands, Tech. Rep., 1998.

[161] P. Tchebychef, *Oeuvres de P.L. Tchebychef*. Imprimerie De L'Acadmie Impriale Des Sciences, 1899, vol. 1, ch. Sur l'interpolation, pp. 541–560.

[162] R. C. Gonzalez and R. E. Woods, *Digital Image Processing*, 2nd ed. Upper Saddle River, New Jersey: Prentice Hall, 2002.

[163] A. N. Akansu, R. A. Haddad, and H. Caglar, "The binomial QMF-wavelet transform for multiresolution signal decomposition," *IEEE Trans. on Signal Processing*, vol. 41, no. 1, pp. 13–19, 1993.

[164] J. Shen, W. Shen, and D. Shen, "On geometric and orthogonal moments," *International Journal of Pattern Recognition and Artificial Intelligence*, vol. 14, no. 7, pp. 875–894, November 2000.

[165] M. M. Goodwin, *Springer Handbook of Speech Processing*. Springer, 2007, ch. The STFT, Sinusoidal Models and Speech Modification, pp. 229–258.

[166] Z. Wang, A. C. Bovik, H. R. Sheikh, and E. P. Simoncelli, "Image quality assessment: From error visibility to structural similarity," *IEEE Trans. on Image Processing*, vol. 13, no. 4, pp. 600–612, 2004.

[167] S. Rueda, J. K. Udupa, and L. Bai, "A comparison of local and global scale approaches in characterizing shapes," in *Proc. of SPIE Medical imaging 2009: Image processing*, J. P. W. Pluim and B. M. Dawant, Eds., vol. 7259, no. 725951, Orlando, FL., U.S.A., February 2009.

[168] S. Abbasi, F. Mokhtarian, and J. Kittler, "Enhancing CSS-based shape retrieval for objects with shallow concavities," *Image and Vision Computing*, vol. 18, no. 3, pp. 199–211, February 2000.

[169] S. Richter, G. Kuehne, and O. Schuster, "Contour-based classification of video objects," in *Proc. of SPIE, Storage and Retreival of Media Databases 2001*, M. M. Yeung, C.-S. Li, and R. W. Lienhart, Eds., vol. 4315, 2001, pp. 608–618.

[170] I. E. Abdou and W. K. Pratt, "Quantitative design and evaluation of enhancement/thresholding edge detectors," *Proceedings of the IEEE*, vol. 67, no. 5, pp. 753–763, May 1979.

[171] W. K. Pratt, *Digital Image Processing: PIKS Scientific Inside*. Wiley, 2007.

[172] Y. Sheng, *Transforms and Applications Handbook*. CRC Press, Taylor & Francis Group, 2010, ch. Wavelet Transform, pp. 10.1–10.53.

[173] G. H. Anderson, *Video Editing and Post Production: A professional guide*. Knowledge industry publications, Inc., 1984.

[174] P. Song, S. Winkler, S. Gilani, and Z. Zhou, "Vision-based projected tabletop interface for finger interactions," in *Human-Computer Interaction*, ser. Lecture Notes in Computer Science, M. Lew, N. Sebe, T. S. Huang, and E. M. Bakker, Eds. Springer-Berlin Heidelberg, 2007, vol. 4796, pp. 49–58. [Online]. Available: http://dx.doi.org/10.1007/978-3-540-75773-3_6

[175] M. Miura and S. Kunifuji, "A tabletop interface using controllable transparency glass for collaborative card-based creative activity," in *Knowledge-Based Intelligent Information and Engineering Systems*, ser. Lecture Notes in Computer Science, I. Lovrek, R. J.Howlett, and L. C.Jain, Eds. Springer-Berlin Heidelberg, 2008, vol. 5178, pp. 855–862. [Online]. Available: http://dx.doi.org/10.1007/978-3-540-85565-1_106

[176] P. Maragos and M. A. Butt, *Mathematical Morphology*. IOS Press, Amsterdam, 2000, ch. Curve Evolution, Differential Morphology and Distance Transforms Applied to Multiscale and Eikonal Problems, pp. 91–129.

[177] H. Breu, J. Gil, D. Kirkpatrick, and M. Werman, "Linear Time Euclidean Distance Transform Algorithms," *IEEE Trans. on Pattern Analysis and Machine Intelligence*, vol. 17, no. 5, pp. 529–533, May 1995.

[178] R. Fabbri, L. da F. Costa, J. C. Torelli, and O. M. Bruno, "2D Euclidean Distance Transform Algorithms: A Comparative Survey," *ACM Computing Surveys*, vol. 40, no. 1, February 2008.

[179] S. Pheasant, *Bodyspace: Anthropometry, Ergonomics and the Design of work*. Taylor and Francis Routledge, 1996.

[180] A. Nag, P. Nag, and H. Desai, "Hand Anthropometry of Indian Women," *The Indian journal of medical research*, vol. 117, pp. 260–269, June 2003.

[181] T. Kanchan and P. Rastogi, "Sex Determination from Hand Dimensions of North and South Indians," *Journal of Forensic Sciences*, vol. 54, no. 3, pp. 546–550, May 2009.

[182] C. de Boor, *A Practical Guide to Splines*, revised edition ed., J.E.Marsden and L.Sirovich, Eds. Springer-Verlag, 2001.

[183] D. L. Swets and J. J. Weng, "Using discriminant eigenfeatures for image retrieval," *IEEE Trans. on Pattern Analysis and Machine Intelligence*, vol. 18, no. 8, pp. 831–836, August 1996.

[184] Janet W. Descutner, *World of dance: Asian dance*, 2nd ed., Elizabeth A. Hanley, Ed. Chelsea house, 2010.

[185] N. Ebenreuter, "Dance movement: A focus on the technology," *IEEE trans. on Computer Graphics and Applications*, vol. 25, no. 6, pp. 80–83, November 2005.

[186] T. Calvert, L. Wilke, R. Ryman, and I. Fox, "Applications of computers to dance," *IEEE trans. on Computer Graphics and Applications*, vol. 25, no. 2, pp. 6–12, March 2005.

[187] K. Kojima, K. Hachimura, and M. Nakamura, "LabanEditor : Graphical editor for dance notation," in *Proc. of the IEEE Int. workshop on robot and human interactive communication*. IEEE, September 2002, pp. 59–64.

[188] T. Takeda, Y. Hirata, and K. Kosuge, "Dance step estimation method based on HMM for dance partner robot," *IEEE trans. on Industrial Electronics*, vol. 54, no. 2, pp. 699–706, April 2007.

[189] B. Stang, M. A. Osterholt, E. Hoftun, J. Kirksaeter, and H. C. Bjorne, *The book of games*, B. Stang, Ed. gameXplore N.A.Inc, 2007, vol. 2.

[190] J. C. Chan, H. Leung, J. K. Tang, and T. Komura, "A virtual reality dance training system using motion capture technology," *IEEE Trans. on Learning Technologies*, vol. 4, no. 2, pp. 187–195, April 2011.

[191] K. Hachimura, K. Takashina, and M. Yoshimura, "Analysis and evaluation of dancing movement based on LMA," in *Proc. of the IEEE Int. workshop on robot and human interactive communication*, August 2005, pp. 294–299.

[192] T. Shiratori and K. Ikeuchi, "Synthesis of dance performance based on analyses of human motion and music," *IPSJ trans. on Computer Vision and Image Media*, vol. 1, no. 1, pp. 34–47, June 2008.

[193] F. Ofli, E. Erzin, Y. Yemez, A. M. Tekalp, Çigdem Eroglu Erdem, A. T. Erdem, T. Abaci, and M. K. Özkan, "Unsupervised dance figure analysis from video for dancing avatar animation," in *Proc. of the Int. conf. on image processing*. IEEE, 2008, pp. 1484–1487.

[194] Y. Iwadate, M. Inoue, R. Suzuki, N. Hikawa, M. Makino, and Y. Kanemoto, "MIC Interactive dance system: An emotional interaction system," in *Proc. of 4th Int. conf. on knowledge-based intelligent engineering systems and allied technologies*, vol. 1, August 2000, pp. 95–98.

[195] V. Mamania, A. Shaji, and S. Chandran, "Markerless motion capture from monocular videos," in *Indian conf. on computer vision, graphics and image processing*, 2004, pp. 126–132.

[196] F. Guo and G. Qian, "Dance posture recognition using wide-baseline orthogonal stereo cameras," in *7th Int. conf. on automatic face and gesture recognition*. IEEE, April 2006, pp. 481–486.

[197] B. Peng, G. Qian, and S. Rajko, "View-invariant full-body gesture recognition via multilinear analysis of voxel data," in *Proc.of ACM/IEEE Int. conf. on distributed smart cameras*, August 2009, pp. 1–8.

[198] A. Soga, R. Boulic, and D. Thalmann, "Motion planning and animation variety using dance motion clips," in *Int. conf. on cyberworlds*, October 2010, pp. 421 – 424.

[199] "Organic Motion powers research into the science of dance," June 2011. [Online]. Available: http://www.organicmotion.com/news/press/pr2011m06d14

[200] L. Deng, H. Leung, N. Gu, and Y. Yang, "Recognizing dance motions with segmental SVD," in *20th Int. conf. on pattern recognition*, August 2010, pp. 1537–1540.

[201] A. Soga, B. Umino, and M. Hirayama, "Automatic composition for contemporary dance using 3D motion clips: Experiment on dance training and system evaluation," in *Int.conf. on cyberworlds*, September 2009, pp. 171–176.

[202] L. W. Campbell and A. E. Bobick, "Recognition of human body motion using phase space constraints," in *Proc. of the 5th Int. conference on computer vision*, June 1995, pp. 624 – 630.

[203] A. SOGAT, M. ENDO, and T. YASUDA, "Motion description and composing system for classic ballet animation on the web," in *Proc. of 10th IEEE Int. workshop on robot and human interactive communication*, 2001, pp. 134 – 139.

[204] M. Yoshimura, K. Kojimal, K. Hachimura, Y. Marumo, and A. Kuromiya, "Quantification and recognition of basic motion okuri in Japanese traditional dance," in *13th IEEE Int. workshop on robot and human interactive communication*. IEEE, September 2004, pp. 205–210.

[205] M. Sakata, M. Marumo, and K. Hachimura, "An analysis of motion features of different characters in Nihon-Buyo dance using motion capture," in *Proc. of the 17th IEEE Int. symposium on robot and human interactive communication*, August 2008, pp. 273–278.

[206] B. orn Rennhak, T. Shiratori, S. Kudoh, P. Vinayavekhin, and K. Ikeuchi, "Detecting dance motion structure using body components and turning motions," in *IEEE/RSJ Int. conf. on intelligent robots and systems*, October 2010, pp. 2264 – 2269.

[207] W. Choensawat, W. Choi, and K. Hachimura, "A quick filtering for similarity queries in motion capture databases," in *10th Pacific Rim Conference on Multimedia: Advances in multimedia information processing*. Springer-Verlag, 2009, pp. 404–415.

[208] R. Kannan, F. Andres, and C. Guetl, "DanVideo: an MPEG-7 authoring and retrieval system for dance videos," *Multimedia Tools and Applications, Springer*, vol. 46, no. 2-3, pp. 545–572, 2009.

[209] A. Salway and K. Ahmad, "Multimedia systems and semiotics: Collateral texts for video annotation," in *IEE Colloquium digest on multimedia databases and MPEG-7*, January 1999.

[210] B. Ramadoss and K. Rajkumar, "Modeling and annotating the expressive semantics of dance videos," *Int. Journal on Information Technologies and Knowledge*, vol. 1, pp. 137–146, 2007.

[211] D. Cabral, U. Carvalho, J. a. Silva, J. a. Valente, C. Fernandes, and N. Correia, "Multimodal video annotation for contemporary dance creation," in *2011 Annual conf. extended abstracts on human factors in computing systems*. ACM, 2011, pp. 2293–2298.

[212] A. Mallik and S. Chaudhury, "Using concept recognition to annotate a video collection," in *Proc. of the 3rd Int. conf. on pattern recognition and machine intelligence, LNCS*, vol. 5909. Springer-Verlag, 2009, pp. 507–512.

[213] D. Hariharan, T. Acharya, and S. Mitra, "Recognizing hand gestures of a dancer," in *Pattern recognition and machine intelligence, LNCS*, vol. 6744. Springer-Verlag, 2011, pp. 186–192.

[214] P. K. Srimani and S. Kavitha, "Recognizing Samyuktha hand gestures of Bharatanatyam using skeleton matching and gradient orientation," *International Journal of Current Research*, vol. 5, no. 6, pp. 1457–1462, June 2013.

[215] Shovana Narayan, *The sterling book of :Indian classical dances*. New Dawn press group, 2007.

[216] Manomohan Ghosh, *Nandikesvara's Abhinayadarpanam: A manual of gesture and posture used in hindu dance and drama*, 2nd ed. Firma K. L. Mukhopadhyay, 1957.

[217] P. V. Subramaniam, *Bharatanatyam*. Samkaleen Prakashan, New Delhi, 1980.

[218] [Online]. Available: http://onlinebharathanatyamacademy.wordpress.com/

[219] S. Bhagyalekshmy, *Music and Bharathanatyam*. Sundeep Prakashan, Delhi, 1991.

[220] V. P. Dhananjayan, *A Dancer on Dance*. Bharata Kalanjali, 1984.

[221] S. Sehgal, *Encyclopedia of Hinduism*, 1st ed. Sarup and Sons, New Delhi, 1999, vol. 2.

[222] Ragini Devi, *Dance dialects of India*, 2nd ed. Motilal Banaridass, 1990.

[223] Anjana Rajan, "Learn the Lingo," The Hindu [Delhi], *Friday Review*, July'09 - January'10 2009-2010.

[224] R. Puri, "Bharatanatyam performed: A typical recital," *Visual Anthropology*, vol. 17, pp. 45–68, 2004.

[225] J. Deer and R. D. Vera, *Acting in Musical Theatre: A Comprehensive Course*. Taylor and Francis, 2008.

[226] B. Andersson and J. L. Geyen, *The DSLR Filmmaker's Handbook: Real-World Production Techniques*. John Wiley and Sons, Inc., 2012.

# List of Publications

### *Journal Publications*

1. S. Padam Priyal and P.K. Bora, “A Robust Static Hand Gesture Recognition System using Geometry based Normalizations and Krawtchouk Moments”, , *Pattern Recognition (Elsevier)*, vol. 46, no. 8, pp. 2202–2219, 2013.

### *Conference Publications*

1. S. Padam Priyal and P.K. Bora, “A Study on Static Hand Gesture Recognition using Moments”, in Proc. of IEEE International Conference on Signal Processing and Communication (SPCOM), IISC- Bangalore , pp. 1–5, July 2010.

2. S. Padam Priyal and P.K. Bora, “Database of Asamyuta Hastas: a step towards intelligent system for Bharatanatyam”, Proc. of Centenary Conference-EE, IISC- Bangalore , pp.15–17, December 2011.